Title
Enabling the identification, quantification, and characterization of organics in complex mixtures to understand atmospheric aerosols

Author
Isaacman, Gabriel Avram

Publication Date
2014

Peer reviewed|Thesis/dissertation

Enabling the identification, quantification, and characterization of organics in complex mixtures to understand atmospheric aerosols

by

Gabriel Avram Isaacman

A dissertation submitted in partial satisfaction of the

requirements for the degree of

Doctor of Philosophy

in

Environmental Science, Policy, and Management

in the

Graduate Division

of the

University of California, Berkeley

Committee in charge:

Professor Allen H. Goldstein, Chair
Professor Robert A. Harley
Professor Dennis D. Baldocchi

Fall 2014

Enabling the identification, quantification, and characterization of organics in complex mixtures to understand atmospheric aerosols

Gabriel Avram Isaacman

Abstract

Enabling the identification, quantification, and characterization of organics in complex mixtures to understand atmospheric aerosols

by

Gabriel Avram Isaacman

Doctor of Philosophy in Environmental Science, Policy, and Management

University of California, Berkeley

Professor Allen H. Goldstein, Chair

Particles in the atmosphere are known to have negative health effects and important but highly uncertain impacts on global and regional climate. A majority of this particulate matter is formed through atmospheric oxidation of naturally and anthropogenically emitted gases to yield highly oxygenated secondary organic aerosol (SOA), an amalgamation of thousands of individual chemical compounds. However, comprehensive analysis of SOA composition has been stymied by its complexity and lack of available measurement techniques. In this work, novel instrumentation, analysis methods, and conceptual frameworks are introduced for chemically characterizing atmospherically relevant mixtures and ambient aerosols, providing a fundamentally new level of detailed knowledge on their structures, chemical properties, and identification of their components. This chemical information is used to gain insights into the formation, transformation and oxidation of organic aerosols.

Biogenic and anthropogenic mixtures are observed in this work to yield incredible complexity upon oxidation, producing over 100 separable compounds from a single precursor. As a first step toward unraveling this complexity, a method was developed for measuring the polarity and volatility of individual compounds in a complex mixture using two-dimensional gas chromatography, which is demonstrated in Chapter 2 for describing the oxidation of SOA formed from a biogenic compound (longifolene: $C_{15}H_{24}$). Several major products and tens of substantial minor products were produced, but none could be identified by traditional methods or have ever been isolated and studied in the laboratory. A major realization of this work was that soft ionization mass spectrometry could be used to identify the molecular mass and formula of these unidentified compounds, a major step toward a comprehensive description of complex mixtures. This was achieved by coupling gas chromatography to high resolution time-of-flight mass spectrometry with vacuum ultraviolet (VUV) photo-ionization. Chapters 3 and 4 describe this new analytical technique and its initial application to determine the structures of unknown compounds and formerly unresolvable mixtures, including a complete description of the chemical composition of two common petroleum products related to anthropogenic emissions: diesel fuel and motor oil. The distribution of hydrocarbon isomers in these mixtures – found to be mostly of branched, cyclic, and saturated – is described with unprecedented detail.

Instead of measuring average bulk aerosol properties, the methods developed and applied in this work directly measure the polarity, volatility, and structure of individual components to allow a mechanistic understanding of oxidation processes. Novel characterizations of these complex

mixtures are used to elucidate the role of structure and functionality in particle-phase oxidation, including in Chapter 4 the first measurements of relative reaction rates in a complex hydrocarbon particle. Molecular structure is observed to influence particle-phase oxidation in unexpected and important ways, with cyclization decreasing reaction rates by ~30% and branching increasing reaction rates by ~20-50%. The observed structural dependence is proposed to result in compositional changes in anthropogenic organic aerosol downwind of urban areas, which has been confirmed in subsequent work by applying the techniques described here.

Measurement of organic aerosol components is extended to ambient environments through the development of instrumentation with the unprecedented capability to measure hourly concentrations and gas/particle partitioning of individual highly oxygenated organic compounds in the atmosphere. Chapters 5 and 6 describe development of new procedures and hardware for the calibration and analysis of oxygenates using the Semi-Volatile Thermal desorption Aerosol Gas chromatograph (SV-TAG), a custom instrument for in situ quantification of gas- and particle-phase organic compounds in the atmosphere. High time resolution measurement of oxygenated compounds is achieved through a reproducible and quantitative methodology for in situ "derivatization" – replacing highly polar functional groups that cannot be analyzed by traditional gas chromatography with less polar groups. Implementation of a two-channel sampling system for the simultaneous collection of particle-phase and total gas-plus-particle phase samples allows for the first direct measurements of gas/particle partitioning in the atmosphere, significantly advancing the study of atmospheric composition and variability, as well as the processes governing condensation and re-volatilization.

This work presents the first in situ measurements of a large suite of highly oxygenated biogenic oxidation products in both the gas- and particle-phase. Isoprene, the most ubiquitous biogenic emission, oxidizes to form 2-methyltetrols and C_5 alkene triols, while α-pinene, the most common monoterpene, forms pinic, pinonic, hydroxyglutaric, and other acids. These compounds are reported in Chapter 7 with unprecedented time resolution and are shown for the first time to have a large gas-phase component, contrary to typical assumptions. Hourly comparisons of these products with anthropogenic aerosol components elucidate the interaction of human and natural emissions at two rural sites: the southeastern, U.S. and Amazonia, Brazil. Anthropogenic influence on SOA formation is proposed to occur through the increase in liquid water caused by anthropogenic sulfate. Furthermore, these unparalleled observations of gas/particle partitioning of biogenic oxidation products demonstrate that partitioning of oxygenates is unexpectedly independent of volatility: many volatile, highly oxygenated compounds have a large particle-phase component that is poorly described by traditional models. These novel conclusions are reached in part by applying the new frameworks developed in previous chapters to understand the properties of unidentified compounds, demonstrating the importance of detailed characterization of atmospheric organic mixtures.

Comprehensive analysis of anthropogenic and biogenic emissions and oxidation product mixtures is coupled in this work with high time-resolution measurement of individual organic components to yield significant insights into the transformations of organic aerosols. Oxidation chemistry is observed in both laboratory and field settings to depend on molecular properties, volatility, and atmospheric composition. However, this work demonstrates that these complex processes can be understood through the quantification of individual known and unidentified compounds, combined with their classification into descriptive frameworks.

Acknowledgements

This work owes by far the most to my loving and amazing wife, Darrow, for her support throughout my time as a grad student, all the way back to beginning - convincing me to move to the Bay Area, helping me find a place to live, and editing my application essays to Berkeley. She has never stopped helping me and working by my side, falling asleep next to me through all-nighters, coming to the office to work on the weekend, and even coming to the field to sit in cramped trailers for days on end. She has happily supported me not only when I needed to work long hours or go away for months, but has also been the driving force for fun in our lives, planning dinner with friends, camping trips, and Fourth of July parties. When she's not around, I start down the path toward crazy old professor, forgetting appointments and showing up at the wrong house for dinner. She is at the top of a long list of family, friends, and colleagues that have made my work possible.

I also owe an enormous debt to my advisor Allen for his years of guidance, insight, and support, and for fighting tooth and nail to get me into Berkeley. He has encouraged me to pursue a wide array of diverse science and research and has allowed me great flexibility in starting many ongoing projects that I am proud to see continue under the excellent direction of the other scientists in the group. I am lucky to have been a part of his group during a time of great collaboration and cooperation, which has yielded friendships as valuable as our science.

I could not have had a better friend and mentor than Dave, who taught me everything I know about fieldwork, gas chromatography, capillaries, and British swearing. For my several years as a grad student, I saw more of him than anyone else (wife included), and am fortunate enough to have enjoyed almost every hour of it. He and Arthur (and hours of science-fiction shows) made the long, long nights at the beam much more fun, though I will forever blame him and beamtime for convincing me to start drinking coffee. Nathan has also been an enormous part of my work, always there for scientific and engineering advice. I will always feel both grateful and guilty for those many late nights he cheerfully stayed with me in the lab, missing time with his family so I could frantically finish up projects in time to catch my flight to Darrow. After data collection, my long hours of analysis were always easier when Drew was in the office to provide a soundtrack of punk music, and I am glad to have carried that friendship beyond the lab after his graduation.

Many scientists have contributed intellectually to this work and have been great sources of inspiration and guidance. Kevin Wilson in particular has been a mentor and friend throughout my research, always willing to give me his time and spend hours on the phone discussing our work. I have also always appreciated the insights and challenging questions of Rob Harley and Ron Cohen, who have always brought different perspectives to my work and have helped me understand how my research fits into larger scientific questions. I would also like to thank Inez Fung and Dennis Baldocchi for serving on my qualifying exam and dissertation committees, ensuring my education has been solid and well-rounded. I have of course also relied on the generous and ongoing funding and fellowships of many agencies and organizations, especially the NSF, EPA, and DOE. My dissertation has only been possible thanks to all of the researcher and students who have helped me improve and understand my data, and all the people who have worked and commiserated with me in the field. Lindsay especially has been the best field-partner I could have hoped for, putting up with snappishness and frustrated-ness, and keeping me from making rash decisions or rocking the boat.

My family has been an important part of this process as I have relied heavily on them for personal and professional advice, and friendship. My parents have provided an endless stream of emotional (and occasionally financial) support, even for those few years I was scraping by in San Francisco when it really looked like I wasn't going to go to grad school or find a full-time job. I am lucky to be so close to Sibren, who has been a great friend and, doing all this 2 years ahead of me, really gave me a great deal of insight into the PhD and academic process. His support of me and my choices have made my decisions easier at every turn (even if making decisions for himself isn't his strong suit), and Tanushree has only made that more true. She has always been a source of great empathy and smart advice. While Rahm may not have contributed much to this work directly, he is worth acknowledging because being an uncle to him is such a bright spot in my life. My academic success is in no small part due to the fact that I have a disconcertingly functional family that likes to spend time together, from the Isaacman beach vacations, to the support the van den Bors have given me in and out of Holland, to the joint holidays combining all my parents and Darrow's parents.

Throughout my PhD I have traveled a lot, and all over this country my friends have – often on one day or one hour notice – dropped what they were doing and spent time with me. If it weren't for the flexibility and friendship of all of these people, I would never have made it through, let alone had as much fun as I did.

Being so far from home would have been much harder if it weren't for my stand-in West Coast family. Thanks to BARSL, weekly sea lion trips across the bay were a welcome break from the lab and frequent dinner parties and trips to Willits made the months and years (and fiberglass insulation) fly by. After leaving, getting to see everyone has made my visits back to the Berkeley seem less like work – thanks especially to Kevi for letting me sleep above the chicken coop on all those visits. My time as a graduate student has been shaped not just by my work, but by nearly every housemate I've had in California, since I have been able to live almost exclusively with close friends: Ryan, Sean, Tommy, Lauren, Iris, and I'm going to count Darrow's housemates, Gordon, Vera, Kika, and Julien. Thanks to all these people and their partners, and a nearly endless list of others – at game nights, on bike rides, and playing kubb – my PhD never felt like a job, it was just a way to have fun, learn, and spend time amongst friends.

So much of this dissertation was written all over the East Coast, and my friends have supported me everywhere: in New Haven, where I've been surrounding by other PhD students motivating me to write, in Durham, where Darrow's housemates and friends gave me warm welcomes and spent days on end in the law library with me, and in DC and Maryland, where old friends taught me about policy-making and that sandals are not professional attire outside of California. Throughout all of this, I've depended heavily on Aaron and Jessalee, who have brought me endless entertainment over the past decade and have donated their friend groups in all of these cities. The list of friends I've relied on through my PhD is long, but all of my friends from home, from Wesleyan, and from the Bay Area have made this time enjoyable and worthwhile, and have offered a bed, or a friend, or advice when I needed it.

Finally I'd like to thank all the inanimate objects I relied on throughout my PhD: Hilgard Hall for not succumbing to any of the many earthquakes, the soft grip 5/32" hex wrench I used almost every day, and the Dremel, with which I did nearly everything. No thanks to the 3/16" wrenches, which are way too easy to lose.

Table of Contents

List of Figures

Chapter 2

Chapter 3

Chapter 4

Chapter 5

Chapter 6

Chapter 7

Appendices

List of Tables

Chapter 1

Introduction

1.1. Scientific background

Atmospheric aerosols have been known for decades to have deleterious health effects (Pope and Dockery, 2006) and climate impacts (Intergovernmental Panel On Climate Change, 2007). However, current regional and global models often substantially underpredict aerosols and poorly predict their chemical and physical properties, owing in large part to the complexity of their composition. In both urban and rural environments, a majority of submicron particulate matter is organic (Jimenez et al., 2009), of which a dominant fraction is Secondary Organic Aerosol (SOA), formed through the atmospheric oxidation of volatile organic compounds (VOCs) resulting in a prevalence of oxygenated aerosols, especially in rural and remote regions (Zhang et al., 2007). Biogenic VOCs (BVOCs), primarily isoprene (C_5H_8), monoterpenes ($C_{10}H_{16}$), and sesquiterpenes ($C_{15}H_{24}$) account for approximately 90% of the estimated global VOC budget (Guenther et al., 1995), with the rest comprised of anthropogenic emissions, largely from fossil fuel combustion. SOA forms from these emissions through their oxidation in the lower atmosphere, primarily by hydroxyl radicals (OH) and ozone and in the presence of sunlight, oxides of nitrogen (NO_x), and sulfate-rich particles.

Oxidation can result in the addition of oxygenated functional groups (functionalization), resulting in lower volatility products, or decomposition into higher volatility products (fragmentation). Initial oxidation steps typically yield functionalized, highly oxygenated, lower-volatility gases that can condense into the particle phase (Goldstein and Galbally, 2007; Hallquist et al., 2009; Kroll and Seinfeld, 2008a). Partitioning between gas-phase "semi-volatile" chemical species and their particle phase component is typically described by thermodynamic equilibrium between condensation and volatilization though this assumption has not been well-tested for ambient aerosol. Continued oxidant exposure can also result in increased fragmentation resulting in loss of particle mass from re-volatilization (Lambe et al., 2012). The balance between formation of semi-volatile condensable species and scission into higher-volatility fragments is influenced by compound structure (Kessler et al., 2010), with some evidence that functionalization and fragmentation depend on branching and cyclization. Significant uncertainty lies both in the relative importance of different chemical mechanisms as well as in the interaction between gas- and particle-phase compounds, but it is clear that the processes that turn VOCs into SOA are dependent on compound size, structure, and functionality.

The dependence of atmospheric processes on chemically specific attributes is complicated by the fact that emissions rarely occur as a single chemical species. BVOC emissions occur as unique combinations of terpenoid compounds (i.e. Bouvier-Brown et al., 2009; Holzinger et al., 2006; Ormeño et al., 2010), while anthropogenic VOC emissions are usually comprised of several hundred different saturated hydrocarbons derived from fossil fuels (Gentner et al., 2012; Worton et al., 2014). These mixtures co-exist in most environments, usually in the presence of other anthropogenic emission such as NO_x and SO_2 that can have a strong effect on chemical conditions. Globally, most carbon in organic aerosol has been shown to be biogenic, both in rural and urban in environments (Bench et al., 2007; Hodzic et al., 2010). However, anthropogenic

emissions of SO_2 have been observed to result in SOA enhancement in some environments (Brock et al., 2003), and OA often correlates with anthropogenic emissions of CO (i.e. Weber et al., 2007). A majority of global aerosol may form through anthropogenic influence on the chemistry of biogenic VOCs (Spracklen et al., 2011), so a complete understanding of atmospheric composition and processes requires knowledge about the fates of both anthropogenic emissions and biogenic emission in the gas- and particle-phase as well as their interactions.

Ambient atmospheric gases and particles contains thousands of organic compounds in trace amounts (Goldstein and Galbally, 2007) due to the variety of emitted compounds reacting through a multitude of available pathways. While the basic oxidation reactions available to organic gas-phase compounds in the atmosphere are well studied, multi-generational oxidation of a compound can yield mixtures of products that are prohibitively complicated to explicitly model (Aumont et al., 2005; Gao et al., 2006; Kroll and Seinfeld, 2008b; Lee et al., 2006a, 2006b). For example, oxidation of a single biogenic precursor is shown in Chapter 2 to quickly yield over 100 unique compounds. Furthermore, laboratory and modeling studies have pointed to an abundance of possible multi-phase processes, such as reactive uptake of gases into the particle through acid-catalyzed oligomerization (Gao et al., 2004b) or organosulfate formation (Surratt et al., 2008), solution and oxidation of oxygenated molecules in cloud droplets (Carlton et al., 2008; Ervens et al., 2008, 2014; He et al., 2013), concentration of organics at the particle surface (Ruehl and Wilson, 2014; Tervahattu et al., 2002), increased particle oxidation through radical propagation (i.e. Nah et al., 2014), and fast oxidation of a minor gas-phase component (Lambe et al., 2009). Many of these pathways have been proposed as potential mechanisms for anthropogenic-biogenic interactions, but ambient observations of their expected products are sparse and their roles in ambient environments are poorly understood.

The plethora of available reaction processes coupled with the variety of available precursor emissions yields an incredible amount of complexity in particles and low-volatility gases. To manage this issue, substantial progress has been made on the bulk analysis of particles. A large array of instrumentation has been refined over the past several decades to measure the physical, optical, hygroscopic, and mass spectrometric signal of particles; extensive reviews of these instruments are provided by McMurry (2000) and Hallquist et al. (2009). Measurements of average particle properties have yielded significant advances in understanding and modeling aerosol formation, but most bulk measurements lack the chemical specificity to probe the roles of specific chemical pathways in the atmosphere or in atmospherically relevant mixtures. In addition, due to the bi-directional flux of organic mass between the gas and particle phases, highly oxygenated semi-volatile compounds in the gas phase must also be studied to fully understand aerosols but have only recently begun to be measured.

Though explicit identification of all component compounds is likely unattainable, a detailed quantitative understanding of this composition has significant benefits. Speciation of organic aerosol improves source attribution by quantifying specific tracers known to originate from a given source or form through a given chemical pathway. These tracers include directly emitted compounds, such as levoglucosan from woodburning and hopanes from diesel exhaust, as well as secondary compounds formed through the oxidation of VOCs, such as phthalic acid and furanones from fossil fuels (Fraser and Lakshmanan, 2000; Mazurek, 2002; Rogge, 1993; Schauer et al., 1996; Simoneit, 2005; Williams et al., 2010b) and a wide array of tracers from BVOC oxidation (Chan et al., 2010; Claeys et al., 2004, 2007, 2009; Jaoui et al., 2005, 2007;

Kleindienst et al., 2009; Szmigielski et al., 2007b). Detailed analysis of aerosol composition has also contributed to a better understanding of formation mechanisms and atmospheric oxidation processes (Gao et al., 2004a; Jaoui et al., 2008; Surratt et al., 2008; Winterhalter et al., 2009) and quantifying known tracer compounds can provide insight into biological and chemical degradation processes (Megharaj et al., 2011; Simoneit, 2005) and contaminant sources (Fraser and Lakshmanan, 2000; Mazurek, 2002; Schauer et al., 1996; Williams et al., 2010b). Ratios of these various tracers provide a means to understand the relative importance of various chemical pathways, i.e. the effect of anthropogenic NO_x on isoprene oxidation in a given environment (Carlton et al., 2009; Worton et al., 2013). In this framework complexity is not a liability, but is instead an opportunity, presenting a nearly limitless number of potential tracers to understand sources and processes.

Several methods have been developed to speciate aerosol, and unambiguously identify and quantify useful tracers. Sample collection on traps or filters is typically followed by extraction with solvents or thermally desorption for analysis by gas or liquid chromatography (GC, LC) coupled to a mass spectrometer (MS) (Cass, 1998; Mazurek, 2002; Schauer et al., 1996; Simoneit, 2005). Resolution and identification of compounds can be improved by coupling together chromatographic columns to separate compounds by multiple chemical properties, i.e. volatility and polarity. Two-dimensional GC (GC×GC) greatly increases the number of compounds that can be chromatographically separated, so has served as useful tool in the classification and understanding of fossil fuels (Mao et al., 2009) and aerosols (Hamilton, 2010; Schnelle-Kreis et al., 2005). However, ambient samples and fossil fuels tend to contain an "unresolved complex mixture" of saturated hydrocarbons that cannot be separated or well-characterized even with traditional GC×GC.

In addition to compositional complexity, atmospheric phenomena occur on the minute to hour timescale (i.e. rain events, temperature fluctuations, and pressure fronts). It is therefore necessary to measure ambient organic tracers with hourly (or faster) time resolution to adequately capture relevant processes. However, traditional extraction of samples from collection substrates typically requires large sample sizes, therefore requiring long sample times, from 12 hours to multiple days. Measurement of organic composition with higher time resolution has been improved through the development of in situ, field-deployable GC/MS instruments. Hourly quantitative measurements of low-polarity tracers in the particle phase using a Thermal desorption Aerosol Gas chromatograph (Kreisberg et al., 2009; Lambe et al., 2010; Williams et al., 2006; and coupled to GC×GC, 2D-TAG: Goldstein et al., 2008; Worton et al., 2012) have been extended to include measurement of semi-volatile, low-polarity gases (SV-TAG: Zhao et al., 2013b). With SV-TAG, gas- and particle-phase compounds are sampled hourly into a high-surface-area collection cell for analysis by thermal desorption into a gas chromatograph/mass spectrometer. Measurements of tracers with hourly time resolution and in both the gas- and particle-phases has yielded insights into source apportionment and the processes controlling gas-particle partitioning (Hayes et al., 2013; Liu et al., 2012; Williams et al., 2007, 2010a, 2010b; Zhao et al., 2013a, 2013b).

1.2. Overview of this work

This work seeks to describe ambient oxidation processes through changes in the molecular composition of atmospherically relevant mixtures. Insights learned from the controlled oxidation of known precursors are coupled with tools and techniques developed for the measurement and characterization of complex mixtures. Measurements of relevant compounds are combined with simplified frameworks for describing compounds lacking identification. The characterization of atmospherically relevant mixtures and their compositional changes are used to yield insights into: the increased oxygenation of particles resulting from continued oxidation following SOA formation, the role of molecular structure in particle-phase oxidation rates and subsequent changes to particle composition, the oxidation and partitioning processes of BVOCs in ambient environments, and the influence of anthropogenic emissions on aerosol formation.

Considering all sources of complexity, the atmosphere is a constantly evolving mixture of thousands of compounds in multiple phases (gas, particle, possible aqueous), from various sources (anthropogenic, biogenic), with various functionalities and structures. It is too complex to fully speciate, but a bulk description is insufficient to fully understand the available oxidation pathways and products. The central goal of this work is therefore to describe atmospherically relevant biogenic, anthropogenic, and ambient particles and gases in terms that are neither too broad to elucidate oxidative transformations nor require explicit identification of all components, and still maintain unambiguous identification of tracers when possible. This is achieved primarily through novel applications and advancements in GC/MS techniques. In Chapters 2 through 4, simplified descriptive frameworks are used to fully characterize particle-phase biogenic (Chapter 2) and anthropogenic (Chapters 3 and 4) mixtures and follow chemical transformations as they are oxidized under controlled, atmospherically relevant conditions. Extension of these frameworks and methods to ambient particles and gases is made possible through several instrument developments detailed in Chapters 5 and 6. Finally, in situ collection and examination of atmospheric samples in Chapter 7 demonstrates the utility of comprehensive chromatographic analyses as well as tracers in elucidating sources and partitioning of gases and aerosols.

While BVOC oxidation has been extensively studied, the products are typically described by bulk properties without chemically specific identification of components. In Chapter 2, the ozonolysis of a sesquiterpene, longifolene, is studied using hourly GC×GC analysis with a TAG instrument. From a single precursor, 154 unique products are observed, but only one or two are identifiable from published libraries of spectra. Empirical classification of unidentified compounds by volatility and polarity is achieved using GC×GC separation to identify groups of compounds with similar chemical properties and functionalities. Continued oxidation was found to increase the number of more polar and less volatile compounds, though total particle mass remained stable throughout the experiment. This work establishes a means to describe biogenic mixtures in a simplified framework not with abstract bulk chemical properties, but as ensembles of individual compounds. In this way, chemical transformations can be studied as the consumption and production of molecules with known properties, and in some cases known identities, to yield detailed understanding of the oxidation processes. While Chapter 2 includes some chemical insights into sesquiterpene ozonolysis, comprehensive description of the products was stymied by an inability to identify most compounds and the limitations of GC in the analysis of polar compounds. Techniques developed in later chapters seek to alleviate these difficulties in future analyses.

While biogenic emissions start relatively well-constrained and progress toward overwhelming chemical variety through atmospheric processing, anthropogenic environmental contaminants typically start as hundreds of hydrocarbon compounds that are subsequently oxidized to form dozens or hundreds of products each. Atmospherically relevant anthropogenic organic emissions are examined through the characterization (Chapter 3) and oxidation (Chapter 4) of motor oil, which has subsequently been shown to be an excellent surrogate for vehicular emissions of primary particulate matter (Worton et al., 2014). Using gas chromatography coupled to an advanced mass spectrometric technique to separate isomers and resolve molecular weights of components, anthropogenic mixtures are classified by molecular structure, including carbon number, branching, cyclization, and the presence of oxygen. The laboratory oxidation of one such mixture provides a better understanding of the role of molecular structure in chemical processes. Surprisingly, the relative oxidation rates of various isomers undergoing particle-phase oxidation are found in Chapter 4 to be significantly different than is predicted for gas-phase chemistry. This difference, and the influence of structure on oxidation chemistry and has since been confirmed in other work (Ruehl et al., 2013) and has been shown to affect the particle composition of ambient aerosol (Chan et al., 2013).

Chapters 2 through 4 discuss insights in the composition and oxidation of biogenic and anthropogenic mixtures. In ambient aerosol these sources come together and interact, so the latter half of this work (Chapter 5 through 7) strives to apply the above tools and knowledge to real environments to yield a complete description of the tracers and chemical characterization of the atmosphere. Significant instrument advances are therefore described in Chapters 5 and 6 to extend the utility of this in situ instrument into the range of chemical properties most commonly observed in the atmosphere. This is necessary because the oxygen-to-carbon ratio of the compounds, as well as the bulk average of most organic aerosols, is beyond that measurable by simple GC methods or therefore by previous versions of TAG (or SV-TAG).

A system of injecting isotopically labeled compounds onto every SV-TAG sample, dubbed the "AutoInject" is detailed in Chapter 5. This advancement significantly improves the quantification capabilities of the TAG system by providing a means to account for point-by-point variability in sample losses and mass spectrometer sensitivity. Robust correction of instrument fluctuations allows for more complex sampling and analysis techniques, such as the introduction of in situ derivatization. Due to interactions between OH groups and GC columns, analysis of highly polar compounds is only possible through "derivatization", in which polar functional groups are replaced with less polar analogues via chemical reaction with a derivatizing agent. Chapter 6 describes the implementation of derivatization into the SV-TAG instrument using a reagent that converts all OH groups into silyl ethers and esters for subsequent analysis by GC. SV-TAG utilizes one-dimensional GC, so does not include separating by polarity to help characterize unknown compounds. However, derivatization provides an additional means to classify compounds in gases and particles by definitively highlighting the presence of OH groups, which is expected to have a strong impact on the solubility, hygroscopicity, and oxidation pathways of a compound. Also included in Chapter 6 is the addition of a second sample collection cell for the simultaneous parallel collection of total gas-plus-particle organic compounds and particle-only organic compounds. These advancements open the door for hourly quantification of the concentration and gas-particle partitioning of nearly any semi- or non-volatile component of the complex mixture of organics in atmosphere.

In Chapter 7, tracers that previously could be quantified only from filter extraction are quantified with hourly time-resolution at two different rural field sites (southeastern U.S., and rural Amazonia, Brazil). Quantification of tracers for the oxidation of isoprene, the most ubiquitous BVOC, show that SOA formation from this compound is primarily dependent on levels of sulfate, providing a strong potential pathway for anthropogenic enhancement of biogenic SOA formation. While these identified tracers yield detailed understanding of various atmospheric reactions, the previous chapters demonstrate that the importance and utility of the hundreds of other present compounds cannot be understated. Work remains to fully characterize ambient aerosols and apply the techniques described in previous chapters, but significant progress has been made by combining mass spectral data with chromatographic separation to yield relevant chemical information about otherwise unknown compounds. The processes governing gas-particle partitioning are explored through known tracers, which provide explicit chemical understanding of specific pathways, as well as a combination of 65 biogenic oxidation products study the chemistry in a broader context. Temporal variability in the gas-particle partitioning of known tracers suggests that partitioning does not occur primarily through thermodynamic equilibrium. This conclusion is supported by the complete lack of correlation between estimated volatility and particle fraction of all measured compounds. However, the fraction in the particle also does not strongly correlate with environmental factors or particle properties, suggesting that condensation and re-volatilization is governed by a complex interaction between aqueous-phase chemistry, thermodynamic equilibrium, particle-phase reactions, and gas-phase loss processes. In addition to the importance of sulfate and the quantification of gas-particle partitioning, the relative compositions and chemistries of the two field sites are explored.

Chapter 2

Understanding evolution of product composition and volatility distribution through in situ GC×GC analysis: a case study of longifolene ozonolysis

Adapted from:

Isaacman, G., Worton, D. R., Kreisberg, N. M., Hennigan, C. J., Teng, A. P., Hering, S. V., Robinson, A. L., Donahue, N. M., and Goldstein, A. H.: Understanding evolution of product composition and volatility distribution through in-situ GC × GC analysis: a case study of longifolene ozonolysis. Atmospheric Chemistry and Physics, 11, 5335-5346. 2011.

Abstract

A method for predicting volatility and polarity based on chromatographic information was developed and applied to the smog chamber ozonolysis of the sesquiterpene longifolene. The products were collected and analyzed using a GC×GC Thermal Desorption Aerosol Gas Chromatograph/Mass Spectrometer (2D-TAG) and a quadrupole Aerodyne Aerosol Mass Spectrometer (AMS). All the secondary organic aerosol (SOA) was produced within the first half hour of the experiment. However, the oxidation level of the organic aerosol, as inferred from the fraction of ion *m/z* 44, suggested continued evolution of the SOA over the subsequent hours. Measurements of speciated organic compounds using 2D-TAG confirm that the composition of the particles changed over the course of the experiment. Nearly 200 oxidation products (thought to be mostly ketones and acids) were observed with 2D-TAG, but most could not be identified definitively due to a lack of standards and the absence of likely sesquiterpene oxidation products in available mass spectral databases. To categorize the observed products, the vapor pressure and oxygen-to-carbon ratio (O/C) of observed compounds were estimated based on their two-dimensional chromatographic retention times relative to those of known standards, establishing a retention time correlation (RTC) method for using 2D-TAG to better constrain important modelling parameters. The product distribution continuously evolved in volatility and oxygenation during 5 hours of oxidation. Using peak area as the best available proxy for mass, we conclude that the product mixture includes many non-negligible products; the most abundant 3 compounds accounted for only half of the total observed peak area and 80% of peak area was spread across 15 compounds. The data provide evidence for three conclusions: 1) 2D-TAG provides valuable volatility and oxygenation information even in the absence of definitive species identification, 2) complex particle-phase chemistry causes continued evolution of particle composition after new particles formation, and 3) minor products contribute significantly to SOA from the ozonolysis of longifolene.

2.1. Introduction

Recent findings have shown that on the order of 100 TgC/year of sesquiterpenes may be emitted globally, accounting for approximately 10% of the global VOC budget (Ormeño et al., 2010). However, oxidation products of many BVOCs, such as sesquiterpenes, likely remain unmeasured due to analytical constraints such as relatively low volatility and high reactivity, but must contribute to SOA (Goldstein and Galbally, 2007). Sesquiterpenes tend to have much higher SOA yields (typically ~70% or higher) than monoterpenes (mostly under 40%) (Lee et al., 2006a; Lee et al., 2006b; Ng et al., 2007) because of their high molecular mass and low-volatility and have been shown to nucleate new particle growth far more efficiently than monoterpenes (Bonn and Moortgat, 2003). These findings taken together suggest sesquiterpenes are likely significant precursors of OA and warrant further study.

Many smog chamber studies have focused on the products of sesquiterpene and monoterpene ozonolysis (Bonn and Moortgat 2002; Bonn and Moortgat 2003; Donahue et al. 2005; Lee et al. 2006a; Zhang et al. 2006; Donahue et al. 2007; Maksymiuk et al. 2009) but due to instrument limitations, compound specific analysis of the particle phase is infrequently conducted. Studies that have identified individual compounds in the particle phase (Claeys et al., 2009; Gao et al., 2004a; Jaoui et al., 2008; Surratt et al., 2008; Winterhalter et al., 2009) rely on filter collection, typically limiting analysis to one sample per experiment. By using the GC×GC Thermal Desorption Aerosol Gas Chromatograph/Time-of-Flight Mass Spectrometer (Worton et al., 2012), this study is the first attempt, that we know of, to understand the change in SOA composition from a single BVOC precursor over time.

Longifolene is one of the dominant sesquiterpenes emitted from ponderosa pine forests (Bouvier-Brown et al., 2009a); it is also emitted in small amounts from agricultural crops (Ormeño et al. 2010). Furthermore, it is a good surrogate compound for the study of sesquiterpene oxidation because, unlike other sesquiterpenes which contain multiple double bonds, it contains only a single exocyclic double bond, potentially simplifying the expected oxidation chemistry and product mixture. As an atmospherically relevant compound with a simpler reaction pathway than other sesquiterpenes, ozonolysis of longifolene is employed in this work as a useful model compound for the study of sesquiterpene oxidation.

Having only one reaction site for ozone, the initial step should be limited to formation of a primary ozonide (POZ) through addition of ozone to longifolene (labeled as species "**1**" in Fig. 2.1) across the double bond (Winterhalter et al. 2000; Atkinson and Arey 2003; Nguyen et al. 2009). The POZ then splits to form either longicamphenylone (species "**2**" in Fig. 2.1) or a Criegee Intermediate (CI). In general, POZ decomposition favors the more substituted CI, suggesting the reaction should proceed preferentially down the lower branch in Fig. 2.1. If stabilized, the CI may react with a ketone to yield a variety of secondary ozonides (SOZ) - potentially including a dimer SOZ - that would likely contribute to the nucleation of new particles because of the rapid decrease in volatility accompanying this increase in molecular weight (Bonn et al. 2002). However, the stabilization of the excited CI competes with unimolecular reactions and complex radical chemistry and the branching between these available pathways is a matter of active debate (Chuong et al. 2004). Consequently, the role of SOZs in the SOA formation from BVOCs is still uncertain, though direct measurements of the product mixture composition may be a valuable tool in understanding the mechanisms.

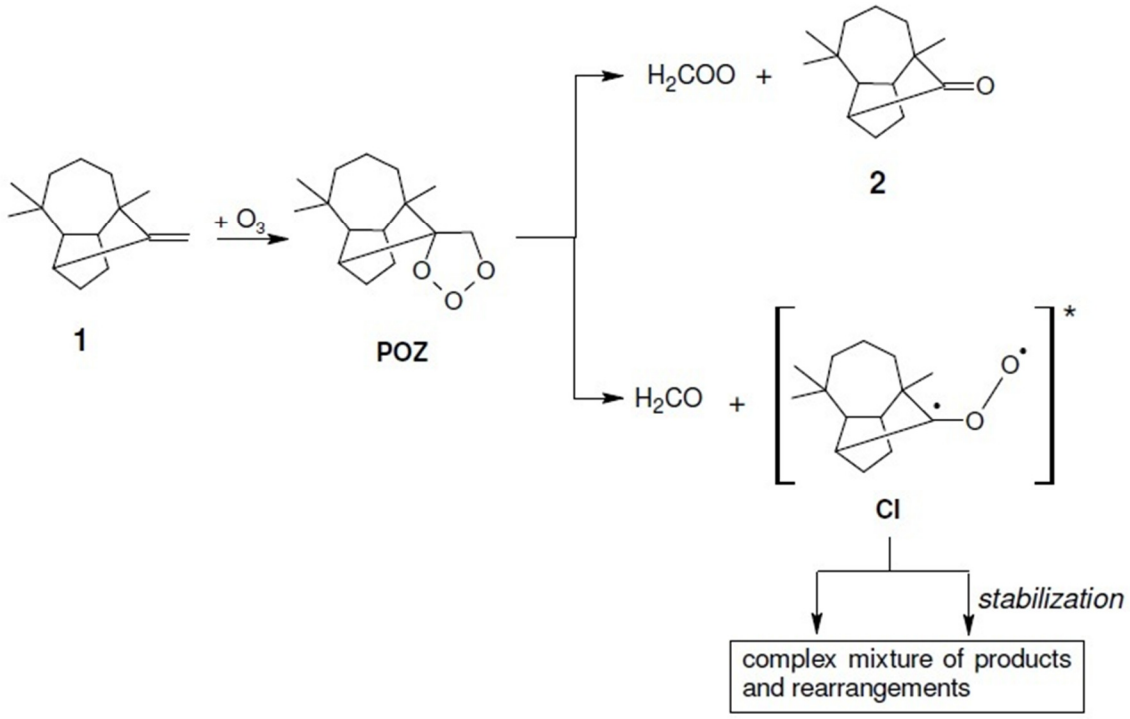

Figure 2.1. Theoretical initial ozonolysis reaction pathway for longifolene (**1**) based on work on β-pinene by Nguyen et al. (2009).

An excellent and extensive modeling treatment of β-pinene ozonolysis, a monoterpene containing a bridge and a single exocyclic double bond, like longifolene, can be found in Nguyen et al. (2009). The ketone formation pathway leading to compound **2** in Fig. 2.1 is expected in 5 - 20% yield in the oxidation β-pinene and is therefore likely to have a similar yield in the longifolene system (Winterhalter et al. 2000; Nguyen et al. 2009). A similar yield of the ketone product is seen for the exocyclic double bond in limonene ozonolysis (Maksymiuk et al., 2009). This reaction pathway proceeds to generate a very complex mixture of products, with at least 7 stable products identified by Nguyen et al. (2009). Aumont et al. (2005) estimate that a C_{15} alkane may form on the order of 10^{10} to 10^{11} compounds after only a few generations, though the contribution of most of these to the overall mass balance is likely to be negligibly small.

Owing to the complexity of VOC oxidation, models are typically simplified by binning oxidation products based on volatility in order to assess their potential in SOA formation. In the commonly used "two-product model" (Odum et al., 1996), SOA yields are modeled using two surrogate compounds that reproduce the partitioning behavior of the mixture as measured in a smog chamber; essentially separating a subset of the product mixture into largely gas-phase and largely aerosol-phase products. This has recently been expanded into a multi-product model that includes oligomerization and uses polarity as a parameter in a addition to volatility (Pankow and Barsanti, 2009). A similar model has been developed by Donahue et al. (2006), in which compounds are grouped into multiple volatility bins that span the gas and condensed phases. This "volatility basis set" (VBS) model accounts for changes in gas-particle partitioning through

multiple generations of oxidation by transferring mass between volatility bins. Compound specific identification is unnecessary for these models as long as the volatility distribution of these compounds can be deduced. The VBS model has recently been expanded into a two-dimensional model (2D-VBS) that includes oxygen to carbon ratio (O/C) as a parameter to better understand the thermodynamics and mixing of organic aerosol and to better constrain its atmospheric evolution (Donahue et al., 2010; Jimenez et al., 2009). This allows the thermodynamics and partitioning of these complex mixtures to be modeled in the context of solvent-species interactions (i.e. oxygenated compounds are less likely to condense onto non-oxygenated aerosol). That both of these frameworks – multi-product models and volatility basis sets – have recently been modified to include a polarity parameter is indicative of the role that oxygenation plays in determining partitioning and SOA formation.

The complexity of organic aerosol makes measurement of products and processes difficult even in simpler scenarios such as longifolene ozonolysis. Bulk analysis – such as with an Aerodyne Aerosol Mass Spectrometer (AMS) – provides the total submicron organic-aerosol mass and some information about average chemical properties. This yields significant insight but often does not provide enough detail on volatility distribution for use in the models described above. An alternate approach is to identify and measure a few useful tracer compounds that provide information about sources or processes. This is, in most cases, a "chromatographic approach," which uses liquid or gas chromatography to separate and speciate complex mixtures to find and apply these tracers. It is the approach for which TAG and 2D-TAG were designed; their high time-resolution allows for detailed analysis of tracer correlation and covariance that can be used to determine the various sources of OA (Williams et al. 2010b). However, ambient aerosol contains thousands of compounds, so comprehensive knowledge of the composition is unattainable. Consequently, chromatographic based techniques provide high levels of detail but not enough bulk information to be useful in models. Therefore, neither the bulk approach nor the chromatographic approach can satisfy all the data needs of the new modeling frameworks.

This work seeks to expand the chromatographic methods by empirically binning compounds based on volatility and polarity, even in the absence of compound identification. Chromatography is limited as to its application for bulk analysis because of difficulties in eluting very polar compounds and thermal decomposition of some compounds (e.g., oligomers). Therefore, this work does not attempt a mass balance nor make claims on the full mass-based volatility distribution. Nevertheless, this method provides insight into the complexity of these systems.

This study lays the groundwork for using a chromatographic approach to place complex atmospheric mixtures into the volatility-polarity models discussed above. This is achieved by correlating retention time to chemical properties. Applying this retention time correlation (RTC) method to 2D-TAG data - an instrument with fairly high time resolution - allows the study of complex condensed-phase product mixtures as their distribution in the volatility-polarity plane changes. In this work, the method developed is applied to SOA formed from longifolene ozonolysis in a smog chamber. Polarity and volatility of the products observed are placed qualitatively into the 2D-VBS framework as a demonstration of the utility of the RTC method. The data are then used to investigate the evolution of the products. As 2D-TAG quantitation capabilities improve, RTC may be used to quantitatively inform these models.

2.2. Experimental

2.2.1. Experimental set-up

The experiment was performed in the Carnegie Mellon University smog chamber using a 10 m^3 Teflon reactor (Welch Fluorocarbons). Longifolene (56 ppb, Fluka, purity ≥ 99 %)) was added by flash vaporization. The reaction was carried out under dry conditions (< 10 % RH) at a constant temperature of 20 ° C. The experiment was carried out in the dark with polydisperse seed aerosol, generated by nebulizing 7 mM (0.9 g/L) ammonium sulfate aqueous solution. An excess of ozone (~1600 ppb) produced from an ozone generator (Azco HTU500ACPS) was added one hour after the addition of seed aerosol and was continuously monitored using an ozone analyzer (Dasibi 1008-PC). The relatively high ozone concentration was necessary because of the relatively low reactivity of the exocyclic double bond in longifolene (Atkinson and Arey, 2003; Shu and Atkinson, 1994). The evolution of the resultant aerosol was continuously measured using a scanning mobility particle sizer (SPMS, TSI 3936) and a quadrupole AMS (Q-AMS, Aerodyne Research Inc.). The AMS data were analyzed using the standard fragmentations and batch tables reported by Allan et al. (2004).

Four 'snapshot' samples were collected and analyzed by 2D-TAG for condensed phase speciated organics during the experiment. TAG is a custom built in situ gas chromatograph, originally described by Williams et al. (2006); incorporation of GCxGC separation into TAG (2D-TAG) is described by Goldstein et al. (2008) and Worton et al. (2012). Air is sampled at 9 lpm and the particles are humidified and impacted onto a passivated metal surface in a custom-designed collection and thermal desorption cell. This cell is heated to 300 ^oC under helium flow and the sample analyzed by a gas chromatograph (Agilent 6890) coupled to an electron impact (EI) time-of-flight mass spectrometer (SAI Kronus ToF-MS). During analysis, the subsequent sample is collected, allowing semi-continuous sampling that is only limited by the length of the chromatographic separation program (2 hours in this work).

The TAG sample schedule is shown in Fig. 2.2. TAG #1 was collected 35 minutes after the addition of the seed aerosol and 15 minutes before ozone addition. The other samples (TAG #2, #3 and #4) were collected between 40 – 45, 155 – 170 and 295 – 310 minutes after ozone addition, respectively. The first two samples (TAG #1 and #2) were collected for 10 and 5 minutes (sample size 0.09 m^3 and 0.05 m^3, respectively) and the latter two samples (TAG #3 and #4) for 15 minutes (sample size 0.14 m^3).

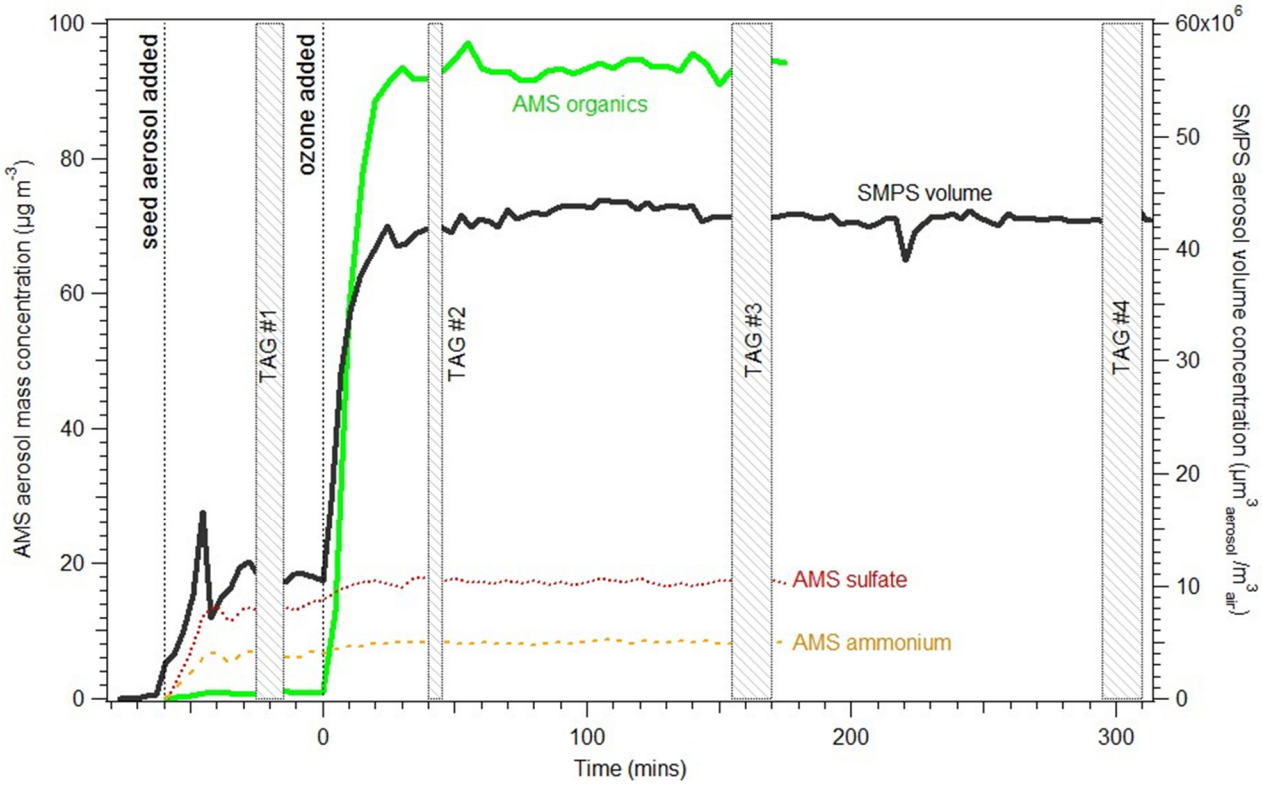

Figure 2.2. Wall-loss corrected aerosol mass and volume concentrations as measured by the AMS and SMPS, respectively.

Collection efficiency is very high for particles larger than approximately 80 nm (Williams et al. 2006). Elution through the chromatographic columns is generally limited to compounds with an O/C of 0.30 or less, though some compounds have been observed by TAG that have an O/C of up to 0.6 (Williams et al. 2010a). Compound identification is performed by comparison of collected EI spectra to the National Institute of Standards and Technology Mass Spectral Library.

2.2.2. Wall loss correction of AMS and SMPS data

Correction for loss of particles to the walls was performed using the extrapolation method published by Pathak et al. (2007). Briefly, wall loss is assumed to be the dominant factor in the change in mass concentration at the end of the experiment, which allows a wall loss rate to be empirically derived and applied throughout the experiment. As wall-loss rates are size dependent (Pierce et al., 2008), the extrapolation method was applied in two ways: 1) calculating and applying size-dependent wall loss rates for each AMS and SMPS size bin, and 2) calculating and applying a single size-independent wall loss rate. However, calculations of the total mass and volume concentrations gave similar results using these two methods, so, for simplification, values shown are calculated using the size-independent wall loss correction method. Though organic vapors are also likely lost to the walls, the resulting suppression of SOA formation is unlikely to occur quickly enough to yield the observed particle mass stability. The complexity of the product mixture observed here may be underpredicted due to vapor loss.

2.2.3. Development of new methodology

Categorizing unidentified compounds can be achieved through comprehensive two-dimensional chromatography, which provides separations based on chemical properties, most commonly volatility and polarity. This empirically maps the distribution of complex mixtures across a two-dimensional space. Consequently, it should be possible to extract from chromatographic data the chemical properties necessary to place compounds in any of the two-dimensional modeling frameworks discussed above.

In order to parameterize volatility and polarity, the two-dimensional chromatographic plane was mapped using a two-dimensional planar fit of O/C and volatility derived from 2D-TAG analysis of known compounds with functionalities similar to those expected from the oxidation of a sesquiterpene (ketones, acids, esters, etc.). Unknown compounds were then assigned an estimated value for these properties based on where they fall in this two-dimensional plane. The columns used by 2D-TAG have been optimized for the separation of atmospheric constituents - the first dimension of 2D-TAG is primarily a volatility separation (Restek Rxi-5ms) while the second dimension separates compounds primarily by polarity (Restek Rtx-200), which is at least partially a function of the O/C (Worton et al., 2012). Therefore the first and second dimension retention times (t_R^1 and t_R^2, respectively), provide information on volatility and oxygenation, thus providing information on chemical properties that are useful for the modeling frameworks discussed above. This retention time correlation (RTC) method is applied here using volatility and polarity separation, but a different column set could be used that separates based on different properties, extending the utility of this method.

We characterized the chromatographic plane by analyzing a standard mixture of 25 known compounds commonly found in ambient aerosols, as well as 10 confidently identified compounds observed in ambient data; these compounds are listed in Appendix A. The vapor pressures, v_P, of these 35 aliphatic compounds with various functionality and known retention times were calculated using the U.S. Environmental Protection Agency Estimation Programs Interface (EPI) Suite (U.S. EPA 2008), which is based on a group contribution method (specifically a modified Grain method, see Lyman (1985) for more details). The calibration compounds include most functionalities commonly observed in atmospheric organic aerosols and were selected to span as much of the 2D-TAG plane as possible given the suite of known standards injected. Using a planar fit to these known compounds (Fig. 2.3a), retention times can be converted into approximate vapor pressures for any aliphatic compound. A similar correlation technique has been used for decades and has been shown in previous studies to be effective within acceptable error using only a single dimension retention time (Hinckley et al., 1990; Jensen and Schall, 1966). In this work we are extending these ideas to include a second dimension. It is clear from the retention times of known compounds that t_R^2 is not entirely independent of vapor pressure in the 2D-TAG system, highlighting the importance of including the second dimension.

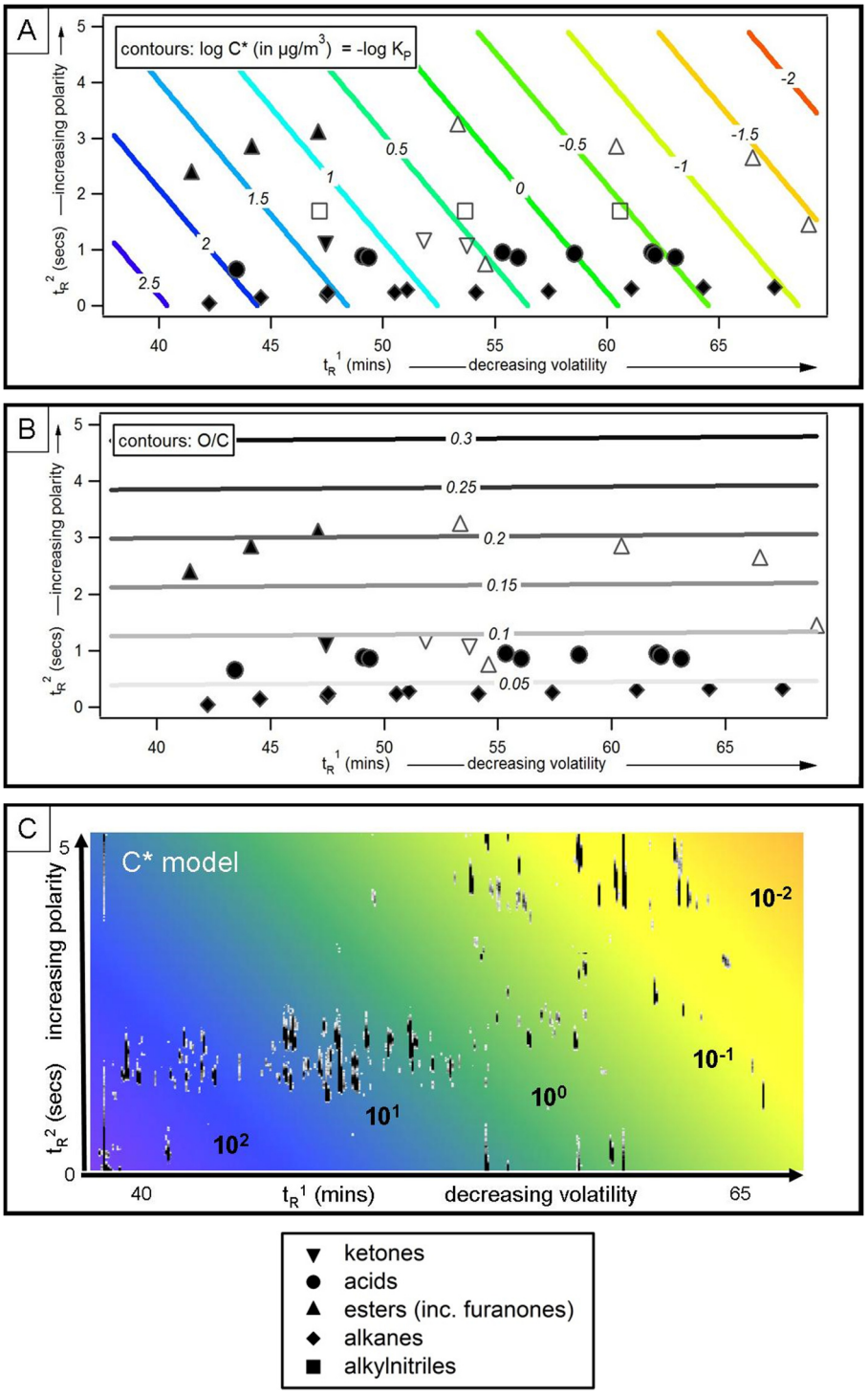

Figure 2.3. (a) Effective saturation concentration C*-fit based on known compounds. (b) O/C-fit based on known compounds. (c) C*-fit applied to TAG #3: color scale matches (a) above. Filled markers are standard compounds, open markers are confidently identified in ambient data. Compounds represent classes relevant to ambient aerosols and are listed in full in Appendix A.

The planar v_P-fit reproduces the vapor pressure of a compound within half an order of magnitude of the calculated value for known compounds, which is within the approximate error of the group contribution methods (Pankow and Asher 2008; U.S. EPA 2008). The EPI method was selected for vapor pressure calculations as it yields a better empirical planar fit than SIMPOL (Pankow and Asher, 2008), the group contribution method used in recent VBS work (Donahue et al., 2010). For more information on the EPI and SIMPOL fits to these compounds, see the Appendix A. Use of one vapor pressure estimation method over another will likely somewhat shift the dependence on t_R^2 but is unlikely to have a significant effect on the results described here. As the use of 2D-TAG increases, more aliphatic compounds in this volatility range will be definitively identified and the fit shown in Fig. 2.3a will be better constrained.

Calculated vapor pressures have been converted to effective saturation concentration, C*, which has been widely adopted by the atmospheric chemistry community and allows data to be placed in the VBS framework (Donahue et al. 2006). The C* of a compound is the aerosol loading (C_{OA}) necessary to cause the condensation of a 50% of the mass of the compound. It is the inverse of the partitioning coefficient, $K_{p,i}$, as defined by Pankow (1994), calculated as:

$$C^* = \frac{1}{K_P} = \frac{MW_i 10^6 \zeta_i v_{P,i}}{760RT} \qquad \text{Eq. 2.1}$$

where MW_i is the molecular weight of species i (g mol^{-1}), ζ_i is an activity coefficient of species i that parameterizes non-ideal behavior of a species, $v_{P,i}$ is the saturation vapor pressure of species i (Torr), R is the ideal gas constant, and T is temperature (K). Because the fit will be applied to unknown compounds, bulk values must be chosen for ζ_i and MW_i. Much of the uncertainty in this calculation comes from ζ_i, which is not well understood and can vary by orders of magnitude depending on species i (Williams et al., 2010a), so as in previous work (Donahue et al., 2006), a value of 1 (pseudo-ideal behavior) is selected here as an approximation. For MW_i, a value of 200 g mol^{-1} is commonly used and is close to the average molecular weight for compounds observed by TAG (Barsanti and Pankow, 2004; Williams et al., 2010a). Though this value is likely 10-20% lower than the actual average molecular weight of aerosol formed by longifolene (MW = 204 g mol^{-1}), this error is small in comparison to uncertainty in ζ_i. Therefore MW_i = 200 g mol^{-1} has been used to be consistent with previous work. The C*-fit allows the partitioning, and therefore the SOA forming potential, of unknown compounds to be inferred using 2D-TAG data.

O/C can be predicted using the same basic approach. A planar fit of O/C as a function of retention time for 32 known compounds (compounds that contain heteroatoms other than oxygen, specifically the three alkylnitriles, are excluded from this fit) shows that O/C is nearly independent of t_R^1 and strongly correlates with t_R^2 in the case of aliphatic compounds (Fig. 2.3b). This O/C-fit allows prediction of the level of oxygenation based on retention times without requiring knowledge of the exact functionality of a given compound - potentially useful information in understanding the age and sources of unknown compounds.

Figure 2.3c shows an example application of the C*-fit to TAG #3 using the same color scale for C* values as Fig. 2.3a. (Figs. 2.3 and 8 are shown using data from TAG #3, when most peaks have been formed but wall loss is less significant than in TAG #4). One challenge is that, to date, no definitively identified aliphatic compounds in 2D-TAG standard or ambient data have t_R^2 values greater than 3 seconds. Therefore, in order to apply the RTC method to all observed peaks, the fit was linearly extrapolated to values of t_R^2 up to 5 seconds. This extrapolation unavoidably increases uncertainty, but relative standard deviation of the slope of this fit - a

measure of the uncertainty in this method - is less than 20% and will be increasingly well-constrained as identification efforts improve and 2D-TAG becomes more widely applied.

Applying both the C*- and O/C-fits derived from the standard mixture allows 2D-TAG data to be placed into the 2D-VBS. The same approach could be used for other proposed two-dimensional spaces such as the ones from Pankow and Barsanti (2009), who propose a number of options for quantifying polarity that may be more precise than a simple O/C. Other measures of polarity can be estimated by deriving appropriate fits to t_R^2, so the RTC method can be used to place aerosol composition into any of the recently proposed volatility-polarity planes that may form the basis of the next generation of model frameworks. Such frameworks cannot yet be quantitatively applied to these data, but ozonolysis of longifolene serves as a qualitative example in which observed peak area is used as the best available proxy for mass.

2.3. Results and discussion

2.3.1. Aerosol concentration and size distribution

Figure 2.2 shows time series of wall loss corrected AMS and SMPS data. The high ozone concentration caused the reaction to proceed quickly; particle formation occurred almost entirely in the first 30 minutes after ozone addition (which occurs at t=0 in all figures). After this rapid formation, the wall loss corrected aerosol mass and volume concentrations as measured by the AMS and SMPS, respectively, remained stable for the remainder of the experiment. The ratio of organics to sulfate from the AMS also remained relatively stable after this initial formation, supporting the conclusion that organic particle formation has ceased. All particle formation therefore occurred before TAG #2 was collected and aerosol mass, once corrected for wall loss, remained unchanged during the subsequent TAG samples (TAG #3 and #4). This allows us to study the evolution of particle composition over approximately five hours.

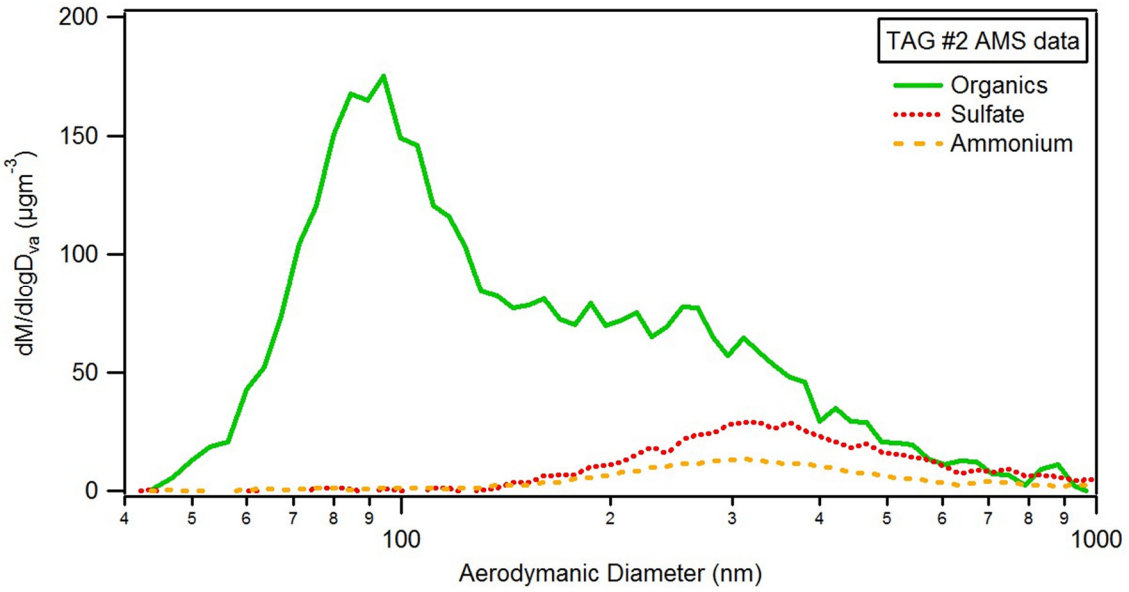

Figure 2.4. Average AMS particle size distribution during TAG #2, collected 40 to 45 minutes after the addition of ozone. These data have not been wall loss corrected in order to avoid artifacts potentially introduced in the correction process.

The size distribution of the aerosol is bimodal and remained largely unchanged after particle formation ends. The size distribution during TAG #2 is shown in Fig. 2.4 without correcting for wall loss to avoid potential size dependent artifacts of the wall loss correction process. The peak in the size distribution at 200-300 nm is expected as organic compounds condense onto the ammonium sulfate seed aerosol, which is mostly in that size range (red and yellow dashed lines in Fig. 2.4). However, the prominent peak at smaller diameters (centered at 90 nm) - where there is no seed aerosol - indicates substantial particle nucleation and growth. This homogenous nucleation of particles by organic compounds requires the rapid production of organic compounds with very low vapor pressures. However, homogenous nucleation may be caused here by the very rapid particle growth caused by the high concentration of ozone and may not be atmospherically relevant.

2.3.2. Evolution of the product mixture

2.3.2.1. Increasing oxidation level

Though particle formation and mass growth reached completion quickly, AMS data show some evidence for the continued evolution of products. The fraction of organic aerosol comprised of ion *m/z* 44 as obtained by the AMS (f_{44}) can be used to estimate the O/C of the aerosol (Aiken et al., 2008) - because *m/z* 44 comes primarily from CO_2^+, high f_{44} is indicative of more oxidized aerosol. Figure 2.5 shows the evolution of f_{44} throughout the period of the experiment for which AMS data are available. When particle formation begins, f_{44} is high due to the partitioning into the particle phase of highly oxygenated, and therefore less volatile, compounds (Kroll and Seinfeld, 2008a). As aerosol loading increases, f_{44} decreases because more volatile, less oxygenated compounds partition into the particle phase (Donahue et al., 2006; Odum et al., 1996). Although production of new particle mass appears to stop after 30 minutes, f_{44} increases throughout the experiment. Particles are lost to the walls as the experiment progresses but are thought to continue to participate in partitioning (Weitkamp et al. 2007), so this slow but continuous increase in f_{44} is unlikely to be entirely an artifact of partitioning, indicating a slow increase in particle oxidation level. Estimated O/C increases from 0.24 about 20 minutes after ozone was added to O/C of 0.30 after three hours of ozone exposure.

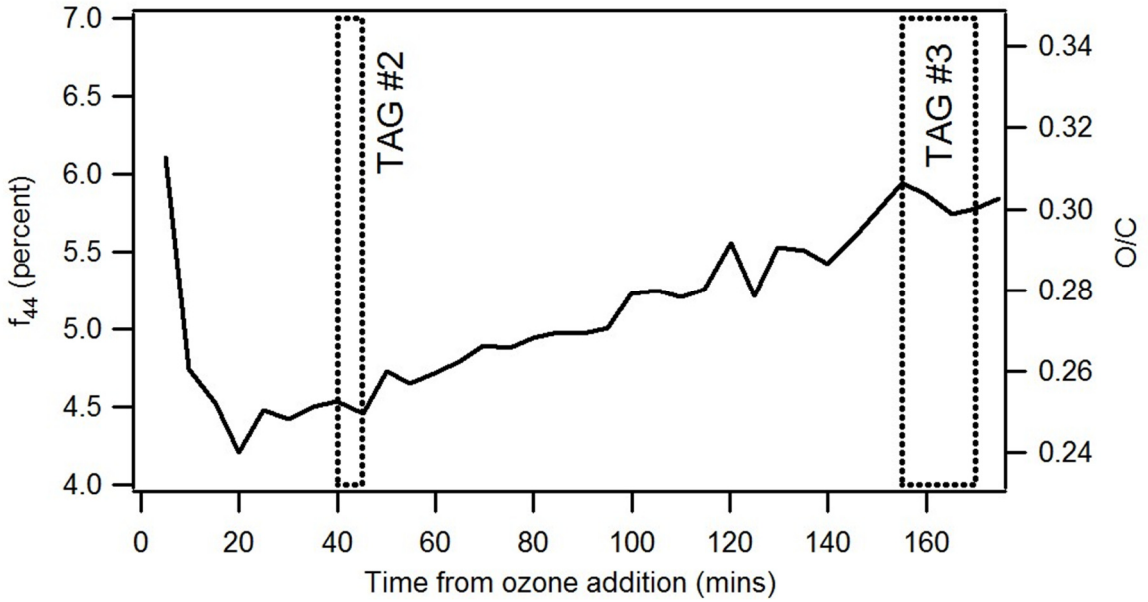

Figure 2.5. Percentage of organic aerosol comprised of *m/z* 44 (f_{44}) over the course of the longifolene ozonolysis. O/C is estimated from this value using the correlation reported by Aiken et al. (2008).

This increase in oxygenation suggests either heterogeneous processing or complex partitioning-oxidation interactions where semi-volatile particle-phase products evaporate, oxidize in the gas-phase, and re-condense. Although the continued oxidation of the condensed phase is common in smog chamber experiments, the oxidant in this case is unclear - the oxidation products of longifolene are not expected to have double bonds that would react with ozone. However, due to the absence of an OH scrubber and the presence of small amounts of water vapor in the chamber, it is possible that some hydroxyl radical chemistry occurs, creating a complex chemical mixture that may continue to oxidize through hydration and/or dehydration reactions. These reaction pathways are speculative, but the continued increase in f_{44} suggests the presence of complex oxidation chemistry, a conclusion supported by increasing complexity and oxygenation of 2D-TAG samples throughout the experiment.

2.3.2.2. Continued functionalization and increasing complexity

Though TAG #2 was collected immediately following particle formation, and TAG #3 and #4 were collected later in the experiment, wall loss corrected aerosol concentrations were stable across all three samples (Fig. 2.2). Owing to the relatively low O/C of the product mixture (< 0.30), most of the particle-phase product should elute through the TAG columns.

Only three likely products of longifolene oxidation are included in available mass spectral libraries, so the vast majority of the observed peaks could not be specifically identified. It was therefore useful to apply the RTC method to categorize and understand the chemical properties of these unidentified products. The C*- and O/C-fits described above were applied to TAG #2, TAG #3, and TAG #4 to provide insight into the chemical and volatility evolution of the condensed phase mixture produced through ozonolysis of longifolene.

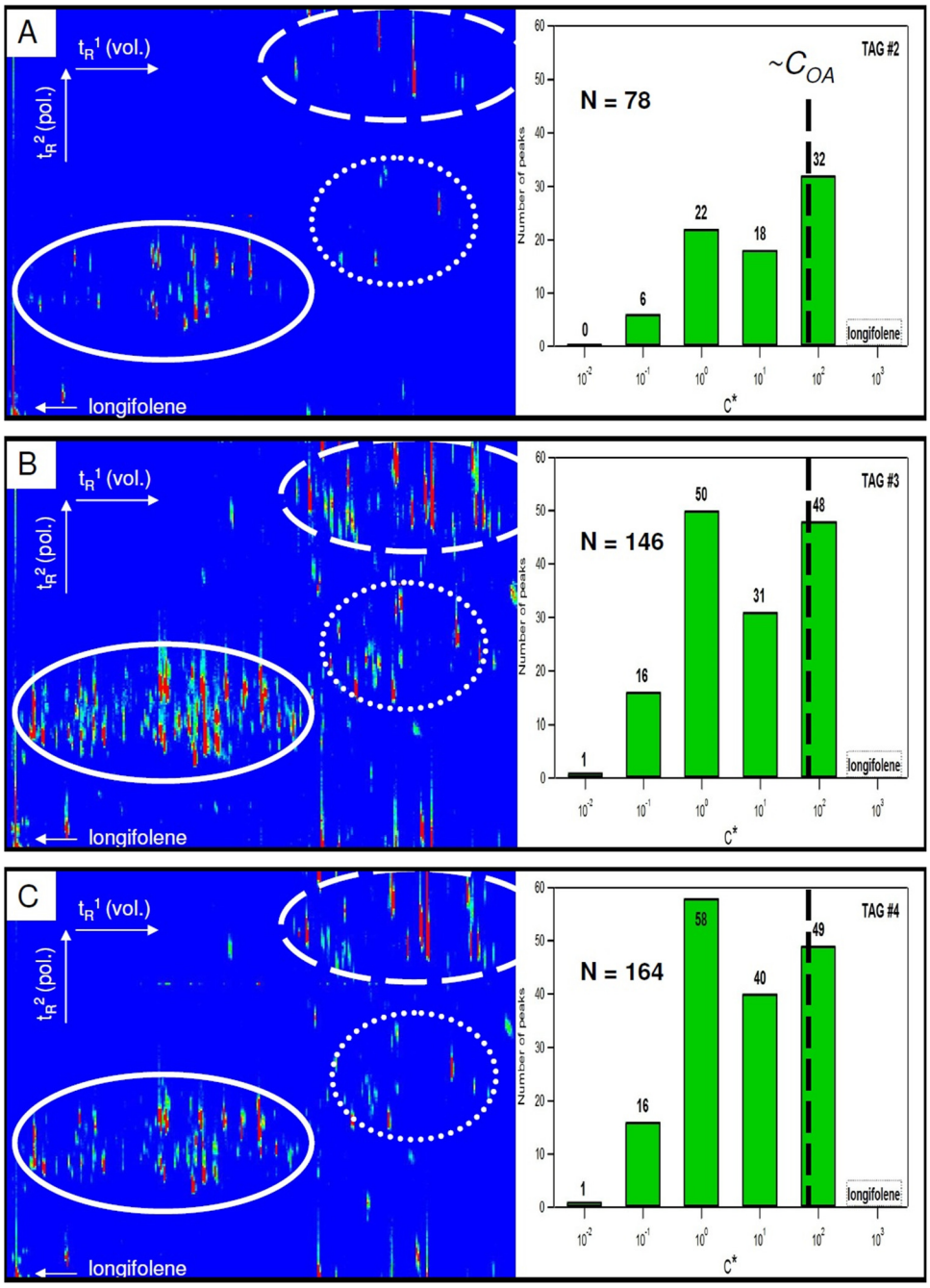

Figure 2.6. GC×GC chromatograms and the number of peaks in each C* bin in samples (a) TAG #2; (b) TAG #3; and (c) TAG #4. The x- and y-axes are t_R^1 (volatility separation) and t_R^2 (polarity separation), respectively, and have the same scale as Fig. 2.3 (approximately 40 to 65 minutes for t_R^1 and 0 to 5 seconds for t_R^2). Color indicates detector response (total ion chromatogram) in arbitrary units (blue is lowest, red is highest). Circled Region 1 (solid line) contains less oxygenated, more volatile compounds while peaks in Regions 2 (dotted line) and 3 (dashed line) are thought to be more oxygenated, less volatile compounds and are discussed in detail in Sect. 2.3.2 of this text. Number of compounds in each C* volatility bin is given on the right along with the total number of observed peaks. Aerosol mass concentration is shown as the line at C_{OA}.

The number of peaks in each volatility bin, as well as the accompanying chromatograms for each snapshot are shown in Fig. 2.6. Any peak in the most volatile C* bin (10^3 μg/m^3) has been neglected because this volatility bin would include compounds not collected by 2D-TAG, making the number of peaks in this bin unknown. In TAG #2, immediately following particle formation, 78 peaks are observed. This increases to 146 peaks in TAG #3 and 164 peaks in TAG #4. The product longicamphenylone (Fig. 2.1, compound **2**), could not be definitively identified though longifolenaldehyde is thought to have been identified.

While the number of peaks grows in every volatility bin between these samples, the overall peak distribution shifts toward less volatile bins over the course of the experiment. For example, in the first sample, TAG #2, most of the products - including the peak thought be longifolenaldehyde - are in the more volatile, less polar Region 1 (Fig. 2.6, solid circle). Based on their location in the two-dimensional plane, these compounds are likely to be the result of single oxygen addition such as ketones or aldehydes. There are a few large peaks, however, in the low volatility, oxygenated Region 3 (Fig. 2.6, dashed circle) that may be the products responsible for homogenous nucleation. Regions 2 (Fig. 2.6, dotted circle) and 3 in this early sample contain relatively few peaks. However, as the experiment progresses, the number of peaks in these regions increases significantly, indicating an aerosol of increasing complexity and increasing oxygenation; peaks in these regions are likely to be products of the addition of multiple oxygen atoms, potentially multi-functional acids or esters formed through multiple generations of oxidation. In addition to a few large peaks, Regions 2 and 3 contain many small peaks that account for only 10 - 20% of the aggregate total peak area because the exponential increase in the number of potential products with each generation distributes the mass over many compounds. It should be noted here that more oxygenated compounds typically exhibit electron impact response factors that are an order of magnitude smaller than those of saturated hydrocarbons, suggesting that using peak area as a proxy underestimates the mass contribution from these compound; the use of peak area in this work is meant for qualitative comparison.

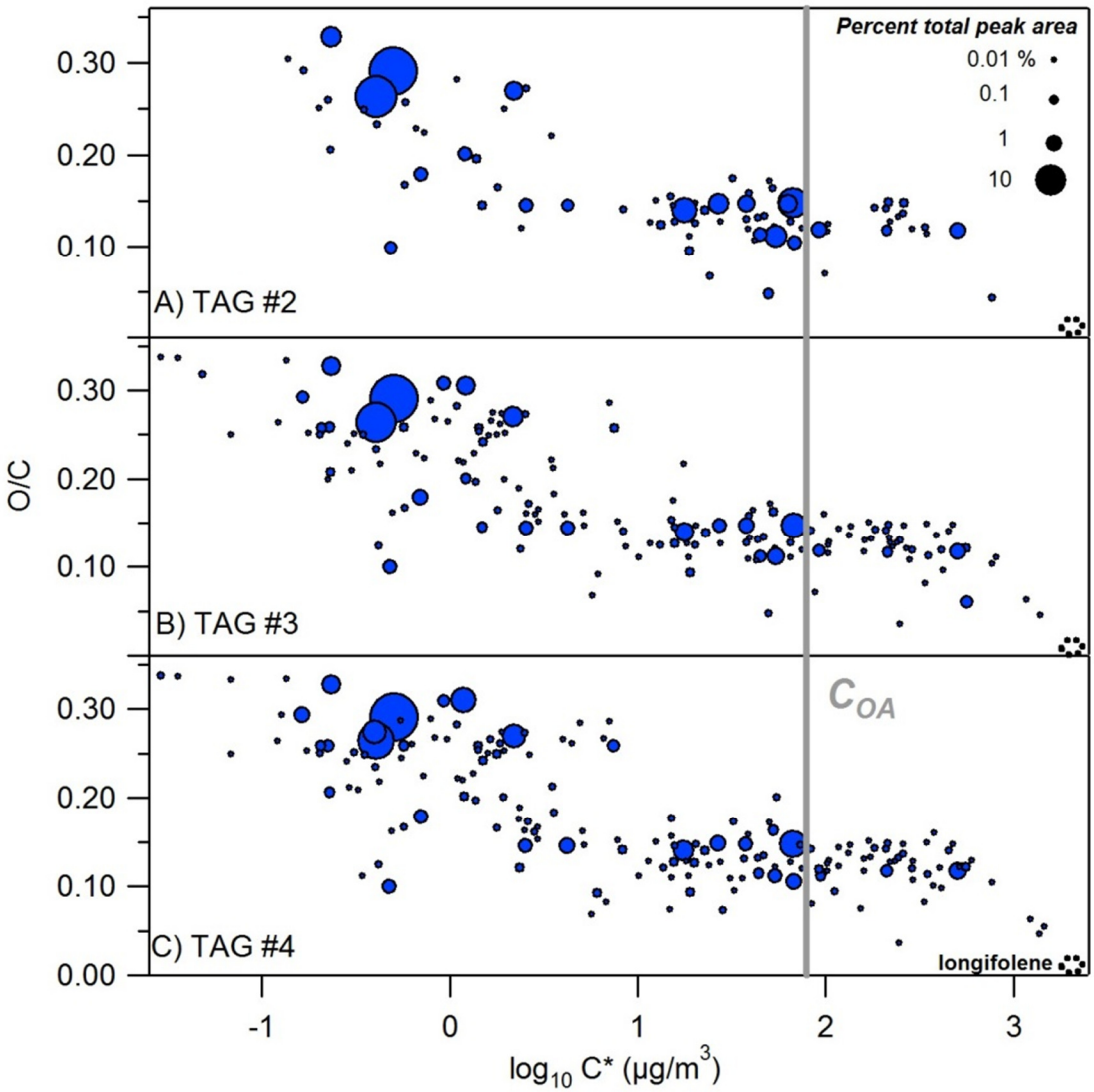

Figure 2.7. Observed peaks in (a) TAG #2, (b) TAG #3, and (c) TAG #4 put into the framework of the two-dimensional volatility basis set (Donahue et al. 2010). O/C and C* are calculated using the RTC method. Marker area is approximately proportional to percent of total peak area for each individual peak. Aerosol mass concentration is shown as the line at C_{OA}.

The distribution of peaks across these regions is shown in the framework of the 2D-VBS in Fig. 2.7. A few large, low-volatility peaks are observed in TAG #2 that are likely the products responsible for homogeneous nucleation, but most of the peaks observed in TAG #2 are in the higher volatility, less oxygenated region. Between TAG #2 and TAG #3, the number of peaks nearly doubles, with many of these new peaks in the regions of lower volatility and increased O/C. This increase in complexity includes the apparent formation of a few larger peaks that each account for a few percent of the total peak area. While the higher volatility, less oxygenated region does change, peaks in this region primarily shrink in relative size and most of the newly formed peaks are negligible. The shift of the peak distribution up (higher O/C) and to the left (lower volatility) in 2D-VBS space suggests continued functionalization throughout the

experiment. Fragmentation of products through gas-phase chemistry likely also occurs but is expected to result mostly in products too volatile to be collected by TAG, and as such were not measured by this instrument.

Average O/C based on peak area increases from 0.21 to 0.23 from TAG #2 to TAG #3. This increase in average O/C and the accompanying shift in peak distribution is consistent with the trend suggested by the evolution of AMS f_{44} shown in Fig. 2.5: that oxidation and aging continue during the period of stable aerosol concentration. Average O/C calculated using the RTC method is expected to be lower than that determined using AMS f_{44} because of low response factors to oxygenated compounds. However, approximately half of the peak area as well as the largest peaks in all samples fall within the AMS f_{44} O/C range of 0.24 to 0.30, and average RTC O/C is only 15-25% less than estimated by AMS f_{44}, suggesting that O/C values calculated using the RTC method are reasonable. In addition, the similarity between the average O/C values estimated by both RTC (0.21 to 0.23) and AMS (0.24 to 0.30) supports the conclusion that 2D-TAG is indeed eluting a representative sample of the aerosol and can therefore be used to provide meaningful information about the bulk product mixture. Toward the end of the experiment, the level of oxidation appears to be relatively stable; average RTC O/C is unchanged and the number and distribution of the peaks does not change as dramatically between TAG #3 and TAG #4 as it did from TAG #2 to TAG#3, though some peaks may have dropped below detection limits as a majority of aerosol has been lost to the walls by the end of the experiment.

Though many of the observed peaks are small, the aggregated area of minor peaks accounts for a non-negligible fraction of the total observed peak area. The number of observed compounds necessary to understand the detected product mixture (Fig. 2.8 - shown using TAG#3) is approximately logarithmic, with 3 peaks accounting for 50% of total peak area and 15 peaks accounting for 80% of total peak area. In other words, while 12 peaks are minor - on average each accounting for less the 3% of total peak area - together they account for nearly a third of observed peak area. Peak area can be thought of as a proxy for mass that eluted through the column (i.e. Ozel et al. 2010), but it is an imperfect measure as discussed above. Nevertheless, Fig. 2.8 suggests that the product mixture contains many significant products and likely cannot be well-described with only one or two compounds. The number of major peaks observed here is approximately of the same order as the number of first and second generation products predicted by Nguyen et al. (2009).

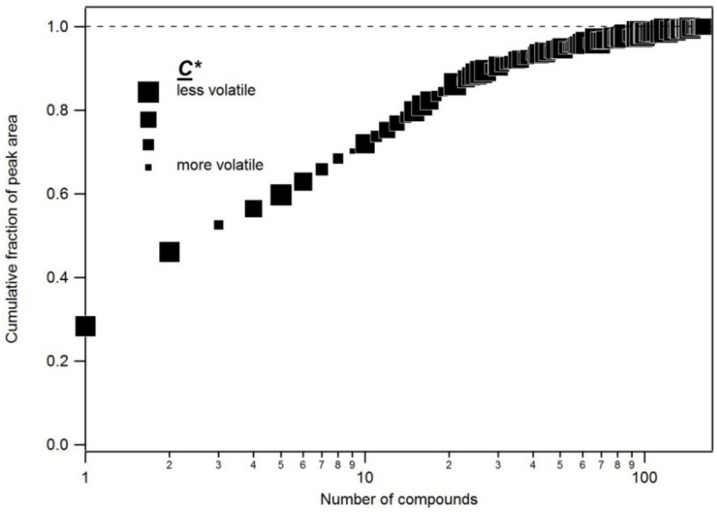

Figure 2.8. Number of compounds required to account for a given fraction of total peak area. Data from the TAG #3 sample. Marker area is approximately proportional to volatility for each individual peak.

2.4. Summary and Conclusions

A retention time correlation (RTC) method was developed to estimate C* volatility and degree of oxygenation (O/C) of complex mixtures from first and second dimension retention times obtained from the 2D-TAG. This method was applied to the ozonolysis of longifolene performed in a smog chamber in the presence of 1600 ppb ozone. In this experiment, O/C values estimated from AMS f_{44} never exceed 0.30 and are similar to those calculated using RTC, suggesting that 2D-TAG collected a representative sample of the aerosol and can therefore be used in conjunction with the AMS to provide some understanding of chemical evolution.

AMS and SMPS data show that under the conditions of these experiments, particle formation proceeded by fast, homogenous nucleation followed by slow continuous oxidation of the particle phase organics, with no further increase in aerosol mass or volume concentration after 30 minutes of ozonolysis. The continued oxidation inferred from AMS f_{44} suggests that atmospheric processing is more complex than simple condensation of oxidized VOCs; either particle-phase oxidation occurs or compounds partition in and out of the particle phase while undergoing oxidation. Samples collected by 2D-TAG during the experiment show an increase in the number of less volatile, more oxygenated products with time, further supporting the conclusion that continued oxidation is not limited to simple gas phase chemistry. Because of the difficulty in definitively identifying most compounds, as well as the complexity of the potential chemistry, the possible pathways for this continued oxidation are unknown, but the increase in f_{44}, corroborated by increases in O/C observed by 2D-TAG suggest it is a real phenomenon that warrants further study.

Nearly 200 peaks were observed by 2D-TAG, a small fraction of the number of potential products generated by comprehensive models (Aumont et al. 2005). The product mixture contained many non-negligible products (between 3 and 15). The major expected product of this reaction, longicamphenylone was not observed in the product mixture, though longifolenaldehyde was.

Studying the evolution of the products in the volatility-polarity plane allows SOA precursors to be categorized not only by SOA yield, as is now common practice, but also by the product mixture volatility distribution. By using an O/C-fit as well as volatility-fit, this work allows more realistic modeling of aerosol formation using either a multi-product model or the 2D-VBS framework. Currently this method is limited to systems with levels of oxygenation lower than is observed in most ambient environments, such as sesquiterpene or monoterpene smog chamber ozonolysis; chamber experiments generate aerosol with levels of oxidation similar to semi-volatile oxygenated organic aerosol (SV-OOA), while more oxygenated low-volatility OOA (LV-OOA) is observed to be a significant factor in ambient aerosol (Jimenez et al. 2009). The study of this transition from SV-OOA to LV-OOA is consequently difficult in laboratory settings. However, 2D-TAG is useful for studying the first few generations of VOC oxidation and the subsequent evolution of the OA, providing an opportunity to understand the aging and processing of SV-OOA. Analysis using the RTC method and 2D-TAG can therefore be used to inform models and improve understanding of the SV-OOA to LV-OOA transition. Future work expanding the O/C range of gas chromatography through use of derivatizing agents may also broaden the applicability of this method for use on LV-OOA and ambient systems.

The RTC method does not yet work well for a mixture of aromatic and aliphatic compounds. Aromatic compounds are retained longer in the second dimension than aliphatic compounds of similar calculated volatility and O/C (Worton et al., 2012) and therefore exhibit a different dependence on t_R^2 in these fits. This necessitates a different planar fit for each class of compounds; in order to properly apply this method, the user must know whether a compound is aliphatic or aromatic and use the appropriate calculated fit. While this is easily tractable in the case study examined here (controlled BVOC oxidation in the absence of any aromatic compounds), it does complicate the application of this method to ambient data. However, as EI spectra tend to have very different character for aromatic and aliphatic compounds, it is likely possible to extend the method described here to a variety of systems - even complex ambient aerosol - by including some mass spectral information.

The bimodal size distribution of the aerosol warrants further study as it may be due to the formation of SOZs. These compounds would likely be too thermally unstable to be observed by thermal desorption coupled to gas chromatography, so its presence can be neither confirmed nor denied by this study, but these data suggest a further need for novel methods of direct measurements such as those employed in this study. Direct measurements of these low volatility first generation products would greatly improve understanding of nucleation in remote forested environments.

2.5. Acknowledgements

This work was supported by the US Department of Energy STTR program, DEFG02-05ER-86235 and the National Science Foundation Atmospheric Chemistry Program Grants 0922562 and 0931934. GI was funded by the US EPA Science to Achieve Results (STAR) program, FP-91781901-0.

Chapter 3

Improved resolution of hydrocarbon structures and constitutional isomers in complex mixtures using Gas Chromatography-Vacuum Ultraviolet-Mass Spectrometry (GC-VUV-MS)

Adapted from:

Isaacman, G., Wilson, K. R., Chan, A. W. H., Worton, D. R., Kimmel, J. R., Nah, T., Hohaus, T., Gonin, M., Kroll, J. H., Worsnop, D. R., and Goldstein, A. H.. Improved resolution of hydrocarbon structures and constitutional isomers in complex mixtures using Gas Chromatography-Vacuum Ultraviolet-Mass Spectrometry (GC-VUV-MS). Analytical Chemistry, 84, 2335-2342. 2012.

Abstract

Understanding the composition of complex hydrocarbon mixtures is important for environmental studies in a variety of fields, but many prevalent compounds cannot be confidently identified using traditional gas chromatography-mass spectrometry (GC-MS) techniques. This work uses vacuum-ultraviolet (VUV) ionization to elucidate the structures of a traditionally "unresolved complex mixture" by separating components by GC retention time, t_R, and mass-to-charge ratio, *m/z*, which are used to determine carbon number, N_C, and the number of rings and double bonds, N_{DBE}. Constitutional isomers are resolved based on t_R, enabling the most complete quantitative analysis to date of structural isomers in an environmentally-relevant hydrocarbon mixture. Unknown compounds are classified in this work by carbon number, degree of saturation, presence of rings, and degree of branching, providing structural constraints. The capabilities of this analysis are explored using diesel fuel, in which constitutional isomer distribution patterns are shown to be reproducible between carbon numbers and follow predictable rules. Nearly half of the aliphatic hydrocarbon mass is shown to be branched, suggesting branching is more important in diesel fuel than previously shown. The classification of unknown hydrocarbons and the resolution of constitutional isomers significantly improves resolution capabilities for any complex hydrocarbon mixture.

3.1. Introduction

Chemical analyses of environmental contamination often rely on chemical speciation of complex organic mixtures. Quantifying known tracer compounds in these environments can provide insight into biological and chemical degradation processes(Megharaj et al., 2011; Simoneit, 2005) and contaminant sources (Fraser and Lakshmanan, 2000; Mazurek, 2002; Schauer et al., 1996; Williams et al., 2010b). Over the past few decades, a variety of liquid and gas

chromatography (LC and GC) techniques have been used with great success to improve understanding of pollutants as well as transformations in intricate natural systems. One of the newest promising techniques is vacuum ultraviolet (VUV) single-photon ionization mass spectrometry (SPI-MS) (Eschner et al., 2010; Hanley and Zimmermann, 2009).

Traditional GC-MS employs electron impact (EI) ionization, where a molecule is ionized by an electron at an energy near the peak of ionization efficiency (usually 70 eV). This technique is broadly applicable, as nearly all organic compounds can be ionized at this energy, and generation of electrons is easily achieved using a filament in a vacuum chamber. However, because the ionization energy (IE) of most large organic compounds lies below 11 eV (Sieck, 1983), EI imparts considerable excess energy to the ionized molecule, causing dissociation into smaller fragment ions. For EI-MS analysis of pure compounds, parent ions are sometimes visible and/or the fragmentation pattern can be used to deduce molecular structure, but because EI of different organic compounds often yields similar fragment ions, interpretation of EI-MS of organic mixtures can be ambiguous. Alternatively, by using photons with energy of 11 eV or less, organic compounds can be ionized with minimal excess internal energy and therefore fragmentation, thus facilitating the identification of a compound by its molecular formula. This "soft" ionization is achieved in SPI-MS with ultraviolet photons in a vacuum (hence "vacuum-ultraviolet", or VUV) generated by a laser (Adam and Zimmermann, 2007), excitation of a rare gas (Zimmermann et al., 2008), or, in the case of this work, synchrotron radiation (Mysak et al., 2005). Soft ionization mass spectrometry has proven to be a valuable tool for analysis of complex mixtures because parent ions can be used for identification. For this reason, GC-VUV-MS analysis is being applied to a wide array of environmental and public health fields (Hanley and Zimmermann, 2009).

Chromatography of many environmental samples yields a large "unresolved complex mixture" that has yet to be well quantified or described. This is because aliphatic hydrocarbons, a significant source of environmental contamination, fragment heavily upon EI ionization, yielding many smaller fragments that are indistinguishable. Consequently large straight-chain alkanes do not yield significantly different mass spectra nor are they distinguishable from branched isomers. Though there is a small parent ion contribution to the mass spectra of many *n*-alkanes, it is not typically large enough to be used for unambiguous identification in a complex mixture. This parent ion is even smaller for branched alkanes, significantly hindering identification of branched hydrocarbons using EI ionization, though such compounds are common in environmental samples. To address co-elution of compounds, gas chromatography can be coupled with a second gas chromatographic separation based on polarity (GCxGC), providing better separation and identification of compound classes in many environmentally-relevant mixtures.(Hamilton, 2010; Schnelle-Kreis et al., 2005) Though useful, this technique typically does not significantly improve resolution of the aliphatic unresolved complex mixture because aliphatic hydrocarbons are not well-retained on the second column (demonstrated by figures in Schnelle-Kreis et al. (2005), Hamilton (2010) and Worton et al. (2012))). However, VUV ionization allows improved identification of hydrocarbons because branched and straight-chain hydrocarbons both display a significant parent ion peak in photoionization mass spectra (see examples in Appendix B). This work uses the capabilities of GC-VUV-MS to develop methods for resolving the "unresolved complex mixture" by classifying compounds according to molecular mass and structure, including separation of structural isomers.

Applications of GC-VUV-MS analyses have often focused on petroleum fuels as sample organic mixtures (Adam and Zimmermann, 2007; Eschner et al., 2010; Geissler et al., 2009; Hanley and Zimmermann, 2009; Mitschke et al., 2006) because of their environmental importance and daunting complexity. Diesel fuel serves as a useful example for typical pollution while its complexity provides an additional test of the resolution and capabilities of a separation technique. Diesel has also been analyzed in great detail using traditional GC-EI-MS techniques (Schauer et al., 1999b), which is useful in comparing results from traditional methods to VUV ionization techniques.

GC-VUV-MS allows separation in the two-dimensional plane of chromatographic retention time (t_R, typically a function of volatility) and ion mass-to-charge ratio (*m/z*). Previous work (Eschner et al., 2010; Geissler et al., 2009) has effectively used this GCxMS plane to identify classes of compounds in complex mixtures by parent ion. Using this method, the volatility distribution of petroleum fuels was shown to approximately agree with GC-MS analysis of diesel fuel (Schauer et al., 1999b), consisting primarily of saturated aliphatic hydrocarbons and polycyclic aromatic hydrocarbons (PAHs). However, the dependence of retention time on chemical structure allows GCxMS analysis to separate not only classes of compounds, but also many isomers. While this has been shown previously (Mitschke et al., 2006), no attempt has been made to explore this capability in depth or determine the structures of unknown compounds. Owing to the limitations of GC-EI-MS in resolving complex hydrocarbon mixtures, only the most dominant branched hydrocarbons, such as pristane and phytane in diesel fuel, have been able to be quantified in past work (Schauer et al., 1999b). Therefore, no complete picture of isomer content of petroleum mixtures is currently available. Isomer separation is a potentially important step forward in understanding fates of fossil fuel contaminants in the environment because structure of a compound strongly affects degradation and oxidation pathways (Kroll and Seinfeld, 2008b; Lim and Ziemann, 2009), which has implications for applications ranging from bioremediation to atmospheric aerosol modeling, as well as providing insights into chemical ecology such as insect interactions (Blomquist and Bagneres, 2010; Martin et al., 2011; van Wilgenburg et al., 2010; Youngsteadt et al., 2010).

Using GC-VUV-MS, we improve the identification of typically unresolved compounds in complex hydrocarbon mixtures and demonstrate the quantitative resolution of structural isomers. Determination of carbon number, compound class, and branching provides structural information about any unknown compound in a mixture. These concepts are shown in the context of diesel fuel, as it is a useful surrogate for many environmental systems, but are intended to be applicable for a wide variety of systems. Distribution of isomers in a diesel sample is shown to be more predictable and constrained than might be expected by the number of potential isomers.

3.2. Experimental

3.2.1. Instrumentation

Samples and standards were analyzed by a GC (6890 Series, Agilent) coupled to a time-of-flight mass spectrometer (TOFMS; HTOF model, Tofwerk). Helium (with splitless flow) was used as a GC carrier gas, with a temperature ramp of 15 ^{o}C per minute from 80 to 320 ^{o}C. The effluent from the GC column (Rxi-5ms, 30 m x 0.25 mm x 0.25 μm, Restek Corporation) entered the TOFMS ionization chamber at vacuum. Molecules in this gas stream were then ionized either by electron impact (EI) ionization using an internal filament or vacuum-ultraviolet (VUV)

photoionization at the Chemical Dynamics Beamline of the Advanced Light Source (ALS) at Lawrence Berkeley National Lab. The photon beam passes through a gas filter and MgF_2 window to remove unwanted undulator harmonics, resulting in photons that are tunable between approximately 8 and 11 eV with a flux of $\sim 10^{15}$ photons/s over the area of a focused spot that is approximately 100 × 200 µm (Heimann et al., 1997). The heated region through which the GC column entered the TOFMS was varied between 150 and 275 °C, as was the temperature of the ionization chamber (see Sect. 3.2.2. below for detailed discussion). The photon beam entered the ionization chamber perpendicular to the column outflow and the EI filament, allowing photoionization without removing the filament.

All standards were purchased from Sigma-Aldrich and AccuStandard. Diesel sample was purchased from AccuStandard. Data analysis was performed using custom processing code written in Igor Pro 6.0.4 (Wavemetrics).

3.2.2. Parameter optimization

Operating conditions can be adjusted by varying temperature and photon energy to minimize fragmentation; lowering these parameters increases the ion fraction observed as the parent ion (f_P) in a mass spectrum by decreasing internal energy (Gloaguen et al., 2006). Experimental conditions were optimized to find a balance between chromatographic separation and minimal fragmentation. This optimization should be performed for all GC-VUV-MS applications and is therefore discussed in Appendix B. A temperature of 150 °C for both the transfer line between the GC and the TOFMS and the ionization chamber in the TOFMS was used in this work as these operating conditions were found to yield little fragmentation without significantly adversely affecting the chromatography in the volatility range of interest. Briefly, fragmentation was observed to be strongly dependent on transfer temperature and not significantly affected by the energy of the ionizing photons (Fig. B.1). However, varying photon energy is an effective means of identifying unresolved compounds by selectively ionizing compounds that differ in ionization energies by more than 0.2 - 0.3 eV, as this is the width of the energy distribution of photons generated at the ALS (Heimann et al., 1997). Photons of 10.5 eV were used for most purposes in this work to ionize all compounds of interest, but photons of 10.0 eV were used to selectively ionize unsaturated hydrocarbons (which have a lower ionization energy (Gloaguen et al., 2006; NIST Mass Spec Data Center S.E. Stein director, 2012)), resolving olefinic and cyclic compounds of identical mass.

3.2.3. Classification by double bond equivalents

In this work, the mass of a given hydrocarbon molecule, i, will be used to classify compounds according to carbon number, N_C, and number of double bonds and rings in their structure, N_{DBE}. Each ring or double bond in the molecule i removes two H atoms compared to the alkane $C_{N_C(i)}H_{2N_C(i)+2}$, reducing the mass of the hydrocarbon, $m(i)$, by twice the mass of hydrogen, $2*m(H)$. $N_C(i)$ can reliably be estimated by the GCxMS characteristics of the molecule as discussed in Sect. 3.3.2. The mass of the alkane therefore equals $m\left(C_{N_C(i)}H_{2N_C(i)+2}\right)$. The number of double bonds and rings, called double bond equivalent number, N_{DBE}, becomes:

$$N_{\mathrm{DBE}}(i) = \frac{m\left(\mathrm{C}_{N_{\mathrm{C}}(i)}\mathrm{H}_{2N_{\mathrm{C}}(i)+2}\right) - m(i)}{2 \cdot m(\mathrm{H})} \qquad \text{Eq. 3.1}$$

Geissler et al. (2009) have shown that each N_{DBE} (adaptation of "class residue" from reference) is expected to represent a different class of compounds common in diesel fuel.

The assignment of DBE classes in this work is based on fuel analysis performed by Schauer et al. (1999), Geissler et al. (2009), and Mitschke et al. (2006). DBE classes are expected to contain saturated and cyclic aliphatic compounds (N_{DBE} = 0 to 3), alkylated benzenes (N_{DBE} = 4) and polycyclic aromatic hydrocarbons (N_{DBE} >= 7). Unsaturated aliphatic hydrocarbons are not expected to be significant components of diesel fuel. For instance, N_{DBE} = 1 is presumed in this and previous work to consist mostly of cycloalkanes, not alkenes. Accurate DBE classification relies on GC separation to distinguish between alkyl and PAH compounds of equal mass (e.g. N_{DBE} = 0 vs. N_{DBE} = 7), which is possible because chromatographic separation is a function of not only molecular formula, but also of chemical structure such as the presences of rings and branches.

3.3. Results and Discussion

3.3.1. Spectra of known compounds

In the Supplementary Information of Isaacman et al. (2012), we provide the first compilation of VUV mass spectra of large organic compounds, with molecular masses primarily in the range of 150 to 400 Da; sample spectra are shown in Fig. B.2. Spectra of 84 known compounds are shown, representing a wide range of functional groups: saturated and unsaturated aliphatic hydrocarbons including hopanes and steranes, polycyclic aromatic hydrocarbons, aliphatic and aromatic acids and esters, aliphatic ketones and aldehydes, oxygenated and multi-functional aromatics, and chloro- and nitro-aromatics. Spectra are collected using VUV ionization at 10.5 eV with transfer temperatures of 150 ^{o}C (for a subset of 38 compounds) and 275 ^{o}C (for all compounds). All spectra are collected by GC-VUV-MS of known compound mixtures.

From the spectra it is clear that transfer temperature has a significant impact on fragmentation. A transfer temperature of 150 ^{o}C increases f_P for all compounds, while higher transfer temperatures enhance fragment peaks. Low temperature operating conditions can therefore be used to focus on resolution by molecular mass as is done in this work. However, using high temperature operating conditions provides some structural information, potentially facilitating identification - as is done in EI - while still providing the molecular mass in most cases; these capabilities may be preferable for identification of compounds in some mixtures.

3.3.2. Classification by carbon number

An injection of diesel fuel (7.5 µg diluted to 1.5 µL with chloroform) was analyzed by GC-VUV-MS to explore resolution capabilities. The sample is shown in the GCxMS plane in Fig. 3.1, where each chromatographic peak is shown as a circle, while the gray areas in the background represent ion abundance. Note that some DBE classes that do not appear to have a significant number of peaks contain long gray areas, indicating a rising background with no identifiable chromatographic peaks. Such areas are likely composed of many small chromatographic peaks

that are not well-resolved but in some cases account for a non-negligible fraction of total detector response. It is clear from Fig. 3.1 that certain DBE classes (colored circles in Fig. 3.1) are more highly populated with peaks than others. This work will focus primarily on the aliphatic DBE classes, as this best utilizes the soft ionization capabilities of VUV-MS; aromatics and PAHs tend not to fragment heavily even using EI ionization owing to resonance stabilization.

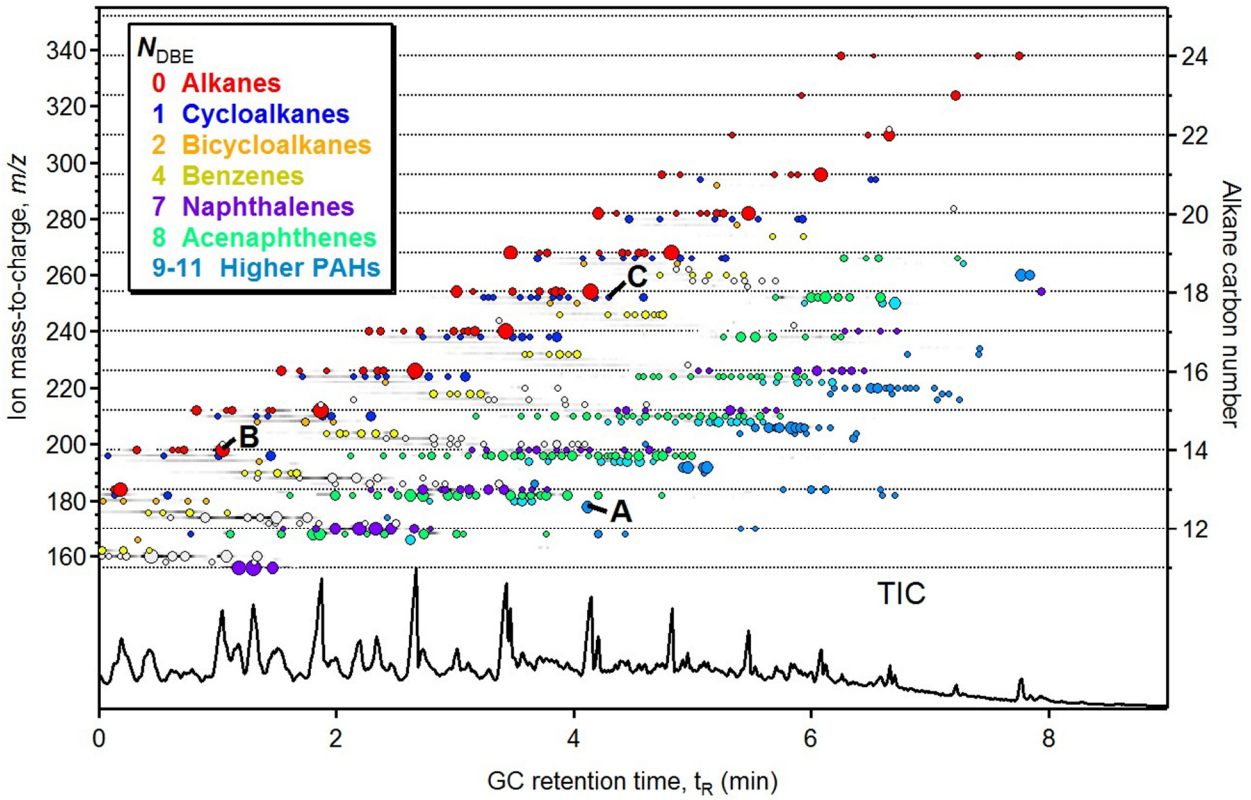

Figure 3.1. GCxMS plot of diesel fuel at a transfer temperature of 150 °C and a photon energy of 10.5 eV. Circles represent peaks and are approximately sized by logarithmic peak height and colored by (N_{DBE}); red: alkanes (0), blue: cycloalkanes (1), orange: bicycloalkanes (2), yellow: benzenes (4), purple: napthalenes (7), green: acenaphthenes (8), blues: higher order PAHs (9-11), and white: unassigned class (3, 5, 6). Gray areas in background are ion abundance and dashed horizontal lines correspond to the mass of alkanes (N_{DBE} = 0). The total ion chromatogram (TIC) at the bottom shows total signal intensity. The blue circle labeled "A" and the red circle labeled "B" are phenanthrene ($C_{14}H_{10}$) and tetradecane ($C_{14}H_{30}$) respectively and are discussed in Sect. 3.3.2. The compounds represented by the blue circle labeled "C" is an unknown compound identified in Sect. 3.3.3 as a C_{18} cycloalkane with a single methyl branch.

The presence of rings and double bonds causes compounds in higher DBE classes to shift toward longer retention times, with aromatics eluting later than aliphatics with the same mass due to interaction with aromatic groups in the phase of the chromatographic column. Compounds of the same carbon number therefore fall in diagonal regions in the GCxMS plane. A clear example of this phenomenon is illustrated by phenanthrene and tetradecane (compounds A and B, respectively) in Fig. 3.1. Though phenanthrene, a C_{14} PAH with N_{DBE} = 10, has a retention time similar to octadecane ($C_{18}H_{38}$) and a mass equal to a C_{13} compound with N_{DBE} = 3, it falls into a

diagonal band of peaks containing tetradecane ($C_{14}H_{30}$). These compounds therefore define an area of C_{14} compounds spanning DBE classes of 0 to approximately 11 (beyond which there are few peaks). There is an analogous band for all observed carbon numbers, so any peak or unknown compound can be classified by N_C and N_{DBE}.

Quantitation of the composition of diesel fuel by carbon number and DBE classifications (Fig. 3.2) using VUV ionization is performed here as a validation against previous analyses of petroleum fuels. Signal intensity at each DBE and carbon number was corrected for transfer efficiency through the GC (dependent on t_R) and was calibrated using one of three standards: hexadecane for aliphatic compounds (N_{DBE} = 0 through 3), dodecylbenzene for alkyl aromatics (N_{DBE} = 4 through 6), and phenanthrene for PAHs (N_{DBE} >= 7). Absorption cross-section and detector response are expected to be structure and functional group dependent (Adam and Zimmermann, 2007) so are neglected here by calibrating to compounds of similar structure. Compounds of N_C below 14 eluted during the chromatographic solvent delay so were not quantified in this work. Consequently smaller aromatics (such as C_2-alkylnaphthalenes and short-chain alkylbenzenes) as well as short-chain alkanes were not measured. In this sample, alkanes account for nearly half (41%), while total aliphatic compounds constitute approximately three-quarters (73%) of the observed mass fraction. Cycloalkanes comprise a more significant mass fraction (14%) of diesel fuel than has been shown in past work, though this may be a function of the specific fuel sample analyzed. The compound distribution shown in Fig. 3.2 approximately agrees with previous diesel fuel characterization(Schauer et al., 1999b) and suggests a volatility distribution similar to that measured by VUV-MS of crude oil (Geissler et al., 2009). Classification by carbon number therefore yields similar results to past work using other methods, demonstrating that quantitation using GC-VUV-MS is an effective method for composition analysis of hydrocarbon mixtures. Characterization by N_C and N_{DBE} may be useful in parameterization of chemically explicit models. Further study of the effects of branching on fragmentation, as well as calibrating with authentic standards for a wider variety of observed compounds, will improve future quantitation by GCxMS analysis.

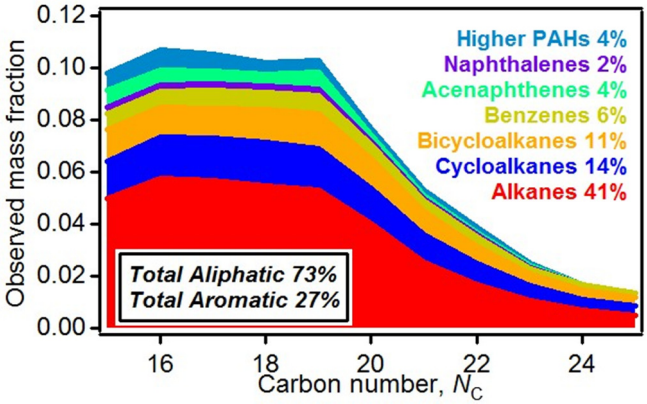

Figure 3.2. Composition of analyzed diesel fuel sample as fraction of total observed mass of each DBE class at each carbon number in the range of C_{15} to C_{25}. DBE classes shown (colored as in Fig. 3.1: N_{DBE} = 0, 1, 2, 4, 7, 8, 9-11) account for 82% of total observed mass. Calibration is approximate and based on measured responses of hexadecane for N_{DBE} = 0 through 3, dodecylbenzene for N_{DBE} = 4 through 6, and phenanthrene for N_{DBE} = 7 through 11.

Though photon energy does not significantly affect fragmentation patterns, it is potentially useful in the identification of unknowns. Comparison of diesel fuel ionization at 10.5 eV and 10.0 eV supports the assumption that most aliphatic hydrocarbons in the sample are saturated and that N_{DBE} = 1 is likely comprised primarily of cycloalkanes, not alkenes. This information on saturation, coupled with N_{DBE} and N_C obtained by GCxMS analysis, provides critical constraints for elucidating the structure of an unknown compound.

3.3.3. Separation of structural isomers

GC-VUV-MS was used to separate and identify structural isomers that are unresolvable using GC-EI-MS. Alkanes are typically quantified by EI-MS using ions with *m/z* 57 (the $C_4H_9^+$ fragment), while VUV-MS allows quantitation based on parent ions; an example of this is shown in Fig. 3.3, which compares two separately collected VUV and EI chromatograms of diesel fuel in the C_{16} to C_{19} retention time window. The large peaks of *m/z* 57 can be identified as *n*-alkane by retention time matching to standards as well as the presence of parent ions, though these are two orders of magnitude smaller than the quantitation ion. However, the interspersed smaller peaks representing branched isomers are undetectable on their parent ions and therefore cannot be identified without authentic standards. Using GC-VUV-MS, each chromatographic peak can be identified by parent ion, allowing identification and quantitation of branched isomers. In many cases, the branched regions observed on *m/z* 57 using GC-EI-MS are shown by GC-VUV-MS to be composed of alkanes of different carbon numbers.

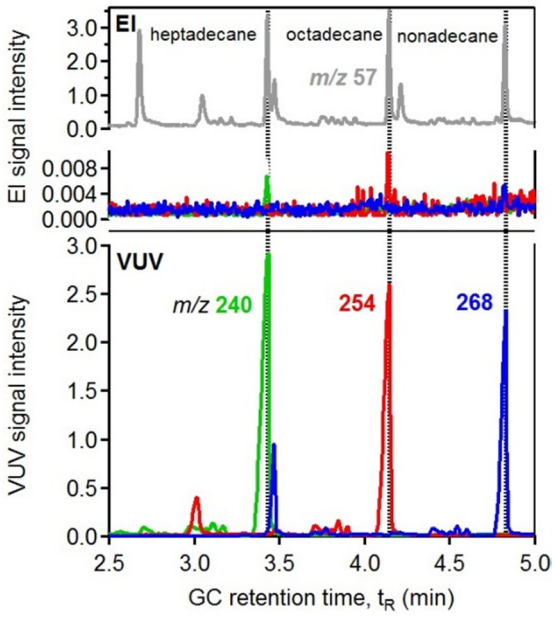

Figure 3.3. Chromatograms of diesel fuel using GC-EI-MS (top) and GC-VUV-MS (bottom). Ions shown are the parent ions of C_{17} (green line, *m/z* 240), C_{18} (red line, *m/z* 254), and C_{19} (blue line, *m/z* 268) alkanes using both EI and VUV, and *m/z* 57 (gray line) using EI, the ion typically used for the quantitation and identification of alkanes. Dashed lines show *n*-alkanes. Branched isomers can be identified by parent ion using VUV but not EI ionization.

The GCxMS plot (Fig. 3.1) shows several structural isomers in each DBE class in diesel fuel. Alkanes (N_{DBE} = 0, red circles in Fig. 3.1) will be used to elucidate isomer separation as they are the largest fraction of diesel, have the clearest isomer patterns, and are not well-resolved using EI-MS. Isomers of a given N_C shift toward shorter retention times as branching increases, so alkane isomers can be compared (Fig. 3.4a) by a relative retention index: the difference (ΔI_K) between the Kovats index (Kovats, 1958) of the isomer and of the *n*-alkane of the same carbon number; by definition $\Delta I_K = 0$ for *n*-alkanes while the earliest-eluting peak with a given N_C has the highest ΔI_K value.

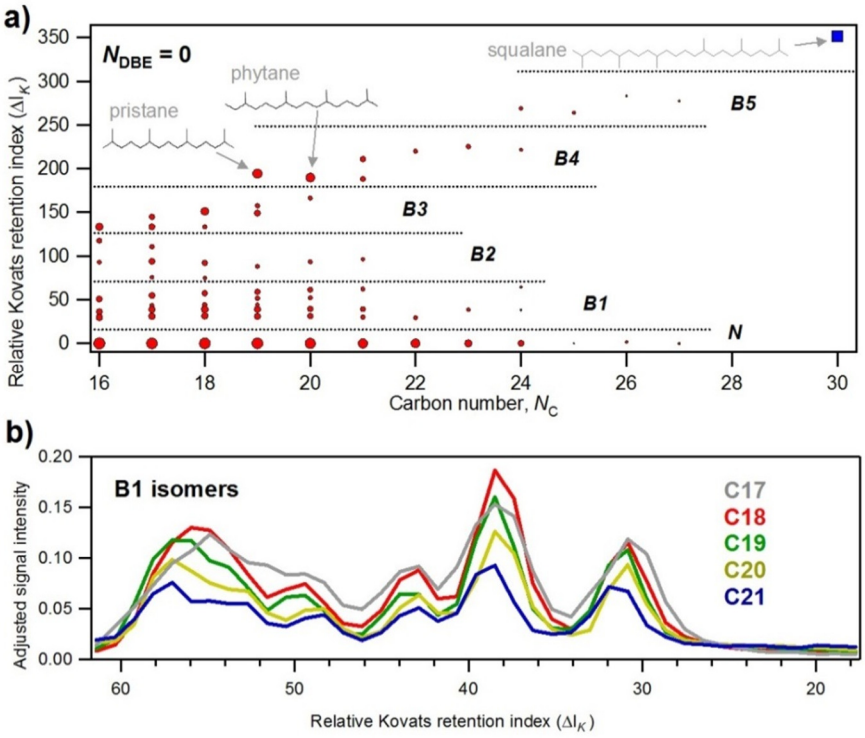

Figure 3.4. (a) Isomer separation of alkanes demonstrated by relative Kovats retention index, the difference between the Kovats index (I_K) of a given peak and that of the *n*-alkane (N) of the same carbon number ($\Delta I_K = 0$). Red circles are peaks found from GCxMS analysis of diesel fuel while the blue square represents squalane, a C_{30} hexamethyl alkane (shown). Pristane and phytane, C_{19} and C_{20} tetramethyl alkanes respectively (shown), are identified by authentic standards. Peaks fall into naturally separated regions shown by dashed lines through the gaps, defining areas of increasing branching from methyl (B1) through C_5-branching (B5). Squalane is in a B6 region that is unpopulated by alkanes observed in this diesel sample. Further discussion of these characterizations can be found in Sect. 3.3.3. (b) Reproducibility of single methyl group isomer (B1) patterns of alkanes (N_{DBE} = 0) from C_{17} through C_{21}. Detector response has been adjusted for GC transfer efficiency so all peaks are on equivalent scales, assuming approximately equivalent detector responses and absorption cross-sections.

Isomer structure can be determined from ΔI_K. The branched endmembers in the C_{19} and C_{20} alkane bands are identified using authentic standards as tetramethyl isomers: pristane and phytane (structures shown in Fig. 3.4a), the two most prevalent branched isomers in diesel fuel.

The range of C_{19} and C_{20} alkane isomers is therefore bracketed by the *n*-alkane (N) and a C_4-branched isomer (B4), with less-branched isomers in between. Due to a lack of available standards, the dependence of retention time shifts on branching location cannot be determined, so an isomer with 4 methyl groups cannot be distinguished from an isomer with a single branch containing a butyl group; therefore this work will refer to C_n-branched (as B*n*) isomers in place of specific identification. Intermediately branched isomers appear to fall into approximately evenly spaced regions separated by natural gaps, suggesting C_1-, C_2-, and C_3-branching. Pristane has a ΔI_K significantly larger than the most branched C_{18} alkane, thus defining the boundary with the B3 region. A similar increase in ΔI_K of the most branched alkane occurs at C_{24}, defining a region of C_5-branched alkanes (B5). Squalane, a hexamethyl C_{30} alkane (blue square in Fig. 3.4a), displays another significant increase in ΔI_K, suggesting a region of C_6-branched (B6) isomers that is unpopulated in the diesel sample analyzed in this work. Boundaries of the regions of C_1- through C_3-branching are inferred from gaps in peaks, though regions B2 and B3 do not have a clear separation point in this sample. Resolved B1 through B3 alkanes are below detection limits for larger alkanes, though some unresolved mass is often present.

As carbon number increases, the degree of possible branching increases correspondingly, so an increase in the width of the alkane band is expected. However, ΔI_K exhibits not a smooth upward trend, but rather a step function punctuated by increases of 30 to 50 every 5 carbon numbers, suggesting a theoretical maximum of branching, with a branch on every fifth carbon such as in the case of pristane. These compounds are thought to be polymers of isoprene (2-methyl-1,3-butadiene, C_5H_8), a biological carbon backbone commonly observed in plants (Langenheim, 1994), biogenic emissions (Guenther et al., 1995) and insects.[18] Only one B4 C_{19} isomer is observed, though the presence of ethyl or propyl branches would allow for multiple possible B4 C_{19} isomers while maintaining five carbons between branches. This preference for methyl groups and absence of more complex branching patterns would be expected for compounds with an isoprenoid origin, though structural changes could also occur during refining processes. These rules allow fewer isomers as branching increases, supported by the large number of B1 peaks at each carbon number compared to relatively fewer isomers of higher branching. In this diesel sample, alkanes typically have 8-10 major isomers, despite the tens or even hundreds of thousands of isomers that are theoretically possible (Goldstein and Galbally, 2007).

These isomer regions are reproducible between carbon numbers, as demonstrated the comparison of C_{17} through C_{21} methyl isomers (Fig. 3.4b). Each carbon number consists of four well-resolved methyl isomers and a broad peak centered at $\Delta I_K \approx 56$ that is likely a co-elution of at least two isomers. The number of methyl isomers observed is a significant fraction of the number of possible isomers; a C_{18} alkane, for instance, has 8 possible B1 isomers, of which 5 or 6 are observed. The same isomers have similar relative intensities at each carbon number. The similarity of the distribution of B1 isomers across all carbon numbers suggests a process either in formation or in petroleum refining that constrains isomer composition.

Quantification of isomers provides an estimate of the importance of branched alkanes in this diesel fuel sample (Fig. 3.5). B4 isomers are quantified based on pristane and phytane, which have similar response factors but fragment approximately twice as heavily as *n*-alkanes. This fragmentation calibration factor is unknown for B1 through B3 isomers, but is expected to fall between *n*-alkanes and B4 isomers, providing upper and lower bounds. Figure 3.5 shows that as alkane carbon number increases, the total mass-fraction of branching increases from approximately 0.4 to 0.6, which may be due to the increase in number of possible isomers. The

B4 isomer is largest at the lowest carbon numbers for which it is present, a pattern that appears to apply to B3 and B5 isomers and may be related to being polymers of isoprene. Though B5 isomers are a large fraction of C_{24} through C_{26} alkanes, these low-volatility alkanes are a small fraction of total observed alkane mass. In total, branched isomers account for 26 to 44% of alkane mass in this diesel fuel sample. Methyl isomers, which are difficult to resolve by GC-EI-MS and therefore not often quantified, are the largest fraction, comprising 10 to 16% of all alkane mass. B4 isomers are a significant fraction of alkanes (5 to 9%), but quantifying only pristane, phytane, and a few other prevalent branched alkanes underestimates branching in diesel fuel by approximately half. Furthermore, understanding not just the mass of branched isomers, but also identifying and classifying them by N_C extends the utility of this analysis into understanding compound-specific reactions and interactions.

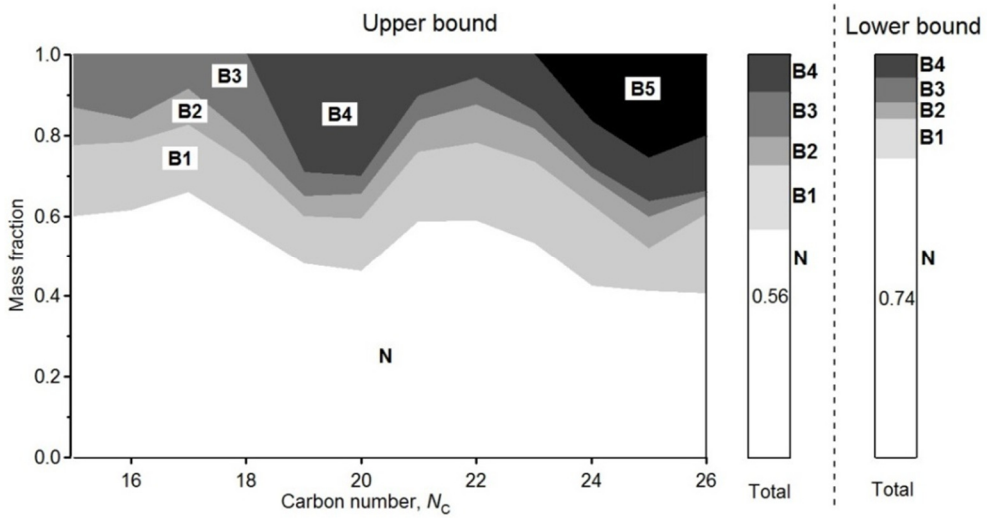

Figure 3.5. Mass fraction of each alkane (N_{DBE} = 0) carbon number composed of branched isomers of type B1 (methyl), B2 (C_2-branched e.g. dimethyl),…B5 (C_5-branched e.g. pentamethyl). Branched isomers have been normalized to *n*-alkanes (N) by f_P. Upper bound calibration assumes f_P for B1 through B3 is similar to B4 and B5 (half that of the *n*-alkane), while lower bound calibration assumes f_P for B1 through B3 is similar to that of the *n*-alkane. Total fraction on right is the fraction at each carbon number weighted by the distribution of alkanes (Fig. 3.2); branched isomers account for between 26 and 44% of total alkane mass.

Branched isomers of higher aliphatic DBE classes are also uniquely resolvable using GC-VUV-MS. Cycloalkanes (N_{DBE} = 1) are shown in Fig. 3.1 to be composed of 10 to 12 different isomers. Quantitative analysis shows these isomers to account for approximately half of the mass of cycloalkanes, though isomer distribution patterns are not as reproducible or clear as those of alkanes. Analysis of complex mixtures by GC-EI-MS would therefore be likely to underestimate the importance of branching for all aliphatic hydrocarbons. Furthermore, GC-VUV-MS allows the branching of previously unknown compounds to be estimated from ΔI_K, further elucidating structure. The utility of the classification scheme developed in this work can be demonstrated on the unknown peak labeled "C" in Fig. 3.1 that is unidentified by GC-EI-MS and lies in the middle of the "unresolved complex mixture." From carbon number separation and DBE class, this compound is expected to be a C_{18} cycloalkane, while its shift in t_R suggests a single methyl branch; the structure of an otherwise unresolved compound can therefore be determined.

3.4. Conclusions

Soft ionization coupled to chromatographic separation allows characterization of compounds based on structural characteristics and mass. GCxMS analysis of complex mixtures was used to classify unknown compounds by carbon number (N_C), number of rings and double bonds (N_{DBE}), and degree of branching based on retention time shifts (ΔI_K). Classification by these parameters provides structural information about unknown compounds in environmentally-relevant hydrocarbon mixtures, allowing identification of aliphatic hydrocarbons that cannot be differentiated using traditional MS techniques. The characterization scheme described in this work therefore provides significantly improved resolution of the "unresolved complex mixture" often present in GC analysis of environmental samples. The structure of any unknown compound in a complex mixture can be well-constrained by N_C, N_{DBE}, and ΔI_K, allowing estimation of reactivity, vapor pressure, and other physical properties that can be useful across a variety of scientific fields. Demonstration of these classification parameters on diesel fuel highlights the importance of isomer analysis. Quantitative analysis of branching using ΔI_K is useful in estimating the prevalence of branched isomers in environmental samples and is expected to provide significant insight into the formation and degradation of contaminants. Photoionization mass spectra of all compounds used in this work are available online (Isaacman et al., 2012) as a reference for other VUV-MS applications; example spectra are shown in Appendix B.

Improved resolution and isomer separation capabilities provided by GC-VUV-MS and GCxMS analysis are useful to any scientific fields that routinely characterize complex hydrocarbon mixtures, e.g. atmospheric chemistry, petroleum refining, microbial and chemical ecology, and bioremediation. Due to differences in chemical decomposition pathways of constitutional isomers, characterization of hydrocarbon branching has potential applications to the modeling of petroleum degradation in atmospheric and biological systems. Furthermore, some biological systems have been shown to be sensitive to isomer composition and branching (Martin et al., 2011; van Wilgenburg et al., 2010). The ability to quantitatively separate isomers and constrain the structure of unknown compounds in complex hydrocarbon mixtures will be useful in the analysis of a variety of samples from wide-ranging disciplines.

3.5. Acknowledgements

The Advanced Light Source as well as K.R.W. and T.N. are supported by the Director, Office of Energy Research, Office of Basic Energy Sciences, of the U.S. Department of Energy under Contract No. DE-AC02-05CH11231. This work was also supported by the Laboratory Directed Research and Development Program of Lawrence Berkeley National Laboratory under U.S. Department of Energy Contract No. DE-AC02-05CH11231, the US Department of Energy STTR Project DE-FG02-08ER-86335, and the National Science Foundation Grant CHE-1012809 and Atmospheric Chemistry Program Grant 0931934. G.I. was funded by the U.S. Environmental Protection Agency (EPA) Science to Achieve Results (STAR) program, Fellowship Assistance Agreement no. FP-91781901-0. This work has not been formally reviewed by EPA. The views expressed in this work are solely those of the authors, and EPA does not endorse any products or commercial services mentioned.

Chapter 4

Heterogeneous OH oxidation of motor oil particles causes selective depletion of branched and less cyclic hydrocarbons

Adapted from:

Isaacman, G., Chan, A. W. H., Nah, T., Worton, D. R., Ruehl, C. R., Wilson, K. R., and Goldstein, A. H.. Heterogeneous OH oxidation of motor oil particles causes selective depletion of branched and less cyclic hydrocarbons. Environmental Science & Technology, 46 (19), 10632-10640. 2012.

Abstract

Motor oil serves as a useful model system for atmospheric oxidation of hydrocarbon mixtures typical of anthropogenic atmospheric particulate matter, but its complexity often prevents comprehensive chemical speciation. In this work we fully characterize this formerly "unresolved complex mixture" at the molecular level using recently developed soft ionization gas chromatography techniques. Nucleated motor oil particles are oxidized in a flow tube reactor to investigate the relative reaction rates of observed hydrocarbon classes: alkanes, cycloalkanes, bicycloalkanes, tricycloalkanes, and steranes. Oxidation of hydrocarbons in a complex aerosol is found to be efficient, with approximately three-quarters (0.72 ± 0.06) of OH collisions yielding a reaction. Reaction rates of individual hydrocarbons are structurally dependent: compared to normal alkanes, reaction rates increased by 20-50% with branching, while rates decreased ~20% per non-aromatic ring present. These differences in rates are expected to alter particle composition as a function of oxidation, with depletion of branched and enrichment of cyclic hydrocarbons. Due to this expected shift toward ring-opening reactions heterogeneous oxidation of the unreacted hydrocarbon mixture is less likely to proceed through fragmentation pathways in more oxidized particles. Based on the observed oxidation-induced changes in composition, isomer-resolved analysis has potential utility for determining the photochemical age of atmospheric particulate matter with respect to heterogeneous oxidation.

4.1. Introduction

Heterogeneous oxidation processes are typically considered in terms of an oxidant uptake coefficient, γ. Measured as the reactive decay of a species upon exposure to an oxidant such as the hydroxyl radical (OH), γ describes the fraction of OH collisions with a compound that result in a reaction (Smith et al., 2009). Oxidation of particles is an efficient process, with 25% to 100% of OH-particle collisions resulting in reaction (Bertram et al., 2001; Che et al., 2009; George et al., 2007; Hearn and Smith, 2006; Kessler et al., 2010; Kroll et al., 2012; Lambe et al., 2009; McNeill et al., 2008; Smith et al., 2009). However, OH uptake by compounds in a particle

is a complex process, influenced by thermodynamic phase, diffusion, particle size and a host of physical parameters, hindering universally applicable parameterization of these processes. In multi-component systems, focusing on relative relationships between rates or OH uptake coefficients of different species reduces uncertainty from physical parameters, providing broader understanding of the oxidation processing of various compounds and theoretically extending utility to other oxidative environments (Donahue et al., 2005b).

OH uptake of compounds is dependent on particle composition (Huff Hartz et al., 2007), so heterogeneous oxidation of hydrocarbons within a motor oil particle (Lambe et al., 2009; Miracolo et al., 2010; Weitkamp et al., 2008) provides a more realistic surrogate system for the atmospheric processing of anthropogenic aerosols than single-component particles. However, these hydrocarbon mixtures are comprised of hundreds to thousands of compounds (Goldstein and Galbally, 2007), most of which are unresolvable using traditional techniques, so past work has generally focused on a small fraction of the chemicals in diesel fuel and motor oil that are resolvable and can serve as molecular markers for these sources. This work provides a more comprehensive analysis of heterogeneous oxidation of these hydrocarbon mixtures by combining gas chromatography with soft photoionization mass spectrometry.

Traditional gas chromatography and mass spectrometry (GC/MS) relies on 70 eV electron impact (EI) ionization. Most organic compounds have an ionization energy below 11 eV (Sieck, 1983), so the excess energy provided by these electrons results in a mass spectrum populated by small fragment ions that are nearly indistinguishable for structurally similar compounds. "Unresolved complex mixtures" containing compounds that cannot be separated chromatographically or through EI mass spectra can be better resolved by "soft ionization" GC techniques that minimize fragmentation, thus preserving the molecular ion for identification. This vastly improves resolution of structural isomers through separation by ion mass-to-charge ratio (m/Q).

Soft ionization is achieved in this work by using vacuum-ultraviolet (VUV) photons generated by synchrotron radiation as an ionization source (described in Chapter 3). Though a variety of other methods of photon generation are available (Adam and Zimmermann, 2007; Hanley and Zimmermann, 2009; Zimmermann et al., 2008), synchrotrons provide the flexibility of adjusting photon energy between 8 and 11 eV, with a reliable and relatively high photon flux (Heimann et al., 1997). The separation and resolution capabilities of VUV-MS are unparalleled when coupled to a gas chromatograph (Eschner et al., 2010; Geissler et al., 2009) for characterizing unknown compounds by carbon number, number of double bonds and rings, and degree of branching (described in Chapter 3), providing a nearly comprehensive compositional analysis of unresolved complex hydrocarbon mixtures.

In this work we apply the separation capabilities of GC/VUV-MS to measure the OH oxidation rates of hydrocarbons in motor oil particles. Comprehensive characterization of the hydrocarbon mixture is accomplished using high resolution (HR) mass spectrometry to separate oxygenated and non-oxygenated peaks in the mass spectrum in order to quantify oxidative decay of each compound class observed in motor oil: alkanes, cycloalkanes, bicycloalkanes, tricycloalkanes, and steranes. Relative reaction rates of resolved individual hydrocarbon classes and structural isomers are reported and combined with compositional analysis to determine the average OH uptake coefficient for total unreacted hydrocarbons. Implications of differences in relative rates are discussed in the context of modeling oxidation of urban organic aerosol, as the composition and fates of particulate hydrocarbons are expected to change with time.

4.2. Experimental

4.2.1. Flow tube reactor

The flow tube reactor used in this work has been previously described in detail (Kroll et al., 2009; Smith et al., 2009), including schematic drawings of the set-up. SAE 15W-40 motor oil particles were produced by homogeneous nucleation of new motor oil at 122 ^{o}C, creating polydisperse aerosol with a log-normal size distribution (mean surface-weighted diameter = ~170 nm) and a concentration of ~2600 μg/m^3; at this particle loading, compounds with volatilities of a C_{22} alkane and lower are expected to be more than 90% in the particle phase. Particles were entrained in nitrogen and passed through an annular charcoal denuder to the flow tube reactor (type 219 quartz, 130 cm long, 2.5 cm i.d.), in which they were exposed to hydroxyl (OH) radicals. The average residence time in the flow tube was ~37 secs. The OH radicals were generated through the photolysis of ozone (corona discharge generator, OzoneLab Instruments) by mercury lamps (λ = 254 nm) in the presence of water vapor (~30% relative humidity). OH exposure (concentration x time) was measured by the decay of *n*-hexane introduced at the top of the flow tube for low OH concentrations. At high OH concentrations, hexane is introduced instead at the bottom of the tube to avoid depletion below the level of detection and calculation of OH exposure includes a multiplicative factor which is found through empirical calibration (uncertainty of ± 5%) before data collection (Kroll et al., 2009). Error in reported OH exposures is dominated by the uncertainty in the gas-phase rate constant, which is 20-30%, though estimated to be closer to 10% (Atkinson, 2003). While OH concentrations generated in this experimental set-up were typically several orders of magnitude larger than atmospherically relevant levels, high OH concentrations have been shown to yield roughly consistent results to longer duration and lower-OH experiments (Che et al., 2009; Renbaum and Smith, 2011).

Hexane concentration in the outflow of the reactor was monitored by a gas chromatograph with a flame ionization detector (SRI Instruments), and particle concentration and size was measured with a scanning mobility particle sizer (TSI). Samples for speciated organic analysis were collected for 10-60 minutes at a flow rate of 0.2-0.6 lpm (mass flow controller, MKS Instruments) on quartz fiber filters (47 mm Tissuquartz, Pall Life Science, pre-baked at 600 ^{o}C) downstream of a charcoal denuder (8 in. 480-channel MAST Carbon) to avoid gas-phase adsorption on the filters. Experiments were performed at seven different OH exposures ranging from 0 to 1.3×10^{12} molecules cm^{-3} s.

4.2.2. GC/VUV-HRTOFMS

Filter samples were analyzed by thermal desorption and gas chromatography coupled to high-resolution vacuum-ultraviolet time-of-flight mass spectrometry (GC/VUV-HRTOFMS). Filter punches (2 to 6 punches of 0.4 cm^2 each) were thermally desorbed under helium using a commercial thermal desorption system and autosampler (TDSA, Gerstel) into a gas chromatograph (Agilent 7890). A first dimension 60 m × 0.25 mm × 0.25 μm non-polar column (Rxi-5Sil MS, Restek) was coupled to a second dimension polar column (1 m × 0.25 mm × 0.25 μm, Rtx-200MS, Restek) with a modulator (Zoex) to allow for GC × GC analysis, although second dimension data will not be presented here. Effluent from the column was analyzed using a high-resolution ($m/\Delta m \approx 4000$) time-of-flight mass spectrometer (HTOF, Tofwerk) coupled to the Chemical Dynamics Beamline (9.0.2) at the Advanced Light Source at Lawrence Berkeley National Laboratory, described in detail by Heimann et al. (1997). Vacuum-ultraviolet photons

were passed through an argon gas cell and a MgF_2 window to remove unwanted high frequency undulator harmonics, providing photons for these measurements of 10.5 eV with a bandwidth of 0.2 eV and a flux of ~10^{15} photons/s over a focus area of approximately 100 × 200 µm.

The initial composition of motor oil (i.e. before oxidation) was quantified by structure and volatility using GC × MS analysis as described in detail Chapter 3. Separation by retention time and m/Q allowed the determination of carbon number (N_C), cyclization (number of double bond equivalents, N_{DBE}), and degree of branching of compounds ("B0" for straight chain, "B1" for a single branch, etc.), providing a basis for understanding the structure of the complex hydrocarbon mixture. Soft ionization provides the molecular weight of a hydrocarbon, which can be used to infer N_C, while N_{DBE} is determined by a difference in m/Q per ring of 2 Th (mass-to-charge, 1 Thomson = 1 Da e^{-1}). This is most accurately described as a measurement of degree of unsaturation, so the term double bond equivalents is used in this and other work, though in the case of motor oil this loss of hydrogens is expected to be due primarily to cyclization. Though resolving compounds solely by mass can be ambiguous, cyclization results in a shift in retention time as a means to distinguish isobaric compounds – for instance, naphthalene, $C_{10}H_8$, and nonane, C_9H_{20}, have the same mass but differ in retention time by several minutes (2 to 3 carbon numbers). Branching also affects retention time, such that a highly branched alkane (i.e. B4) elutes significantly earlier than a straight-chain alkane (B0) of the same carbon number, allowing separation of compounds by number of branches. Motor oil contains little unsaturated aliphatic or polycyclic aromatic mass (Mao et al., 2009), so the hydrocarbon fraction can be grouped into classes of branched and straight-chain hydrocarbons including alkanes, cycloalkanes, bicycloalkanes, and tricycloalkanes (N_{DBE} = 0 through 3, respectively), alkylbenzenes and steranes, (N_{DBE} = 4), and tetralins and hopanes (N_{DBE} = 5).

Calibrations of GC/MS response were performed for each compound class based on a variety of relevant compounds of similar volatility and structure. These calibration response factors are expected to correct for thermal desorption efficiency (volatility dependent), GC transfer efficiency (volatility and structure dependent), and photoionization cross-section and efficiency (structure dependent). This calibration method, using structurally relevant compounds, has been shown to achieve approximately 90% mass closure in the case of diesel fuel and compare quantitatively to compounds measured by traditional methods (Gentner et al., 2012). Multi-point calibrations were performed for C_{12}-C_{28} *n*-alkanes, two branched alkanes: phytane (B4, C_{19}) and squalane (B6, C_{30}), one cycloalkane: pentadecylcyclohexane (C_{21}), C_9-C_{15} *n*-alkyl benzenes, and a mixture of polycyclic aromatic hydrocarbons, providing response factors for N_{DBE} = 0, 1, 4, and 7+. A comparison between branched and unbranched alkanes and polycyclic aromatic hydrocarbons (naphthalene, methyl naphthalene, dimethyl naphthalene, methyl biphenyl, dimethyl biphenyl, phenanthrene, pyrene, methyl pyrene) was used to determine the effects of branching on the GC/MS response of cyclic compounds. Calibration curves for these compounds are provided in Fig. C.1 and are shown to be reasonably linear. Response factors for N_{DBE} classes without known standards were determined through interpolation of the known response factors. Authentic standards were purchased from Sigma-Aldrich, AccuStandard, and TCI.

4.2.3. High-resolution data processing

All data processing was performed using custom code written in Igor Pro 6.22 (Wavemetrics). High-resolution data was analyzed using a technique similar to that described by DeCarlo and

co-workers (DeCarlo et al., 2006) and incorporated into the Peak Integration by Key Analysis (PIKA) software tool (Sueper, 2012), widely used in the atmospheric sciences for analysis of HTOF data. The spectrometric signal at a given nominal mass was deconvoluted into component peaks by minimizing the residual of a fit based on exact masses of candidate C_xH_y and $C_xH_yO_z$ peaks likely to be present. To account for deviations from Gaussian peak shapes and drifts in mass calibration, a peak shape was selected and mass calibration was performed using frequently and regularly spaced per-deuterated normal alkanes (C_{12}, C_{16}, C_{20}, C_{24}, C_{28}; C/D/N Isotopes) spiked onto the filter before desorption. Candidate peaks to be fit were selected based on the composition of unoxidized motor oil particles, which is shown in Fig. 4.1 to not contain a significant fraction of polycyclic aromatic hydrocarbons, in approximate agreement with literature motor oil composition (Mao et al., 2009). This also conveniently avoids uncertainty from a nominal mass containing multiple potential hydrocarbons with different mass defects. Oxidized peaks were allowed to have up to four oxygen atoms, of which at most one was expected to be a hydroxyl group. These constraints reflect typical limitations of GCs, which have poor transfer efficiency for large, highly oxygenated compounds, especially hydroxyl groups (i.e. compounds presented by Williams et al. (2010b)). Though variations of these deconvolution parameters were explored, these constraints were found to provide a satisfactorily low residual signal and the fit was not significantly improved by allowing additional oxygen atoms.

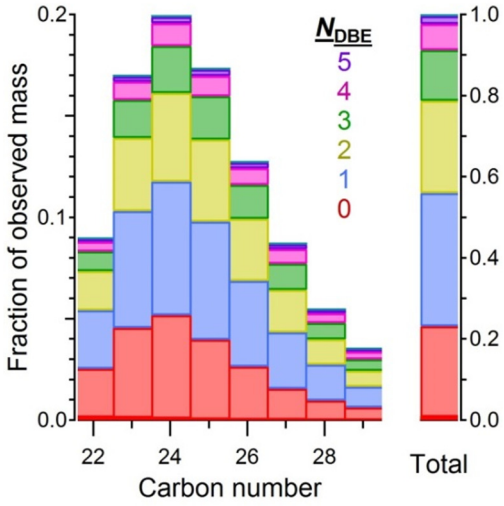

Figure 4.1. Contribution of each compound class to total observed mass. Except for straight-chain alkanes (shown in dark red) all mass is branched, and classes (N_{DBE}) include alkanes (0, red), cyclocalkanes (1, blue), bicycloalkanes (2, yellow), tricycloalkanes (3,green), steranes and alkylbenzenes (4, pink), and hopanes and tetralins (5, purple).

The validity of peak deconvolution was investigated to confirm that signal was properly attributed despite the small difference in mass defect between oxygenated and non-oxygenated compounds in the carbon number range of interest. The same list of candidate peaks was used regardless of OH exposure to avoid potential biases and peak deconvolution of unoxidized motor oil particles found little oxygenated mass, confirming that hydrocarbon mass was not incorrectly identified as oxygenated. Furthermore, peak-fitting of known compounds in the volatility range of interest yields accurate molecular formulas with less than 10% of mass attributed incorrectly.

The described peak-fitting method was found to yield log-linear decay of the hydrocarbon signal (R^2 > 0.7 for nearly all individual hydrocarbon classes), as well as reasonable growth of the oxygenated signal suggesting relatively accurate attribution of signal between oxygenated and non-oxygenated fractions. Most of the signal is found to contain one to three oxygen atoms, though peak-assignment in this work will be limited to oxygenated versus non-oxygenated.

4.2.4. Relative rate calculations

Uptake coefficients can be derived through the measurement of the decay of a compound, *i*, upon exposure to OH to yield an effective rate constant, $k_{eff,i}$, that is a direct measure of reaction rate, influenced by physical factors such as particle diameter and phase state (Donahue et al., 2005b; Lambe et al., 2009):

$$\frac{\partial \ln C_i}{\partial t} = k_{eff,i} C_{OH} \qquad \text{Eq. 4.1}$$

Assuming that chromatographic signal (S_i) is a linear function of analyzed mass (supported by calibration curves shown in Fig. C.1), the theoretical relationship between the concentration of OH radical (C_{OH}), the concentration of a compound (C_i), and time (t) can be expressed in an empirically useful form:

$$\ln \frac{S_{t,i}}{S_{0,i}} = k_{eff,i} \{C_{OH} t\} \qquad \text{Eq. 4.2}$$

where the OH exposure, $\{C_{OH} t\}$, is determined from the decay of the gas-phase tracer, hexane. Using Eq. 4.2, $k_{eff,i}$ can be calculated from the slope of the chromatographic signal of *i* at time *t* ($S_{t,i}$) relative to initial measured signal ($S_{0,i}$) (normalized for sample volume) as a function of OH exposure. To account for errors in apportioning mass by high-resolution data processing, which are poorly constrained, 1000 different values for $k_{eff,i}$ were calculated for each analyte of interest by varying the data points included in Eq. 4.2 (i.e. which values of $S_{t,i}$ were considered valid). Samples with the lowest hydrocarbon fractions (the most oxidized filters) were randomly included or excluded, as these samples are more likely to have points below detection limit (which was allowed to vary in this analysis), or incorrect peak deconvolution from the high-resolution analysis. In addition, the threshold for goodness of fit necessary to be considered was varied around a mean of R^2 = 0.70 (Gaussian distribution with a standard deviation of 0.10). Rates and uptake coefficients reported in this work are the averages and standard deviations of these 1000 computations.

Measured reaction rates cannot adequately be described by $k_{eff,i}$ as this quantity is a strong function of physical parameters such as particle surface area, density, mixing, and phase state. Therefore, the heterogeneous oxidation rate can more accurately be considered in terms of the fraction of OH collisions with a compound of interest, *i*, that result in the loss of the compound, given as the effective OH uptake coefficient, γ_{eff}, after Smith et al. (Smith et al., 2009):

$$\gamma_{eff,i} = \frac{4 \times k_{eff,i} \times D_{p,surf} \times \rho \times N_A}{6 \times \bar{c} \times M_i} \qquad \text{Eq. 4.3}$$

where $D_{p,surf}$ is the mean surface weighted diameter, ρ is the particle density (approximately 0.8 g cm^{-3} for a hydrocarbon mixture), N_A is Avogadro's number, $\bar{c}$ is the average speed of the OH

radical, and M_i is the molecular weight of i. Measured effective reaction rate constants can include secondary radical chain chemistry or gas-phase processing (Lambe et al., 2009), yielding an effective uptake coefficient of significantly greater than 1.

In a complex system such as motor oil, the fraction of OH collisions with unreacted hydrocarbons resulting in reaction, γ_{eff}^{tot}, can be directly measured from the decay of total hydrocarbon mass, providing an overall rate for the transformation of unoxidized to lightly oxidized particles. The total uptake of OH by hydrocarbons in the particle must also be the sum of the relative uptake of all component compounds, assuming a well-mixed particle so that there is no preferential uptake by surface compounds. OH-hydrocarbon collisions resulting in loss of a given hydrocarbon, i, are therefore dependent on the probability of interaction with that compound, a function of the mole fraction of the compound, χ_i:

$$\gamma_{eff}^{tot} = \sum_i \chi_i \gamma_{eff,i} \qquad \text{Eq. 4.4}$$

Total hydrocarbon OH uptake measured through these two methods should be approximately equal in the case of internally consistent measurements.

4.3. Results and Discussions

4.3.1. GC × MS analysis

Characterization of the unresolved complex mixture in unoxidized motor oil particles (Fig. 4.1) showed a significant contribution from alicyclic compounds with little polycyclic aromatic hydrocarbon mass, as observed in previous work (Mao et al., 2009). While some compound classes contained a resolvable B0 isomer, such as *n*-alkanes and *n*-alkylcyclohexanes, greater than 90% of the mass in all compound classes was observed as branched isomers. The mass of the motor oil particles was centered on C_{24} compounds, a lower carbon number than in directly injected motor oil, which was observed qualitatively to have a center of mass several carbon numbers larger though was not quantified in this work. This difference is due to the relatively low temperature homogeneous nucleation of the motor oil particles, which results in particles depleted in less volatile compounds, but is not expected to affect the kinetics results presented here, which depend on the initial composition of the particles not the parent motor oil.

GC × MS analysis provides a useful tool for understanding the oxidation processes by component hydrocarbons when coupled with high-resolution peak deconvolution of mass spectra (Fig. 4.2). The oxygenated fraction (blue signal in Fig. 4.2) shifts toward longer GC retention time than hydrocarbons (red signal) of a given carbon number. Retention time, a proxy for volatility, of a given *n*-alkane (black circles in Fig. 4.2) is similar to that of a ketone of approximately two carbon numbers smaller as would be expected based on volatility calculations (Chapter 2; Kroll and Seinfeld, 2008a). The complexity of the mixture is demonstrated by the lack of well-defined peaks in either the oxygenated or non-oxygenated fraction, but classification of these large unresolved signals by structure based on GC × MS allowed calculation of relative reaction rates for different structural classes.

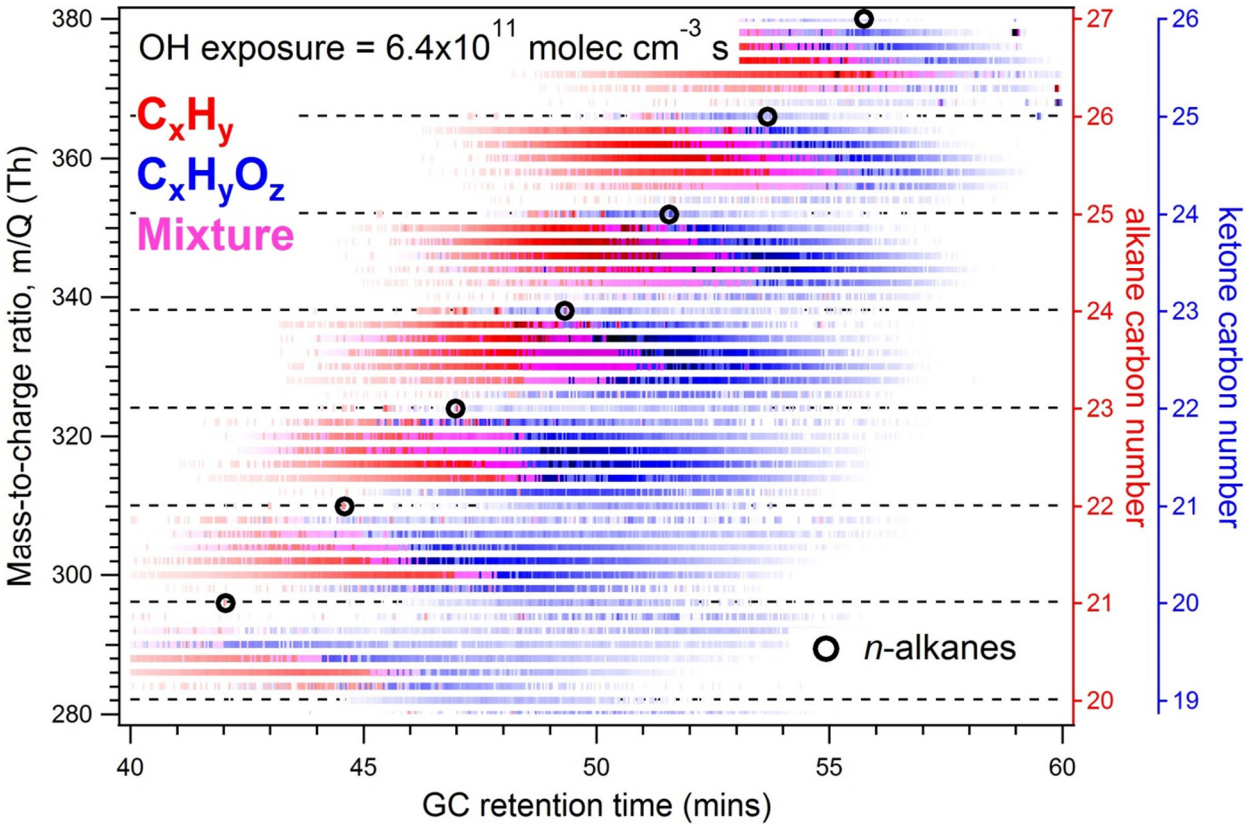

Figure 4.2. GC x MS plot of intermediately oxidized motor oil ($6.4x10^{11}$ molec cm^{-3} s, approximately half the exposure of the most oxidized sample). Points with a majority of the observed signal (greater than 55%) in the hydrocarbon fraction are shown in red, while majority oxygenated points are shown in blue. Points with no clear major fraction (evenly split, ± 5%) are shown in purple. The locations of normal alkanes are circled in black.

The oxidation of tetracosane (C_{24}) and its lightly branched (B1 and B2) isomers provides an excellent case study of the oxidative decay of hydrocarbons, as shown in Fig. 4.3, where the nominal mass signal at m/Q = 338 Th is separated into oxygenated and non-oxygenated signal fractions. In unoxidized particles, all mass is contained in the hydrocarbon fraction (C_xH_y) as expected, while oxidation results in a relative increase of the oxygenated fraction ($C_xH_yO_z$). As OH exposure increases, well-resolved alkane isomer peaks are increasingly difficult to distinguish using nominal mass resolution but are extracted through high-resolution analysis. Though the shape of each isomer region remains similar, the relative intensity of each region changes. B1 and B2 isomers in this region decay at roughly the same rate, but the *n*-alkane decays much more slowly; the most abundant B1 isomers reduce from approximately 3 times the peak height of the *n*-alkane to half its height in the most oxidized sample. These observed differences in oxidation rates between isomers can be quantified using a relative rates approach.

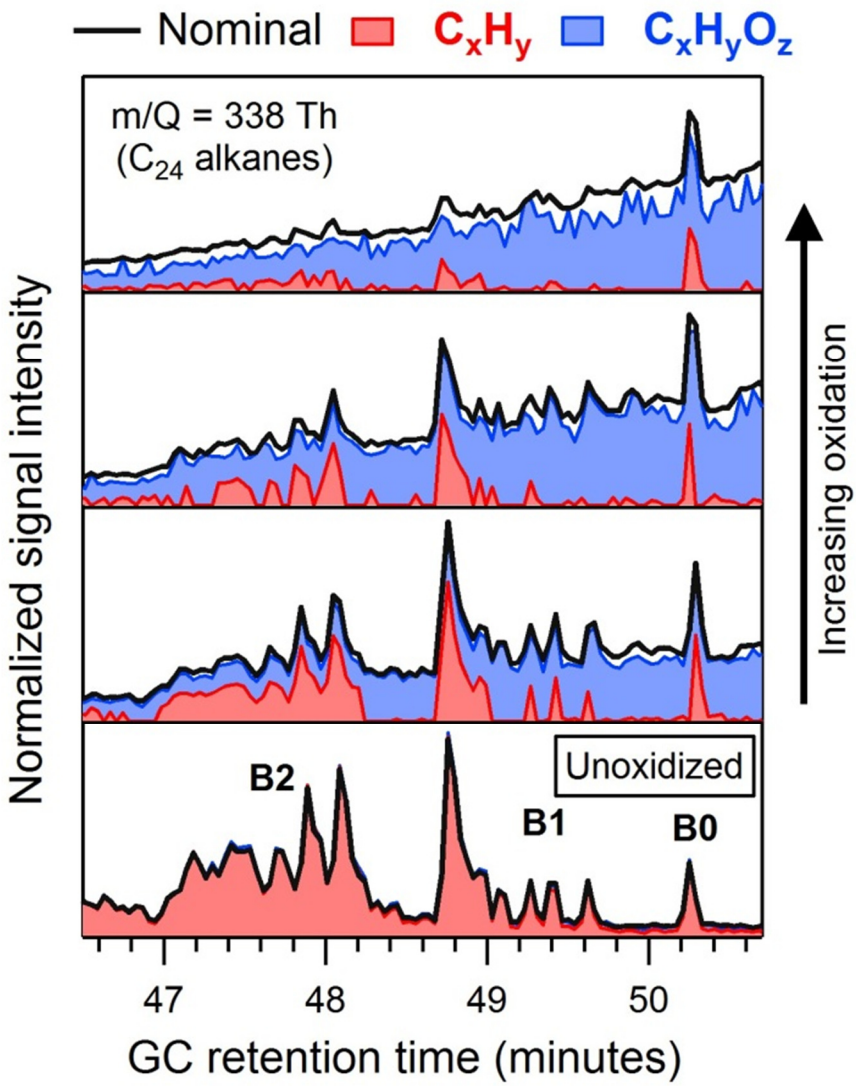

Figure 4.3. Oxygenated and hydrocarbon fractions of m/Q = 338 Th in the region of straight (B0) and lightly branched (B1, B2) C_{24} alkanes at four OH exposures (from bottom to top): unoxidized, 6.4×10^{11}, 7.3×10^{11}, and 1.3×10^{12} molec cm^{-3} s^{-1}. Nominal mass signal (black line) is deconvoluted into hydrocarbon (red) and oxygenated (blue) fractions. Approximately 20% of signal is unassigned in the most oxidized panel, likely due to low signals that do not cross the background threshold for peak-fitting.

4.3.2. Structurally resolved relative rates of oxidation

Calculation of relative rates is demonstrated on C_{24} alkane isomers in Fig. 4.4, in which the slope of the linear regression ($R^2 > 0.85$ for all isomers shown in Fig. 4.4) equals the effective rate constant, $k_{eff,i}$ as described by Eq. 4.2. As was qualitatively observed in Fig. 4.3, tetracosane (the B0 isomer) was removed at a significantly slower rate than branched isomers. Lightly branched (B1 to B3) C_{24} isomers reacted more than 50% faster than the straight chain alkane, while more branched isomers oxidized approximately twice as fast.

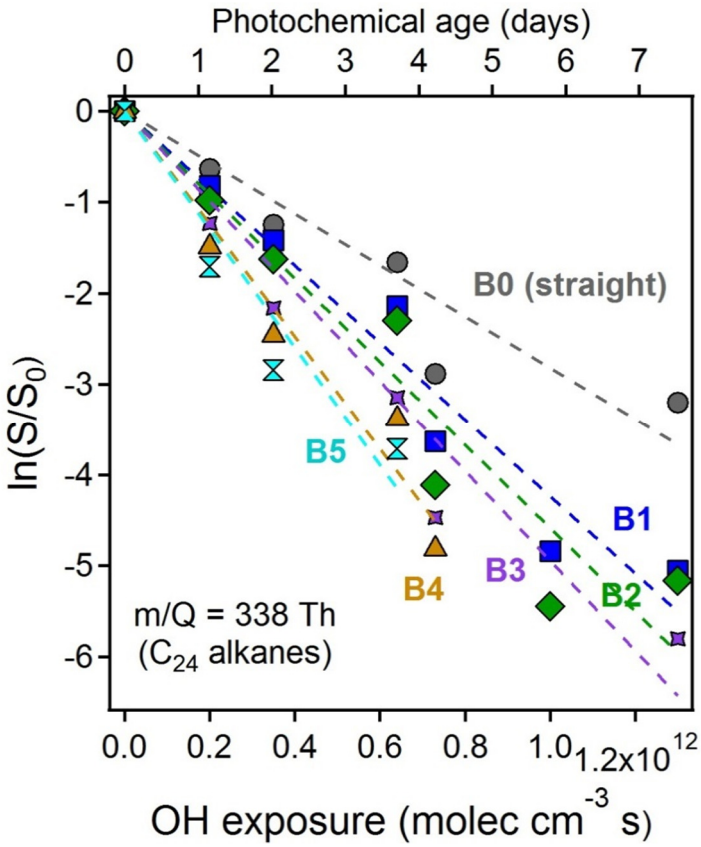

Figure 4.4. Relative decay of C_{24} straight (B0: gray circles) and branched alkanes (B1: blue squares, B2: green diamonds, B3: purple crosses, B4: gold triangles, B5: cyan hourglasses) as shown by logarithmic decrease of measured detector signal (S) relative to initial signal (S_0) with OH exposure. Steeper slopes indicate faster oxidation rates. Uncertainty in fits is shown by error bars in Fig. 4.5a. Approximate photochemical age is calculated assuming an OH concentration of $2x10^6$ molec cm^{-3}

Effective rate constants were measured for all observed compound classes and resolved isomers and converted to effective uptake coefficients using Eq. 4.3 (Fig. 4.5). Uptake coefficients were near or less than 1 for all compounds, while previous work conducted at atmospherically relevant particle concentrations found γ_{eff} values for compounds in this volatility range to be an order of magnitude larger than those shown in Fig. 4.5 (Lambe et al., 2009). This supports the conclusion of Lambe and co-workers that a significant amount of oxidation of these compounds in the atmosphere occurs through gas-phase processes, while confirming that due to the high particle concentrations the data presented in this work provide insight primarily into particle-phase and heterogeneous reactions. The values of γ_{eff} measured here are not descriptions of oxidation in atmospheric conditions, but rather an idealized investigation into the kinetics of the heterogeneous processes affecting these compounds. The carbon number dependence of γ_{eff} observed for all compound classes (Figs. 4.5a-b) may be due to the presence of some gas-phase oxidation of the lighter hydrocarbons though this effect is not expected to be large because alkanes C_{23} and larger are predicted to be almost entirely in the particle phase.

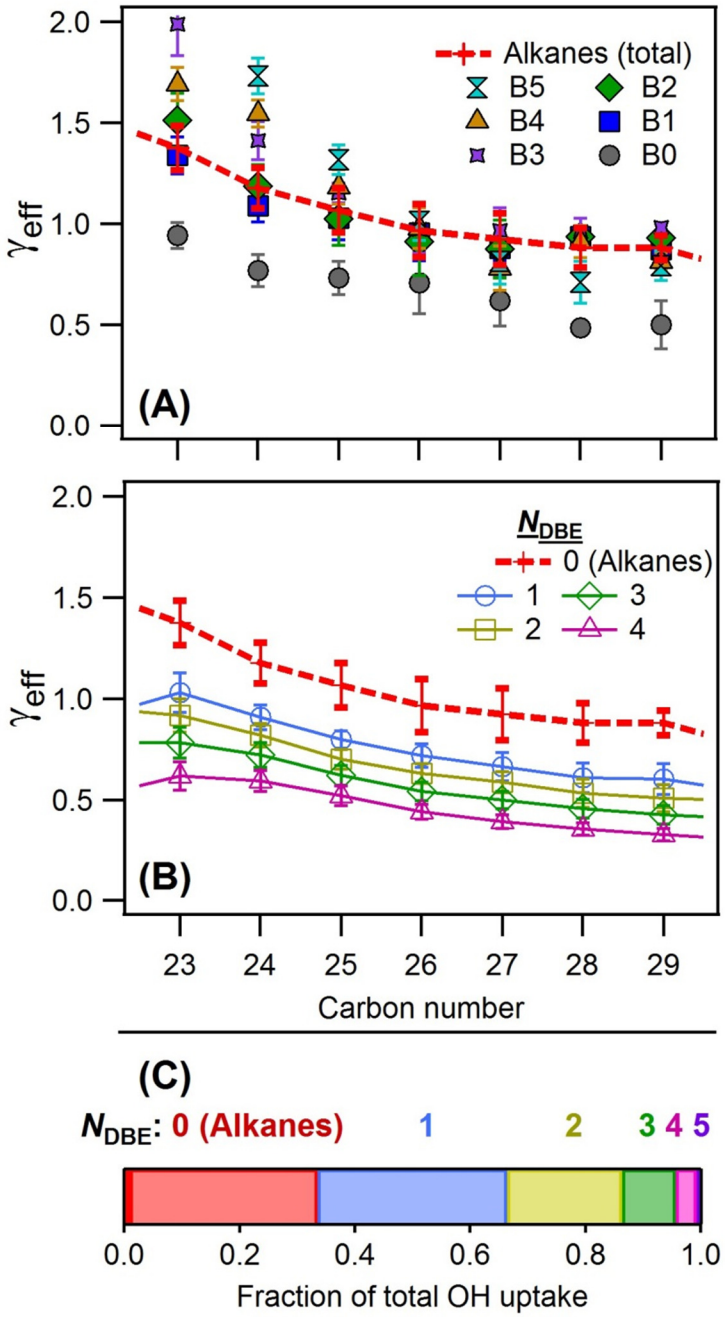

Figure 4.5. Effective uptake coefficients of (a) alkane isomers, and (b) cyclic compounds; the total alkane values (red dashed line) are the same in both plots. (c) Contribution of each compound class to total observed mass and total OH uptake. The measured total uptake coefficient, γ_{eff}^{tot}, equals 0.72 ± 0.06. Colors and symbols are the same used in Figs. 4.1 and 4: classes (N_{DBE}) measured include alkanes (0, red; straight chain in darker red), cycloalkanes (1, blue), bicycloalkanes (2, yellow), tricycloalkanes (3,green), steranes and alkylbenzenes (4, pink), and hopanes and tetralins (5, purple). A majority of the mass in all compound classes is branched. Values shown are averages and standard deviations (error bars) of 1000 computations in which variables were randomly varied to gauge sensitivity to poorly constrained error.

While γ_{eff} is a useful means of displaying the data and making comparisons across carbon numbers and laboratory environments, discussing average relative values provides insight into effects of structure on OH uptake. Figure 4.5 is shown in relative terms in Appendix C (Fig. C.2) to provide more detail to the interested reader beyond the average relative values and comparisons discussed below. From Fig. 4.5a it is clear that branched isomers had faster oxidation rates than straight alkanes of the same carbon number in all cases. Across all carbon numbers, lightly branched (B1 and B2) alkanes account for a majority of the alkane mass and reacted on average 48% faster than straight alkanes, while more heavily branched isomers (B3 through B5) reacted 67% faster. Branching increases volatility, so dependence of γ_{eff} on number of branches may be an artifact of gas-phase processing. Indeed, this dependence on degree of branching was not observed for higher molecular weight alkanes, which are less likely to be affected by partitioning; above C_{26}, all branched isomers reacted approximately 44 ± 14% faster than *n*-alkanes of the same carbon number.

The effects of volatility and partitioning can be accounted for using chromatographic retention time, as it is a function of vapor pressure (Chapter 2). A fit of *n*-alkane uptake coefficients with respect to retention times yields a polynomial function modeling expected γ_{eff} for theoretical *n*-alkanes of a given approximate volatility. Branched isomers of all carbon numbers were found to react 28 ± 11% faster than modeled straight chain alkanes of the same retention time, regardless of number of branches (data shown in Fig. C.3). Based on volatility corrections and the rates of high molecular weight alkanes, we infer heterogeneous OH uptake to be 20-50% faster for all branched alkane isomers.

The reason for increased OH uptake by branched alkanes is unknown. Previously reported models predict branching to have a smaller effect on reaction rates than observed in this work. While calculations based on structure-activity relationships predict a straight chain C_{24} alkane to react less than 10% slower than branched isomers, this work suggests differences in oxidation rates are non-negligible and may be masked by uncertainties in these relationships of up to 40% for acyclic alkanes (Kwok and Atkinson, 1995).

Cyclization was also observed to affect oxidation rate. Although cyclic aliphatic compounds were expected to react with OH radicals faster than acyclic hydrocarbons (Kwok and Atkinson, 1995) based on structure activity relationships, we observed the inverse (Fig. 4.5b). Cycloalkanes reacted 27 ± 3% more slowly than *n*-alkanes, and with the addition of each ring, the observed heterogeneous OH uptake of cyclic compounds decreased by an additional 20 ± 8%. This unexpected result is in relative agreement with previous observations of a 30% difference in the relative rates of hopanes and steranes (Weitkamp et al., 2008), whose structures differ by the presence of one ring. The values shown in Fig. 4.5b were calculated from total integrated signal of each compound class at each carbon number, composed almost entirely of branched isomers. An increase in relative oxidation rate from branching in cyclic hydrocarbons analogous to that observed in alkane isomers has been observed in the specific case of cholestane and androstane (Weitkamp et al., 2008), but isomers were not sufficiently resolved in higher N_{DBE} classes to provide this level of detail.

The mechanisms for the observed dependence of relative rates on cyclization and branching remain poorly understood and should be an area of focus for future studies, especially on the importance of this effect under atmospherically relevant conditions and gas-phase oxidation. Physical factors such as multi-phase particles and differences in diffusion rates are not thought to account for differences in relative rates because timescales of diffusion (estimated for alkanes

from Vardag et al. (1991)) are expected to be several orders of magnitude faster than reactive OH uptake and good log-linear decay of all isomers supports the assumption of a well-mixed particle. Observed differences in reaction rates between structural isomers are therefore thought to be due at least in part to previously unstudied chemical mechanisms.

4.3.3. Overall OH uptake by hydrocarbon mass

Relative rates measured here agreed with the small number of previously published results (Lambe et al., 2009; Weitkamp et al., 2008) but this work represents a much more comprehensive analysis of OH uptake by chemically reduced hydrocarbons in complex particles. Combining measured relative OH uptake coefficients with compositional analysis using Eq. 4.4, the overall uptake coefficient, γ_{eff}^{tot}, of the hydrocarbon mass in the particles was calculated to equal 0.86 ± 0.08, suggesting efficient OH uptake by unreacted hydrocarbons. This value was calculated with an initial composition, so represents an initial uptake coefficient that is in agreement with previous work on a compositionally similar complex hydrocarbon mixture (Kroll et al., 2012). However, differences in relative rates are expected to change the composition of the hydrocarbon mixture with time, so a more accurate value for average OH uptake by the hydrocarbon mixture can be calculated by measuring decay of the total hydrocarbon mixture. This direct measurement technique yielded a value of 0.72 ± 0.06. As the particulate matter becomes enhanced in cyclic compounds the overall reaction rate of hydrocarbons decreases, so the average uptake coefficient is expected to be lower than the initial uptake coefficient, as observed.

OH uptake is not equally efficient across structural classes, so the products of OH oxidation cannot be estimated solely from compositional analysis. Instead, the contribution of each compound class to the overall OH uptake can be determined as shown in Fig. 4.5c. Compounds that react more efficiently with OH account for a larger fraction of total OH uptake than the mass fraction would predict, such that branched alkanes account for approximately 20% of the mass of the particles, but ~33% of all OH uptake. An additional ~33% of hydroxyl radicals are expected to react with cycloalkanes, while the final third react with polycyclic aliphatic hydrocarbons. These fractions are of course dependent on particle source composition but are a reasonable estimate for the oxidation of hydrocarbon mass in atmospheric particles and highlight the importance in understanding relative OH uptake.

4.4. Atmospheric Implications

Heterogeneous oxidation rates of hydrocarbons in motor oil particles by hydroxyl radicals were observed in this work to be structurally dependent. While this has been demonstrated in previous work to be important for tracer method source attribution, it also has important implications for oxidation chemistry and aerosol transformations. Because branched alkanes are found to react 44 ± 14% faster than *n*-alkanes of the same carbon number (~30% faster when correcting for differences in volatility), the ratios of branched to straight alkanes are expected to change with atmospheric oxidation. Furthermore, particles are expected to become enhanced in cyclic compounds with atmospheric oxidation due to the observed 20 ± 8% decrease in oxidation rate with the addition of each ring. Consequently, the initial heterogeneous OH uptake by hydrocarbons in particles is dominated by less cyclic and more branched compounds and the composition is a function of photochemical age, with aged aerosols expected to be enhanced in

polycylic and straight-chain hydrocarbons. However, to fully constrain these compositional transformations, experiments under more atmospherically relevant conditions and analyses of the structural dependence of gas-phase reaction rates are necessary, as relevant properties of ambient aerosols or gases may differ from motor oil particles.

The application of GC x MS to oxidized motor oil yields new tools for studying ambient aerosol, alleviating the need to rely on only a few low-abundance well-resolved tracers. Newly accessible compounds provide a unique opportunity to use the composition of hydrocarbon particles as a photochemical clock, in which the ratio of compounds such as straight and branched or cyclic alkanes can be used to infer photochemical age. In contrast to most widely accepted gas-phase tracers of photochemical age (i.e. benzene and toluene as in ref. (de Gouw et al., 2005)), compounds studied in this work are semi-volatile in the atmosphere, partitioning between gas and particle phase, and thus provide a means for measuring oxidation in mixed-phase or heterogeneous environments, assuming reliable knowledge about the composition of the initial particle.

The selective depletion of branched and relatively less-cyclic compounds affects not just oxidation rates, but also the expected products and pathways. Because tertiary carbon atoms have unique chemical pathways upon oxidation that can lead to decomposition, branching is expected to increase fragmentation into more volatile products upon oxidation, leading to loss of aerosol mass (Kessler et al., 2010). Alternately, cyclization, which slows reaction rates, provides fragmentation sites but also yields less volatile functionalized products due to ring-opening. The reaction products of the highly cyclic compounds measured in this work are not well-studied, but previous work has shown increased oxygen-to-carbon ratios in aerosol from a tricylic precursor relative to acyclic precursors (Lambe et al., 2012). Shifts toward cyclic products with aerosol age will therefore affect oxidation products, pathways, and properties, though the details of these transformations and the influence of gas-phase processes remain understudied. While multiple generations of oxidation increase fragmentation of the oxidized products (Lambe et al., 2012), the inverse is true for the transition from unreacted hydrocarbons to lightly oxidized compounds. Enhancement of cyclization with photochemical age increases the importance of ring-opening functionalization pathways in the oxidation of hydrocarbons in aged particulate matter.

In areas downwind of major urban centers or subjected to significant anthropogenic influence, the hydrocarbon fraction of the aerosols will have a different chemical composition and different reaction products than freshly emitted particulate matter owing to the structural dependence of oxidation mechanisms. Buried in the previously unresolved complex mixtures in these ambient aerosols is information about sources and photochemical age. Though these applications are complicated by the presence of non-petroleum-based hydrocarbon mixtures, future analyses of ambient environments can provide a basis for understanding source profiles. Improved understanding of the fates of branched and cyclic hydrocarbons is necessary to further constrain the fate of atmospheric aerosols, as they comprise a large fraction of the observed mass but are poorly resolved in current inventories.

4.5. Acknowledgements

We would like to thank Kathryn R. Kolesar for assistance operating the flow tube reactor. The Advanced Light Source as well as KRW and TN are supported by the Director, Office of Energy Research, Office of Basic Energy Sciences, of the U.S. Department of Energy under Contract No. DE-AC02-05CH11231. CRR, AHG, and KRW are supported in part by the Laboratory Directed Research and Development Program of Lawrence Berkeley National Laboratory. Contributions by UCB personnel were supported in part by the National Oceanic and Atmospheric Administration award No. NA10OAR4310104. G.I. was funded by the U.S. Environmental Protection Agency (EPA) Science to Achieve Results (STAR) program, Fellowship Assistance Agreement No. FP-91781901-0. This work has not been formally reviewed by EPA. The views expressed in this work are solely those of the authors, and EPA does not endorse any products or commercial services mentioned.

Chapter 5

A versatile and reproducible automatic injection system for liquid standard introduction: Application to in situ calibration

Adapted from:

Isaacman, G., Kreisberg, N. M., Worton, D. R., Hering, S. V., and Goldstein, A. H.: A versatile and reproducible automatic injection system for liquid standard introduction: application to in-situ calibration. Atmospheric Measurement Techniques, 4, 1937-1942. 2011.

Abstract

The quantitation of trace organic compounds in ambient organic aerosol is difficult due to the chemical complexity of these mixtures, but is needed to provide insight into their sources and formation processes. Compound-level characterization of organic aerosols is typically performed through sample collection followed by gas or liquid chromatography. With these methods, introduction of liquid standards has long been used as an effective means of quantifying trace compounds, but automating this technique for use with in situ instrumentation has not previously been achieved. Here we develop an automatic injection system (AutoInject) for the introduction of liquids into a custom collection and analysis cell for improved quantitation in chromatographic measurements. The system consists of chilled reservoirs containing liquid standards from which a sample loop is loaded and then injected into the cell. The AutoInject is shown to be reproducible over 106 injections with a relative standard deviation of 1.5%, and have negligible injection-to-injection carryover. A 6-port selector allows injection of different liquid standards separately or simultaneously. Additionally, automatic injection of multiple sample loops is shown to generate a linear multi-point calibration curve. Tests conducted in this work focus on use with the Thermal desorption Aerosol Gas chromatograph (TAG), but the flexibility of the system allows it to be used for a variety of applications.

5.1. Introduction

Accurate quantitation using chromatographic methods relies on measuring detector response relative to directly introduced authentic standards using a multi-point calibration, often with a correction for variation in sample recovery or detector drift. The most common technique for correcting for run-to-run variability is to spike each filter with a known quantity of some liquid internal standard (Mazurek et al. 1989; Schauer et al. 1996; Offenberg et al. 2011). However, though this method has been used with great success to quantify compounds on filters, it poses a significant drawback when applied to in situ data collection; specifically, the 24-hour per day presence and vigilance of an operator. An alternate method appropriate to field measurements is the use of a regularly injected complex mixture - a "tracking standard" - to monitor long-term

trends in detector response, coupled with regular multi-point calibrations (Kreisberg et al., 2009). Though shown to be effective, this field method assumes monotonic changes in detector response and does not correct for variations related to changes in transfer efficiency and detector response. Therefore, combining these two methods by injecting both internal standards on every run as well as regular tracking standards would greatly improve the accuracy of in situ quantitative speciation. This dual calibration approach is the objective of the automatic injection system (AutoInject) described in this work. The AutoInject was developed and tested specifically for the Thermal desorption Aerosol Gas chromatograph (TAG) field instrument, an in situ quantitative gas chromatograph used to study aerosol composition (see Williams et al. 2006 for details).

Common laboratory-based liquid introduction systems typically do not meet requirements for field use. The most common mechanisms in laboratory data collection are "XYZ" automatic systems, in which a robotic arm with a syringe withdraws an aliquot from a vial containing a known liquid, moves to the instrument inlet, and injects the syringe (e.g. those sold by Agilent Technologies for GC or Waters Technologies for LC). This approach is infeasible in the case of custom field instruments, however, as (a) it usually requires vertical injection which is not possible on some instruments (including TAG), (b) frequent septum piercing caused by syringe injection leads to coring and sample contamination, and (c) it is typically bulky, involves many moving parts, and usually does not provide temperature stabilization.

Several field-applicable standard introduction systems have been developed for high pressure liquid chromatography (HPLC) and gas-phase calibration. Automated liquid introduction systems have been recently developed for LC (van Midwoud et al., 2011) in which flow rate is controlled by syringe pumps. These systems have the capability to switch between liquids by controlling pump rates and valve states, but the volumes of solvent used (in some cases many milliliters per injection) generates more waste than is preferred for field use. Jardine et al. (2010) recently developed an elegant system that uses a stepper motor to introduce liquid into a helium stream at much lower flow rates to be evaporated and delivered to a TD-GC or other in situ instrument. However, due to the low vapor pressure of many compounds relevant to atmospheric aerosols, such a scheme is impractical for the study of particle-phase compounds.

In this work we develop a new method for the introduction of fixed volumes of liquid into a custom cell that is versatile and quantitative. Field deployment is emphasized by generating minimal waste (< 30 uL per injection) and relying on pressure gradients to create flow, thereby minimizing moving parts. Several hundred injections were tested to address the ability of the automatic injection system to meet the following goals:

1) Injection of a known volume must be reproducible.
2) Injection-to-injection carryover must be minimal and the presence of the system must have a negligible effect on blanks.
3) Quantity of liquid should be variable to facilitate multi-point calibrations.
4) Manual injection should be possible, allowing for injection of standards not contained within the system.

5.2. AutoInject Description

A schematic of the Automatic Injection System (AutoInject), which occupies a total space of 40 cm x 35 cm x 15 cm, is shown in Fig. 5.1a. Pressurized reservoirs, selected using a multiport selector, deliver liquid to fill a sample loop of known volume, which is injected via a 6-port valve into a custom cell. Up to four reservoirs of liquid are kept in a custom refrigerator consisting of an insulated, machined aluminum block cooled using an on-off controlled Peltier device (Custom Thermoelectric) capable of sustaining sub-freezing temperatures. The reservoirs are pressurized to 30 psig with helium distributed through a 6-way manifold. Reservoirs (shown in Fig. 5.1b) consist of a standard 10 mm x 75 mm Pyrex test tube capped with a 10mm compression fitting (Swagelok Company) using teflon ferrules. The cap has two drilled holes, through which 1/16 in outer diameter (o.d.) stainless steel tubing is inserted and silver brazed, with one tube reaching to the bottom of the reservoir for liquid delivery and one tube at the top for pressurization. The liquid delivery tube of each reservoir is connected to a 6-port selector valve (Upchurch Scientific V-1241) by 50 cm of 125 μm diameter (i.d.), 1/16 in o.d. tubing made of polyether ether ketone (PEEK), a non-reactive, opaque polymer, which prevents exposure to light. The small i.d. of this tubing minimizes the volume of liquid that is temporarily stored outside of the cooled block and is therefore not cooled. The 6-port selector is connected by 20 cm of 60 μm i.d. PEEK tubing to a 6-port valve (Rheodyne MXP7900) configured for sample loop injection. All liquid downstream of the selector must be injected or discarded during each injection cycle, so small i.d. tubing is necessary to minimize waste. All tubing was purchased from Upchurch Scientific.

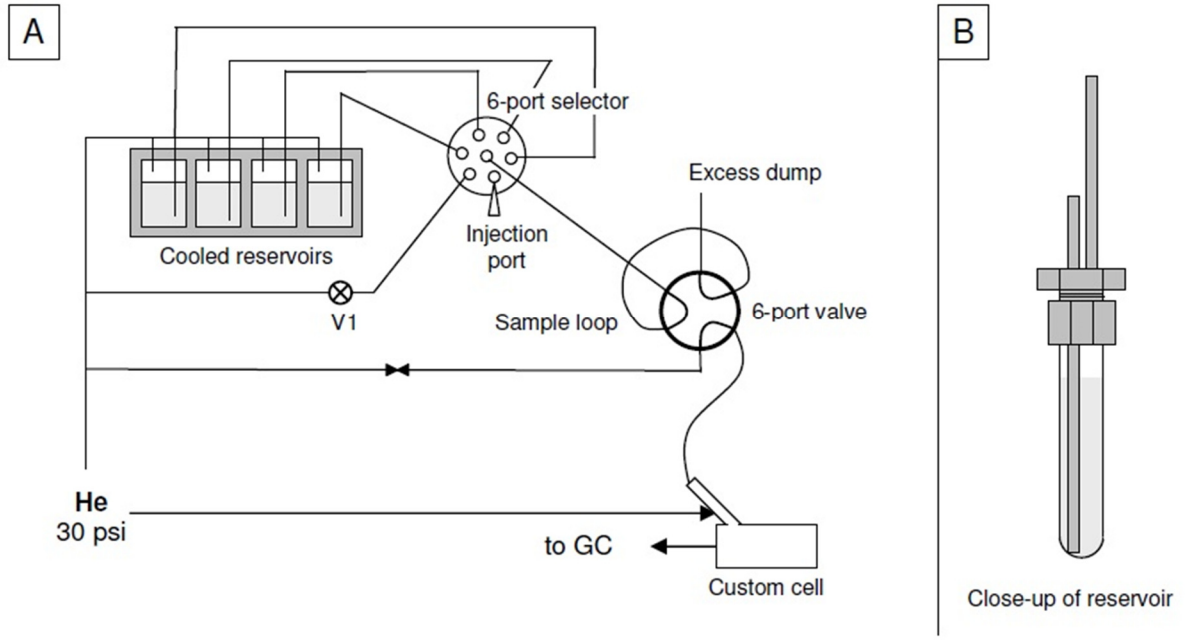

Figure 5.1. Overview of the automatic injection system (AutoInject) showing (a) the schematic diagram of the system in "load" and (b) a close-up of a standard reservoir. The custom cell used in these studies is the Collection and Thermal Desorption (CTD) cell of the TAG instrument (Williams et al. 2006).

5.2.1. Operation procedure

With the 6-port valve in the load position (pictured in Fig. 5.1), the liquid loads a sample loop of known volume (see Sect. 5.2.2), with excess going to a waste container; in this case, waste is injected onto glass wool at the bottom of a vial containing activated charcoal, facilitating evaporation of solvent that is then scrubbed to prevent emissions. In the inject position, the sample loop is flushed with helium into the custom cell via a 15 cm x 1/32 in o.d. x 250 μm i.d. stainless steel capillary. Injection helium is restricted by 1 m of 60 μm tubing, maintaining helium flow below 2 ccm. Additionally, a check valve on this line prevents back flow from the cell even in the presence of a pressure gradient. Following injection, excess liquid remaining in the lines is purged with helium through the selector port connected directly to helium. When idle, the helium port is selected with the shut-off valve (V1) closed, so neither liquid nor helium is wasted and the restriction of the injection helium minimizes helium waste. All valves (6-port selector, 6-port valve, and helium valve) are actuated automatically through computer controlled contact closures using a custom written Labview program (National Instruments Corporation).

The custom cell into which liquid was introduced for this study is the collection and thermal desorption (CTD) cell on the Thermal desorption Aerosol Gas chromatograph (TAG) described in Kreisberg et al. (2009). This CTD cell has a built-in helium purged injection port with a septum seal for needle insertion for manual injections. The injection capillary of the AutoInject was inserted into this port with a compression fitting (Swagelok Company), eliminating the need for the septum. The injected liquid standard was thermally desorbed at 300 ^{o}C and analyzed using a gas chromatograph (GC) coupled for most tests to a flame ionization detector (FID; Agilent Technologies) and for carryover tests to a time-of-flight mass spectrometer (Kronus ToF-MS; Scientific Analysis Instruments).

A typical injection cycle lasts approximately 45 seconds per reservoir used: approximately 20 seconds to load and inject a single loop volume and 15 seconds to helium purge the line between the valve and selector, with some time for transitions in between. For all experiments in this study, injection of a standard was followed by injection of solvent to clean the lines. Minimizing loop load time minimizes waste and load timing is strongly dependent on helium pressure and tubing i.d., so the shortest load time possible to fully load the loop was determined.

5.2.2. Sample loop

The sample loop used in these tests was a 15 cm x 1/16 in o.d. x 180 μm i.d. stainless steel sample loop (Rheodyne). The internal volume injected, consisting of the loop itself plus dead-volume within the valve and fittings, was found to be 4.0 ± 0.1 μL for the conditions and valve described above by comparing FID response of one loop of standard to a multi-point calibration using the same standard done by manual injection. Any 1/16 in o.d. tubing can be used as a sample loop, making the AutoInject highly flexible for custom applications.

5.3. Results

5.3.1. Stability tests

The two primary necessities for a useful automatic injection system are the capability for long-term, highly reproducible injections, and the capability to switch standards with minimal cross contamination.

The reproducibility of liquid injections using the AutoInject was studied through the injection of a standard containing 2 ng/μL n-alkanes from C_8 to C_{40} and polycyclic aromatic hydrocarbons (PAHs) spanning a similar volatility range in chloroform. All tests focus on the volatility range of C_{15} to C_{35} as this is where nearly all compounds are observed by TAG. In Fig. 5.2, the FID response to compounds in each run, relative to the average response across 106 injections of each compound, demonstrates the high reproducibility of the AutoInject. The dashed line marks the standard deviation, σ, of 1.5%. The root mean square (RMS) error for all peaks is below 2.5% and averages 1.4%. Some compounds that partially co-elute in the chromatographic separation have been binned in order to minimize measuring errors not intrinsic to the AutoInject, especially difficulties in drawing baselines for, and therefore accurately quantifying, co-eluting peaks. However, deviations from unity are, in most cases, not well correlated between different compounds ($R^2 = 0.27 \pm 0.16$), suggesting that a large fraction of error is not from AutoInject instability (i.e. injecting more or less liquid) but rather from other sources, such as inaccuracies in chromatogram integration due to chromatographic baseline variations.

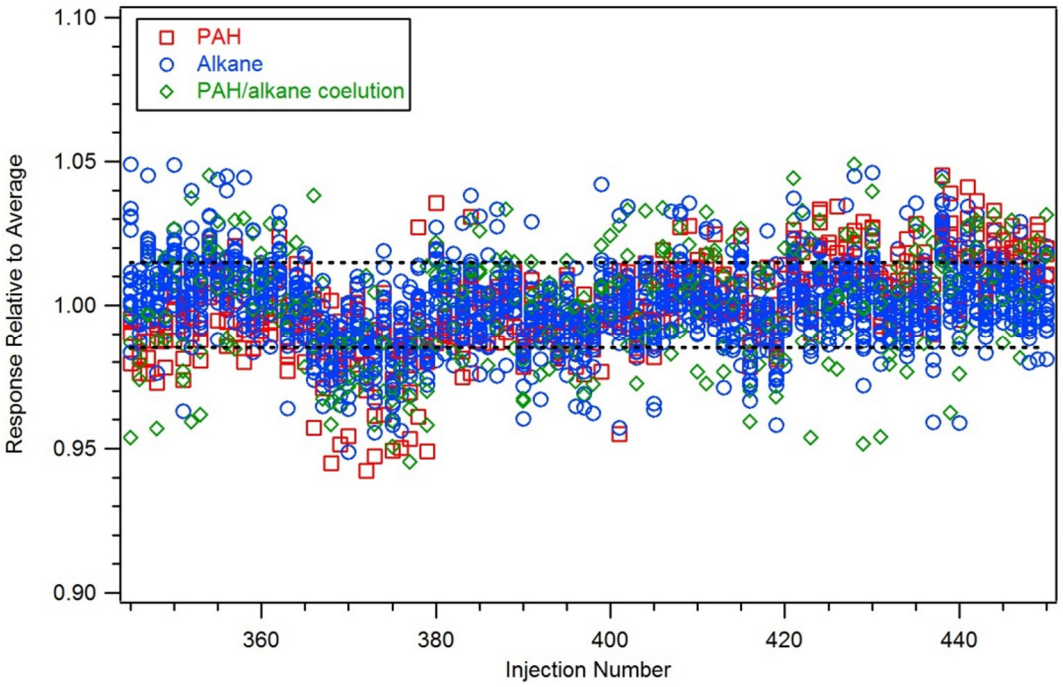

Figure 5.2. Stability of the AutoInject over 106 runs. FID detector response of a given compound is shown relative to the average response of that compound over all runs shown. Symbols differentiate PAHs, alkanes, and co-eluting peaks that contain both PAHs and alkanes while the dashed line represents the standard deviation of relative response for all standard compounds measured (1.5%).

In continuous operation, a reservoir, which has a volume of approximately 3 mL, contains enough liquid for more than 150 injections under the conditions and timing used in these tests. In the case of the TAG instrument, this allows the instrument to be run for at least one week, with hourly internal standard injections, without the need to refill a reservoir or expose the operator to chemicals. This length of time is of course dependent on the volume of the sample loop, the volume of the transfer lines, the volume of the reservoirs, and the duration of the load timing.

5.3.2. Carryover tests

The liquid carryover from one injection to the next was quantified by alternating between injection of a standard containing a complex 110-component mixture representing classes known to be atmospherically relevant (n-alkanes, PAHs, aromatic acids, straight chain acids, ketones, esters, etc.) and injection of an equal volume of a similar complex mixture containing 21 deuterated compounds. The number of solvent rinses following each injection was varied to determine the volume of solvent injection necessary to eliminate carryover. To accurately quantify carryover, a ToF-MS was used, allowing for specific ion extraction and, consequently, an improved level of detection. While the absence of a solvent rinse results in significant carryover (sometimes greater than 20%), this is greatly reduced by a single solvent rinse (Fig. 5.3). No statistically significant decrease in carryover was observed when employing more than a single rinse, suggesting that carryover after a single solvent rinse is negligible and any remaining carryover is external to the AutoInject.

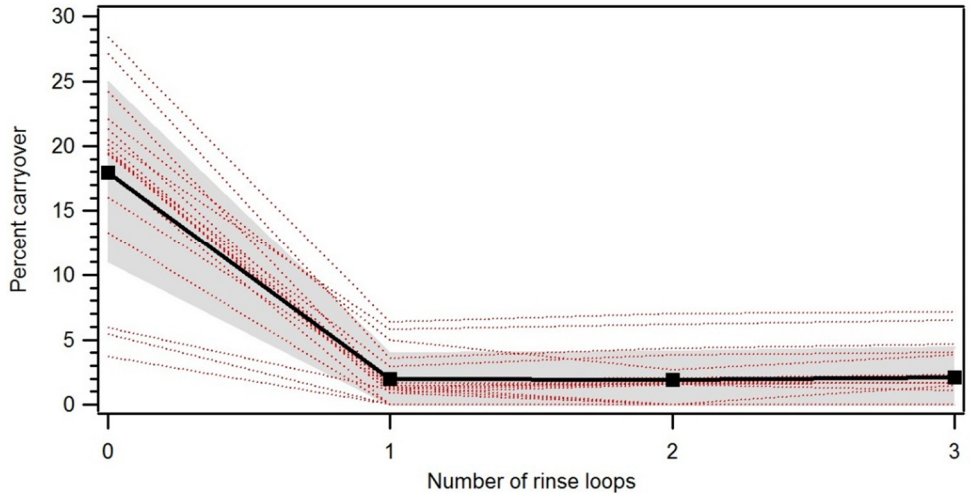

Figure 5.3. Injection-to-injection carryover tests for 18 representative compounds (dashed red lines) and overall average (solid black line with standard deviation in gray area). Compounds shown are a selection of deuterated alkanes (n-hexadecane-d_{34}, n-eicosaned_{42}, n-tetracosane-d_{50}, n-octacosane-d_{58}, n-dotriacontane-d_{66}), deuterated polycyclic aromatic hydrocarbons (dPAHs; phenanthrene-d_{10}, fluoranthene-d_{10}), straight chain acids (hexadecanoic acid, octadecanoic acid, eicosanoic acid), PAHs (phenanthrene, fluoranthene), and other atmospheric relevant compounds (5α-cholestane-d_6, 5α-cholestane, 2-pentadecanone, retene, benzophenone, and dihydro-5-octyl-2(3H)-furanone).

Given low carryover, injection of standards from two different reservoirs in the same injection cycle is possible. Injection of PAHs and alkanes in the same injection cycle from two different reservoirs was shown to yield the same FID response within reproducibility error as injection of each separately.

5.3.3. Multi-point calibration tests

Useful capabilities beyond the necessary requirements of the AutoInject were also tested, including injection of multiple loops of a standard, and manually loading the sample loop.

Multi-point calibrations were performed by injection of one to three loops of 2 ng/µL n-alkanes in chloroform followed by one loop of solvent (Fig. 5.4). The order of multi-loop injections within a "calibration cycle" was varied (1-2-3, 3-1-2, 2-3-1, etc.) with an injection of a single loop of standard in between each calibration cycle (the calibration cycles are shown connected by lines in Fig. 5.4). In each of the two series of calibration cycles (red squares and blue circles in Fig. 5.4), detector response is shown relative to the average response of single loop injections that were interspersed between the calibration cycles. Solvent blanks show the carryover to be less than 1% in these series. These calibrations lie on to the 1:1 line, as expected, with an overall slope of 1.01 ± 0.01 and an intercept of -0.01 ± 0.02, demonstrating the capability of using the AutoInject for generating multipoint calibration curves.

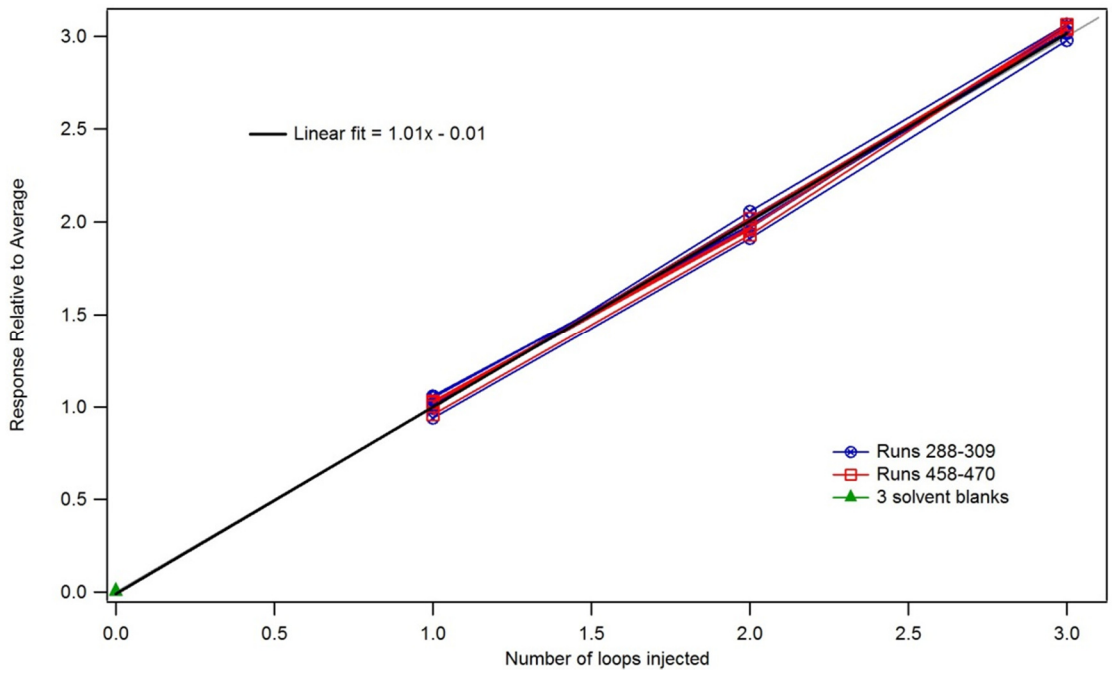

Figure 5.4. Demonstration of injection of multiple loops of straight chain alkanes (C_{15} to C_{35}) used as a multi-point calibration. Connected points are "calibration cycles" performed at two different times in the testing (blue and red, see Sect 5.3.2 for further discussion). Average FID detector response is shown relative to the average response for single loops injections interspersed between these calibrations. A linear fit (black line) is on top of the 1:1 line (gray line).

5.3.4. Manual loading tests

A manual injection port (Rheodyne) connected to one port of the 6-port selector (shown in Fig. 5.1) was used to manually fill the sample loop. This "pseudo-manual" injection method allows for injection of small amounts of any liquid without needing to fill a reservoir and showed similar reproducibility (σ = 2.3%) to automated injections. This capability extends the use of multi-point calibration methods by allowing for the occasional injection of significantly more concentrated or dilute standards than are necessary for automated running conditions (i.e. weekly pseudo-manual injections of a very dilute standard) without the need for an additional reservoir.

5.4. Conclusions

In this work, a new device and method for the reproducible injection of liquid standards, dubbed the "AutoInject," was developed. Multiple chilled reservoirs were connected to a 4.0 ± 0.1 μL sample loop via a 6-port selector (used to select a reservoir) and a 6-port-valve (used to load and inject the sample loop). Liquid injection with the AutoInject was shown to be highly reproducible, with a relative standard deviation of 1.5% and negligible carryover after one solvent rinse. Use of the 6-port selector allows for up to three different liquid standards plus a solvent rinse reservoir to be available for injection, either alternated or simultaneously. Each reservoir contains enough liquid for more than 150 injections. Furthermore, through injection of multiple loops, the AutoInject was shown to generate linear multi-point calibrations. The range of these calibrations can be extended beyond the range of standards in the reservoirs through the use of an injection port to manually load the sample loop.

Through these capabilities, the AutoInject is able to fulfill a variety of liquid injection needs. For instance, internal standards can be injected onto every sample, while a tracking standard can be used for regular calibration and/or multi-point calibrations. Multi-reservoir switching capabilities greatly extend the utility of the system, allowing for use of multiple standards in each run, such as co-injection of internal and calibration standards to be used for cross calibration or regular injection of two standards that cannot be stored together. Regular introduction of standards will greatly improve the quantitation of instruments such as the TAG and other instrumentation measuring a similar range of chemicals. Furthermore, waste generation is kept low in this system, minimizing ecological impact and personal hazard of calibration in the field.

The components of the AutoInject make it a highly versatile device that can be adapted to any instrument that relies on regular liquid injections for any purpose. Injection volume is variable through sample loop selection, loop load times are dependent on reservoir pressure, and reservoir volumes can be increased by using larger test tubes. The flexibility of the injection capillary allows for injection into any custom sample cell. In addition, the AutoInject is ideal for field use as it is compact, versatile, and relies on a minimum of moving parts for increased reliability.

In future studies using the TAG instrument, the AutoInject will be used for repeated injections of an internal standard, as well as regular multi-point calibrations and tracking standards. This system could also be used for regular injection of a derivatizing agent, greatly expanding the capabilities of in situ gas chromatography. The combined capabilities of this automated calibration system offers the potential to significantly improve the accuracy and extend the utility of TAG and other particle-phase in situ instrumentation.

5.5. Acknowledgements

Many thanks to A. Lambe, B. Williams, and T. Hohaus for field-testing a prototype system. This work was supported by the US Department of Energy STTR program, DE-FG02-05ER-86235 and DE-FG02-08ER-86335, and the National Science Foundation Atmospheric Chemistry Program Grants 0922562 and 0931934. GI was funded by the U.S. Environmental Protection Agency (EPA) Science to Achieve Results (STAR) program, Fellowship Assistance Agreement no. FP-91781901-0. This work has not been formally reviewed by EPA. The views expressed in this work are solely those of GI, and EPA does not endorse any products or commercial services mentioned.

Chapter 6

On-line derivatization for hourly measurements of gas- and particle-phase Semi-Volatile oxygenated organic compounds by Thermal desorption Aerosol Gas chromatography (SV-TAG)

Adapted from:

Isaacman, G., Kreisberg, N. M, Yee, L. D., Worton, D. R., Chan, A. W.H., Moss, J. A., Hering, S. V., and Goldstein, A. H.: On-line derivatization for hourly measurements of gas- and particle-phase Semi-Volatile oxygenated organic compounds by Thermal desorption Aerosol Gas chromatography (SV-TAG), Atmospheric Measurement Techniques, in press, 2014.

Abstract

Laboratory oxidation studies have identified a large number of oxygenated organic compounds that can be used as tracers to understand sources and oxidation chemistry of atmospheric particulate matter. Quantification of these compounds in ambient environments has traditionally relied on low time-resolution collection of filter samples followed by offline sample treatment with a derivatizing agent to allow analysis by gas chromatography of otherwise non-elutable organic chemicals with hydroxyl groups. We present here an automated in situ instrument for the measurement of highly polar organic semi-volatile and low-volatility compounds in both the gas- and particle-phase with hourly quantification of mass concentrations and gas-particle partitioning. The dual-cell Semi-Volatile Thermal desorption Aerosol Gas chromatograph (SV-TAG) with derivatization collects particle-only and combined particle-plus-vapor samples on two parallel sampling cells that are analyzed in series by thermal desorption into helium saturated with derivatizing agent. Introduction of MSTFA, a silylating agent, yields complete derivatization of all tested compounds, including alkanoic acids, polyols, diacids, sugars, and multifunctional compounds. In laboratory tests, derivatization is found to be highly reproducible (<3% variability). During field deployment, a regularly injected internal standard is used to correct for variability in detector response, derivatization efficiency, desorption efficiency, and transfer efficiency. Error in quantification from instrument fluctuations is found to be less than 10% for hydrocarbons and less than 15% for all oxygenates for which a functionally similar internal standard is available, with an uncertainty of 20-25% in measurements of particle fraction. After internal standard corrections, calibration curves are found to be linear for all compounds over the span of one-month with comparable response on both of the parallel sampling cells.

6.1. Introduction

For GC analysis, filter samples are typically reacted with a derivatizing agent following solvent extraction to form esters and ethers from hydroxyl groups, which suffer from poor transfer through GC columns due to hydrogen bonding interactions. Diazomethane, a common derivatizing agent, selectively converts acid groups into methyl esters and has been used to quantify acids and diacids in petroleum sources (Fraser et al., 1998; Schauer et al., 1999b, 2002), meat-cooking (Schauer et al., 1999a), and biological processes (Simoneit, 2005). Source profiles containing these derivatized acids in combination with hydrocarbons (including alkanes, hopanes, steranes, and polycyclic aromatic hydrocarbons), and biomass-burning tracers (Fraser and Lakshmanan, 2000; Ramdahl, 1983) have been used extensively in the analysis of particle matter in urban environments (Fraser et al., 1999; Hildemann et al., 1991; Kubátová et al., 2002; Lough et al., 2006). Alternately, derivatization can be performed using silylating agents, which exhibit broader reactivity, converting all OH groups into silyl esters and ethers. A large number of such reagents are available with minor variations in volatility and reactivity (Fluka Chemie AG, 1995), but the most commonly used in atmospheric applications is BSTFA (N,O-bis(trimethylsilyl)trifluoroacetamide), which yields trimethylsilyl (TMS) protecting groups as a derivatized product. Using BSTFA derivatization, many compounds have been identified in the laboratory controlled oxidation of common biogenically emitted compounds, including isoprene (Chan et al., 2010; Claeys et al., 2004; Kleindienst et al., 2009; Szmigielski et al., 2007b), some monoterpenes (Claeys et al., 2007, 2009; Jaoui et al., 2005), and some sesquiterpenes (β-caryophyllene: Jaoui et al., 2007); these tracers are regularly used for source apportionment in rural environments (i.e. Edney et al., 2003; Kleindienst et al., 2007, 2010; Kourtchev et al., 2005; Lewandowski et al., 2007; Offenberg et al., 2011; Zhang et al., 2009). Analysis by LC/MS allows measurement without prior derivatization of these and similar tracers, including compounds not observable by GC/MS (i.e. Gao et al., 2006; Surratt et al., 2008), but this technique is typically less comprehensive than derivatized GC/MS. LC analyses rely on careful selection of an elution solvent and, in most cases, quantification using electrospray ionization (ESI) MS, which is highly structurally dependent (Oss et al., 2010). Consequently the technique has focused primarily on high-molecular weight compounds and oligomerization processes (Hallquist et al., 2009), which cannot be well-studied using GC/MS.

Derivatization can be performed in situ without the need for solvent extraction and offline reaction. Docherty and Ziemann (Docherty and Ziemann, 2001) demonstrated that co-injecting BSTFA into a hot GC inlet alongside the sample efficiently derivatizes organic acids, which is thought to proceed by fast reactions occurring in the gas-phase after volatilization of the derivatizing agent and the analytes. Desorption of filters into a stream of derivatizing agent has been used in the analysis of atmospheric samples and laboratory oxidation experiments using both diazomethane (Sheesley et al., 2010) and silylating agents (Orasche et al., 2011; Ruehl et al., 2013; Zhang et al., 2013), but it is not yet a widely used technique.

Since most previous particle phase tracer measurements have relied upon offline analysis, the time resolution of sample collection has typically been on the order of several hours to several days. Through development of the Thermal desorption Aerosol Gas chromatograph (TAG), Williams and co-workers (Kreisberg et al., 2009; Williams et al., 2006) were able to measure non-polar and low-polarity tracers with hourly time-resolution, resulting in insights into particle formation pathways and source apportionment (Williams et al., 2010a, 2010b; Worton et al., 2011). A newer version of this instrument uses a high-surface area filter to collect gas- and

particle-phase low-volatility and semi-volatile compounds, considered here as any compounds expected to partition between the gas- and particle-phase under typical atmospheric conditions. (SV-TAG, described by Zhao et al., 2013b). This has expanded the utility of this instrument into measurements of gas-to-particle conversion pathways (Zhao et al., 2013b). However, while this instrument provides the highest available time-resolution for the measurement of organic tracer compounds, it has thus far been limited to hydrocarbons and less-polar oxygenates (oxygen-to-carbon ratio lower than 0.3 in most cases). Most known tracers for the oxidation of biogenic compounds are too polar to be measured by previous TAG instruments, often with an oxygen-to-carbon ratio between 0.5 and 1.

Here we describe modifications to SV-TAG to enable measurements of highly polar oxygenates with hourly time resolution through the inclusion of in situ derivatization. To validate the implementation, we demonstrate here that derivatization occurs to completion, has linear calibrations, and is reproducible, including a quantification of error.

6.2. Methods

6.2.1. SV-TAG overview

The instrument described in this work is shown in Fig. 6.1. Briefly, it is a modified Semi-Volatile Thermal desorption Aerosol Gas chromatograph (SV-TAG), a custom in situ instrument for quantifying gas- and particle-phase semi- and low-volatility organic compounds in the atmosphere (Kreisberg et al., 2009; Williams et al., 2006; Zhao et al., 2013c). SV-TAG measures organic compounds in both the gas- and particle-phase through collection into a custom collection cell containing a reusable, high-surface area metal fiber filter, the implementation and operation of which is described in detail by Zhao and co-workers (2013b). Two identical cells are used in parallel to collect simultaneous measurements with and without passing through a denuder to directly measure gas-particle partitioning. Thermal desorption of these compounds includes in situ derivatization and subsequent analysis by gas chromatography/mass spectrometry. Quantification of mass concentration and particle fraction is achieved with hourly time resolution. The implementation of two important novel instrument components are described and validated here: parallel dual-cell sampling system (Sect. 6.2.1.2) and in situ derivatization (Sect. 6.2.1.3).

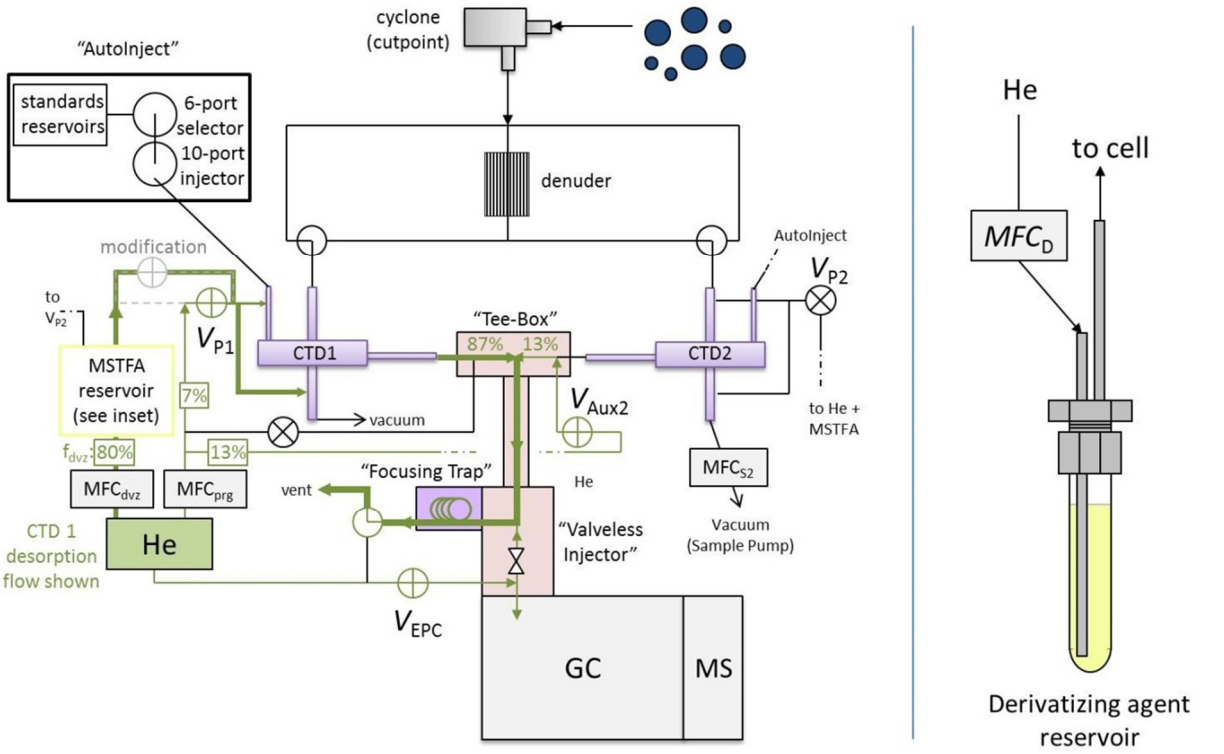

Figure 6.1. Schematic of dual-cell SV-TAG with in situ derivatization. Two parallel Collection and Thermal Desorption cells (CTD) simultaneously sample, one directly collecting gas plus particle phase compounds and one through a denuder that removes all gas phase compounds thus collecting only particles. Each sample is transferred in series to the GC/MS through a two-stage purge-and-trap thermal desorption process. Purge helium is saturated with derivatization agent by passing through a reagent reservoir (inset). Derivatized and underivatized desorption flows are controlled independently using MFC_{dvz} and MFC_{prg}, respectively. Liquid standards are regularly introduced by the AutoInject. After SOAS, derivatized flow paths were decoupled from non-derivatized flow paths (modification shown in dashed gray – path with flow added, path without flow removed). Green arrows show helium flow during desorption of CTD1 assuming $f_{dvz} = 0.80$, where width is approximate relative flow rate.

6.2.1.1. Description of SV-TAG and operation

Sample is collected at 10 L min^{-1} into a custom Collection and Thermal Desorption cell (CTD), which contains a high surface area metal fiber filter in a housing that can be cooled through forced air cooling, or heated. This filter CTD (F-CTD) quantitatively collects gas-phase compounds with a volatility as high as tetradecane, which is found almost entirely (> 99%) in the gas phase under ambient conditions (Zhao et al., 2013c). In sampling or analysis scenarios not requiring gas-phase collection, the original impactor CTD (I-CTD) can be installed, which can be more easily cleaned of nonvolatile contaminants such as black carbon. For field measurements, this work uses an F-CTD to collect gas-phase compounds. As noted, some lab experiments reported in this work utilizes the I-CTD. Samples can be collected directly or by first passing through a 500-channel activated carbon denuder (30 mm OD x 40.6 cm; MAST

Carbon), shown to efficiently remove gas-phase species (Zhao et al., 2013c). Comparison between undenuded ("total", gas plus particle) samples and denuded ("particle") samples provides a direct measurement of gas-particle partitioning of semivolatile compounds, an area of active research. Simultaneous dual-cell collection removes the need for interpolation between consecutive samples to quantify gas-particle partitioning. Gas-particle partitioning is measured using a denuder-difference technique, which is expected to result in lower error than a filter-difference measurement, as is discussed in detail by Zhao et al. (2013b). Briefly, filter-based removal of particles is expected to result in adsorption and possible re-volatilization of low-volatility gases resulting in measurement artifacts (Storey et al., 1995). Artifacts from sampling through a denuder, such as re-partitioning and subsequent removal of particle-phase compounds after the removal of the gas phase, have been suggested as a potential source of error (Kamens and Coe, 1997) but are minimized in this instrument by keeping denuder residence time low (~1 s).

Samples are transferred from the CTD to the GC/MS in a two-step thermal desorption process. First, compounds are desorbed from the cell into a stream of helium saturated with derivatizing agent, ramping between 30 ^{o}C and 315 ^{o}C over 8 minutes with relatively high helium flow rates (20-150 sccm two-stage desorption flow as described by Zhao et al., 2013b), and re-concentrated onto a focusing trap held at 30^{o}C through forced air cooling. This focusing trap, consisting of approximately 100 cm of metal, thick phase column (MXT-5, 0.53mm ID x 5µm phase thickness; Restek), is then heated to 315 ^{o}C for 5 minutes and back-flushed (~2 sccm) through a custom valveless interface (Kreisberg et al., 2014) onto the head of the GC column for analysis by mass spectrometry. For this work a non-polar column (Rtx-5Sil MS, 20m x 0.18mm x 0.18µm; Restek) was installed in a gas chromatograph (7890A; Agilent Technologies) modified to accommodate SV-TAG hardware, coupled to a commercially available mass spectrometer (5975C; Agilent Technologies). GC analysis of each sample occurs in 14 minutes, with a ramp of 23.6 ^{o}C min^{-1} from 50 to 330 ^{o}C (hold 2.2 min) and a helium flow rate of 1 sccm. Analysis is performed with custom software written in Igor Pro 6.3 (Wavemetrics).

Calibration and correction for run-to-run variability is performed through regular injection of liquid standards into the CTD using an automatic injection system ("AutoInject"). A 2-position valve containing a 4 uL sample loop is loaded from any one of multiple chilled reservoirs holding the standards (details in Chapter 5). For the dual-cell system, a 10-port 2-position valve containing two standard loops of the same volume was used, one for each cell. Both standard loops are loaded simultaneously with the same standard then injected at the same time into their respective cells immediately following sampling so that the samples and the internal standards are subjected to the same conditions. Approximately 25 isotopically labeled (mostly perdeuterated) standards representing most atmospherically relevant functional groups are introduced into every sample to correct for changes in instrument sensitivity and transfer efficiency. Calibrations are performed using more than 100 authentic standards spanning a broad range of functional groups and known tracer compounds. Calibration injections are performed approximately once every 6-8 hours at different concentrations to yield a multi-point calibration approximately every day or two. All chemical standards used were purchased at >98% purity from Sigma-Aldrich or C/D/N Isotopes.

6.2.1.2. Implementation of dual-cell system

Outfitting SV-TAG with a parallel dual-cell system provides flexibility for improved measurements and detailed method comparisons. Parallel cells are sampled simultaneously then analyzed in series; samples can be collected or analyzed in two different ways. In a typical field deployment, gas-particle partitioning is targeted by collecting samples with different treatments: one cell collects an undenuded sample (gas plus particle), while the other collects a denuded sample (particle only, all gas-phase species removed). The roles of the cells are swapped with each sample to avoid cell-to-cell bias. The dual-cell SV-TAG instrument can therefore directly measure gas-particle partitioning without any need for interpolation between points, a source of error in previous measurements of partitioning with TAG (Williams et al., 2010a; Worton et al., 2011; Zhao et al., 2013b). Alternately, when comparing methods of derivatization, each cell can be subjected to different treatments (i.e. derivatized and non-derivatized), allowing direct comparison between methods on ambient samples.

To ensure identical sample size of each cell, sample flow is regulated independently through two matching mass flow controllers (e.g. MFC_{S2} shown for cell 2). For thermal desorption, the cells are joined to the valveless interface via a custom "tee-box" manifold (Fig. 6.1) consisting of three 1/16" passivated VICI tees in a housing maintained at 300°C, which allows desorption of one cell at a time. During desorption of CTD1, used as an example in Fig. 6.1, helium from valve V_{P1} purges CTD1 while the purge valve on CTD2, V_{P2}, is closed to prevent accidental transfer of volatiles. Desorption helium flushes the collection cell from both above and below the internal collection filter, with the split between these flow paths governed by restricted capillaries as described by Zhao et al. (2013b); substantially more flow passes through the filter from below as shown by differences in arrow widths in Fig. 6.1. During desorption, helium also flows through auxiliary flow valve V_{Aux2}, which introduces flow downstream of CTD2 to prevent any desorption flow from CTD1 reaching CTD2. Using restrictive capillaries, a passive 1:7 split between the flow paths of V_{P1} and V_{Aux2} ensures that 13% of total purge flow goes through the auxiliary channel with the other 87% divided between derivatized and underivatized purge flow. This auxiliary flow prevents cell-to-cell contamination with >97% efficiency (Kreisberg et al., 2014).

Sampling and analysis of both cells occurs with hourly time resolution. A typical duty cycle consists of 22 minutes of sampling on both cells, injection of standards (2 min), two-step desorption (12 min) and chromatographic analysis (14 min) of CTD1, then desorption and analysis of CTD2 while collection of the subsequent sample begins after exactly 60 min. The valveless interface decouples the collection cells from the GC, allowing hourly time resolution by performing GC/MS analysis during CTD desorption and sampling.

6.2.1.3. Implementation of in situ derivatization

Derivatization is implemented by saturating helium with derivatizing agent, and using that saturated helium as a portion of the total CTD purge flow during thermal desorption. Desorption flow is controlled as the sum of helium flow through two mass flow controllers, MFC_{dvz}, which passes through the derivatizing agent reservoir (Fig. 6.1 inset), and MFC_{prg}, which does not. The reservoir consists of a standard 10 mm x 75 mm glass test tube with a custom modified compression fitting cap (Swagelok) with two 1/16" (1.6 mm) OD tubes inserted and soldered.

Helium is introduced at the bottom of the reservoir and bubbled through the derivatizing agent, ensuring saturation. This reservoir is the same as those used for liquid-flow of standards in the AutoInject, connected in reverse to provide gas-flow. A constant stream of derivatizing agent is thus introduced so that all compounds are volatilized from the CTD into an environment rich in reagent. Excess reagent passes through the focusing trap (Fig. 6.1) during desorption, minimizing the amount of unreacted derivatizing agent reaching the GC column. Derivatization occurs during the first 7 minutes of the two-step thermal desorption process, with the final minute purged without derivatizing agent to prevent introduction of reagent onto the GC column. Due to this purge method, only species less volatile than the derivatizing agent can be analyzed.

The quantity of derivatizing agent introduced to the sample can be optimized by controlling the fraction of total purge flow that is routed through the reagent reservoir, $f_{dvz} = MFC_{dvz} / (MFC_{dvz} + MFC_{prg})$. However, we describe here some limitations to this control. To prevent the derivatization of the cell that is not being desorbed, it is necessary to ensure that V_{Aux} does not receive any derivatizing agent, so, due to the 1:7 passive split, greater than 13% of total flow must be purge flow at all times. Maximum derivatization is therefore $f_{dvz} = 0.87$, though in practice $f_{dvz} = 0.80$ is rarely exceeded to ensure proper division of flows (illustrated in Fig. 6.1). To make certain that V_{Aux} gets flow from MFC_{prg} and because surface tension in the MSTFA reservoir prevents bubbling of <~2 sccm, neither purge nor derivatization flow are ever regulated to be between 0 and 4 sccm. The fraction of desorption flow that is derivatized at low total flows is limited by these constraints. For example, at 20 sccm, f_{dvz} cannot be less than 0.25 or greater than 0.75. Despite these limitations, independent control of derivatized and non-derivatized flow provides a useful tool for probing derivatization efficiency (demonstrated in Sect. 6.3.1) and optimizing amount of reagent used. In typical collection of ambient data, f_{dvz} is set to the practical maximum of 0.80 to ensure complete derivatization.

6.2.1.4. Selection of derivatization agent

Dozens of derivatizing agents exist in the literature to improve GC analysis for a wide variety of functional classes (Blau and Halket, 1993), but the most commonly used reagents for atmospheric organic tracer analysis are silylating agents, primarily BSTFA, due to their efficiency and broad reactivity (all OH groups). As previous research has demonstrated the utility of this agent for efficient, fast, gas-phase derivatization (Docherty and Ziemann, 2001), silylating agents in the chemical family of BSTFA are used in this work. MSTFA (N-methyl-N-(trimethylsilyl) trifluoroacetamide) has been used for the dual-cell SV-TAG presented here due its similar reactivity but higher reagent and byproduct volatility than BSTFA (Fluka Chemie AG, 1995), allowing all non-analytes to be efficiently purged across the focusing trap. MSTFA has an estimated vapor pressure approximately equal to decane (C_{10} alkane) so is sufficiently volatile to not impede the analysis of any species targeted by SV-TAG, which is limited in its sample collection to species no more volatile a C_{14} alkane (Sect. 6.2.1.1). The implementation of in situ derivatization presented in this work allows complete flexibility of derivatizing agent and an effective means for measuring derivatization efficiency, so use of derivatizing agents targeting specific volatilities or functional groups is an area for future exploration. Derivatizing reagents were purchased through Sigma-Aldrich (>98% purity, synthesis grade).

6.2.2. Laboratory evaluation methods

6.2.2.1. Derivatization efficiency

Derivatization efficiency was tested through repeated automatic injection of a complex mixture of polar and non-polar compounds containing most functional groups present in known atmospheric tracer compounds and spanning a wide-range of volatilities. Response of 43 oxygenated compounds introduced by an automated liquid standard injector is examined under varying derivatization conditions. To provide a conservative test, injected quantities of most constituents were larger than expected from atmospheric sampling. Total injected mass was 2.0 µg per analysis with approximately half the mass comprised of compounds containing functional groups expected to be derivatized (hydroxyl groups). For each compound, detector response relative to detector response under high derivatization conditions ($f_{dvz} > 0.5$) was measured for 8-10 replicate injections at 9 levels of MSTFA, from 1% to maximum derivatized flow ($f_{dvz} = 0.80$), taking into consideration the flow limitations discussed in Sect. 6.2.1.3. In considering derivatization efficiency, responses of all oxygenated compounds were normalized to the nearest *n*-alkane in volatility to correct for any fluctuations in detector sensitivity and matrix-dependent transfer. A complete list of compounds injected and their relative retention times is provided in Appendix D, including 5 oxygenated compounds with no OH groups such as ketones, 25 compounds with 1 OH groups, 8 compounds with 2 OH groups, and 5 compounds with 3 or 4 OH groups (which have been combined to improve statistics), spanning a volatility of tridecane (C_{13} alkane) to tetratriacontane (C_{34} alkane). While these compounds span the functionalities of most known tracers, the fate of some compound classes – i.e. hydroperoxides, organonitrates, and organosulfates – upon reaction with silylating agents is generally not well-understood. Further study is necessary to understand measurement of these atmospherically relevant compounds by thermal desorption GC/MS.

6.2.2.2. Derivatization reproducibility

Under laboratory conditions, reproducibility was measured through repeated injection of an atmospheric aerosol sample: a filter extraction of a high-volume (67 m^3 h^{-1}) quartz fiber filter collected in the Sierra Nevada Mountains of California as part of the Biosphere Effects on Aerosols and Photochemistry Experiment (Worton et al., 2011). The filter was collected during the day of 1 October 2009 for approximately 11 hours (total 726 m^3 of air sampled). One-half of the filter was extracted into 50 mL of methanol with 1 hour of sonication, blown dry under a gentle flow of nitrogen gas, and diluted to 10 mL. BSTFA was introduced as a derivatizing agent for 50 consecutive injections of one AutoInject loop (4 µL) into an I-CTD. In each injection, over 1400 peaks were identified above detection limits, most of which are expected to be polar compounds due to the extraction into a polar solvent. To measure reproducibility, each injection was compared to the average of all injections in the series.

Responses of internal standards over one-month of field data during two separate field campaigns are used to estimate error in correcting for run-to-run variability and reproducibility in real-world data. Dual-cell SV-TAG with derivatization was first deployed as part of the Southern Oxidant and Aerosol Study (SOAS) in the summer of 2013 in rural Alabama (32.903 N, 87.250 W, near Brent, AL,) in the Southeast U.S. The period of measurement was 1 June 2013 through 15 July 2013. Data presented here consist of calibrations and injections of internal

standards from the period of 4 June 2013 – 2 July 2013 ("Study 1"). Samples were collected with 1.5 hour time resolution through 18 June 2013, then hourly time resolution for the remainder of the field campaign. Following SOAS, minor instrument modifications were made to avoid exposing non-derivatized flow paths to derivatizing agent through the introduction of parallel flow paths and an additional valve (shown in Fig. 6.1 in dashed gray lines). Reproducibility and stability of the modified instrument was tested using internal standards injected on top of ambient samples collected in rural Brazil in a rainforest region from 14 February 2014 to 13 March 2014 (referred to hereafter as "Study 2"). The internal standard used during this period was an order of magnitude more dilute than that used during Study 1. MSTFA was used as the derivatizing agent during both campaigns. To accommodate long-term drifts in detector sensitivity and significantly changing sample matrices, reproducibility in field data is quantified using ratios of internal standards, not simply response, the reasons and implications of which are discussed in Sect. 6.3.2. The internal standards used for correcting run-to-run variability in these deployments were: perdeuterated C_{14}-C_{32} *n*-alkanes (even carbon numbers only), decanoic acid-d_{19}, tetradecanoic acid-d_{27}, hexadecanoic acid-d_{31}, octadecanoic acid-d_{35}, pentadecanol-d_{31}, cholesterol-d_6 (Study 1 only), hexanedioic acid-d_4, 3-hydroxy pentanedioic acid-d_5, glucose-$^{13}C_6$ (Study 2 only), and pentaerythritol-2-^{13}C.

6.3. Results and discussion

Effective, quantitative derivatization must be shown to be complete and reproducible, with linear or predictable response. Dual-cell SV-TAG with derivatization was shown to meet these requirements through a series of laboratory tests, as well as field deployment to the Southeastern U.S. and rural Brazil.

6.3.1. Derivatization efficiency

Derivatization is shown in Fig. 6.2 as a function of quantity of derivatization agent introduced, and is found to occur to completion during normal instrument operation. In a scenario of incomplete derivatization, a small reduction in reagent would be expected to reduce the response of all derivatized compounds in proportion to the number of OH groups on each compound. For a large number of oxygenated compounds injected into dual-cell SV-TAG, a reduction in signal is not observed when fraction of derivatizing agent, f_{dvz}, is reduced significantly from its maximum (here set at 0.80). For all 43 compounds shown, detector response leveled off by f_{dvz} = 0.50 (50% derivatized purge flow) suggesting maximum possible derivatization, and in most cases f_{dvz} = 0.30 was a sufficient fraction of derivatization flow to maximize signal. Increased derivatization flow also decreased variability in detector response, suggesting more reproducible derivatization.

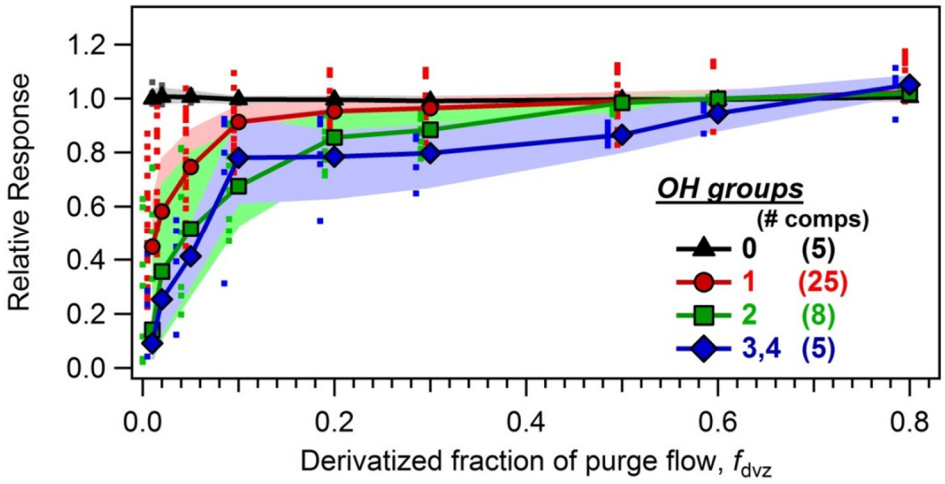

Figure 6.2. Response of 43 oxygenated compounds dependent on quantity of MSTFA introduced, normalized to the average response of each compound at f_{dvz}> 0.5. Solid lines and symbols are the median relative response of all injections at each derivatization level with the interquartile range shown as the shaded area. Compounds used are listed in Appendix D. Average response of each compound at each derivatization level is shown as a small dot of the appropriate color (slightly offset to the left) to show spread of the data.

With severely reduced quantities of derivatizing agent, detector response was greatly diminished due to incomplete reaction because these compounds cannot be measured by traditional gas chromatography in the absence of derivatization. Compounds containing more hydroxyl groups are more sensitive to a dramatic reduction in f_{dvz}, as is expected from stoichiometric limitations caused by consumption of the reagent. The injected mixture contained ketones with no hydroxyl groups to test for possible formation of a silylated enol. However, the analysis of these compounds (Fig. 6.2, black triangles), as well as hydrocarbons, was not found to be adversely affected by the introduction of derivatizating agent. Previous work (Orasche et al., 2011) has shown improved recovery of polycyclic aromatic hydrocarbons using derivatization, but that was neither observed nor specifically tested here.

6.3.2. Reproducibility of derivatization

Derivatization was found to be highly reproducible in a laboratory setting through the repeated injection of a complex mixture. A methanol extraction of a filter collected in the Sierra Nevada Mountains of California in the summer of 2009 was injected 50 consecutive times into an I-CTD to quantify the reproducibility of derivatization of an atmospherically relevant complex mixture (Fig. 6.3). Figure 3a shows a comparison of all peaks in one of these injections to the average areas, which is found to deviate from unity by less than 1%, with a correlation coefficient of 0.998, across approximately four orders of magnitude in peak area. These correlation metrics are consistent across all 50 injections (Fig. 6.3b), with a slope almost always within 2% of unity and very high correlation coefficients (r^2 > 0.994). Given a 1-3% reproducibility error of the AutoInject (Chapter 5), repeated derivatization of an identical mixture occurs with very little or no variability.

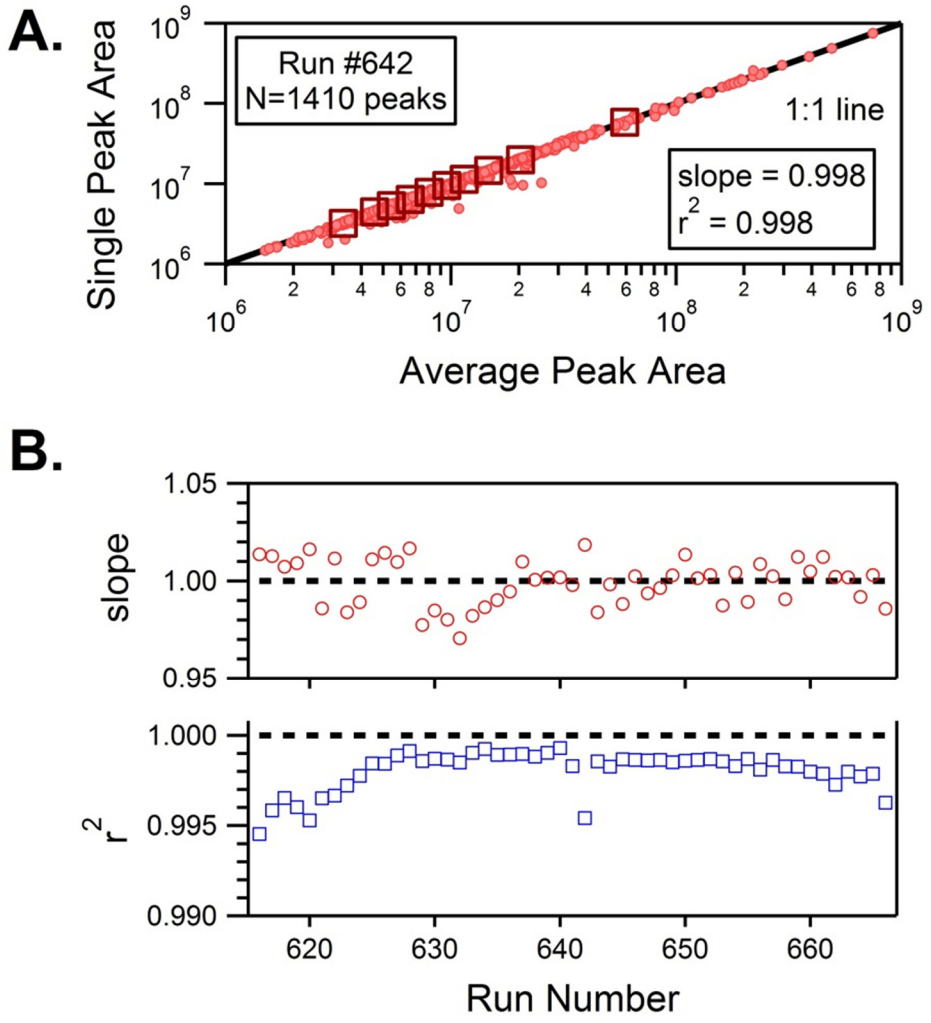

Figure 6.3. Comparison of reproducibility of injection and derivatization of 50 consecutive injections of a methanol extraction of a filter collected in the Sierra Mountains of California. Responses of 1410 peaks in each injection were compared to the average response of each peak. This comparison is shown for (A) the injection in the middle of the series, where pink circles show all peaks compared and red squares show peaks binned by size into 10 equal bins (140 peaks each). (B) The slope (red circles) and correlation coefficient (blue squares) is shown for all comparisons in the series. Perfect correlation (slope = 1, r^2 = 1) is shown as a dashed line

Satisfied with > 98% reproducibility under ideal laboratory conditions, reproducibility under more difficult field conditions was assessed using approximately one month of internal standard injections on top of ambient samples during two periods of data collection – Study 1 in the southeastern U.S. and Study 2 in a rural Brazil rainforest region. Direct reproducibility is difficult to accomplish due to non-ideal working conditions in the field (i.e. temperature fluctuations, power outages, high humidity, drifts in detector sensitivity) and significant changes in sample loading due to atmospheric variability, which is known to affect transfer efficiency.

Reproducibility is instead achieved by correcting changes in derivatization and sample transfer efficiency by using isotopically labeled internal standards injected into each sample. The extent to which derivatization is reproducible and these errors can be corrected is quantified by comparing internal standards to each other, e.g. in a perfect correction scenario all compounds suffer the same changes in efficiency, so the ratio of any two compounds is unchanging and derivatization can be said to be reproducible, or at least predictable and therefore quantifiable. In a non-ideal correction scenario, some fluctuation of this ratio is expected, so correction/reproducibility error is quantified as the relative standard deviation (σ) from the average of a ratio of two internal standards. The error from various possible correction scenarios is presented in Fig. 6.4 and Table 6.1 using response of internal standards injected on top of a wide range of organic loadings.

#	Internal standard used	Standard deviation	
	oxygenate-to-oxygenate		
		Study 1	*Study 2*
1	**Random *n*-acid (*n*-acids only)**	**13.5%**	**12.5%**
2	**Nearest *n*-acid (*n*-acids only)**	**10.0%**	**8.6%**
3	Nearest *n*-acid[1]	32.5%	21.1%
4	Similar number of OH groups[2]	36.7%	20.4%
5	Nearest oxygenate	38.0%	24.0%
6	Octadecanoic acid[1]	36.0%	27.3%
	oxygenate-to-hydrocarbon		
7	Octadecane	61.5%[3]	36.7%[3]
8	Nearest alkane[1]	61.1%[3]	32.5%[3]

[1]Cumulative distribution of error shown in Appendix D; [2]nearest oxygenate with same number or ±1 OH group; [3]strongly non-Gaussian error, poorly represented by standard deviation

Table 6.1. Standard deviation in error for correction of run-to-run variability of oxygenates using a variety of possible scenarios for pairing analytes to internal standards. Full distribution of error for scenarios in bold are shown in Fig. 6.4. In all cases, "nearest" refers to closest in volatility.

Figure 4 highlights the correction scenarios that apply to operational conditions typically used in deployment of SV-TAG with derivatization. Given the wide range of alkanes present in the internal standard, perdeuterated alkanes that are close in volatility can be used to correct variability in response to hydrocarbon analytes. The ratio of one perdeuterated alkane (representing a hydrocarbon analyte) to the next closest in volatility has a relative standard deviation of 8.4% (Fig. 6.4a) during Study 1 and 11.2% during Study 2. More than 80% of all points fall within these standard deviations. Transfer efficiency can change dramatically between 2 carbon numbers for species of high molecular weight, so a large fraction of this error is due to real differences in response caused by variations in sample loading; when considering only hydrocarbons not affected strongly by transfer efficiency changes (smaller than C_{28}), such as sesquiterpenes, standard deviation of error for Study 2 is reduced to 6.1%.

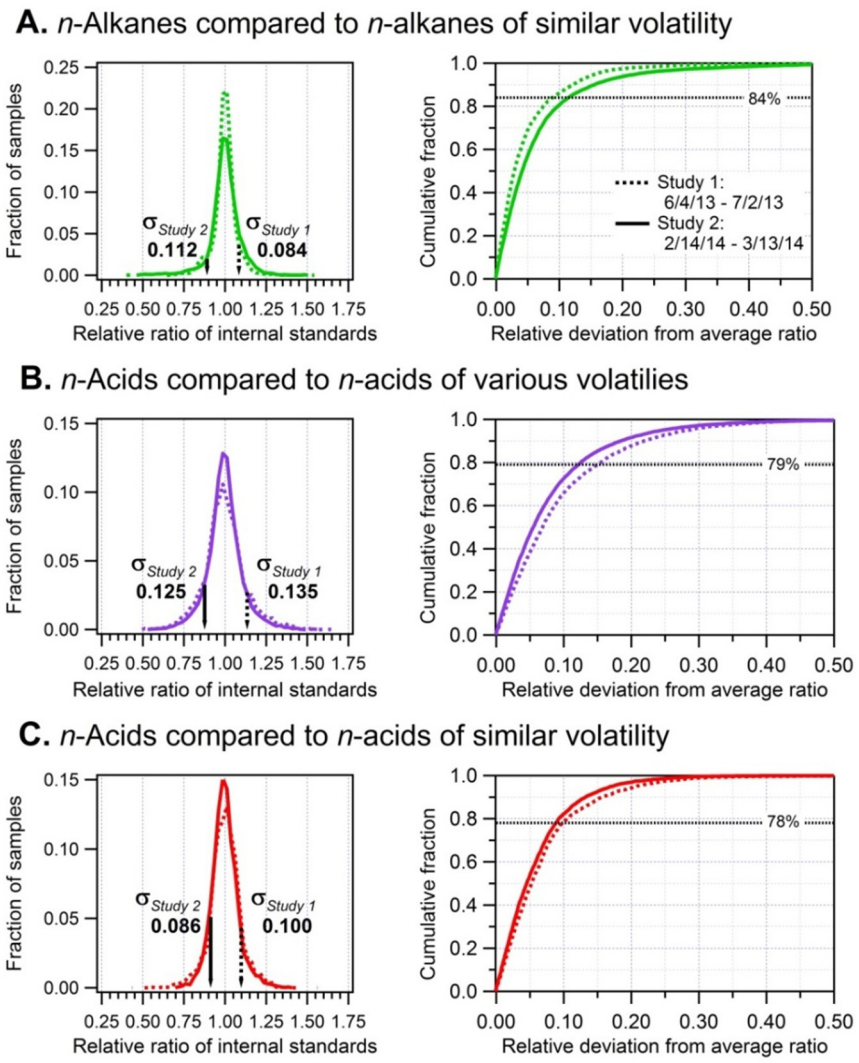

Figure 6.4. The ratio of two internal standards relative to their average ratio, with relative standard deviations shown. Distributions of error from two periods of field data collection (dashed: Study 1, solid: Study 2) are shown for scenarios most closely representing operating conditions of TAG: (A) correction of alkanes using alkanes with similar volatilities to quantify precision in hydrocarbon measurement, (B) correction of alkanoic acids using randomly assigned alkanoic acids to quantify precision in most oxygenate measurements, and (C) correction of alkanoic acids using the alkanoic acid closest in volatility to quantify precision in analytes for which a very similar internal standard is present. In all cases, approximately 80% of all samples fall within the standard deviation of the average (exact percentage in each scenario shown as dotted line).

Error in correction for run-to-run changes in derivatization efficiency depends strongly on available internal standards due to its dependence on functionality. In typical field deployment of TAG, most atmospherically relevant oxygenated compound classes that can be detected by thermal desorption, derivatized GC are represented by at least one internal (isotopically labelled) standard: mono-carboxylic acids, di-carboxylic acids, polyols, sugars, and hydroxy acids. Most

of these compound classes are limited to only one internal standard due to cost and availability of isotopically labelled standards, but several perdeuterated *n*-alkanoic acids are present. The ratio of one *n*-alkanoic acid to another with no regard to volatility therefore serves as a reasonable model for error in correction of run-to-run variability of identified compounds and therefore applies broadly to most oxygenated compounds measured in typical SV-TAG operation. Figure 6.4b is the result of assigning each of 4 perdeuterated *n*-acids randomly to each other 10 times. Based on this representative scenario, the measurement precision is found to have a standard deviation of 13% for any compound for which a reasonably chemically similar internal standard is used under normal operating conditions. This is higher than the error inherent in hydrocarbon correction as it includes variability in derivatization efficiency, an additional source of error. To reduce error, compounds may be targeted with specific internal standards (i.e. pentaerythritol-2-^{13}C to accurately quantify 2-methyltetrols, a common biogenic oxidation product). Error for such a targeted compound is best modeled by correcting *n*-acids using the next nearest n-acid in volatility (Fig. 6.4c) to represent correction using an internal standard that is both chemically and structurally similar. This scenario has an error of approximately 10% in correction for run-to-run variability. In both scenarios shown for correction of oxygenates, standard deviations encompass nearly 80% of the error (dotted lines in Fig. 6.4).

The scenarios for error in Fig. 6.4 are those that apply to most compounds under typical operation of TAG. However, error depends on the availability of chemically similar standards, so estimates of error have been provided in Table 6.1 for various scenarios representing possible selections of internal standards (scenarios highlighted in Fig. 6.4 are shown in bold).

In the absence of a wide array of internal standards, a small range of oxygenates can be used with similar functionality (scenario 4) or volatility (scenarios 3, 5) with an error of 20-30%. Note that based on scenario 3, an oxygenated compound can be measured with a precision of ~20% even in the absence of definitive identification, providing an estimate of error in cases where absolute concentrations are unnecessary such as comparison between parallel sampling cells. If necessary, a single oxygenate can be used to correct simply for overall changes in derivatization efficiency (scenario 6), with a corresponding increase in error (30-40%). However, correction of oxygenates using hydrocarbon internal standards (scenarios 7, 8) results in a significantly non-Gaussian distribution of errors and very high-error (see Appendix D for cumulative error distribution), indicating that there are some relevant changes in derivatization efficiency that must be corrected for with oxygenated internal standards. For scenarios involving correction using relatively similar internal standards, error is found to be similar across both instrument deployments despite varying environmental conditions owing to the use of a large suite of internal standards. However, error estimates diverge under scenarios modeling the use of less similar internal standards, with some reduction in error following instrument modifications between campaigns. This highlights the importance of careful internal standard selection and the benefits of employing atmospherically relevant internal standards.

6.3.3. Quantitation

Linear response of derivatized compounds within the range of expected analyte abundances is necessary for accurate quantification of oxygenated tracer compounds. A suite of over 100 authentic standards was injected at various levels 2 to 3 times per day throughout Study 1 during the SOAS field campaign. Daily schedules typically included injection of a single AutoInject

loop of "concentrated" standard (12-32 ng of each compound) and one injection of 1 to 3 loops of "dilute" standard (1.2-3.2 ng of each compound per loop), with occasional injections of 2 loops of concentrated standard. Once corrected for variability using internal standards (per Sect. 6.3.2), calibration curves were found to be linear in nearly all cases. Examples of 4 calibration curves spanning several atmospherically relevant functional classes are shown in Fig. 6.5, with quantities injected that are approximately in the range expected in the atmosphere for typical sample sizes, and instrument response normalized to the response of one loop of concentrated standard. Several correction scenarios shown in Fig. 6.4 are represented: correction of a hydrocarbon using a hydrocarbon of similar volatility (6.5a: hexadecane corrected using hexadecane-d_{34}), correction of an oxygenate using an oxygenate of similar functionality (6.5b: ketopinic acid, a mono-carboxylic acid, biogenic oxidation product, corrected using tetradecanoic acid-d_{27}) and correction of an oxygenate (alkanoic acid) using a nearly identical oxygenate (6.5c: tridecanoic acid corrected using tetradecanoic acid-d_{27}, 6.5d: erythritol corrected using pentaerythritol-2-^{13}C).

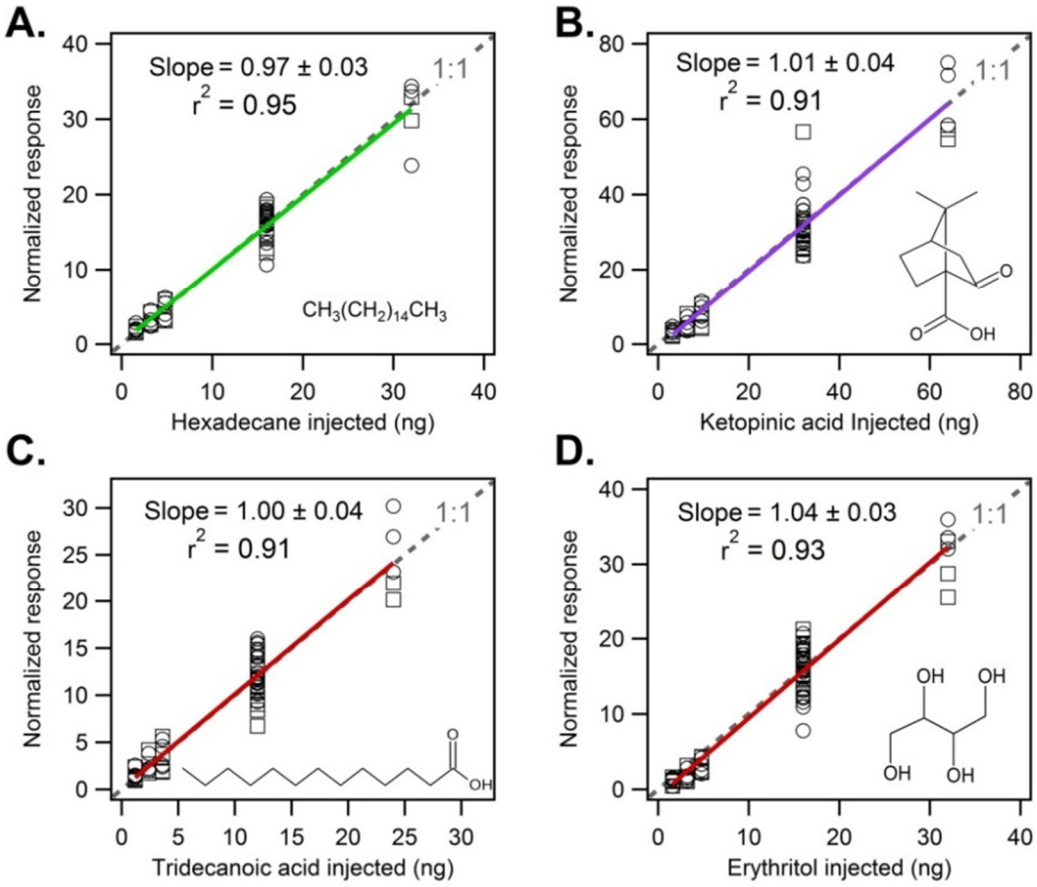

Figure 6.5. One month of multi-point calibrations of sample compounds during Study 1 (both cells shown as circles and squares). Response is corrected using a structurally similar deuterated internal standard injected into every run, as is standard operating procedure to correct for run-to-run variability (line color represents the scenario of correction from Fig. 6.4). The average response of the instrument to one loop of concentrated standard is used to normalize all data to demonstrate 1:1 linearity.

Calibrations are in all cases linear and spread in the data is typically limited to 10-20%, within the precision error for run-to-run variability correction estimated by detailed error analysis in Sect. 6.3.2. Following correction by internal standards, both cells fall on the same calibration curves because any difference in sensitivity to a compound between the cells is mirrored in the sensitivity to a chemically similar internal standard. Consequently, uncertainty in mass concentrations is dominated by the correction for instrument and derivatization variability. As the ratio of both cells, uncertainties in variability correction combine to yield approximately 20-25% uncertainty in particle fraction. Appendix D contains a discussion of propagation of error in mass calibration, equalization between the two cells, and particle fraction, as well as the equations necessary to calculate uncertainty on a point-by-point basis.

Sensitivity to compounds is dependent on functionality, such that limits of detection and quantitation are compound specific. Calibrations shown in Fig. 6.5 extend down to approximately 1-2 ng injected mass, though in most cases analyte signal at this level is still 10-100 times chromatographic background signals. As an example, erythritol as shown in Fig. 6.5d during Study 1 is 20 times larger than background at 1.6 ng and during Period 2 is 10 times background at 0.6 ng. Consequently, though limits of detection must be calculated individually for each analyte of interest, a reasonable average estimate is on the order of tenths of a nanogram, though in some cases it is lower than 0.1 ng. When operating with hourly time resolution, sample is collected for approximately 20 minutes at 10 lpm, yielding conservative limits of detection of 1-2 ng m^{-3} (~0.1 ppt), which is below measured concentrations for most analytes of interest. However, detection limits can be arbitrarily scaled through increasing or sacrificing sampling time and therefore time-resolution. Though sample and injected standards sit on Cell 2 throughout desorption of Cell 1, there is no indication of a loss of volatile compounds. Carryover of sample from one cell into the other cell or subsequent sample occurs independent of volatility at less than 3% (Kreisberg et al., 2014).

6.3.4. Sample Field Data

A sample of the data available using dual-cell SV-TAG with derivatization is shown in Fig. 6.6, a short sample timeline from the SOAS field campaign. Three days of hourly concentrations of gas- and particle-phase pinic acid, a product of the atmospheric oxidation of α-pinene, demonstrates clear diurnal variation, as well as many short spikes in concentration. These features are indicative of atmospheric and biological processes that are occurring with higher time-resolution than is available using traditional measurement techniques.

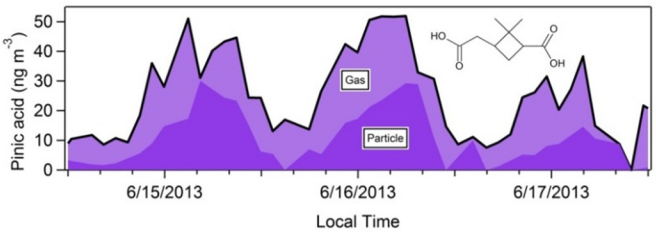

Figure 6.6. Sample final data of pinic acid, a tracer for the oxidation of α-pinene, a common monoterpene. Gas-phase concentration (light purple) is measured as the difference between total concentration (black line) and particle-phase concentration (dark purple).

6.4. Conclusions

We present here an instrument for hourly measurement of both gas- and particle-phase oxygenated organic compounds in the ambient atmosphere. Though quantification of organic tracers has provided significant insight into atmospheric oxidation chemistry and aerosol formation pathways, traditional measurement techniques require sample times of several hours to several days, as well as offline sample processing. By modifying SV-TAG, a field deployable instrument, to include on-line derivatization, known and novel organic tracers can be quantified hourly in situ. Inclusion of a dual-cell, parallel sampling system allows simultaneous measurement of both gas- and particle-phase components through a denuder difference method. Automation of the dual-cell SV-TAG with derivatization provides improved time-resolution over traditional measurement techniques with decreased operator interaction and offline sample preparation, minimizing exposure to derivatizing agent and solvents.

Derivatization is found to be reproducible, complete, and linear in all laboratory and field tests performed. Field-deployable, in situ derivatization of polar compounds is found to be robustly quantifiable within approximately 10-20% by using internal standards to correct for variability in detector sensitivity and derivatization efficiency (range represents similarity of internal standard to analyte). Non-polar compounds can also be measured by this instrument with an error of <10%. This quantification of error is based on real-world data with significantly changing background matrixes (polluted days, clean days, denuded samples, etc.) and is robust across two different field campaigns. Absolute error in concentrations for a given compound depends strongly on available standards. For compounds with authentic or nearly identical chemical calibration standards, error is expected to be limited to correction for derivatization and transfer efficiency as discussed in this work (i.e. 15%), while error will increase as chemical similarity decreases between the analyte of interest and the chemical surrogate used for quantification. Quantification by chemical surrogates is estimated to yield errors between 33% and 50% (Jaoui et al., 2005) and is therefore expected to be the main source of error for this instrument, as is the case for traditional offline methods.

Atmospheric phenomenon often occur on the scale of hours (i.e. break-up of inversion layers, rain events, etc.), so the time resolution provided by dual-cell SV-TAG with derivatization will enable a far more detailed analysis of atmospheric chemical pathways with similar accuracy as lower-time-resolution techniques. Furthermore, direct, hourly measurement of gas-particle partitioning will provide observational constraints to assess the relative importance of a wide variety of partitioning pathways that have been studied in great detail in laboratory experiments. Future exploration of alternative derivatization agents is also expected to expand the utility of this instrument.

6.5. Acknowledgements

Instrument development work was supported by the US Department of Energy SBIR/STTR under grant DESC0004698. GI is supported by the National Science Foundation (NSF) Graduate Research Fellowship (NSF Grant: DGE 1106400). Data collected as part of the SOAS field campaign was funded by NSF Atmospheric Chemistry Program Grant #1250569. Internal standard reproducibility data collected in Brazil was thanks to the NSF Atmospheric Chemistry Program Grant #1332998. Filter collection for the BEARPEX campaign was funded by NSF Atmospheric Chemistry Program Grant #0922562

Chapter 7

Gas-Particle partitioning and temporal variability of biogenic oxidation products in rural organic aerosol

Abstract

Most of the reactive carbon in the atmosphere is emitted as biogenic volatile organic compounds, which oxidize to form secondary organic aerosol (SOA). A major fraction of atmospheric particulate matter is thought to form through anthropogenic influence on the oxidation of biogenic emissions, but little is understood about the chemical pathways dominating this interaction. In this work we quantify known biogenic oxidation products with hourly time-resolution, many for the first time, using a novel instrument during two field campaigns in rural locations: the Southeastern Oxidant and Aerosol Study (SOAS) in 2013 in the southeastern U.S., and GoAmazon2014/5 in Amazonia, Brazil downwind of Manaus. A Semi-Volatile Thermal desorption Aerosol Gas chromatograph (SV-TAG) was coupled with in situ derivatization to investigate the oxidation chemistry of isoprene and monoterpenes and provide unprecedented direct measurements of the gas-particle partitioning of their oxidation products. Concentrations of oxygenated compounds in both the gas- and particle-phase are highly variable, forming quickly during periods of high precursor concentrations and being removed efficiently by wet deposition. 2-Methyltetrols, known isoprene oxidation products, are found to account for an estimated 20-35% of isoprene-derived SOA, which comprises typically 5-20% of total organic aerosol in both locations. Other isoprene products, i.e. C_5 alkene triols, are also observed in both regions to comprise a large fraction of isoprene SOA. Oxidation products of α-pinene (pinic, pinonic, hydroxyglutaric acids, etc.) are measured in relatively high concentrations in the southeastern U.S., but are observed at substantially lower concentrations in Amazonia. Formation of SOA from isoprene is found to be dependent on sulfate concentrations, at least in part due to the indirect effect of sulfate enhancement of particle-phase liquid water. Using SV-TAG, the gas-particle partitioning of 65 biogenic oxidation products is measured hourly, including for many compounds that have not yet been unambiguously identified, and found to be poorly explained by a traditional thermodynamic equilibrium partitioning model. Most measured oxygenated compounds, regardless of volatility, are observed for the first time to have a gas- as well as particle-phase component, in contrast with the typical assumption applied to source attribution and modeling studies that known tracer compounds are primarily in the particle-phase. Small, highly oxidized species are observed to have a much higher particle fraction than expected, so solubility of organic compounds is proposed as an important factor in particle uptake of organics in relatively wet environments. Anthropogenic emissions therefore directly impact organic aerosol composition through both the enhanced formation and increased particle fraction of biogenic oxidation products due to increased particle-phase water.

7.1. Introduction

Most reactive carbon emitted globally to the atmosphere is biogenic, consisting predominately of isoprene, monoterpenes, and other terpenoid compounds (Guenther et al., 1995). Reactions of

these gas-phase species with atmospheric oxidants yield lower-volatility oxygenated gases that condense to form secondary organic aerosol. This SOA comprises the majority of atmospheric particulate matter and is typically highly oxidized, but measurements of specific components have been very limited, especially with time resolution adequate to understand atmospheric phenomena (Goldstein and Galbally, 2007; Jimenez et al., 2009; Zhang et al., 2007). Observations have determined that even in urban areas, ambient particle-phase carbon is mostly biogenic or non-fossil in origin (Hallquist et al., 2009; Hodzic et al., 2010), but often correlates with combustion-related compounds (Brock et al., 2003; Weber et al., 2007). This interaction between biogenic carbon emissions with anthropogenic pollutants may be responsible for most global secondary organic aerosol (SOA) (Spracklen et al., 2011), so recent work has focused on reaching a detailed understanding of the oxidation pathways of biogenic compounds under varying reaction conditions.

As the dominant global biogenic volatile organic compound (BVOC), isoprene oxidation has been a particular focus of laboratory study. Following oxidation by hydroxyl radical in the gas-phase and formation of the peroxy radical, isoprene in the presence of oxides of nitrogen (NO_x) can react with NO to form methacrolein, which, proceeding through methyl peroxyacetyl nitrate (MPAN), has been proposed to form a highly reactive epoxide, methacrylic acid epoxide (MAE) (Lin et al., 2013). Alternately, instead of reaction with NO and NO_2, the isoprene peroxy radical can react with HO_2 to form isoprene hydroxyhydroperoxide (ISOPOOH), which goes on to also form an epoxide, isoprene epoxydiol (IEPOX) (Chan et al., 2010; Paulot et al., 2009; Surratt et al., 2010). Secondary organic aerosol can form through either channel – reaction with NO_x or reaction with HO_2 – via the uptake of epoxides into the particle and subsequent ring-opening reactions to yield a suite of highly oxygenated compounds (Lin et al., 2013, 2012; Nguyen et al., 2014a), though reaction with HO_2 is expected to dominate in rural and remote regions. The impact of anthropogenic pollutants can be studied in part through ratios of products: i.e. 2-methylglyceric acid is formed through reaction with NO_x (Surratt et al., 2006; Szmigielski et al., 2007b), while dominant products from IEPOX uptake are two "2-methyltetrols" (2-methylerythritol and 2-methylthreitol; structures in Fig. 7.2) and three "C_5 alkene triols" (*cis,trans*-2-methyl-1,3,4-trihydroxy-1-butene and 3-methyl-2,3,4-trihydroxy-1-butene; structures in Fig. 7.2) (Claeys et al., 2004; Kleindienst et al., 2009; Kourtchev et al., 2005; Wang et al., 2005). The production pathway of C5 alkene triols is poorly understood, so there is no mechanistic understanding of the ratio between these compounds and 2-methyltetrols. However, NO-HO_2 competition between formation of ISOPOOH and methacrolein is only one of several potential sources for anthropogenic influence.

SOA formation from isoprene oxidation through reaction with HO_2 may be altered by environmental conditions affecting reactions of IEPOX. Uptake of IEPOX into the particle is followed by acid-catalyzed ring-opening reaction with a nucleophile, which can be water to yield a 2-methyltetrol, sulfate to yield an organosulfate, another molecule to yield an oligomer, etc. The formation, as well as the composition and volatility, of IEPOX-derived SOA is therefore dependent on inorganic particle composition as well as on particle acidity and liquid water content (Worton et al., 2013) – two properties strongly driven by anthropogenic emission of SO_2 and inorganic ions (Carlton and Turpin, 2013). However, these relationships are poorly constrained. Increased acidity has been shown to facilitate formation of high-molecular-weight oligomers (Gao et al., 2004b) and organosulfates (Surratt et al., 2008), but has also recently been shown to be unnecessary for the uptake of IEPOX (Nguyen et al., 2014a) provided the particle contains a sufficient nucleophile concentration. Furthermore, though oligomers (Gao et al.,

2004a; Kalberer et al., 2004; Szmigielski et al., 2007b) and organosulfates (Hatch et al., 2011; Surratt et al., 2008; Worton et al., 2013) have been observed to be an important component of SOA in some environments, observations of high-molecular-weight products are still relatively sparse and stymied by their thermal and chemical decomposition through most analytical techniques. Formation of these compounds, though, is a potential pathway for anthropogenic influence on SOA formation from isoprene and other BVOCs and is expected to be exhibited in part through their effects on particle volatility.

Anthropogenic influence on IEPOX uptake and BVOC oxidation is studied in this work through data from two sites with a mixture of high anthropogenic and biogenic emissions, where the complex chemical interactions between these compounds are particularly relevant. In the southeastern U.S., aerosol concentrations have a strong summer maximum (Goldstein et al., 2009) consistent with the dominance of biogenic carbon, but also correlate well with tracers for combustion (Weber et al., 2007). The Southeastern Oxidant and Aerosol Study (SOAS) in northern hemisphere summer of 2013 was designed to elucidate these relationships in the heavily forested and highly populated southeastern U.S., where up to half of biogenic SOA is controlled through the impacts of anthropogenic sulfate, nitrogen, and combustion emissions (Carlton et al., 2010). The chemical influence of anthropogenic emissions on biogenic SOA formation was additionally targeted through the GoAmazon2014/5 field campaign in Amazonia, Brazil, where the large city of Manaus provides an ideal natural experiment using measurements sites upwind, inside, and downwind of the city. Emissions of reactive carbon are dominated throughout Amazonia by biogenic compounds (Martin et al., 2010) and during the wet season atmospheric conditions are amongst the most pristine the world, with similar particle properties and loadings as the remote ocean (Andreae, 2009). This biogenic environment gets modified by Manaus with high emissions from combustion in the city that influences chemistry of downwind sites (Kuhn et al., 2010; Trebs et al., 2012). The influence of this isolated, developing city is used in this campaign to study the effect of anthropogenic emissions on otherwise natural aerosol.

Many of the compounds known to form through BVOC oxidation with and without anthropogenic influence are semi-volatile – they are expected to exist in both the gas and particle phase under typical ambient conditions. Under thermodynamic equilibrium between the gas and particle phase, the volatility and the gas-particle partitioning of a compound can be considered in terms of saturation concentration C^0, the ambient loading of organic aerosol at which a compound is partitioned evenly between the particle and gas phase (Donahue et al., 2006; Odum et al., 1996; Pankow, 1994). Predicted particle fraction, F_P, of a compound can be calculated as:

$$F_{P,predicted} = \left(1 - \frac{\gamma C^0}{C_{OA}}\right)^{-1} \quad \text{Eq. 7.1}$$

where C_{OA} is the mass of ambient organic aerosol and C^0 is calculated from the temperature dependent vapor pressure. Deviations from ideality are expected in the atmosphere and can be expressed in terms of an activity coefficient, γ. Barriers to equilibrium, e.g. partitioning of a non-polar compound into a polar particle, can yield a lower-than-expected fraction in the particle-phase ($\gamma > 1$). Conversely, processes such as solution in an aqueous phase or reactive processes can increase uptake into the particle, yielding an effective activity coefficient, γ_{eff}, less than 1. The roles of solubility and particle-phase reactions are uncertain in part because the gas-particle partitioning has never before been measured for most known BVOC oxidation products. A higher-than-expected particle fraction has been observed for some slightly oxygenated compounds (oxygen-to-carbon ratio = 0.1 to 0.3), but measurements of gas-particle partitioning

are largely non-existent for compounds more closely resembling those dominating global SOA (Williams et al., 2010a; Zhao et al., 2013b).

To understand oxidation pathways and aerosol sources in ambient environments, many techniques have been developed to identify and quantify compounds of interest. Through controlled laboratory oxidation, many "tracer compounds" have been identified to come from specific sources or through known oxidation pathways. A large suite of known tracer compounds allow relatively comprehensive apportionment of ambient aerosol from many sources: direct emissions from biomass burning (levoglucosan: Fraser and Lakshmanan, 2000)) and fossil fuels (Fraser et al., 1999; Schauer et al., 1996, 1999b, 2002), as well oxidation products of vehicular emissions (Rogge et al., 1993; Sheesley et al., 2010; Simoneit, 2005), isoprene (Claeys et al., 2004; Szmigielski et al., 2007b; Wang et al., 2005), some common monoterpenes (Claeys et al., 2007, 2009; Jaoui et al., 2005; Lewandowski et al., 2007; Szmigielski et al., 2007a), and at least one common sesquiterpene (Jaoui et al., 2007). Though equilibrium partitioning theory predicts a gas-phase component for most known tracers, source attribution studies have traditionally assumed these compounds exist primarily or entirely in the particle-phase. This discrepancy results in poorly constrained errors, both from sampling artifacts during filter collection and from atmospheric degradation of tracer compounds through gas-phase reactions. However, these assumptions have yet to be significantly challenged due to a complete lack of observational constraints of gas-particle partitioning.

Despite uncertainties in partitioning, quantification of summed concentrations of tracers has yielded significant advances in average regional source apportionment over periods of months or seasons (i.e. Kourtchev et al., 2008; Offenberg et al., 2011). Though each tracer provides unique information about chemical oxidation pathways, detailed analysis of chemical variability has been hindered by the relatively low time-resolution of traditional tracer analyses using collection of particles onto a substrate. Solvent extraction of these samples for subsequent analysis by gas or liquid chromatography (GC or LC) has typically relied on collection onto filters for 12 hours to several days. Consequently, detailed understanding of temporal variability has been limited. Analysis by GC, though common for tracer-based studies, requires reaction of the solvent extract with a "derivatizing" agent to form less-polar analogues from polar groups that would otherwise be non-elutable due to hydrogen bonding reactions with the chromatography column. Though on-line methods for derivatization have been described (Docherty and Ziemann, 2001; Sheesley et al., 2010), offline techniques are still used for most tracer analyses.

Quantification of tracer compounds with time-resolution sufficient to study atmospheric variability has been achieved through development of the (Semi-Volatile) Thermal desorption Aerosol Gas chromatograph (SV-)TAG (Kreisberg et al., 2009; Williams et al., 2006; Zhao et al., 2013b; Chapter 6). This has allowed improved, time-resolved source apportionment in urban regions (Gentner et al., 2012; Williams et al., 2007, 2010b; Zhao et al., 2013a), but the limitation of GC for analysis of highly oxygenated compounds has restricted the chemical range observed in previous TAG instruments to relatively low polarities. The addition of in situ derivatization and a two-channel sampling system described in Chapter 6 allows for the first hourly measurements of most BVOC oxidation products and the first direct observations of their gas-particle partitioning. This provides an unprecedented opportunity to understand the processes controlling SOA formation and explore the assumptions made in traditional source attribution methods. In this work, known oxidation products of isoprene and α-pinene, a common monoterpene, are quantified hourly to determine the factors controlling their uptake into the

particle and SOA formation in rural regions. Furthermore, thermodynamic equilibrium is found in this work to poorly describe the observed gas-particle partitioning of most highly oxygenated compounds prevalent in the atmosphere.

7.2. Experimental

7.2.1. Measurement locations

Both measurement locations are situated in rural areas where atmospheric composition is expected to be dominated by regional oxidation of BVOC emissions (Fig. 7.1, colored by dominant land cover: forests in green, cropland in yellow, and urban in red).

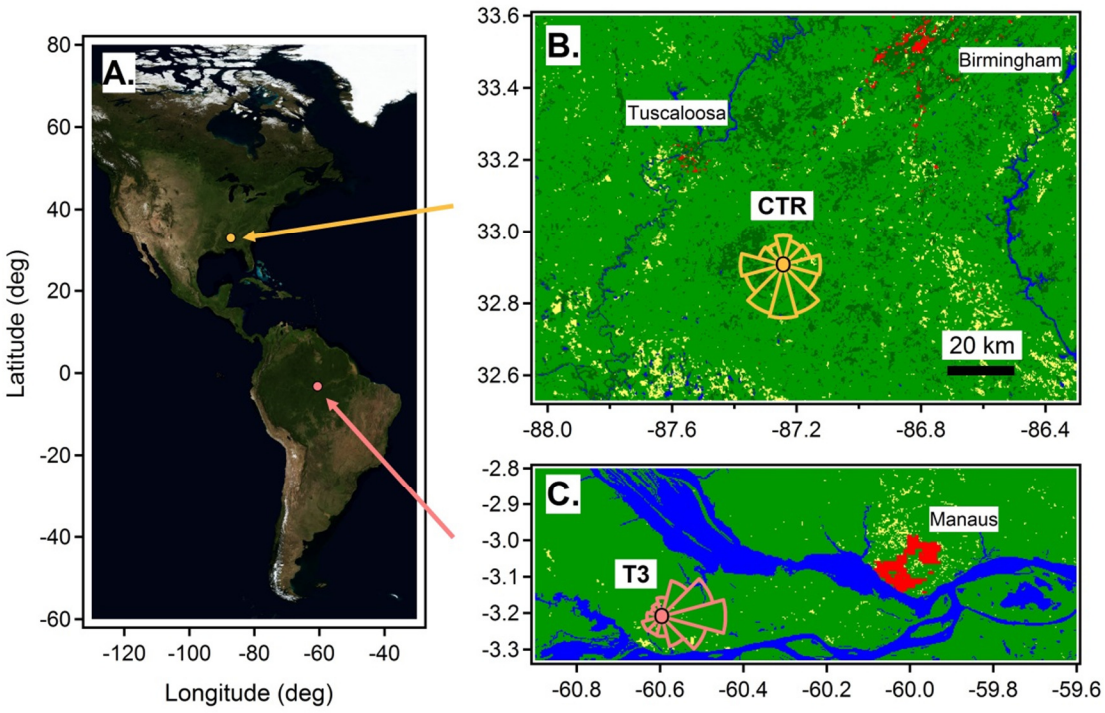

Figure 7.1. Location of measurements from (a) a global perspective in natural color (Stockli et al., 2005), and a close-up of the landcover surrounding (b) SOAS measurements at the CTR site and (c) GoAmazon2014/5 measurements at the T3 site. A windrose is shown at both groundsites. Major nearby urban areas are labeled. Land is colored by the majority of its landcover based on 0.3 km x 0.3 km data from GlobCover2009 (Arino et al., 2012): broadleaf vegetation in light green, coniferous vegetation in dark green, cropland in yellow, urban in red, water in blue.

7.2.1.1. SOAS: Southeastern U.S.

Measurements in the southeastern United States were collected as part of the Southern Oxidant and Aerosol Study ("SOAS") at the Centreville, Alabama groundsite ("CTR"; 32.903 N, 87.250 W; timezone: UTC-5), shown in Fig. 7.1b. Data collection lasted from June 1 to July 15, 2013. Concentrations of oxidized tracer compounds are reported from approximately June 4 to July 5, with some data coverage from July 5 to July 12. SV-TAG samples are collected for 50 minutes

every 1.5 hours until June 18, and the first 22 minutes of each hour thereafter. The site is rural, primarily forested with a mixture of deciduous and coniferous trees. Emissions of VOCs in this region are expected to be predominantly biogenic with relatively little local influence. Anthropogenic emissions from Tuscaloosa, AL (~30 km NW) or Birmingham, AL (~80 km NE) are expected to have some influence on regional oxidation chemistry, though winds were more often southerly during this period, as seen in Fig. 7.1b. Samples were collected at ~5 m a.g.l. in a clearing on a small hill (elevation gain of 10-20 m from the tree line) tens of meters from the tree line in most directions: 40m from the tree line to the east and west and 130 m south of the CTR measurement tower and tree line. The tree line is 250 m from the site toward the southwest, which is also the location of the nearest road.

7.2.1.2. GoAmazon2014/5: Amazonia, Brazil

Data was collected in rural Brazil as part of the GoAmazon2014/5 field campaign, which consisted of several ground sites and aircraft in the vicinity of Manaus, Brazil. Data presented in this work was collected during the wet season Intensive Operating Period 1 (IOP1: Feb 1 to March 31, 2014) at the "T3" ground site (3.213 S, 60.599 W; timezone: UTC-4) shown in Fig. 7.1c, a rural location 60 km west (and consequently downwind) of Manaus. Samples were collected at ~5 m a.g.l. at the eastern edge of the measurement site; the tree line begins approximately 500 m east (upwind) of the sample inlet. T3 is bounded on the west edge by a little used gravel road (50 m from sample inlet) and is surrounded by mostly unused pastureland. A diesel generator at the west edge of the measurement site provided power during municipal power outages so these periods have been removed from comparisons with bulk aerosol measurements (i.e. AMS organics, see description below). Atmospheric composition at the site is expected to be comprised predominately of regional biogenic emissions and oxidation products, with periods of strong anthropogenic influence from Manaus. Data coverage during IOP1 for compounds measured by SV-TAG spans Feb 14 to March 27, 2014, with samples collected during the first 22 minutes of every hour. These measurements are hereafter referred to simply as "GoAmazon."

7.2.2. Instrumentation

7.2.2.1. SV-TAG: Semi-Volatile Thermal desorption Aerosol Gas chromatograph

Organic tracer compounds are measured in the particle and gas phases using a Semi-Volatile Thermal desorption Aerosol Gas chromatograph employing two parallel sampling cells and in situ derivatization. The instrument used in this work is identical to the one described in detail in Chapter 6 (schematic shown as Fig. 6.1), so is only discussed in brief here. Air is sampled through a PM_1 cyclone at 10 lpm into each custom Filter Collection and Thermal Desorption cell (F-CTD), consisting of a high surface-area metal fiber filter in a stainless steel housing to allow controlled heating and forced air cooling. In addition to particles, the F-CTD quantitatively collects and retains gas-phase compounds with a volatility at least as high as tetradecane, allowing direct measurement of gas-particle partitioning for low volatility gases using a denuder difference technique (Zhao et al., 2013c). Simultaneous collection of a "particle" sample and a "total" gas-plus-particle sample is achieved using a multi-channel carbon monolith denuder (500 channels, 30 mm OD x 40.6 cm; MAST Carbon) to remove all gases upstream of one collection

cell. Particle fraction, F_P, is calculated from the direct comparison between the two samples. Gas-phase semi-volatile compounds are expected to easily condense on surfaces, so residence time in the inlet is minimized by sub-sampling 20 lpm from the center stream of a ~200 lpm, 6" stainless steel duct (cleaned with isopropanol and heat treatment) with a height of approximately 5 m. Sample flow is brought from this duct to the collection cells through ~1 m of 3/8" stainless steel tubing.

Samples are thermally desorbed from the cells into a helium stream 80% saturated with MSTFA (N-Methyl-N-(trimethylsilyl) trifluoroacetamide), which converts all hydroxyl groups into silyl esters and ethers. It must be noted that the reactions of silylating agents with some atmospherically relevant functional groups, such as hydroperoxides, organosulfates, and organonitrates, have not been extensively studied, and may yield products indistinguishable from hydroxyl analogues. Following thermal desorption, sample is re-condensed onto an intermediate focusing trap (~100 cm of 0.53mm ID x 5µm MXT-5 chromatography column; Restek), which is then backflushed and heated to transfer analytes to the GC column. This two-step purge-and-trap method allows high desorption flows (up to 150 sccm) and removes compounds too volatile to be trapped, such as excess derivatizing agent and by-products. Once transferred to the GC column (Rtx-5Sil MS, 20m x 0.18mm x 0.18µm; Restek), the sample is analyzed through a commercially available GC/MS (7890A/5975C; Agilent Technologies). All chromatographic data was reduced and analyzed using custom analysis code written in Igor Pro 6.3 (WaveMetrics), which forms the basis of the publicly available software TAG ExploreR and iNtegration (TERN; Isaacman and Sueper, 2014).

Compounds are quantified using a combination of isotopically labeled internal standards to correct for run-to-run variability in sample transfer efficiency and instrument response, and regular multi-point calibrations of approximately 100 authentic standards. All tracers and internal standards quantified in this work are shown in Fig. 7.2. Pentaerythritol-2-^{13}C (a tetrol) is used to correct levoglucosan (a triol), 2-methyltetrols, and C_5 alkene triols, while hexanedioic acid-d_4 is used for pinic acid (a C_9 diacid). In the case of unidentified compounds thought to be oxygenated, pentadecanol-d_{31} is used as an internal standard to provide a single, simple correction for variability of derivatization efficiency and MS sensitivity. Authentic standards are used in this work for quantification of levoglucosan and pinic acid, using the response on select ions *m/z* 204 and *m/z* 171, respectively. Both 2-methylerthritol and 2-methylthreitol (*m/z* 219) are quantified using the response of erythritol (*m/z* 217), corrected by a factor of 3.0 based on a multi-point calibration of co-injected authentic 2-methyltetrols and erthythritol on a different thermal desorption GC. For these compounds, uncertainty in mass is approximately 15%, calculated using the methods described in Appendix D. C_5 alkene triols (*m/z* 231) are quantified using the calibration factor of 2-methyltetrols assuming identical total (not select) ion response; lack of an authentic standard results in unconstrained uncertainty in mass accuracy of 30-50% (Jaoui et al., 2005). F_P is measured as a direct comparison of analyte signal at each point, with approximately 20% uncertainty for all identified compounds and approximately 30-40% uncertainty for unidentified compounds. Time-integrated (i.e. diurnal or campaign-long) median or average particle fractions are measured with much more certainty as they are a function of sample size. In this work, uncertainties on diurnal averages of particle fraction of identified compounds are ~5%, while median particle fraction across the entire campaign of any compound can be measured with <5% uncertainty.

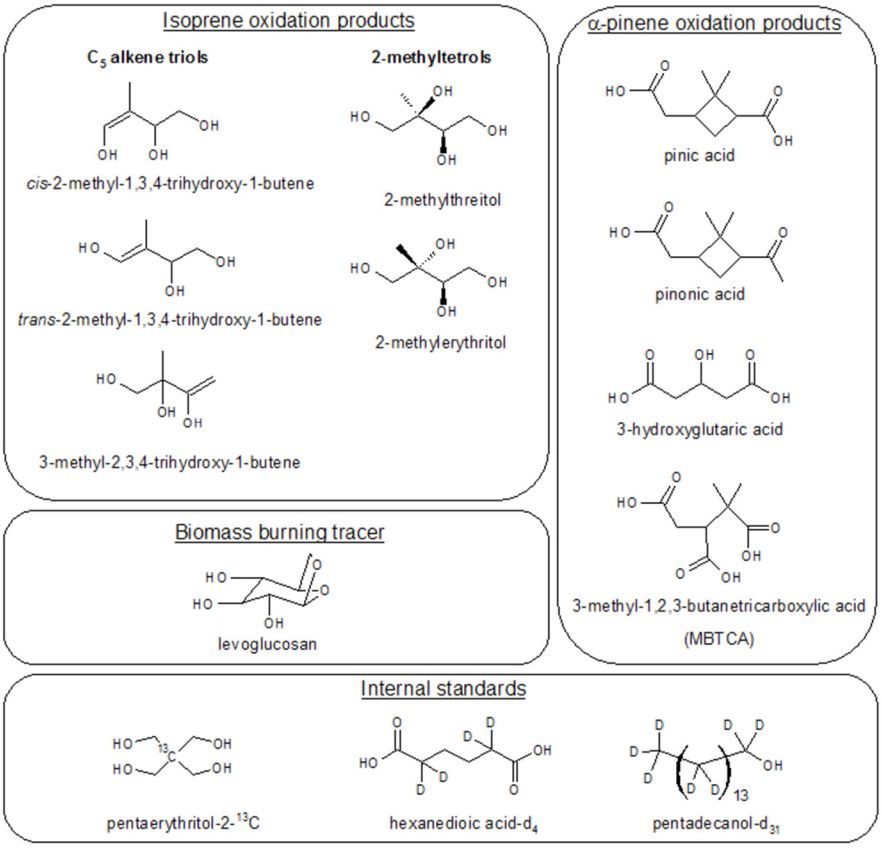

Figure 7.2. Structures of tracer compounds quantified in this work and the internal standards used to correct for run-to-run instrument variability.

7.2.2.2. Supporting instrumentation

Meteorological data (temperature, wind speed, relative humidity) was collected at both sites. In addition, concentrations of relevant atmospheric components were measured by collaborators:

AMS: Aerodyne Aerosol Mass Spectrometer. Non-refractory submicron particle-phase mass at both field sites was measured by an Aerodyne High Resolution Time-of-Flight Aerosol Mass Spectrometer (AMS) to quantify organics, sulfate, nitrate, ammonium, and chloride (DeCarlo et al., 2006). An aerodynamic lens (Liu et al., 2007) focuses submicron particles into a beam for volatilization by a 600 ^{o}C vaporizer and analysis by electron impact mass spectrometry. Data analysis is performed using standard AMS software (SQUIRREL, PIKA) available online (Sueper, 2012). Positive Matrix Factorization (PMF) is used to deconvolute the high-mass-resolution organic component into several "factors" following the methodological recommendations of Paatero and Tapper (Paatero and Tappert, 1994) and Ulbrich et al. (Ulbrich et al., 2009). Methodological details of the PMF analysis are beyond the scope of this work, discussed instead in other manuscripts currently in preparation by collaborators who ran the AMS instruments.

PTR-ToF-MS: Proton Transfer Reaction Time-of-Flight Mass Spectrometer. Precursors of known oxidation products are quantified at both field sites using a High Resolution Time-of-Flight Proton Transfer Reaction Mass Spectrometer (PTR-ToF-MS), which is described in detail

elsewhere (Lindinger et al., 1998) and is used widely to quantify atmospheric concentrations of biogenic compounds (i.e. Jardine et al., 2011; Karl et al., 2010; Park et al., 2014). For isobaric compounds, such as monoterpenes, the sum of isomers is reported.

Particle-phase liquid water. Concentrations of particle-phase liquid water were measured at SOAS as the difference between dried and unperturbed particle volume using instrumentation described by T. K. V. Nguyen et al. (2014). Particles are sampled under atmospheric temperature and relative humidity using a differential mobility analyzer and a condensation particle counter to quantify particle volume and size distribution. The sample flow is then cooled at the inlet to remove water vapor and allowed to warm, resulting in a drop in water vapor saturation ratio that drives water out of the particle. Particle volume at RH ≈ 10% is compared to the unperturbed volume to calculate the mass of the water present in ambient particles.

7.3. Results and Discussion

7.3.1. Temporal variability of isoprene oxidation products

Concentrations of 2-methyltetrols, a dominant product from isosprene oxidation, are observed in relatively large concentrations at both locations. Figure 7.3 shows the concentrations of 2-methyltetrols (sum of two isomers) in both the gas- and particle-phase throughout the SOAS and GoAmazon campaigns (Fig. 7.3a and c, respectively). Concentrations are highly variable, with hourly fluctuations in mass and longer term trends over the field campaigns that qualitatively follow trends in organic and sulfate aerosol mass (Figs. 7.4b,d). While rain events were not uncommon during both measurement periods, several particularly heavy rain events have been highlighted on July 4, 2013 (SOAS) and March 8 and 12, 2014 (GoAmazon). In addition to removing particles from the atmosphere, as evidenced by rapid declines in AMS organic and sulfate mass, these events also remove the gas-phase component of 2-methyltetrols. While the rain event on March 8, 2014 only briefly decreases concentrations, this is observed in gas- as well as particle-phase mass, suggesting efficient scavenging and wet deposition of highly oxygenated gases.

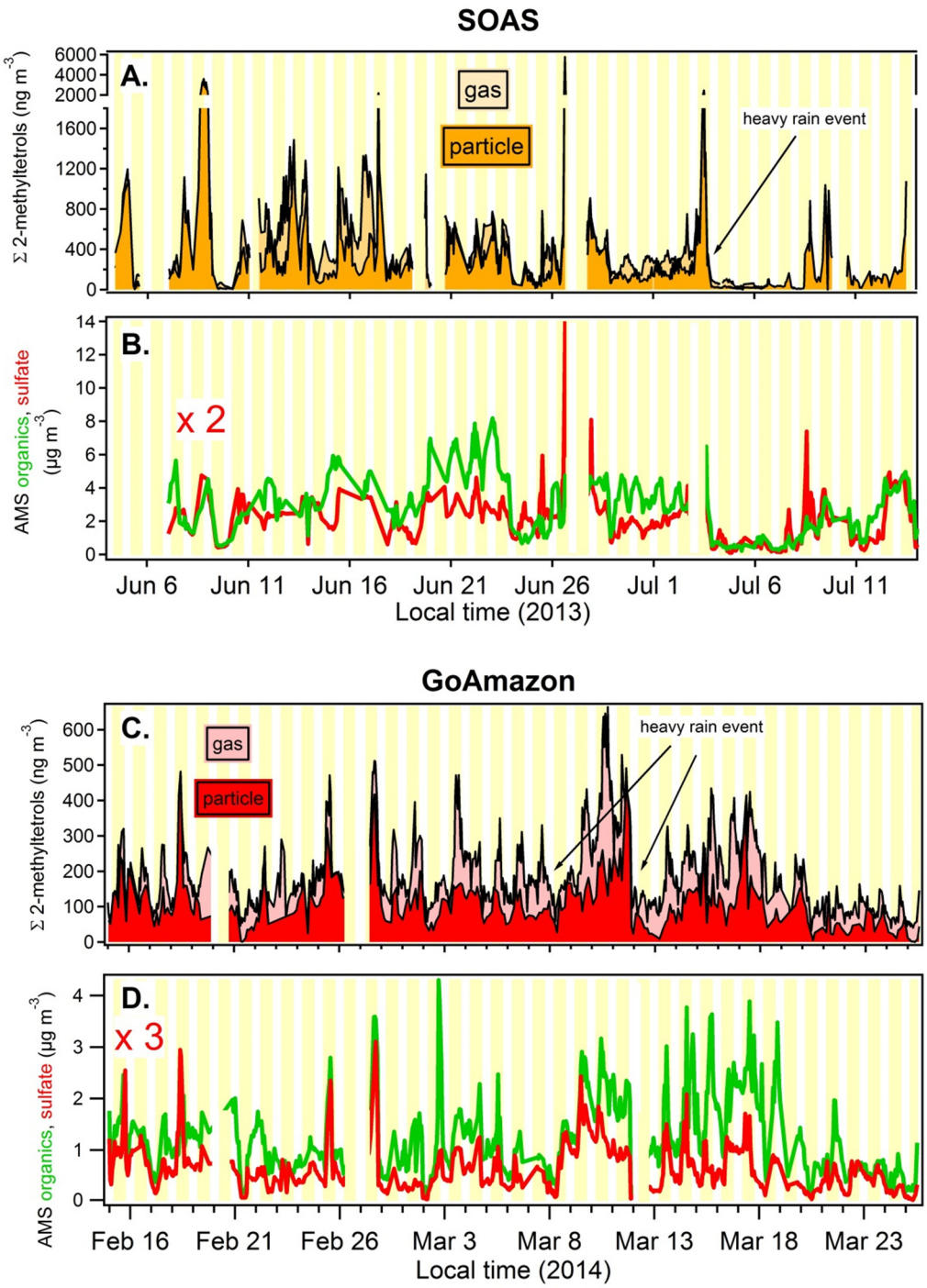

Figure 7.3. Mass concentrations of particle-phase and total gas-plus-particle-phase 2-methyltetrols (sum of both isomers) as well as AMS organics (green lines) and sulfate (red lines). Gas-phase concentrations are visible as the difference between particle-phase (dark shading) and total (light shading) concentrations. Daylight hours are shown in background as 0600-1800 local time. Data was collected during SOAS of (a) 2-methyltetrol concentrations (dark yellow shading) and (b) AMS organic and sulfates, and during GoAmazon of (c) 2-methyltetrol concentrations (red shading) and (d) AMS organic and sulfates.

Despite relatively stable organic aerosol mass loadings during SOAS, concentrations of 2-methyltetrols fluctuate significantly, likely due to rapid changes in aerosol composition from local influence. This is not observed to the same degree during GoAmazon, which exhibited a relatively constant background of particle-phase compounds with some diurnal viariability and multi-day events, suggesting that the atmospheric composition is predominately controlled by large-scale regional chemistry.

7.3.1.1. Influence of sulfate

On June 25 and 26, 2013, sulfate concentrations rapidly spiked to their campaign peak (Fig. 7.4). This event is associated with only a marginal increase in organic mass, but concentrations of 2-methyltetrols increased to approximately the same degree as sulfate mass. During this same period there is an increase in organic mass during the night of June 26 that is not associated with increased sulfate or tracer mass. This event demonstrates that sulfate is an important factor in the reaction pathway that forms 2-methyltetrols through IEPOX uptake and that other formation pathways are also important sources of aerosol at this site. This conclusion is supported by the correlations of particle-phase 2-methyltetrols with organic and sulfate mass (Fig. 7.5). Despite qualitatively similar temporal variability shown in Fig. 7.3, correlation between 2-methyltetrols and total organic mass (Fig. 7.5 a-b) is relatively poor because other sources of OA are present (i.e. monoterpene oxidation), but sulfate mass correlates reasonably well (Fig. 7.5c-d). This relationship may be driven by the role of sulfate as a ring-opening nucleophile in the reactive uptake of IEPOX, or may be indirect due to sulfate enhancement of the acidity or liquid water content of the particle. Comparison on an hourly basis yields more scatter than comparing daily averages (r^2 shown using daily averages), which may be due in part to reaction lifetimes. Concentration of particle components (i.e. tracer concentrations, LWC, etc.) change with oxidation, volatilization, and deposition, so formation of 2-methyltetrols may occur under somewhat different particle conditions than currently observed; averaging by day removes some of these issues of timescale by effectively binning data in days with i.e. more sulfate, or less particle-phase water.

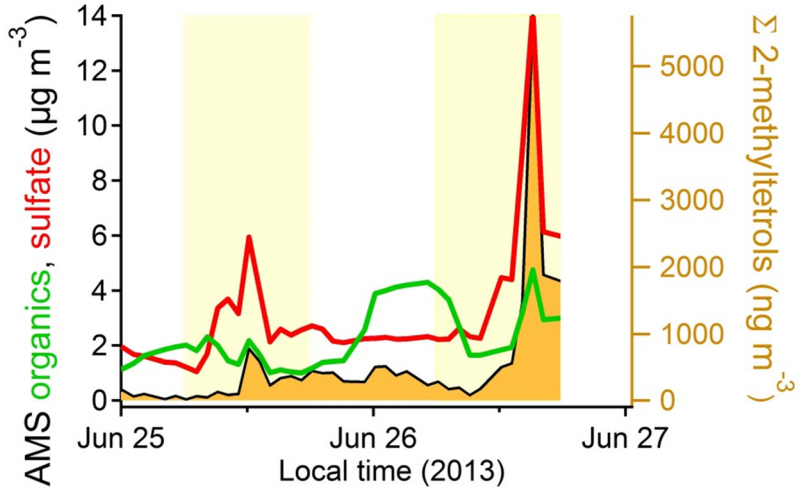

Figure 7.4. Concentrations on 25 and 26 Jun 2013 at the SOAS groundsite of particle-phase 2-methyltetrols (dark yellow shading), AMS organics (green line) and AMS sulfates (red line).

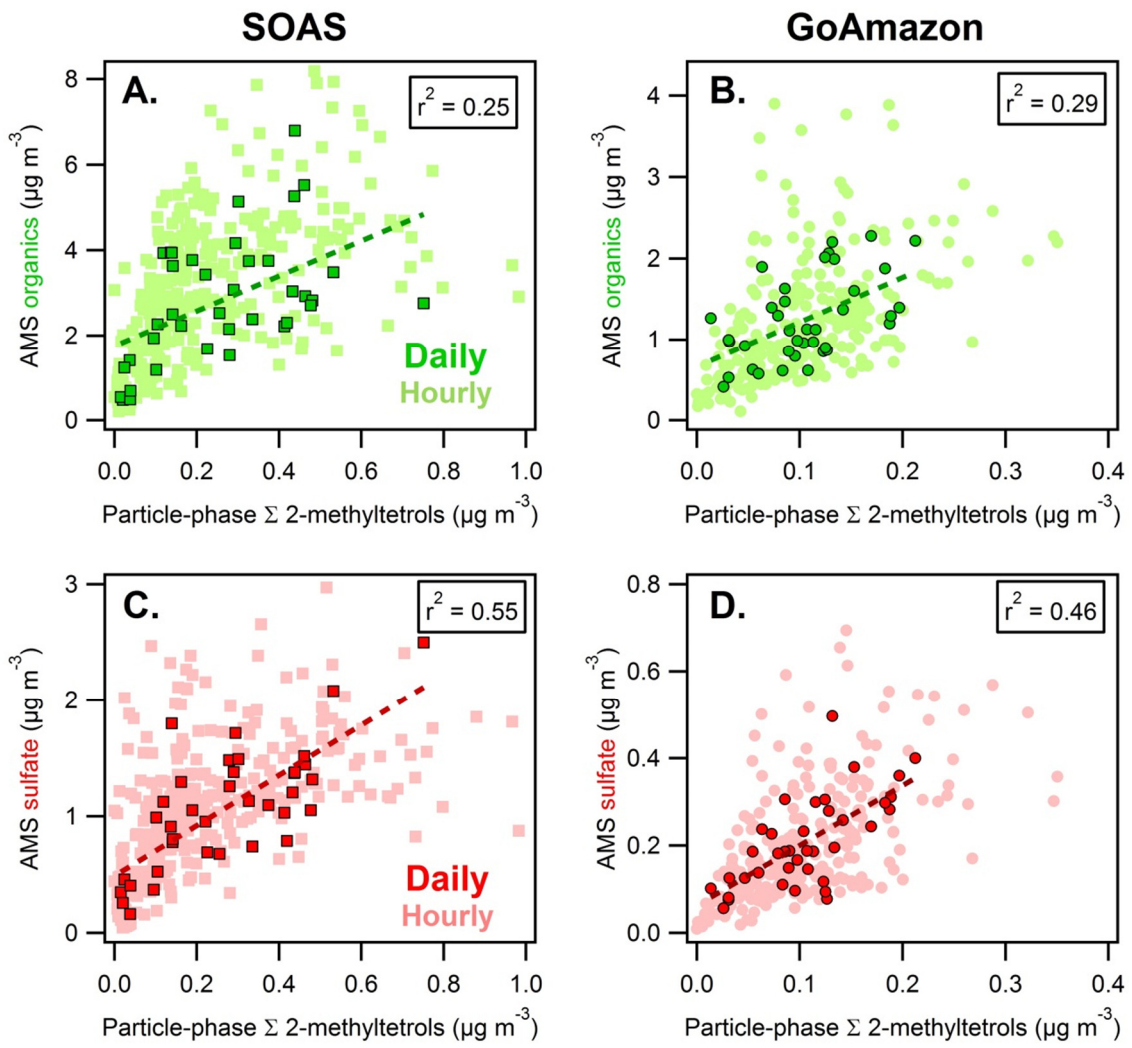

Figure 7.5. Correlations of daily (large, outlined symbols) and hourly (small symbols) concentrations of particle-phase 2-methyltetrols during SOAS and GoAmazon, respectively, with (a,b) AMS organics and (c,d) AMS sulfate. r^2 coefficients are shown for correlation with daily data.

Both the direct and indirect roles of sulfate in SOA formation from IEPOX are found to be important in these environments. Due to high levels of sulfate, particles in the southeastern U.S. are relatively acidic (pH < 2) and contain large amounts of liquid water, so reactions of IEPOX are not expected to be limited by acidity or water. Indeed, a recent multi-variable linear regression informed by the tracers discussed here (Xu et al., 2014) supports the conclusion that IEPOX-derived SOA is predominately controlled by the availability of sulfate as a nucleophile, with little additional explanatory value from acidity and LWC. However, 2-methyltetrols are formed through nucleophilic attack of the epoxide by water, while addition of sulfate yields organosulfates, so this presence of high concentrations of 2-methyltetrols implies that reaction of IEPOX is occurring in large part with water as a nucleophile. Though the fate of organosulfates in the SV-TAG instrument is not well-known and measurements of 2-methyltetrols may be

partially convoluted with analogous organosulfates, this is unlikely to explain a majority of the measured mass because organosulfates are not expected to be larger than particle-phase mass of 2-methyltetrols (Chan et al., 2010) even in the southeastern U.S. Furthermore, convoluted organosulfate mass is only expected in the particle-phase, so frequent observations of 2-methyltetrols with only a small particle fraction suggests that organosulfate derivatization is at most a minor source of error. The correlation of 2-methyltetrols,products formed through IEPOX reaction with water, with sulfate implies that the role of sulfate in isoprene SOA formation is, at least in part, indirect, through enhancement of particle-phase liquid water. Direct measurements of organosulfates are necessary to further understand this issue.

7.3.1.2. Prevalence of isoprene SOA

During both measurement periods, oxidation of isoprene was observed to be a significant source of SOA. On average, the sum of both 2-methyltetrol isomers in the particle phase accounted for 8% of organic aerosol mass during SOAS, and 10% during GoAmazon (Fig. 7.6). The dominance of these tracers is different between sites, regularly comprising 10-15% of observed organic mass in the Amazonia region during the wet season, while only rarely reaching this fraction in the southeastern U.S. The SOAS groundsite was surrounded by a complex mixture of deciduous and coniferous vegetation and is observed have a higher concentration of monoterpenes with respect to isoprene, consistent with a relatively lower contribution of 2-methyltetrols to organic aerosol, while T3 in Amazonia appears to be dominated by isoprene oxidation products, with nighttime OA from biomass burning sources. Levoglucosan, a common tracer for biomass burning, increases at night (Fig. 7.7) with frequent spikes in concentration indicating influence from local sources. These peaks are often associated with spikes in total organic aerosol mass that are not accompanied by increases in 2-methyltetrols, as demonstrated by the biomass burning events shown in Fig. 7.7 on the nights of March 14, 17 and 18.

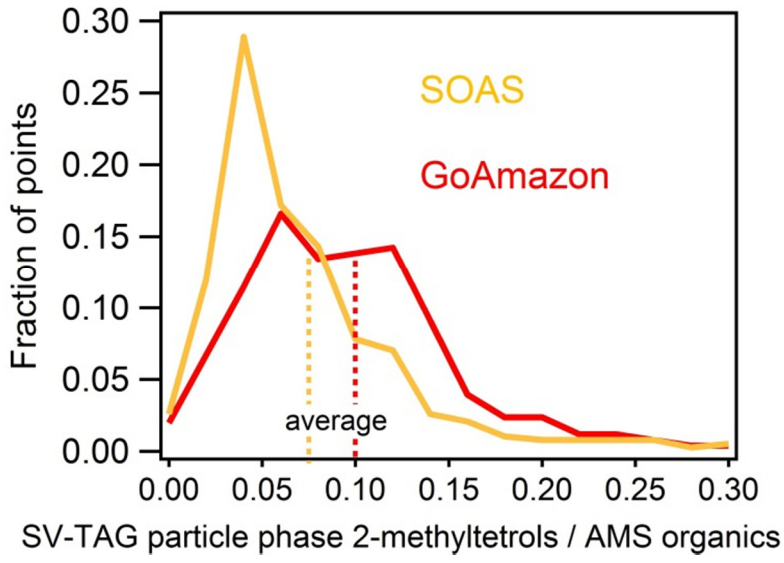

Figure 7.6. Frequency of observations of the ratio of observed particle-phase mass of 2-methyltetrols to AMS organic mass during SOAS (dark yellow) and GoAmazon (red).

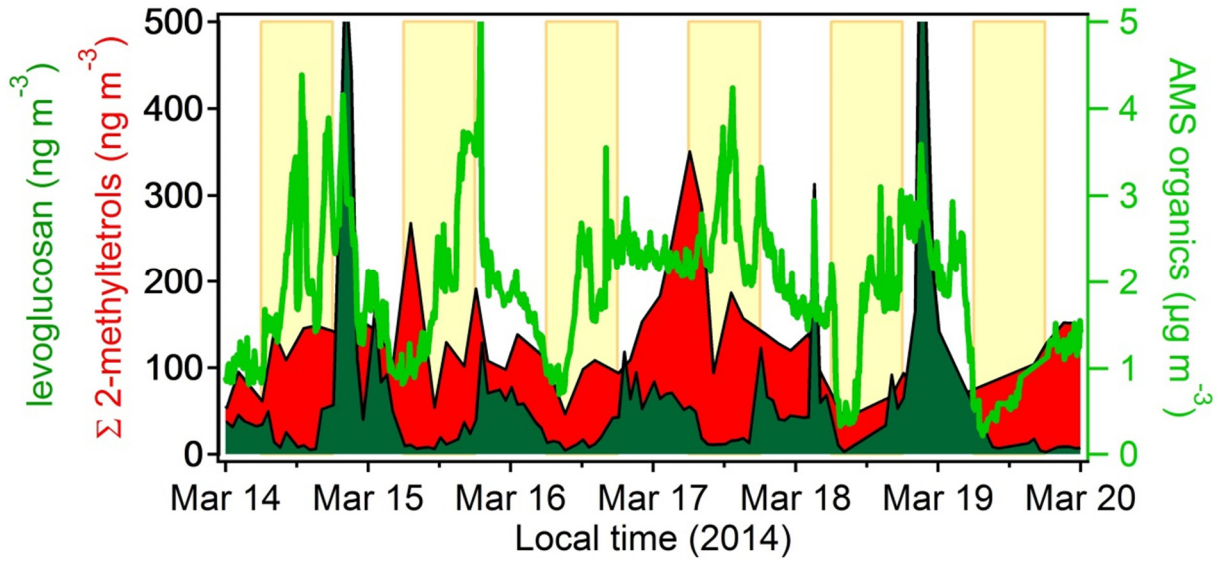

Figure 7.7. Concentrations from 14 through 19 Mar 2014 at the GoAmazon "T3" groundsite of particle-phase 2-methyltetrols (red shading), levoglucosan (dark green shading), and AMS organics (light green line).

At many field sites with large biogenic emissions, including those discussed in this work, Positive Matrix Factorization of AMS data has identified a factor identified as SOA mass formed through isoprene oxidation (Budisulistiorini et al., 2013; Robinson et al., 2011). Though the detailed composition of this fraction of organic mass has not been characterized, it has been shown in laboratory studies to form through reactive uptake of IEPOX (Budisulistiorini et al., 2013). In situ measurements of known IEPOX products are shown here to correlate very well with this "IEPOX-OA" AMS factor (Fig. 7.8) at both field sites (hourly data r^2 = 0.59 and 0.60 for SOAS and GoAmazon respectively), corroborating the identification of this factor as a reasonable proxy for IEPOX-derived SOA. However, as shown in Fig. 7.8, particle-phase 2-methyltetrols make up a smaller fraction of mass identified as IEPOX-OA mass during SOAS (~20%) than GoAmazon (~35%). Previous laboratory studies used for tracer analyses have identified these compounds as ~20% of SOA mass formed from isoprene oxidation in the absence of NO_x (Kleindienst et al., 2007, accounting for response differences between standards used for quantification in this and referenced studies), in good agreement with the ratio measured at SOAS. The IEPOX-OA factor at GoAmazon may underestimate the contribution of isoprene or IEPOX to SOA due to multi-generational oxidation of the products yielding a product mixture that cannot be separated or identified as isoprene derived mass. Applying the laboratory and SOAS ratio of 20% to the histogram in Fig. 7.6, isoprene SOA from reaction of IEPOX accounts for a majority fraction, and in some cases nearly all, of OA measured during the GoAmazon campaign. However, variations in reaction conditions likely impact the efficiency of 2-methyltetrol formation with respect to other IEPOX reaction products, so this simple ratio provides only an estimate. Interestingly, while 2-methyltetrols and C_5 alkene triols have a similar correlation with IEPOX-OA at SOAS, C_5 alkene triols correlate extremely well (r^2 = 0.88) with this factor at GoAmazon. This difference cannot yet be well-explained owing to a lack of detailed knowledge about the formation processes of C_5 alkene triols.

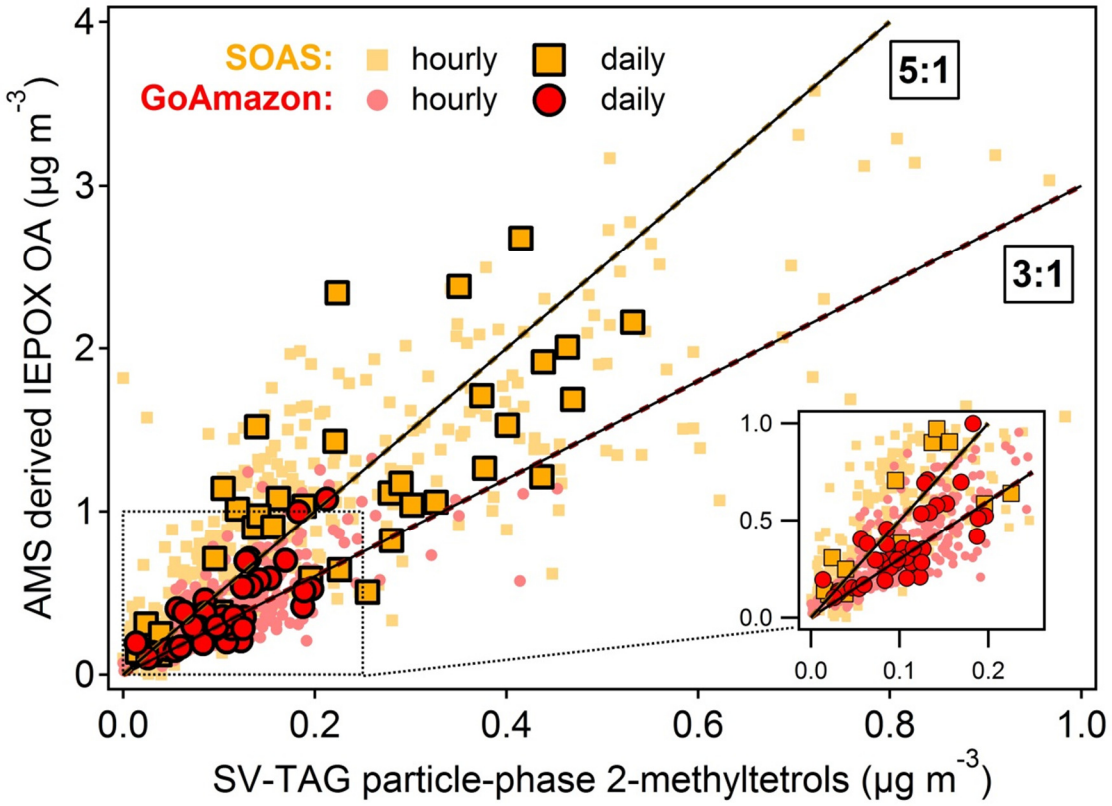

Figure 7.8. Ratio of the IEPOX-OA AMS PMF factor, associated with SOA formed through IEPOX uptake, to particle-phase 2-methyltetrols at SOAS (dark yellow squares) and GoAmaozn (red circles). Daily averages are shown as large, outlined symbols, while small symbols are hourly data. Lines shown are approximate slopes of linear regression fits (r2 ≈ 0.60), but are intended only to guide the eye.

7.3.2. Diurnal trends: impact of precursor emission patterns

All identified isoprene and monoterpne oxidation products are found to have diurnal variability that approximately follows diurnal trends in precursor emissions (Fig. 7.9). Isoprene emissions depend strongly on light as well as temperature, so tend to have a strong maximum during the day at both sites, with concentrations that are approximately three times higher at the SOAS groundsite compared to GoAmazon (Fig. 7.9a). Oxidation products of isoprene are observed to have a similar diurnal pattern, with daytime maxima at both sites (Figs. 7.9c-d) though the peak in oxidation products is less pronounced than that of its precursor. Diurnal patterns in total concentrations are driven primarily by increased gas-phase mass with relatively stable particle-phase mass (dashed lines), which results in diurnal trends in F_P (Figs. 7.9f-h). Oxidation of isoprene and uptake of IEPOX is therefore thought to occur on the timescale of hours during periods of high isoprene concentration, which coincide with increased temperatures and decreased liquid water content that may drive volatilization of 2-methyltetrols out of the particle. Ongoing oxidation to form oligomers and high-molecular-weight products of 2-methyltetrols coupled with cooler temperatures yields an apparent increase in particle fraction at night, resulting in a relatively stable regional background of these compounds that typically does not

drop to zero at night at either site. As observed in Fig 7.3, 2-methyltetrols measured during GoAmazon have a less prominent daytime peak, likely driven by high local emissions of isoprene local to SOAS groundsite.

The role of precursor emissions and rapid oxidation are demonstrated by differences between the two measurement locations in observed diurnal trends in pinic acid, an oxidation product of the common monoterpene α-pinene. Monoterpenes in North America are generally described by a temperature-dependent model, with little or no dependence on light (Geron et al., 2000, 2010; Guenther et al., 1995). These emission patterns result in nighttime maxima in concentrations due to continued emissions of monoterpenes coupled with a nighttime decrease in boundary layer height, as is observed for SOAS data in Fig. 7.9b. However, as GoAmazon data demonstrates, this is not true for some tropical regions, which can have light dependent monoterpene emissions and daytime maxima in concentrations (Chen et al., 2009; Jardine et al., 2011; Karl et al., 2004; Rinne et al., 2002). Diurnal patterns of pinic acid (Fig. 7.9e) follow the same general temporal patterns as its precursor, supporting rapid formation of oxidation products, though the hourly correlation between precursor and total pinic acid is poor (r^2 = 0.03 and 0.17 for SOAS and GoAmazon, respectively). Concentrations of pinic acid are substantially lower (~20x) at the GoAmazon groundsite than observed during SOAS, which is in agreement with higher monoterpene concentrations. However, this comparison is strongly influenced by the distribution of monoterpene species, which can vary significantly between plant species, though α-pinene is a dominant component of monoterpene emissions in both environments (Geron et al., 2000; Kuhn et al., 2007). Some previously reported oxidation products of pinic acid and pinonic acid have been observed at both sites (i.e. 3-hydroxyglutaric acid and MBTCA) in similar concentrations, so while total α-pinene products are substantially lower in concentration at GoAmazon compared to SOAS, SOA formed from its oxidation is comprised of more highly oxidized compounds.

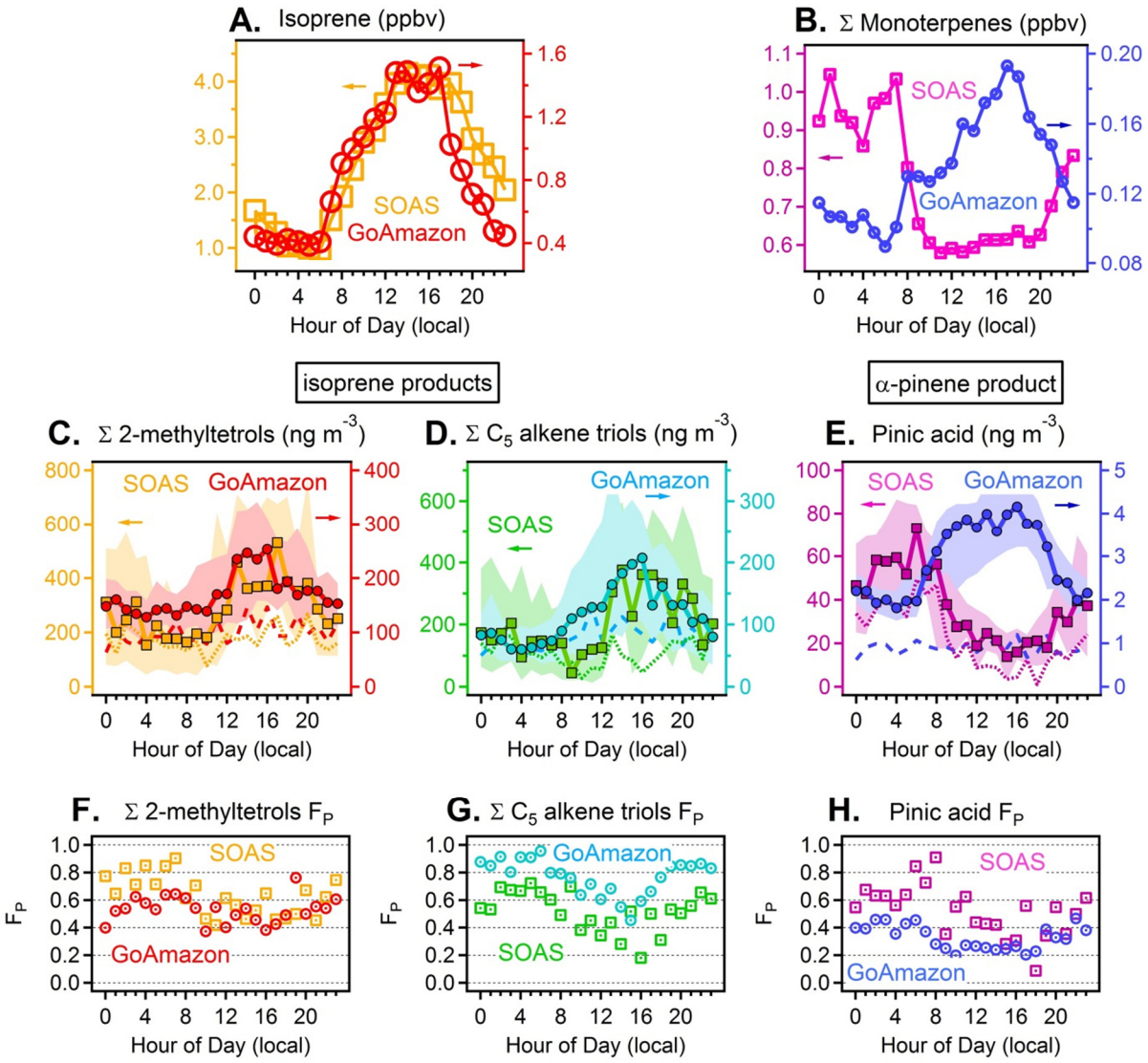

Figure 7.9. Diurnal plots of known BVOCs, oxidation products, and particle fraction. Medians of total concentration are shown as lines through symbols (squares: SOAS, left axis; circles: GoAmazon, right axis) with the interquartile range shown as the shaded region. Median particle-phase concentrations are shown as dashed lines. Diurnal concentrations are shown for (a) isoprene (yellow: SOAS; red: GoAmazon), (b) sum of monoterpenes (purple: SOAS; blue: GoAmazon), (c) sum of 2-methyltetrols (yellow: SOAS; red: GoAmazon), (d) sum of C5 alkene triols (green: SOAS; cyan: GoAmazon), and (e) pinic acid (purple: SOAS; blue: GoAmazon). Diurnal patterns of the particle fraction are shown for these compounds with open symbols in the same color scheme for (f) 2-methyltetrols, (g) C_5 alkene triols, and (h) pinic acid. The colors and closed symbols used for 2-methyltetrols and pinic acid in this figure are used for these compounds throughout this work.

7.3.3. Gas-particle partitioning of oxygenated compounds

7.3.3.1. Temporal variability and decreased daytime F_P

Nearly all identified tracer compounds are partitioned between the gas and particle phase and have a higher fraction in the particle-phase at night (Fig. 7.9f-h). This is expected in part due to cooler temperatures resulting in condensation as observed in some of the comparisons between measurement locations: the GoAmazon field campaign had higher temperatures than SOAS and a higher F_P is observed during SOAS for 2-methyltetrols and pinic acid. However, changes in temperature and organic aerosol mass are insufficient to explain observed gas-particle partitioning. C_5 alkene triols have a higher particle fraction during the warmer GoAmazon campaign and diurnal trends vary somewhat between compounds, with most identified compounds more in the particle phase than predicted by thermodynamic equilibrium (Fig 7.10). While 2-methyltetrols and pinic acid both exhibit broad decreases in daytime F_P, C_5 alkene triols have a sharp minimum in the late afternoon. Particle fraction is therefore not being driven primarily by meteorological conditions or equilibrium partitioning, at least for some compounds. Ongoing particle-phase oxidation may prevent re-volatilization through formation of high-molecular-weight products that may increase apparent F_P if they are measured as their hydroxyl analogues. However, for oligomeric decomposition to account for observed enhancement in F_P, these compounds must exist almost entirely as polymers (i.e. 80-90% of 2-methyltetrols). This is not thought to be the case as previous studies by instrumentation not reliant on thermal decomposition have quantified particle-phase 2-methyltetrols in their monomeric form in concentrations similar to particle-phase concentrations observed here (Lin et al., 2012). Consequently, instrument convolution of oligomers may somewhat enhance apparent F_P, but are unlikely to fully account for observations. However, formation of an oligomeric shell due to continued oxidation may result in kinetic barriers to re-partitioning of measured compounds (Roldin et al., 2014; Shiraiwa et al., 2013; Zhou et al., 2013), though this is not expected at the high levels of relative humidity observed during both campaigns (typically 60 to 99%) (Zhou et al., 2013).

Vapor pressures for 2-methyltetrols and pinic acid were calculated using a structure activity relationship (SIMPOL: Pankow and Asher, 2008) and used to calculate a predicted fraction in the particle phase at each hour based on thermodynamic equilibrium partitioning as described in Eq. 7.1. An average error of 0.4 atm in log(vapor pressure) exists the in the structure activity with up to twice this error for polylols (Compernolle et al., 2011; Pankow and Asher, 2008). Comparison between measured and calculated F_P is shown in Fig. 7.10 for 2-methylerythritol and pinic acid assuming ideal partitioning ($\gamma = 1$, a reasonable assumption due the highly oxygenated nature of both the tracers and the bulk aerosol). While the median F_P of pinic acid during both measurements periods is within vapor pressure error of unity, errors are insufficient to explain observed particle fractions of 2-methyltetrols. Furthermore, the temporal variation of both compounds is poorly described by ideal thermodynamic equilibrium and this poor correlation is insensitive to the exact value of the calculated vapor pressure. The observed deviation of particle fraction can be expressed in terms of an effective activity coefficient, γ_{eff}, below 1. Williams (2010a) and co-workers found alkanoic acids and some other oxygenates to be best described by $\gamma_{eff} \approx 0.1$ or lower, a range consistent with this work's observations in both SOAS and GoAmazon. To explain predicted F_P of 2-methylerythritol, γ_{eff} must vary between 1 and approximately 0.01. The variation in γ_{eff} is expected to be related to solubility into liquid water present in the particle, formation of thermally decomposed high-molecular-weight

products, or kinetic barriers to re-volatilization. Consequently, observed F_P of 2-methyltetrols depends on environmental or particle-phase factors, but no simple relationships have been found between γ_{eff} and particle composition; correlations with pH, anion-to-cation ratio, liquid water content, and sulfate concentration are shown in Appendix E to poorly explain observations ($r^2 < 0.1$ in all cases). Observed F_P is likely a result of a combination of these processes and is thus difficult to predict at any single point in time, though trends in partitioning of various compound classes can provide some insight.

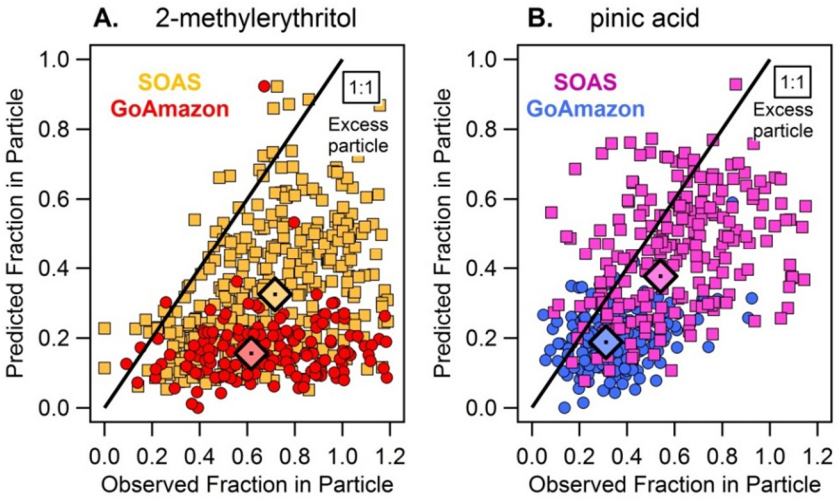

Figure 7.10. Particle fraction predicted by equilibrium partitioning (calculated from Eq. 7.1) compared to observed hourly particle fraction for (a) 2-methylerythritol (yellow squares: SOAS; red circles: GoAmazon) and (b) pinic acid (purple squares: SOAS; blue circles: GoAmazon). Median fraction in the particle for each compound during each campaign is shown as a filled, outlined diamond.

7.3.3.2. Dependence of F_P on chemical characteristics

Median particle fraction of unknown compounds can be calculated from SV-TAG measurements even in the absence of unambiguous identification (see Chapter 6). Hourly particle fraction was calculated during the GoAmazon field campaign for 65 compounds that correlated well ($r^2 > 0.8$) with known oxidation tracers; compounds correlating well with internal standards or known contaminants were excluded from this analysis. Like the tracer compounds measured, these compounds are assumed to be highly oxygenated and formed through oxidation of biogenic emissions. Though mass spectral matches fail to unambiguously identify most compounds, the mass spectra of many of them are consistent with compounds previously identified in ambient aerosols and laboratory studies of BVOC oxidation (Claeys et al., 2007, 2009; Edney et al., 2003; Jaoui et al., 2005; Kubátová et al., 2002), such as hydroxy and dihydroxy dicarboxylic acids and substituted tricarboxylic acids. Median particle fraction for these compounds are shown in Fig. 7.11 as a function of their retention time in the chromatogram, using an alkane-based retention index (i.e. retention time of pentadecane = 1500). Identified compounds are labeled and classified as isoprene products (red) or monoterpene products (blue) while unknown compounds are colored based on whether they correlate better with a known isoprene tracer or a known monoterpene tracer (no unidentified compounds in this analysis correlate well with levoglucosan, green).

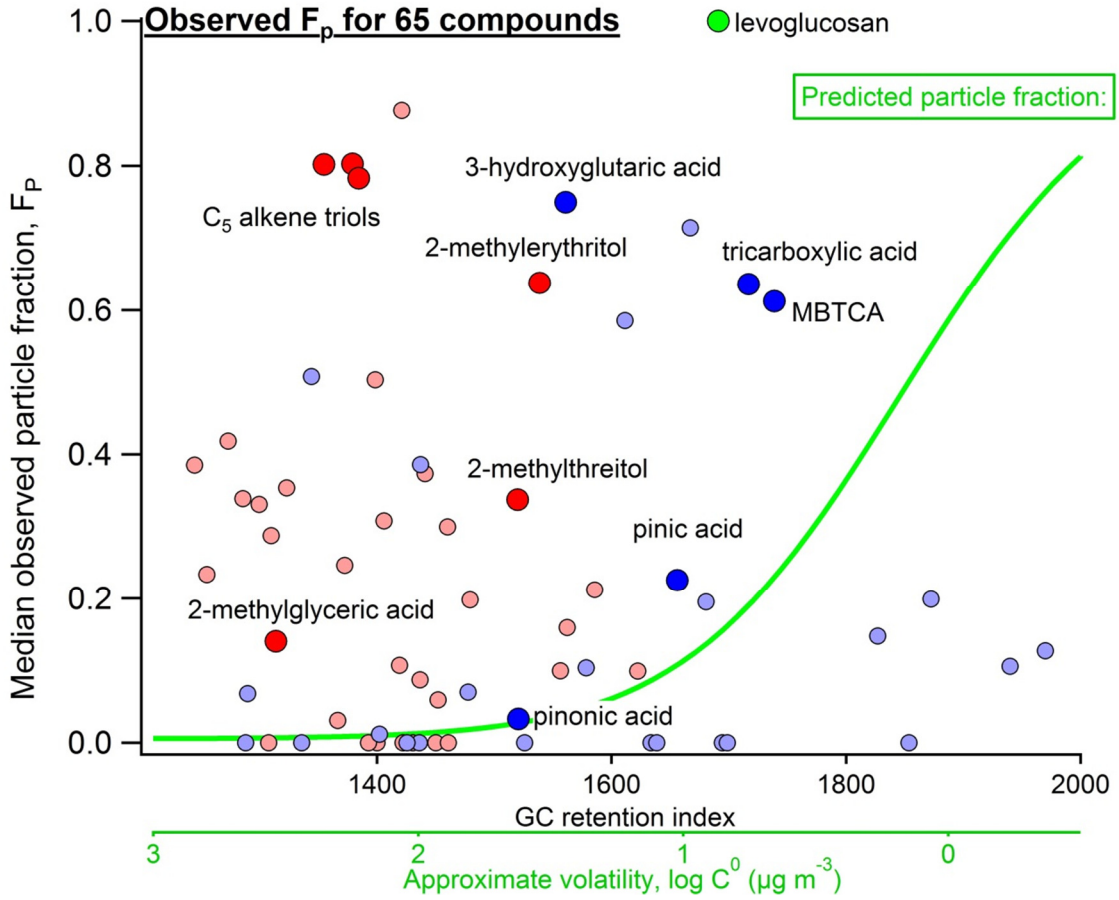

Figure 7.11. Median observed particle fraction, F_P, as a function of GC alkane-based retention index for all compounds that correlate with one of the identified (labeled) BVOC oxidation products. Known compounds are larger, outlined symbols. Compounds correlating with one of the labelled monoterpene oxidation products are blue, while those correlating with isoprene oxidation products are red. Levoglucosan is shown in green. Approximate volatility is calculated from retention index as described in the text, and the particle fraction predicted by this volatility (green line) is calculated with an average C_{OA} of 1.2 µg m-3.

Chromatographic separation occurs in part through a temperature ramp, so relative vapor pressure within a compound class can be estimated based on retention time (i.e. Chapter 2) to within error of vapor pressure structure activity relationships (log error of ± 0.4). Extension of this relationship to derivatized compounds finds that including the number of derivatized groups on a compound is sufficient to predict the vapor pressure of the underivatized compound to within approximate error of vapor pressure calculation (Fig. E.2). Simple classification of compounds by highly oxygenated (greater than 1 derivatized group) or less oxygenated (0 or 1 derivatized group) yields only marginally higher error (log error of ± 0.6). Approximate vapor pressure of the unknown compounds shown in Fig. 7.11 is calculated assuming all compounds have greater than 1 derivatized group.

Like 2-methyltetrols and pinic acid, nearly all compounds shown in Fig. 7.11 have a higher median F_P than predicted by thermodynamic absorption partitioning (median C_{OA} = 1.2 µg m^{-3}). Many highly volatile compounds have a large particle-phase component and F_P is independent of any clear relationship with volatility. This is likely a combination of the effects of equilibrium partitioning and solubility, which are inversely correlated (Hodzic et al., 2014). Equilibrium absorptive partitioning is a reasonable description for large compounds, while small compounds deviate from predictions, suggesting the influence of solubility. Isoprene-correlated unknowns tend to have higher volatility and stronger enhancement of particle fraction, while monoterpene oxidation products are larger and tend to more closely agree with predicted partitioning. This is observed for known compounds as well as unknown; small compounds with many hydroxyl groups display a significantly larger particle-phase component than expected. Thermal decomposition of oligomers measured as particle-phase mass of the monomer may be responsible for some of the particle-phase component but for the reasons described in Sect. 7.3.3.1, particle-phase enhancement is more likely explained by solubility parameters considering the large concentration of particle-phase liquid water. An additional enhancement in particle fraction is expected through the efficient dry deposition of gas-phase oxygenated compounds, which has been observed as a significant loss mechanism for related compounds (Worton et al., 2013) and is expected to suppress the gas-phase component. Uptake into the particle via acid-base chemistry is not shown to be important as the four compounds definitively identified as acids lacking hydroxyl groups are in approximate agreement with predicted F_P. It is clear from Fig. 7.11 that thermodynamic equilibrium is an inadequate description of gas-particle portioning for most compounds formed through oxidation of biogenic emissions.

7.4. Atmospheric implications

Hourly quantification of BVOC oxidation products provides unprecedented detail about the chemical processes of the atmosphere. Efficient wet deposition of gases as well as particles is observed in ambient measurements, and formation of particle-phase products and subsequent volatilization is observed to occur quickly. These high-time-resolution fluctuations in the concentrations of known tracer compounds highlight the need for fast measurements of oxygenated gas- and particle-phase aerosol components in order to understand the sources and sinks of reactive carbon. Organic aerosol at both rural locations studied in this work is shown to be comprised in large part by SOA formed by isoprene oxidation, and the chemistry that controls formation of this mass is observed to be influenced by anthropogenic emissions. Increased particle water due to elevated sulfate levels in the southeastern U.S. is found to be a significant factor in isoprene SOA, and this correlation with sulfate is also observed in Amazonia, Brazil during the wet season. SOA formed through IEPOX uptake accounts for a large, if variable, fraction of organic mass in these rural environments, so the impact of water and sulfate on ring-opening reactions is a source of substantial anthropogenic influence on biogenic SOA formation.

Nearly all compounds observed in this work were found to be partitioned between the gas and particle phase, regardless of the phase in which they were formed. However, particle fraction of a given compound does not correlate well with predicted equilibrium partitioning due to the effects of solubility and high-molecular-weight products. Small, highly oxygenated compounds that are too volatile to condense are regularly found in the particle phase with no clear correlation with environmental factors or particle composition, though solubility into particle-phase liquid water is expected to play an important role given the chemical functionality of these compounds.

Larger compounds are adequately described by thermodynamic equilibrium, so both solubility and absorptive partitioning need to be considered in gas-particle partitioning. Particle-phase oxidation yielding low-volatility products such as oligomers likely impacts the partitioning of BVOC oxidation products both directly and through potential kinetic effects cause by oligomeric films, but time-resolved measurements of these components are still largely unavailable. These potential kinetic effects and the absence of fast thermodynamic equilibrium implies that gas-phase loss mechanisms may substantially impact observed gas-particle partitioning. Solubility of BVOC oxidation products is another pathway for anthropogenic enhancement of particle-phase biogenic aerosol mass. Increased liquid water content of particles can increase not just the formation of oxidation products, but also their retention in the particle-phase, preventing their removable by gas-phase oxidation. Further identification of unknown oxidation products in the particle- and gas-phases, as well as a better understanding of the formation processes of some known compounds (i.e. C_5 alkene triols) will help inform the chemical processes controlling gas-particle partitioning.

7.5. Acknowledgements

GI is supported by the National Science Foundation (NSF) Graduate Research Fellowship (NSF Grant: DGE 1106400). Data collected as part of the SOAS and GoAmazon field campaign was funded by NSF Atmospheric Chemistry Program Grants #1250569 and 1332998, respectively. The author would like to thank collaborators and organizers of both the SOAS and GoAmazon field campaigns for facilitating collection of these measurements, including E. Egerton, K. Baumann, A. G. Carlton, J. L. Jimenez, A. Manzi, R. de Souza, S. Martin and P Artaxo. Specifically, SV-TAG data collection occurred with the help of L. D. Yee, N. M. Kreisberg, S. V. Hering, and A. H. Goldstein. AMS data was collected through the hard work of W. Hu, P. Campuzano-Jost, B. B. Palm, D. A. Day, S. S. de Sá, and L. Alexander. PTR-MS data was collected by P. Misztal (SOAS) and Y. Liu (GoAmazon). Liquid water measurements at SOAS were collected by T. K. V. Nguyen. Thanks to D. R. Worton for assistance with E-AIM modeling.

Chapter 8

Future Work

While this work contains advances in understanding particle-phase oxidation, instrument capabilities, and simplified characterization of atmospherically relevant mixtures, several potential milestones remain for future research. The goals discussed here range from addressing specific lacks in instrument capabilities, to comprehensive implementation of the ideas and methods discussed in preceding chapters.

The compositions of anthropogenic and biogenic mixtures are characterized in this work by volatility, polarity, presence of OH groups, and a variety of structural features. Each mixture studied in this work is classified using different subsets of these properties depending on data availability and precursor compounds, but these classifications have not been comprehensively applied to ambient samples. Ambient data are very complex, containing hundreds of chromatographically resolved compounds as well groups of poorly resolved isomers. Chemical description of these mixtures therefore relies on semi-explicit or parameterized characterizations. However, application of a simplified framework to ambient aerosol is significantly more difficult than unmodified extension of the concepts described in Chapters 2 through 7. The application and development of the techniques described in this work have relied on knowing the precursor reagents and designing the conceptual framework accordingly, i.e. classification by carbon structure in the case of oxidation of motor oil. To the extent that the currently described structural descriptive frameworks have been applied to ambient aerosol, they have been limited to subsets of the aerosol mass, i.e. the hydrocarbon mixture present in atmospheric samples due to fossil fuel emissions (Chan et al., 2013). Complete characterization of ambient aerosol instead requires a novel adaptation of the developed frameworks to completely describe the system, likely including some description of compound functionality, carbon backbone structure, and volatility. Understanding ambient atmospheric mixtures in a form that preserves information about chemical structure will allow oxidation processes to be observed as the sum of the chemical reactions that are occurring, not just bulk transformations of measured chemical properties. Creating the best framework for ambient mixtures will require creativity and novel data-processing methods to determine the best way to simplify the complexities of structure and molecular identity without losing important chemical information.

The data necessary to reach the goal of comprehensive, chemically semi-explicit characterization of ambient aerosol is only now available, since ambient measurements by SV-TAG do not use two-dimensional GC or photoionization, which is necessary to classify compounds by volatility, polarity and molecular weight. However, filter samples collected at several field sites have recently been analyzed with derivatization using the advanced GC and MS instrumentation described in Chapters 3 and 4. To facilitate the characterization of these ambient data, samples of controlled laboratory BVOC oxidation could be collected for analysis using the same instrumentation, which was not yet developed at the time data was collected for Chapter 2 (longifolene oxidation). Comprehensive analysis of oxidation of a known, atmospherically relevant, precursor presents a complex system for the development of a simplified framework, but one that is still easier to understand than ambient data. Furthermore, to better understand and

constrain structures and molecular identities of organic compounds in the atmosphere, the frameworks developed through GC×GC of these samples for complete characterization of aerosol can be supplemented and compared against other for understanding functionality have been applied to atmospheric aerosol. Fourier transform infrared (FTIR) spectroscopy has, for instance, been relatively widely used to measure the functionality of atmospheric particles (Hallquist et al., 2009; Turpin et al., 2000), but lacks any separation by volatility or molecular identification. This and other spectroscopic methods can and should be compared employed to create a more complete picture of the chemical properties of atmospheric components.

Current chemical understanding has focused on specific chemical pathways of compounds known to be dominant components, i.e. isoprene oxidation under various conditions. This approach can yield significant global insights, but falls short of being able to predict the products in an arbitrary atmospheric environment that does not fall into the combination of precursors or reactive environments explicitly studied. The goal to characterize mixtures by structure instead of measured bulk properties stems in part from the idea that chemistry of a mixture can be described, if imperfectly, as the combination of reactions between individual molecules and atoms. For example, reaction of a saturated hydrocarbon with a hydroxyl radical can be well described using a structure-activity relationship to predict the isomer distributions, rates, and products of hydrogen abstraction (Atkinson, 1987, 1997, 2003). By extension, knowing the structural properties of a mixture that control these variables (i.e. ratios of primary, secondary, and tertiary carbons) will allow some understanding or prediction of the chemical pathways and products. This idea has not been tested on a large or atmospherically relevant scale – it is not known if the dominant reactions in the atmosphere can be considered as the sum of their structural components. While the atmosphere is extraordinarily complex and cannot be completely understood by structure or explicitly modeled, a structurally informed classification framework would allow for some improved prediction of the oxidation of pathways of atmospheric organic mixtures. For example, using the framework described in Chapter 3, description of vehicular emissions by structure has been shown to roughly explain SOA formation in an urban environment (Gentner et al., 2012). To further determine the feasibility of using simplified frameworks to predict chemistry of a wider variety of compounds, controlled laboratory oxidation of model compounds can be studied individually, as part of a mixture, and as structural analogues of other compound. For example, the products of dodecylcyclohexane oxidation may be at least partly predictable by understanding the chemical reaction pathways of dodecane and cyclohexane; likewise, the distribution of functional groups formed through oxidation of various terpenes is expected to be dependent on the number and location of double bonds and may be able to be characterized or parameterized as such.

While the offline techniques used to build these frameworks provide more detail, they are built primarily on the in-depth analysis of small numbers of samples. The higher time resolution provided by in situ measurements is important for a comprehensive understanding of aerosol, but also generates thousands of chromatograms over the course of a field campaign. In part to tackle this data volume, gas chromatography has traditionally been relied upon only for identification of known compounds. However, as demonstrated throughout this work, even unknown compounds provide valuable information; to focus on only known compounds is to discard most of the data collected. Expedited processing that makes use of all collected data is possible through the parameterization of ambient SV-TAG data by adaption of comprehensive frameworks developed from more detailed, offline, GC×GC data. Though SV-TAG lacks polarity separation or advanced mass spectrometry methods, compounds can be classified by available information (i.e.

volatility, mass spectral information) as in Chapter 7. Data analysis techniques remain to be developed to efficiently and robustly tackle these large datasets in a useful way. In typical chromatographic analysis, analytes of interest are identified in one or two chromatograms and then chromatographic peaks are integrated separately in each sample throughout the dataset. Any potential compounds of interest that are not present in the samples used for identification are likely overlooked. Instead, all chromatograms should be considered as a single dataset, with compounds of interest identified via variability throughout the dataset, and integration of peaks informed by trends in the data to ensure data quality. Such an approach would greatly reduce necessary processing timing and would likely yield many new atmospheric tracers. The complexity of the necessary analysis algorithms is a substantial barrier to the automated implementation of such a "whole dataset" approach. However, it is already possible to explore novel ways to view changes in chromatograms and mass spectra across time to identify potential new compounds of interest.

While comprehensive analysis of the chromatographic development is not yet a completely realized goal, SV-TAG has yielded unprecedented time resolution and measurements of gas-particle partitioning of known organic tracers. However, instrument limitations still prevent the unambiguous measurement of some compound classes known to be significant fractions, specifically organosulfates, organonitrates, and organic hydroperoxides. All three compound classes are expected to be prevalent and potentially important in the formation of new particles (Ehn et al., 2014; Perring et al., 2010; Surratt et al., 2008), but measurements of these compounds in the particle phase are sparse and typically integrated over many hours or days. Current SV-TAG operation involves thermal desorption of analytes, followed by reaction with a derivatizing agent; this process may convert these thermally and chemically labile species into compounds that are indistinguishable from those containing the analogous hydroxyl group. Due to the difficulty in obtaining and transporting atmospherically relevant compounds of these classes, little is known about their analysis in this instrument. In some cases, these species may survive analysis but cannot be identified due to lack of known mass spectral signatures, so use of element-specific detectors (i.e. a nitrogen phosphorous detector, NPD, or a sulfur chemiluminescence detector, SCD) may highlight these compounds. Experimentation with alternative derivatization agents may also provide a means to separate or selectively react with such compounds, but little research exists about derivatization of these compound classes and they are likely to be multi-functional. Multi-stage derivatization or entirely different analysis techniques may be necessary to target these compound classes, but hourly (or faster) measurement of these species in the particle phase would be an important and substantial advancement in aerosol measurements.

It is clear from Chapter 7 that our understanding of gas-particle partitioning is poor, with a much larger particle fraction for most compounds than predicted by thermodynamic equilibrium. This may be due in part to the thermal decomposition of oligomers or the other high molecular weight compounds discussed above. It is still uncertain if the compounds being measured by SV-TAG are due in part to thermal decomposition of oligomers (or derivatization of i.e. organosulfates), but if so, polymerization reactions may be keeping oxygenated compounds in the particle phase and driving gas-particle partitioning by preventing re-volatilization of compounds from the particle. Though some studies have suggested that organic aerosol may be comprised of 50-80% oligomers (Angove et al., 2006; Kalberer et al., 2004), identified oligomers typically account for only a very small fraction of organic mass (Lin et al., 2012). The role of these high molecular weight compounds needs to be studied in more detail, either through instrumental changes, or

controlled laboratory testing. Adjusting operational parameters may result in more or less thermal decomposition of oligomers, providing a means to probe their prevalence. Alternately, analysis of samples by these thermal decomposition techniques can be combined with methods to quantify oligomers in order to constrain their impact on observed gas-particle partitioning. Laboratory studies of gas-particle partitioning coupled with quantification of oligomers may shed some light on its driving factors. Furthermore, partitioning measurements in regions dominated by biogenic emissions but containing relatively little particle-phase water would improve understanding of the role of water in these processes.

The areas of future research described here are a limited window into the significant progress that can still be made using the methods described in this work. Comprehensive description of ambient aerosol as well as its chemical oxidation pathways remains to be achieved, as has simplified processing of all chromatograms across a dataset. This large-data approach would be improved through future instrument advances to focus on important compound classes, especially oligomers, which may be a dominant factor in understanding particle formation, condensation, and volatilization.

Appendix A

Vapor pressure calculation from GC×GC retention times for low-polarity compounds

Both the EPA Estimation Program Interface (EPI) Suite and the SIMPOL group contribution method show an error on the order of half an order of magnitude in calculated vapor pressures in the volatility range of the compounds used in this work (Pankow and Asher 2008; U.S. EPA 2008). Therefore, the decision to use one over the other is a question of empirical fit to the data. Figure A1 shows the precision of the planar fit in the case of the EPI method and the SIMPOL method (Figs. A.1a and b respectively), where the calculated values are used to create a planar fit and then the known compounds are mapped back on to this fit. The values calculated and those estimated from the fit fall along the 1:1 line in both cases, but fall much closer to the line in the case of the EPI method. Furthermore, and perhaps more importantly, the error in the SIMPOL fit is strongly functional group dependent, suggesting a systematic error that is likely to adversely affect the v_P-fit. In addition, SIMPOL does not include a group contribution for a nitrile group, so alkylnitriles are excluded from this fit though they are known to be present in the atmosphere. The error of these fits is shown in Fig. A.2 as the residual of the planar fit (that is, how far off of the 1:1 line a compound falls). The standard deviation for the error of the EPI method is 0.5 orders of magnitude, which is approximately the error expected from a group contribution method. The error for the SIMPOL method is twice that. The EPI method is therefore selected because it has a better fit, less systematic error, and a method that allows a fit to be drawn based on a more inclusive suite of compounds. It must be noted that this is not necessarily a universal decision and does not speak to the accuracy of one method over another. Instead, this simply suggests that the properties that affect retention times for the particular columns used in this work are more closely mirrored by the parameterization of the EPI method. Future applications of this method should perform a similar sensitivity analysis.

Table A.1. List of 25 known and 10 confidently identified aliphatic compounds used in parameter fits. Forward Match (FM) and Reverse Match (RM) are measures of the certainty of the NIST library search match; in general, higher numbers indicate greater certainty. All of the compounds in this table have been identified with high certainty. For a more in depth discussion, see Worton et al. (2011). [a]FM and RM are shown only for compounds identified in ambient samples. All other compounds used are from known standards.

Compound	t_R[1]	t_R[2]	*Compound class*	*O/C*	*FM*[a]	*RM*[a]
n-Tetradecane	40.3	0.0	alkane	0.00		
5-Hexyldihydro-2(3H)-furanone	41.5	2.3	ester	0.20		
n-Pentadecane	42.3	0.1	alkane	0.00		
n-Dodecanoic acid	43.5	0.7	acid	0.17		
5-Heptyldihydro-2(3H)-furanone	44.2	2.8	ester	0.18		
n-Hexadecane	44.6	0.1	alkane	0.00		
5-Octyldihydro-2(3H)-furanone	47.1	3.1	ester	0.17		
Tetradecanenitrile	47.2	1.7	nitrile	-	674	740
2-Pentadecanone	47.4	1.1	ketone	0.07	800	878
n-Heptadecane	47.5	0.2	alkane	0.00		
Pristane	47.6	0.2	alkane	0.00		
Myristoleic acid	49.1	0.9	acid	0.14		
n-Tetradecanoic acid	49.4	0.9	acid	0.14		
n-Octadecane	50.6	0.2	alkane	0.00		
Phytane	51.1	0.3	alkane	0.00		
6,10,14-Trimethyl-2-pentadecanone	51.8	1.2	ketone	0.06	617	684
6-Nonyltetrahydro-2H-pyran-2-one	53.3	3.2	ester	0.14	617	684
Hexadecanenitrile	53.7	1.7	nitrile	-	876	927
2-Heptadecanone	53.8	1.1	ketone	0.06	715	767
n-Nonadecane	54.2	0.2	alkane	0.00		
Hexadecanoic methyl ester	54.6	0.7	ester	0.12	779	816
cis-9-Hexadecenoic acid	55.4	1.0	acid	0.13		
n-Hexadecanoic acid	56.0	0.9	acid	0.13		
n-Eicosane	57.4	0.3	alkane	0.00		
cis-10-Heptadecenoic acid	58.6	0.9	acid	0.12		
5-Dodecyldihydro-2(3H)-furanone	60.4	2.8	ester	0.13		
Octadecanenitrile	60.6	1.7	nitrile	-	794	824
n-Heneicosane	61.1	0.3	alkane	0.00		
(Z,Z)-9,12-Octadecadienoic acid	62.0	1.0	acid	0.11		
(Z)-9-Octadecenoic acid	62.2	0.9	acid	0.11		
n-Octadecanoic acid	63.1	0.9	acid	0.11		
n-Docosane	64.3	0.3	alkane	0.00		
5-Tetradecyldihydro-2(3H)-furanone	66.5	2.6	ester	0.11	688	724
n-Tricosane	67.5	0.3	alkane	0.00		
bis(2-ethylhexyl) hexanedioic ester	69.0	1.4	ester	0.18	859	874

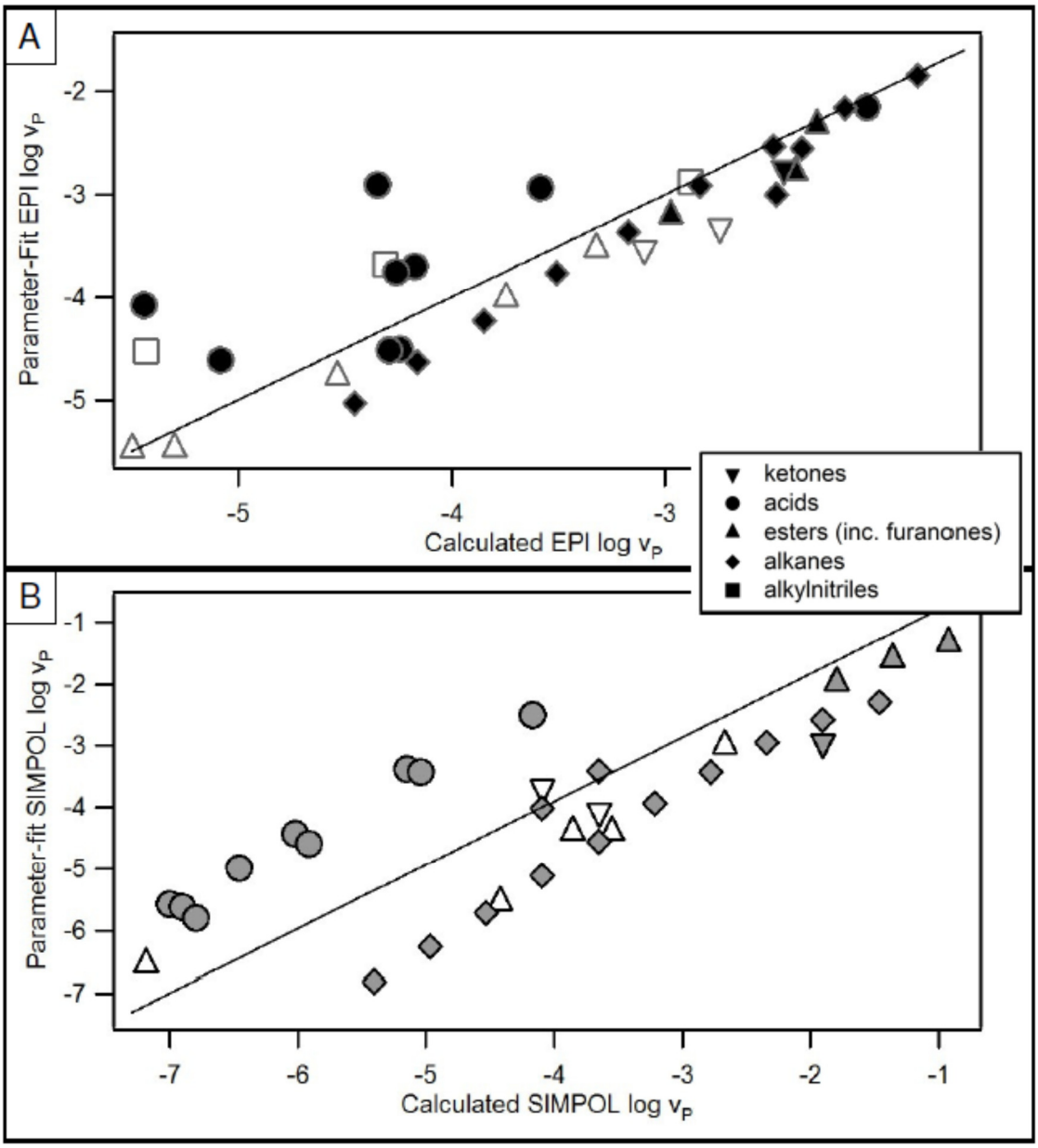

Figure A.1. Vapor pressures as calculated by the (a) EPI method and (b) SIMPOL method compared to the values estimated from the planar fit. Filled markers are standard compounds, open markers are confidently identified in ambient data

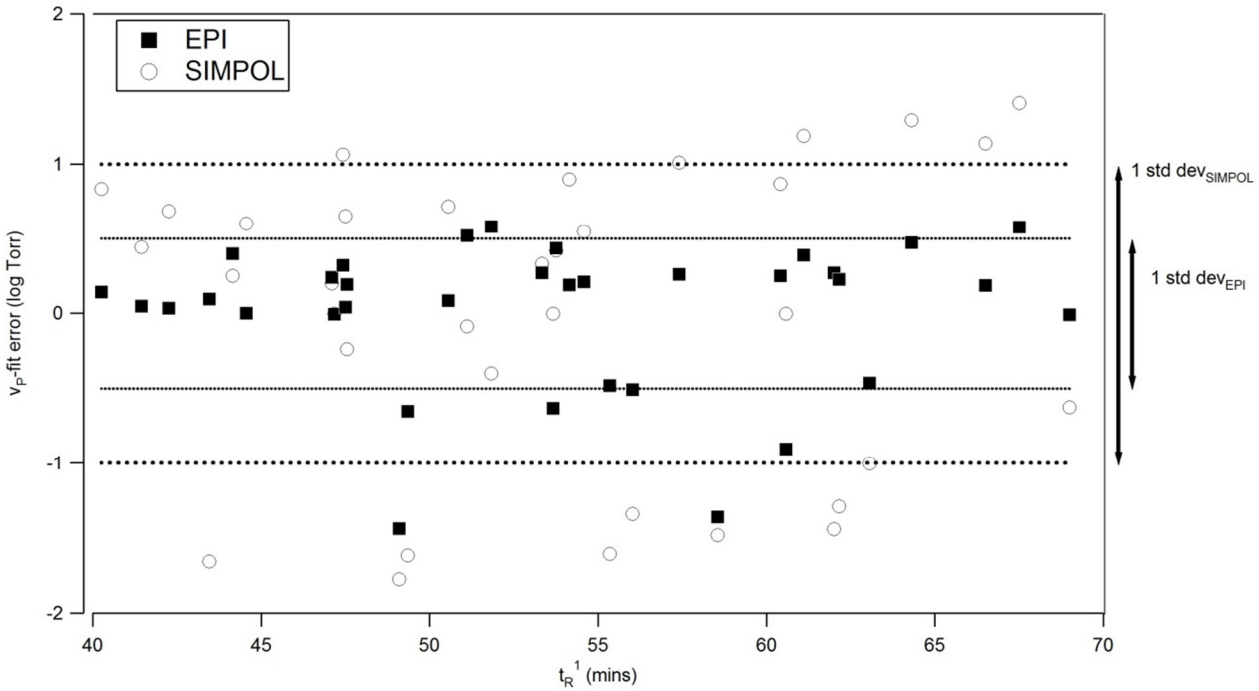

Figure A.2. Error of the EPI and SIMPOL planar fits as the difference between the value estimated from parameter fit and the value originally calculated by the method.

Appendix B

Vacuum ultraviolet mass spectra of sample compounds and dependence on chromatographic and ionization parameters

This appendix contains a discussion of optimization of the parameters used to collect mass spectra, as well as sample mass spectra of known compounds using vacuum ultraviolet (VUV) ionization at transfer temperatures of 150 °C and 275 °C. Parent ion is shown in bold.

Fragmentation using VUV ionization is sensitive to temperature at the time of ionization as well as energy of the ionizing photons. In gas chromatography, the elution of compounds is dependent upon heating the chromatographic column using a temperature ramp that is optimized for speed and resolution so cannot be significantly modified. However, the temperature of the transfer line between the GC and the TOFMS, as well as the temperature of the ionization chamber in the TOFMS, can be varied; in this work, these temperatures were always modified together to create a uniform "transfer temperature." Using an injection of a standard containing C_8 through C_{40} *n*-alkanes, fragmentation was observed to be strongly dependent on transfer temperature (Fig. B.1). The gap between internal energy and IE widens as IE decreases with carbon number, causing the associated downward trend in f_P observed in Figure S-1. Branched alkanes fragment approximately twice as much as straight-chain alkanes and are more sensitive to photon energy because they tend to have lower ionization energies.

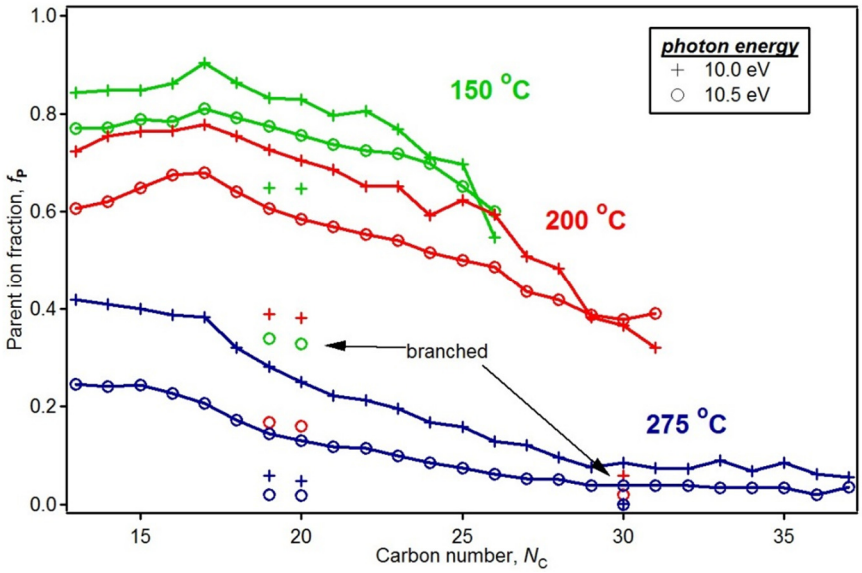

Figure B.1. Fraction of ion abundance in the mass spectrum observed as the parent ion peak (f_P) for *n*-alkanes in the range of C_{14} to C_{37} at differing transfer temperatures (green: 150 °C; red: 200 °C; blue: 275 °C) and photon energies (open circles: 10.5 eV; crosses 10.0 eV). Branched alkanes shown are pristane (C_{19}), phytane (C_{20}), and squalane (C_{30}).

In contrast to transfer temperature sensitivity, photon energy was observed to have a much smaller effect on f_P in the mass spectra of the compounds presented here, including acids, ketones, esters, and aromatics. Straight-chain alkanes in the C_{10}-C_{30} range are expected to have ionization energies at or near 10 eV, while the ionization energies of aromatics and other unsaturated hydrocarbons are expected to be significantly lower. Photon energy can therefore be used as a parameter to determine the presence of double bonds in a compound. Application of this technique in this work suggests that most hydrocarbon mass in this diesel sample is fully saturated.

In Fig. B.1, lower volatility alkanes are not shown at low transfer temperatures because under these conditions they cannot be efficiently transferred to the TOFMS, demonstrating the balance between fragmentation and chromatographic transfer needs. The optimized parameters for any GC-VUV-MS application vary depending on analyte volatility range of interest. Diesel fuel, the hydrocarbon mixture used in this study, is not expected to contain significant organic mass in the range of C_{26}-C_{40}, so a transfer temperature of 150 ^{o}C (green line in Fig. B.1) was used in this work. This provides minimal fragmentation, improving detection of the compounds studied in this work.

Mass spectra of three sample compounds are shown in Fig. B.2 at high and low transfer temperatures. Spectra of 84 injected compounds are available in the Supplementary Information of Isaacman et al. (2012).

Figure B.2. VUV mass spectra docosane, phytane, and isopimaric acid with a transfer line temperature of (a-c) 150 °C and (d-f) 275 °C.

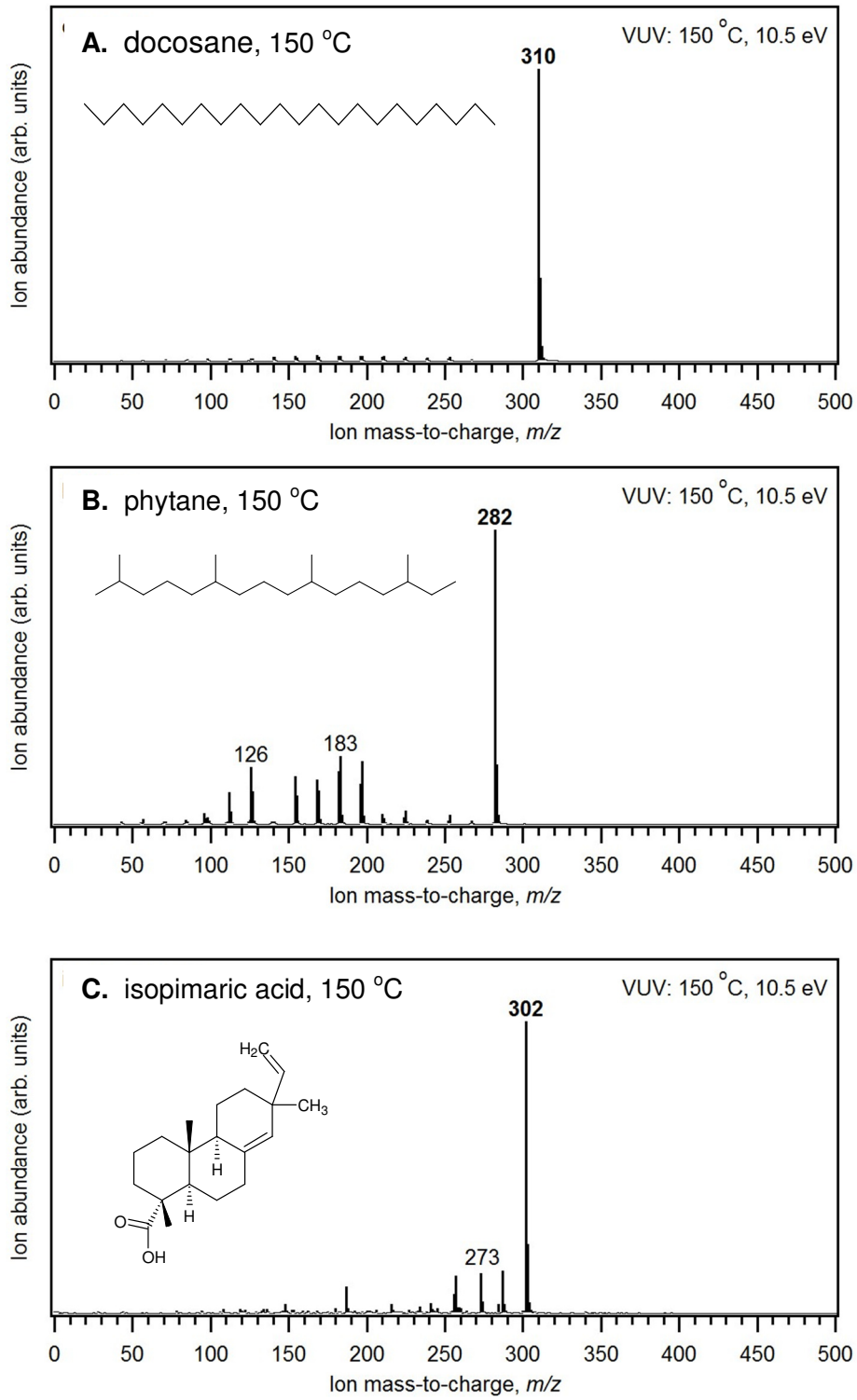

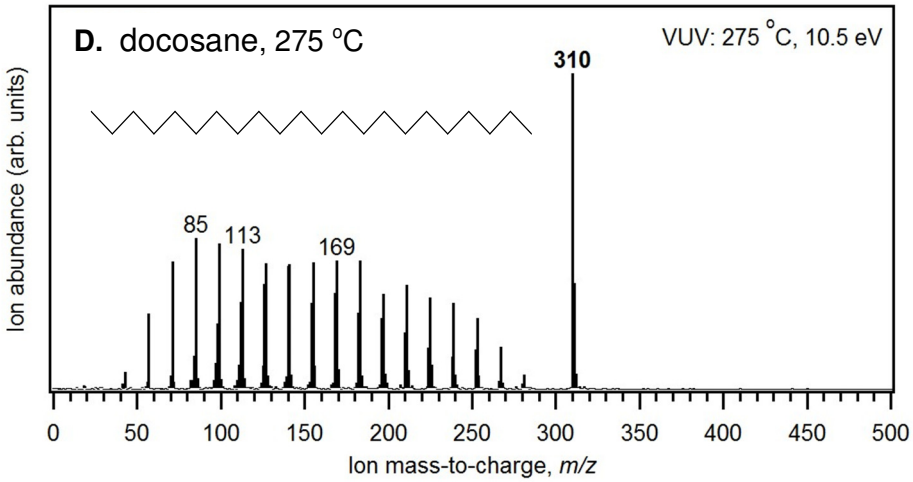
D. docosane, 275 °C
VUV: 275 °C, 10.5 eV
310
85
113
169
Ion abundance (arb. units)
0 50 100 150 200 250 300 350 400 450 500
Ion mass-to-charge, m/z

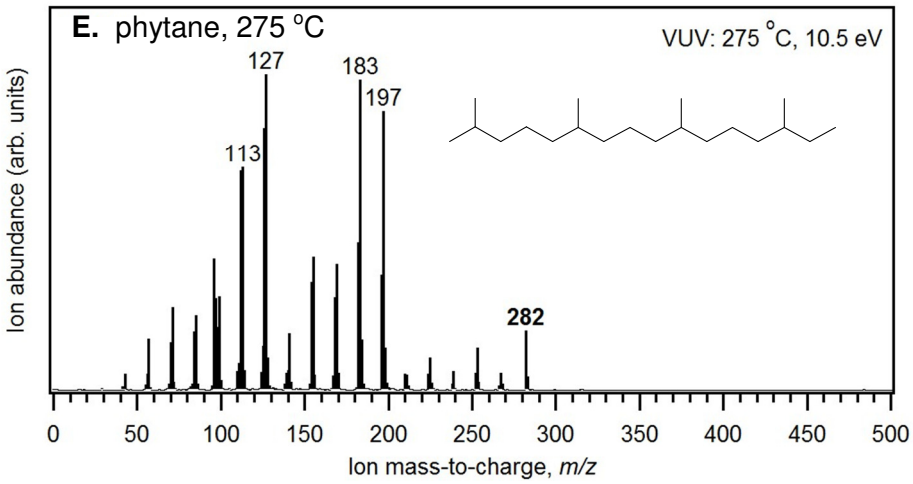
E. phytane, 275 °C
VUV: 275 °C, 10.5 eV
127
183
197
113
282
Ion abundance (arb. units)
0 50 100 150 200 250 300 350 400 450 500
Ion mass-to-charge, m/z

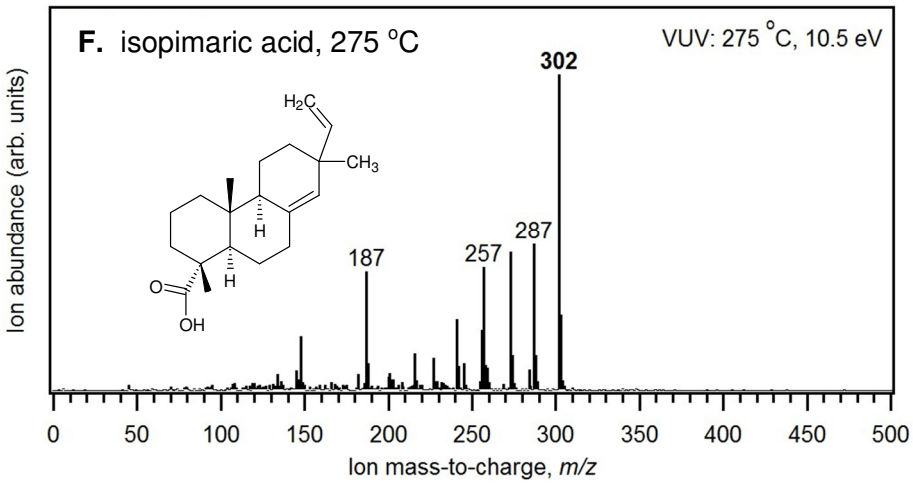
F. isopimaric acid, 275 °C
VUV: 275 °C, 10.5 eV
302
H2C
CH3
H
H
O
OH
187
257
287
Ion abundance (arb. units)
0 50 100 150 200 250 300 350 400 450 500
Ion mass-to-charge, m/z

Appendix C

Quantification of relative rates in motor oil oxidation

C.1. GC/VUV-HRTOFMS calibration and linearity

Calibration of GC/VUV-HRTOFMS data in this work was performed through the use of authentic standards, as discussed and listed in Sect. 4.2.2. The calibration curves for these compounds are shown in Fig. C.1.

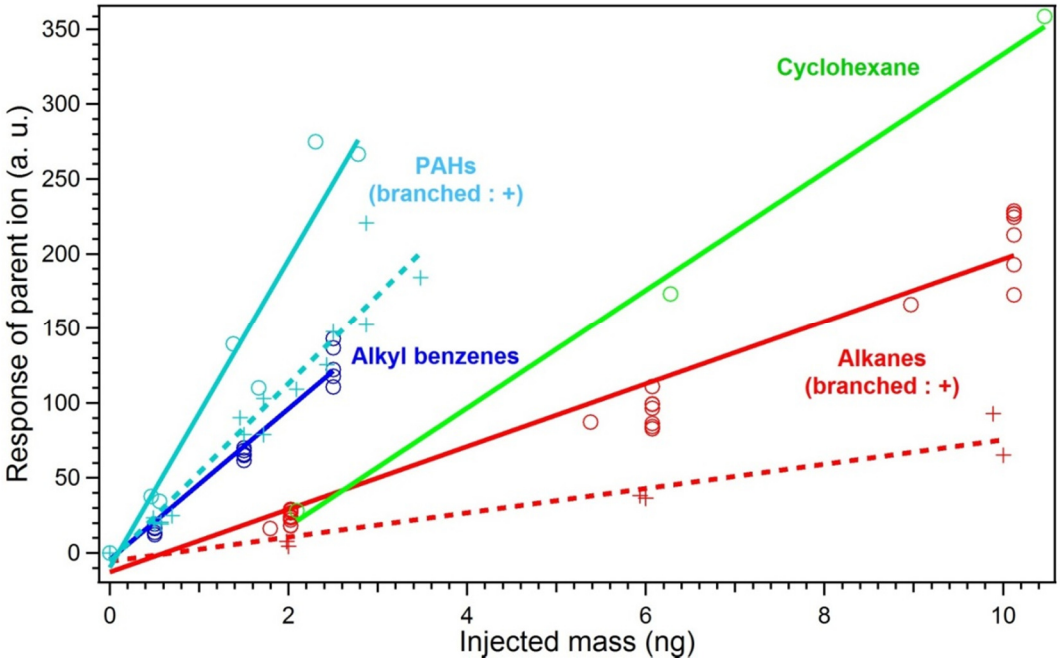

Figure C.1. Calibration curves for injected compounds. Full list of compounds is presented in Sect. 4.2.2 of the text.

Kinetics results presented in this work are calculated using Eq. 4.2, reproduced here:

$$\ln \frac{S_{t,i}}{S_{0,i}} = k_{eff,i}\{C_{OH}t\} \qquad \text{Eq. C.1}$$

where the OH exposure, $\{C_{OH}t\}$, is determined from the decay of the gas-phase tracer, hexane. As discussed in the text, $k_{eff,i}$ is calculated from the slope of the chromatographic signal of i at time t ($S_{t,i}$) relative to initial measured signal ($S_{0,i}$) (normalized for sample volume) as a function of OH exposure. Chromatographic signals are related to mass (M) through a response factor (α):

$$S_{t,i} = \alpha M_{t,i} \qquad \text{Eq. C.2}$$

In a linear response regime such that α is a constant, chromatographic signal can be used directly in Eq. C.1 without the need for quantitative calibration:

$$\frac{S_{t,i}}{S_{0,i}} = \frac{\alpha M_{t,i}}{\alpha M_{0,i}} = \frac{M_{t,i}}{M_{0,i}} \qquad \text{Eq. C.3}$$

Therefore, though absolute calibration curves are necessary to quantitatively characterize the composition of the motor oil particles, the bulk of this work relies on relative quantitation that does not necessitate calculation of absolute response factors, instead relying on the assumption of linearity. Linearity is demonstrated clearly for known compounds (Fig. C.1), so is assumed for compound classes lacking authentic standards. Cycloalkanes exhibit a non-linearity at low concentrations possibly due to a scarcity of available data, but this is below the measured signal intensity for these samples (intensity typically > 50 a. u.), so the linearity at higher concentrations has been highlighted.

C.2. Relative uptake coefficients

In order to compare the results presented in this work to previous research, data in Chapt. 4 is displayed in terms of γ_{eff}. However, to more broadly apply these results, it is useful to discuss the measured values in average, relative terms, as we have done in Sect. 4.3.2. The data used to generate the average values discussed in that section are shown in Figure C.2, in which branched alkanes are displayed relative to straight-chain alkanes, and cyclic compounds are displayed relative to total alkanes, which is typically dominated by the B1 and B2 isomers. C_{28} and C_{29} *n*-alkanes exhibit slightly lower average uptake coefficients than expected based on trends from lower molecular weight alkanes, resulting in higher than expected relative uptake coefficients. This may be an artifact of measurement errors caused by low abundances of large *n*-alkanes in the initial motor oil particles, as the absolute uptake coefficients (shown in Fig. 4.4) for lower molecular weight branched alkanes do not exhibit the same spikes. The enhancement of branching on uptake coefficients is included in Figs. C.2 and C.3.

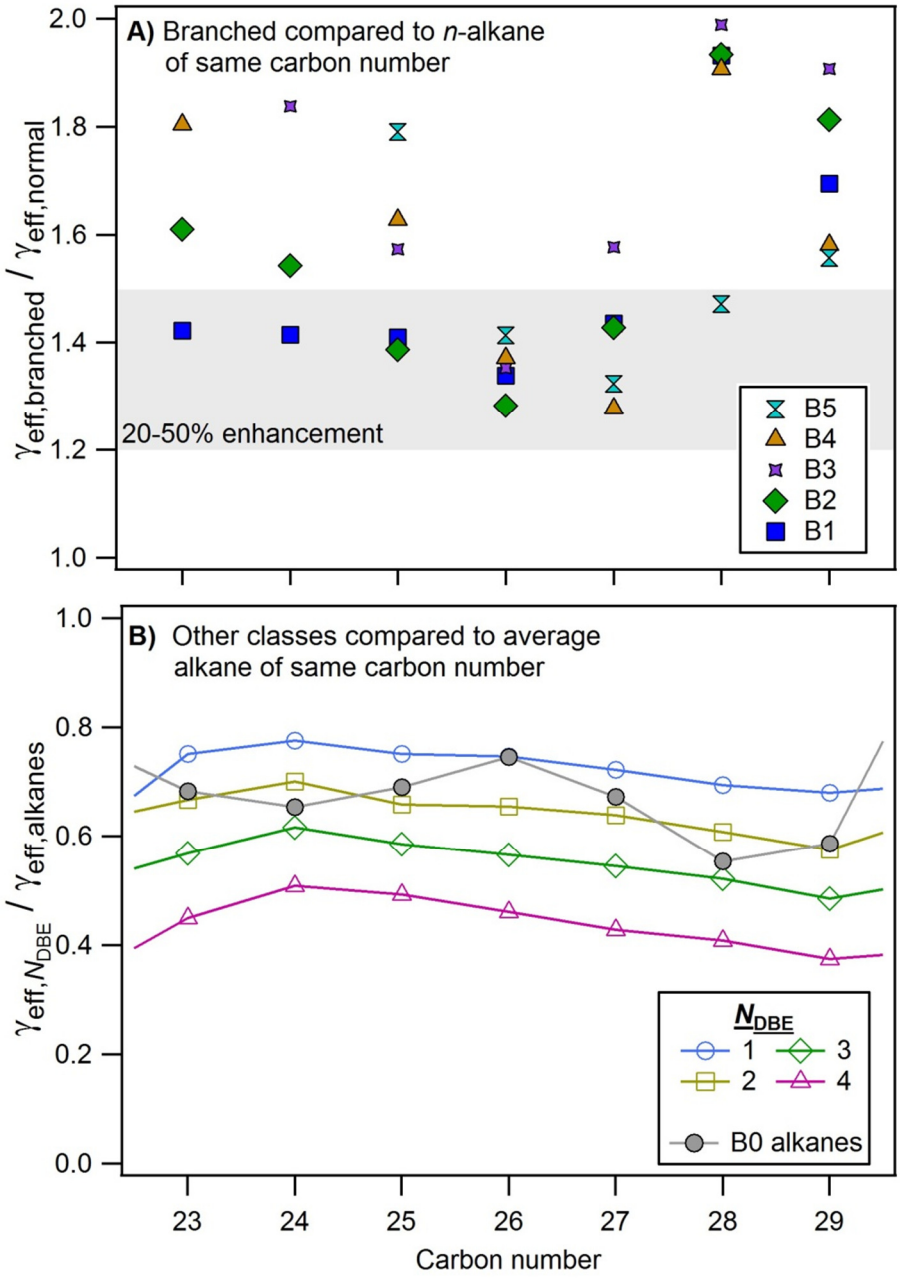

Figure C.2. Relative uptake coefficients of a) branched alkanes compared to *n*-alkanes of the same carbon number and b) cyclic compounds (N_{DBE} = 1 through 4) and straight-chain alkanes compared to average alkanes of the same carbon number.

Volatility correction was performed to account for the effects of partitioning on measured relative uptake coefficients. As discussed in the text, branched alkanes were compared to the expected uptake coefficient of an *n*-alkane of equivalent volatility based on a polynomial fit through the known data (Fig. C.3). An increase in the relative rates of the lower molecular weight compounds is observed, similar to that seen in Fig. C.2 and likely due to similar measurement errors.

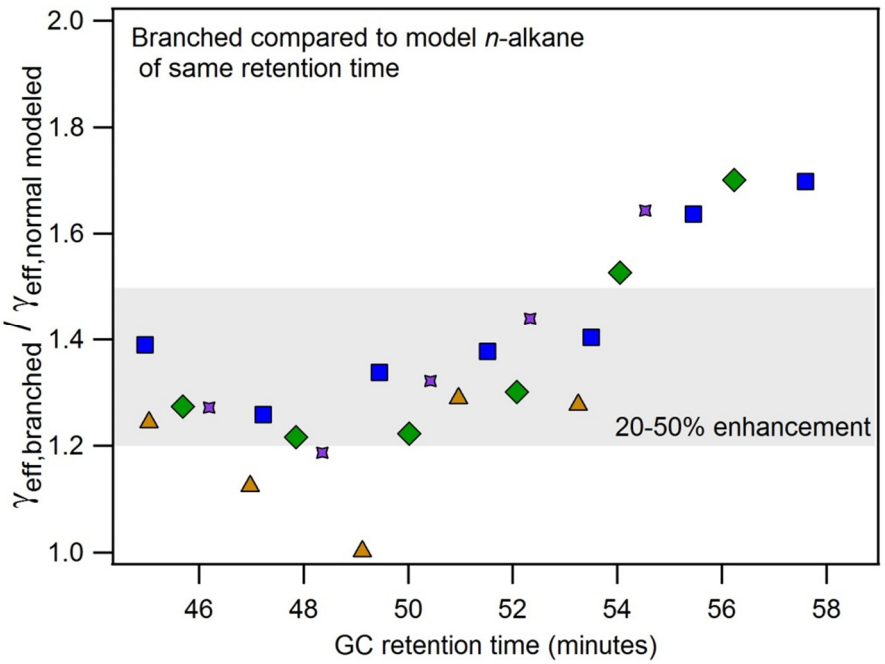

Figure C.3. Relative uptake coefficients of branched alkanes compared to modeled *n*-alkanes of similar volatility

Appendix D

Uncertainty in quantification and partitioning measured by dual-cell SV-TAG with derivatization

D.1. Derivatization efficiency tests

As discussed in the text, derivatization efficiency is tested using repeated injection of a mixture including 43 oxygenated compounds. In Table S1, names of the compounds injected and their molecular formulas and number of OH groups are shown, as well as the retention index of the derivatized compound. For every OH group, the derivatized compound eluted contains a trimethylsilyl group, adding C_3H_8Si to the formula of the observed peak. Observed relative retention times are shown as a Kovats-like (Kovats, 1958) retention index relative to *n*-alkanes, with i.e. *n*-pentacosane (C_{15}) having an index of 1500. Compounds span a retention time of approximately tridecane to tetratriacontane, but most (38 compounds) elute earlier than pentacosane.

Table D.1. Compounds injected to assess derivatization efficiency: name, molecular formula, number of OH groups, and retention index of the derivatized peak relative to an *n*-alkane series.

Injected Compound Name	Molecular Formula	Number OH Groups	Derivatized Retention Index
Glyceric acid	$C_3H_6O_4$	3	1323
2,6-Dimethoxyphenol (Syringol)	$C_8H_{10}O_3$	1	1398
3,3-Dimethylglutaric acid	$C_7H_{12}O_4$	2	1433
n-Decanoic acid	$C_{10}H_{20}O_2$	1	1453
Threitol	$C_4H_{10}O_4$	4	1493
Erythritol	$C_4H_{10}O_4$	4	1501
Ketopinic acid	$C_{10}H_{14}O_3$	1	1507
cis-Pinonic acid	$C_{10}H_{16}O_3$	1	1526
3-Methoxy-4-hydroxybenzaldehyde (Vanillin)	$C_8H_8O_3$	1	1537
2-Methoxy-4-propenylphenol (Isoeugenol)	$C_8H_{10}O_3$	1	1568
Diethyltoluamide	$C_{12}H_{17}NO$	0	1582
Benzophenone	$C_{13}H_{10}O$	0	1645
cis-Pinic acid	$C_9H_{14}O_4$	2	1663
γ-Dodecalactone	$C_{12}H_{22}O_2$	0	1688
Levoglucosan	$C_6H_{10}O_5$	3	1698
α-Bisabolol	$C_{15}H_{26}O$	1	1742
n-Tridecanoic acid	$C_{13}H_{26}O_2$	1	1746
1,9-Nonadioic acid	$C_9H_{16}O_4$	2	1791
1,10-Decadioic acid	$C_{10}H_{18}O_4$	2	1887
Methyl palmitate	$C_{17}H_{34}O_2$	0	1924
n-Hexadecanol	$C_{16}H_{34}O$	1	1956
cis-9-Hexadecenoic acid	$C_{16}H_{30}O_2$	1	2022
Homosalate	$C_{16}H_{22}O_3$	1	2025

n-Hexadecanoic acid	$C_{16}H_{32}O_2$	1	2041
1,12-Dodecadioic acid	$C_{12}H_{22}O_4$	2	2082
Methyl stearate	$C_{19}H_{38}O_2$	0	2125
n-Heptanoic acid	$C_{17}H_{34}O_2$	1	2139
n-Octadecanol	$C_{18}H_{38}O$	1	2154
cis,cis-9,12-Octadecadienoic acid	$C_{18}H_{32}O_2$	1	2206
cis-9-Octadecenoic acid	$C_{18}H_{34}O_2$	1	2213
cis-11-Octadecenoic acid	$C_{18}H_{34}O_2$	1	2220
n-Octadecanoic acid	$C_{18}H_{36}O_2$	1	2240
1,14-Tetradecanoic acid	$C_{14}H_{26}O_4$	2	2275
n-Eicosanol	$C_{20}H_{42}O$	1	2349
Isopimaric acid	$C_{20}H_{30}O_2$	1	2353
16-Hydroxyhexadecanoic acid	$C_{16}H_{32}O_3$	2	2385
12-Hydroxyoctadecanoic acid	$C_{18}H_{36}O_3$	2	2423
Abietic acid	$C_{20}H30O_2$	1	2433
Deoxycholic Acid	$C_{24}H_{40}O_4$	3	3065
Cholesterol	$C_{27}H_{46}O$	1	3166
β-Stigmasterol	$C_{29}H48O$	1	3297
β-Sitosterol	$C_{29}H_{50}O$	1	3360
Lupeol	$C_{30}H_{50}O$	1	3441

D.2. Derivatization reproducibility tests

When correcting analytes for run-to-run variability using internal standards, an internal standard must be selected to use for the correction. Several possible selection criteria are available for correction of oxygenated compounds. Table D.1 in the main text lists the schemes tested for correction of all oxygenates with hydroxyl groups and the error of each scenario, measured as the relative standard deviation from the average ratio of one internal standard to another one selected based on the criteria of the scenario. Figure D.1 shows the cumulative error distribution for a subset of the test scenarios selected to apply to most, if not all, operating conditions. Correcting for compounds using an internal oxygenated standard of only similar volatility (i.e. in the case of analytes of unknown structure or a functionally similar internal standard is unavailable) is modeled by correcting all oxygenates to the nearest *n*-acid in volatility, of which there are 4 of various volatility in the standard used (Fig. D.1a). The error present in correcting for only general changes in derivatization efficiency is quantified by correcting all oxygenates using a single, relatively stable oxygenate, *n*-octadecanoic acid-d_{35} (Fig. D.1b). Under operating conditions requiring minimal internal standards or maximizing standard stability by not including oxygenates, oxygenates can be corrected for variability in transfer efficiency and detector sensitivity using only alkanes of similar volatility, but this results in large errors with a relatively non-Gaussian distribution (Fig. D.1c). Due in part to operational improvements after the SOAS field campaign, Study 2 has lower error in all cases shown in Fig. D.1 owing to more reproducible measurements of multi-functional acids.

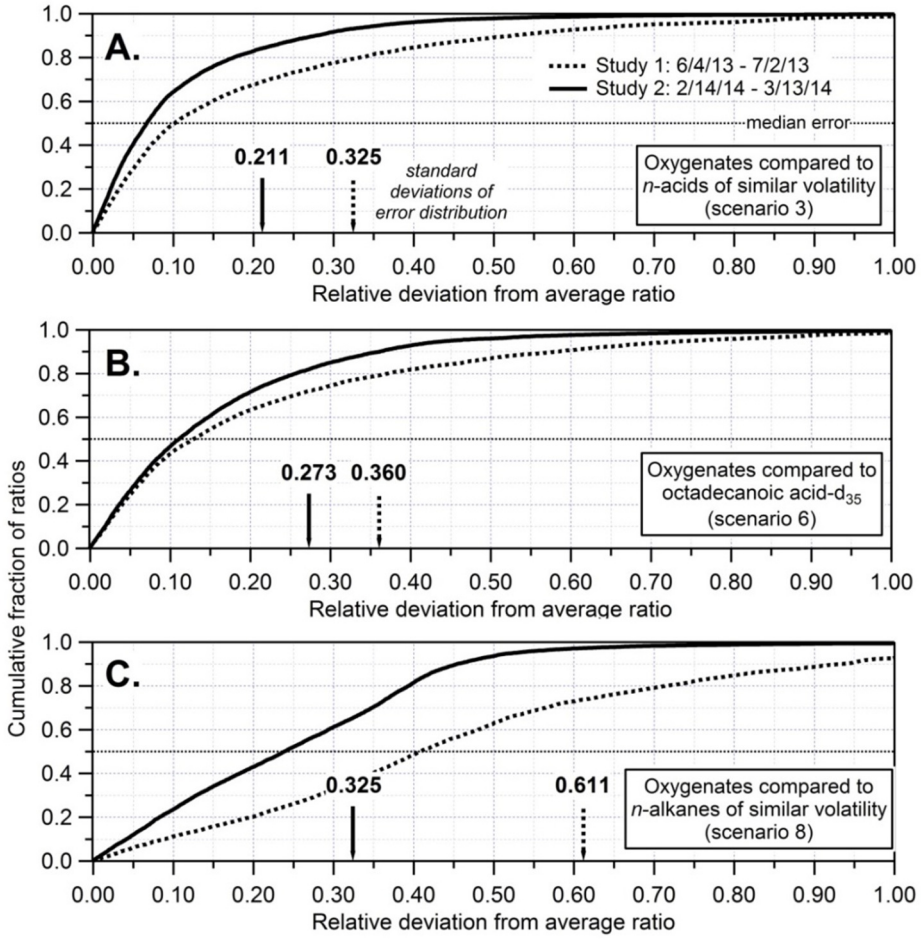

Figure D.1. Cumulative distribution of error in correction of oxygenates for run-to-run variability in derivatization efficiency and instrument response measured as relative deviation of two internal standards from their average ratio. Boxes and Sect. D.2 describe each correction scenario, which are numbered corresponding to Table 6.1 in the main text. Arrows show relative standard deviation for each study. Dotted line is median error (50% of points halve less than this error).

D.3. Total uncertainty

The main text of this manuscript addresses reproducibility and precision in derivatization. To explicitly calculate total uncertainties in reported masses and fractions in the particle, the two independent cells of the instrument also have to be calibrated and then compared. Uncertainty in mass calibration using a linear calibration curve is described by NIST (2012) and is applied in Sect. S3.1 without significant modifications to recommended practices. Differences between parallel sampling cells are removed through normalization to the mean response of the two cells to identical samples, with the magnitude and uncertainty in this normalization included in estimation of mass uncertainty as described in Sect. D.3.2. Finally, in Sect. D.3.3, uncertainty in particle fraction is found to be a function of this normalization, as well as derivatization precision as discussed in the main text, but not mass calibration.

Known compounds are found below to be quantified with 20-25% accuracy, though detailed error analysis is actually compound-, study-, and even point-specific. By calculating fraction in particle before performing mass calibration, partitioning can be measured with less uncertainty than simply compounding the error in two compared mass measurements. Fraction in particle is thus found to also be measured with approximately 15-25% uncertainty; formal estimation of this error is confirmed through empirical estimates. Calculating F_P from signals also allows measurement of particle fraction even for compounds which are not unambiguously identified or for which no authentic standard exists. Data from this instrumented is found to be best reported as total mass and fraction in the particle, with particle mass calculated from these two value, because particle mass is typically lower and thus more uncertain than total mass.

D.3.1. Uncertainty in mass calibration of a single cell

Raw signal, R_A^i, of an analyte in either cell, i, is ratioed to the raw signal of an internal standard, R_{IS}^i, to generate a corrected signal, S_A^i, that accounts for any systematic variability in instrument response. The uncertainty in this correction for run-to-run variability is detailed in the main text and is defined here as σ_S^i, a relative uncertainty in precision. It depends on the similarity between the analyte and the internal standard, but in typical operation is usually 10-15% depending on the compound (and includes uncertainty in the AutoInject injections).

Calibration curves as shown in Fig. 6.5 are calculated in terms of calibrant corrected signal, S_c^i, (raw calibrant signal, R_c^i, ratioed by internal standard, R_{IS}^i), against mass injected (using the AutoInject) for all injections within a given operational period. A linear fit of calibrants ($S_C^i = a^i + b^i M_C^i$) is used, such that the mass of an analyte M_A^i is:

$$M_A^i = \frac{S_A^i - a^i}{b^i} \qquad \text{Eq. D.1}$$

Absolute error in mass for any point, j, $\Delta_{M_j}^i$, is derived from the linear fit (NIST/SEMATECH, 2012):

$$\Delta_{M_j}^i = \sqrt{\left(\frac{1}{b^i}\right)^2 {\Delta_S^i}^2 + \left(\frac{-1}{b^i}\right)^2 {\Delta_a^i}^2 + \left(\frac{-\left(S_{A_j}^i - a\right)}{{b^i}^2}\right)^2 {\Delta_b^i}^2 + 2\left(\frac{-1}{b^i}\right)\left(\frac{-\left(S_{A_j}^i - a\right)}{{b^i}^2}\right)\sigma_{ab}^i} \qquad \text{Eq. D.2}$$

Where Δ_S^i is absolute uncertainty in the corrected signal (S_A^i multipled by σ_S^i), Δ_a^i and Δ_b^i are the absolute uncertainty in the intercept and slope, respectively, and σ_{ab}^i is their covariance. Injections of only internal standard (lacking any calibrant) are used as zeroes to constrain the intercept. Inclusion of an intercept term therefore amounts to background subtraction, which is observed in most cases to be within uncertainty of the origin, suggesting background subtraction is minor and any error introduced is included in the error of the intercept term, Δ_a^i.

Error in mass can also be calculated empirically from the fit as the difference between measured and injected mass (NIST/SEMATECH, 2012)

$$\Delta_{M_j}^i = M_{A_j}^i - (\text{mass injected}) \qquad \text{Eq. D.3}$$

As signal approaches the intercept, the relative calibration error increases in importance due to the uncertainty in the intercept term, even when constrained by injections of "zeros". This is demonstrated in Fig. D.2, in which the uncertainty for calibration of pinic acid is calculated both formally from Eq. D.2 (blue squares) and empirically from Eq. D.3 (red circles) and normalized to the observed mass. The formal calculation is in good agreement with the empirical measurements.

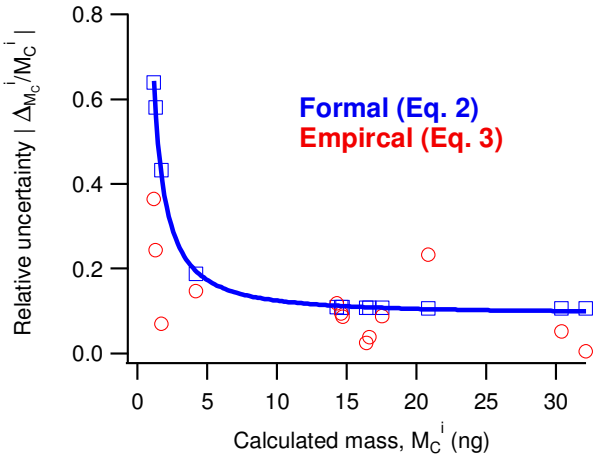

Figure D.2. Relative error in mass calibration of pinic acid during one operational period, calculated with the formal equation (blue) and as the residual of the linear fit for each point (red).

While Δ_M^i is point-specific, uncertainty in the intercept, Δ_a^i, is negligible for large samples so uncertainty for most points is dominated by error in the corrected signal and the slope, which are a constant fraction independent of measured mass. However, uncertainty can be very large at measured masses near the lower limit of the calibration range (Fig. D.2). The detection limit for this compound (3 times the background chromatographic signal) is approximately 0.5 ng on column, in good agreement with Fig. D.2 as uncertainty in the measurement approaches 100% near the detection limit. For compounds with concentrations typically higher than the detection limit, relative mass uncertainty, σ_M^i, can be considered to be 15% (assuming σ_S^i = 10%), though it should be explicitly calculated for each compound. For cases in which most points fall well above detection limit, an average estimate of error for each compound is sufficient, though it is in all cases more desirable to report absolute uncertainty for each measurement when possible.

The uncertainty introduced by the intercept term is expected to be more important in denuded samples, where signals are typically lower, though including an adequate zero or blank measurement can help reduce this source of uncertainty. Consequently, it can reasonably be expected that $M_A{}^{den}$ typically has a higher uncertainty than $M_A{}^{byp}$. The degree to which this is the case depends on uncertainty in the intercept term and the size of denuded signals relative to bypass signals, but suggests error will typically be lower in bypass samples.

D.3.2. Normalizing between cells

In an ideal world, the parallel sampling cells are exactly the same, but this is not the case due to small but consistent differences in derivatization efficiency and/or transfer losses not accounted for by the calibration, so there is a need to correct for these differences. Generating continuous timelines of mass concentrations or to calculate fraction in the particle relies on this correction because during typical operation a sample is denuded on one cell and bypass on the other, then the cells are switched to avoid bias. Variations on this sampling scheme can be employed, but in all schemes there is a fundamental need to intercompare cells. To correct for systematic differences between the cells, bypass samples are periodically collected simultaneously in both cells, providing a direct comparison using real air samples. This comparison is shown in Fig. D.3 using both fully calibrated masses (Fig. D.3a) and uncalibrated signals (Fig. D.3b). Note that calibrating the signal reduces the difference between the cells, but also marginally increases the relative uncertainty in the slope.

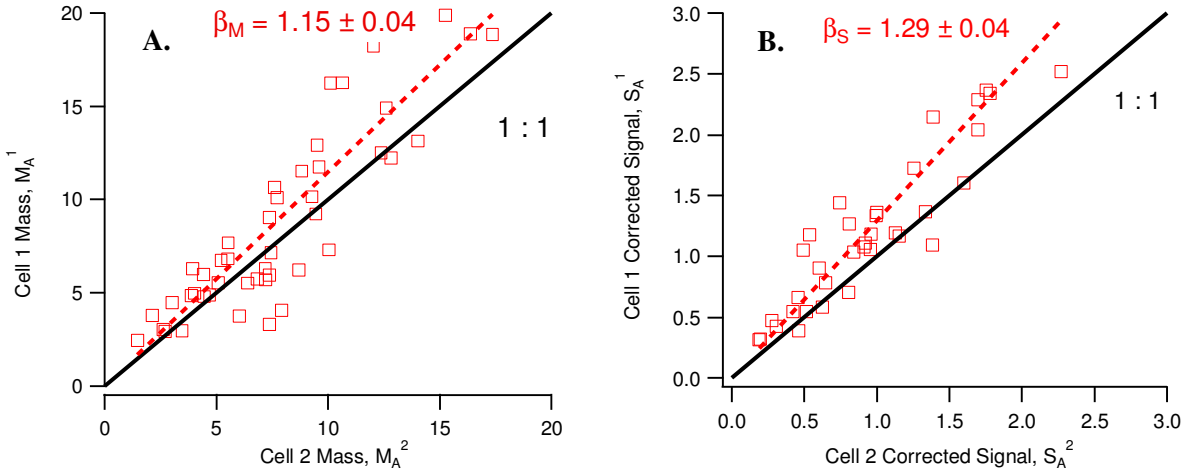

Figure D.3. "Bypass-bypass" comparison of pinic between two cells, Cell 1 and Cell 2, in (a) mass terms, M_A^1 and M_A^2 and (b) signal terms, S_A^1 and S_A^2.

The bypass-bypass comparison of identical samples on the two cells prior to normalization provides an equalization factor, E_M^i, to adjust the cells to their mean value. This equalization can be applied across an entire measurement period, or to subsets thereof. It has been observed that there can be some temporal variability in cell-to-cell differences, so when possible, equalization is performed in small subsets, comparing only the bypass-bypass points nearest in time to each point. This is unlikely to affect average calibrated values, but is expected to yield more accurate temporal and diurnal variability.

The equalization factor is calculated from the best-fit slope, β, (Fig. D.3) which is forced through zero because sample cannot exist on one cell and not the other, so an intercept has no physical meaning. In most cases the intercept is within uncertainty of the fit so forcing through zero simplifies calculations with no detriment to the fit. The equalization factor is therefore:

$$E_M^2 = 0.5(\beta + 1) \quad \text{and} \quad E_M^1 = 0.5(\frac{1}{\beta} + 1) \qquad \text{Eq. D.4}$$

$$\text{and, in relative terms, } \sigma_{E_M} = \sigma_{\beta_M} \text{ (in the shown example, approximately 4\%)} \qquad \text{Eq. D.5}$$

To equalize the cells, the original mass calculated is multiplied by this factor:

$$\text{Adjusted mass, } M_A^{i\,*} = E_M^i \times M_A^i \qquad \text{Eq. D.6}$$

$$\text{with error: } \sigma_{M_p}^{i\,*} = \sqrt{\left(\sigma_M^i\right)^2 + \left(\sigma_{E_M}\right)^2} \qquad \text{Eq. D.7}$$

This error accounts only for uncertainty in precision, designated with subscript *p*, which incorporates uncertainty in the equalization factor, σ_{E_M}, but does not account for systematic errors or instrument biases. The equalization factor is itself a systematic error in accuracy, while other additional instrument uncertainties, σ_I, may also contribute to accuracy error, to yield:

$$\text{total error in mass measurement, } \sigma_M^{i\,*} = \sqrt{\left(\sigma_{M_p}^{i\,*}\right)^2 + (\sigma_I)^2} \qquad \text{Eq. D.8}$$

Because equalization modifies the absolute calibrated mass in each cell, systematic biases must be as great as or greater than the magnitude of the equalization factor. Additional known sources of error, i.e. uncertainty in sample volume, liquid injection, etc., may also cause systematic uncertainties and instrument errors. However, because cells are largely independent – i.e. separate sample volume control and liquid injection volumes – many potential significant sources of instrument error would negatively impact E_M. For example, if uncertainty in sample flow were 10%, it is unlikely the bypass-bypass comparison for any compounds would ever be in good agreement. Therefore, E_M incorporates in large part most other large uncertainties so is expected to be dominate instrument error:

$$\text{total instrument error, } \sigma_I = |E_M - 1| + \sigma_1 + \sigma_2 + \ldots \approx |E_M - 1| \qquad \text{Eq. D.9}$$

Final precision uncertainty for the example compound (pinic acid) is therefore approximately 15% (Eq. D.7: $\sqrt{(15\%)^2 + (4\%)^2}$), with an additional bias error greater than 8% for a total error of approximately 20%. It should be noted that any compound for which an authentic standard error is unavailable has an additional bias error, which is in most cases difficult to constrain.

D.3.3. Uncertainty in Partitioning Fraction, F_P

Fraction in the particle, F_P, is calculated by comparing a "bypass" sample in one cell to a simultaneously collected "denuded" sample in the other cell, which requires equalization between the cells. Though this can most intuitively be considered in mass terms, $F_{P,M}$, calculation of F_P relies solely on the ability to intercompare samples on different cells, not necessarily quantitative mass measurements. F_P can therefore also be considered in signal terms, using a signal-based equalization factor, which will be shown here to result in reduced uncertainty:

$$F_{P,M} = \frac{M_A^{den}}{M_A^{byp}} \times \beta_M \quad \equiv \quad F_{P,S} = \frac{S_A^{den}}{S_A^{byp}} \times \beta_S \quad \text{(in the case where Cell 2 denuded)} \qquad \text{Eq. D.10}$$

As a comparison between the cells, systematic biases in accuracy do not add uncertainty to this calculation. Instead, only uncertainty in precision and the equalization factor are relevant:

$$\sigma_{F_{P,M/S}} = \sqrt{\left(\sigma_{M/S}^{den}\right)^2 + \left(\sigma_{M/S}^{byp}\right)^2 + \left(\sigma_{E_{M/S}}\right)^2} \quad \text{Eq. D.11}$$

In signal terms, the bypass-bypass ratio, β, is expected to be higher than in mass terms, as is observed in Fig. D.3. However, the magnitude of the equalization does adversely affect uncertainty in F_P because uncertainty in intercomparison between cells does not depend on the size of this equalization, only on the uncertainty in the ratio, which is similar or slightly lower in signal terms. Given that σ_M^i is a function of both signal uncertainty, σ_S^i, and calibration error, formulating Eq. D.11 in signal terms using only σ_S^i necessarily yields lower uncertainty.

The formal calculation of error in Eq. D.11 can be tested against an empirical error estimate by investigating scatter around the cell-to-cell equalization line in an ideal case. When the internal standard is very similar to the analyte, as in the example compound (pinic acid – $C_9H_{14}O_4$, using as an internal standard a deuterated adipic acid – $C_6H_6D_4O_4$), the scatter around the equalization line, β, is a result of the uncertainties in corrected signals (σ_S^i) as well as any uncertainties in cell-to-cell equalization and is therefore a good estimate of the error in F_P, similar to Eq. D.3 (NIST/SEMATECH, 2012). The standard deviations of the residual from the equalization line for pinic acid in signal and mass terms (Fig. D.3) are 14% and 18% respectively, very similar to the calculated errors of $\sigma_{F_{P,S}} \approx 15\%$ and $\sigma_{F_{P,M}} \approx 20\%$, so formal calculation of error is found to be reasonable.

If no internal standard is available that is similar to the analyte of interest, equalization using bypass-bypass analyses may result in a bias when comparing bypass to denuded samples due to compound differences in sensitivity to sample concentration. Instead, a formal estimation of error from Eq. D.11 is the best estimate because calculation of σ_S^i using the scenarios shown in the main text does includes error caused by differences between analyte and internal standard. From the estimates in Table D.1, an internal standard containing approximately the same number of OH groups is sufficient to greatly reduce this error. However, a large suite of internal standards is recommended and is typical in SV-TAG operation, allowing relatively unbiased measurement of F_P for all compounds with a robust formally estimated error of 15-25%

It should be noted that particle fraction is calculated as the ratio of one cell to another, so a value of greater than 1 is possible due to measurement uncertainties. Uncertainties are reported as standard deviations, so greater than approximately 70% of points with a particle fraction greater than 1 should be within uncertainty of 1.00, and compounds entirely in the particular phase are expected to be measured as an approximately normal distribution around $F_P = 1$. An example of such a compound is hydroxy glutaric acid (Fig. D.4), which is calculated from Eq. D.11 to have an unceratinty, $\sigma_{F_{P,S}}$, of approximately 22% using deuterated hydroxy glutaric acid as an internal standard. The distribution of points is centered on $F_P = 1.02 \pm 0.02$ (standard error) with a distribution well-described by $\sigma_{F_{P,S}}$ (97% of points with $F_P > 1$ are within 2 $\sigma_{F_{P,S}}$). Uncertainty in the particle fraction is only a weak function of signal size as demonstrated by Fig. D.4, in which larger analyte signals (green line) have a slightly narrower distribution around $F_P = 1$ than signals smaller than the internal standard (red line), which is approximately 4 times the level of quantification. Therefore, due to errors in chromatographic integration and mass spectrometric background signals, it is possible that the average estimation of error underpredicts uncertainty at signals very close to the limit of detection.

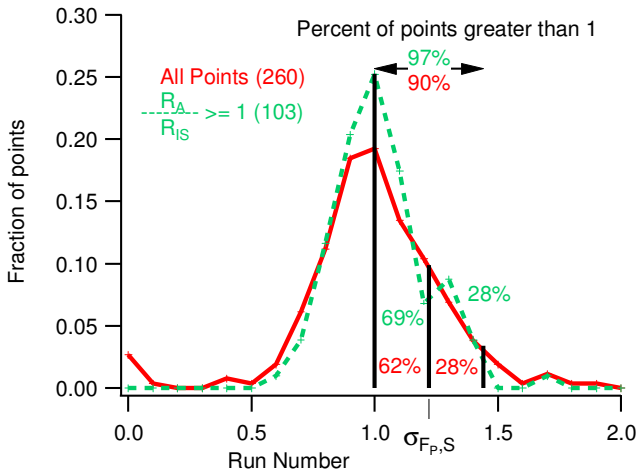

Figure D.4. Histogram of fraction in particle, $F_{P,S}$, for hydroxy glutaric acid for all points (red), and for points greater than the internal standard (green). $\sigma_{F_{P,M/S}} = 22\%$ from Eq. D.11.

While the formal error estimate of partitioning relies on the precision of the instrument and the ability to compare the cells, systematic biases can exist that must be explored. Both penetration of gases through the denuder and loss of gases to the inlet, for instance, will bias the instrument toward a higher F_P. Using various forms of zeroes, no evidence is found in SOAS data for a non-negligible influence of either of these potential biases. However, such biases need to be considered and generally added into F_P error if appropriate.

Appendix E

Supporting information for studying of the chemical characteristics on particle fraction

E.1. Effect of particle composition on FP

Deviation of observed particle fraction from that predicted by equilibrium partitioning is parameterized by an apparent activity coefficient, γ_{eff}, calculated from a rearrangement of Eq. 7.1:

$$\gamma_{eff} = \frac{C_{OA}}{C^0}\left(1 - {F_{P,observed}}^{-1}\right) \quad \text{Eq. E.1}$$

Hourly calculation of this parameter for both isomers of 2-methyltetrols is compared in Fig. E.1 to particle composition. Uptake of IEPOX into the particle and subsequent formation of 2-methyltetrols is expected to be influence by particle acidity, liquid water content, and sulfate (both directly and through a sulfate-driven increase in the two former parameters). Acidity can be estimated from AMS data as an ion charge balance, such as the anion-to-catio ratio. Total ionic charge is computed as the molar balance of dominant inorganic ions:

$$\text{Anion-to-cation ratio} = \frac{2M_{SO_4}[{SO_4}^{2-}] + M_{Cl}[Cl^-] + M_{NO_3}[{NO_3}^-]}{M_{NH_4}[{NH_4}^+]} \quad \text{Eq. E.2}$$

where species concentrations are in mass units and $M_{species}$ is the molecular weight of each species. The anion-to-cation ratio as formulated in Eq. E.2 is greater than 1 in cases of excessive negative charges, when the particle is expected to be acidic. Acidity is modeled more explicitly from these mass concentrations using the Extended Aerosol Inorganics Model (E-AIM model II, http://www.aim.env.uea.ac.uk/aim/aim.php, Clegg et al., 1998; Wexler and Clegg, 2002), which uses temperature and relative humidity to thermodynamically constrain the concentration of free hydrogen ions and particle-phase liquid water content from which pH is calculated. This model does not include the organic contribution to liquid water content, which has been shown to be as high as 20-36% of particle-phase water (Speer et al., 2003; Xu et al., 2014), but this relatively minor correction is not expected to significantly impact the lack of clear relationship between γ_{eff} and liquid water of pH in Figs. E.1c-d.

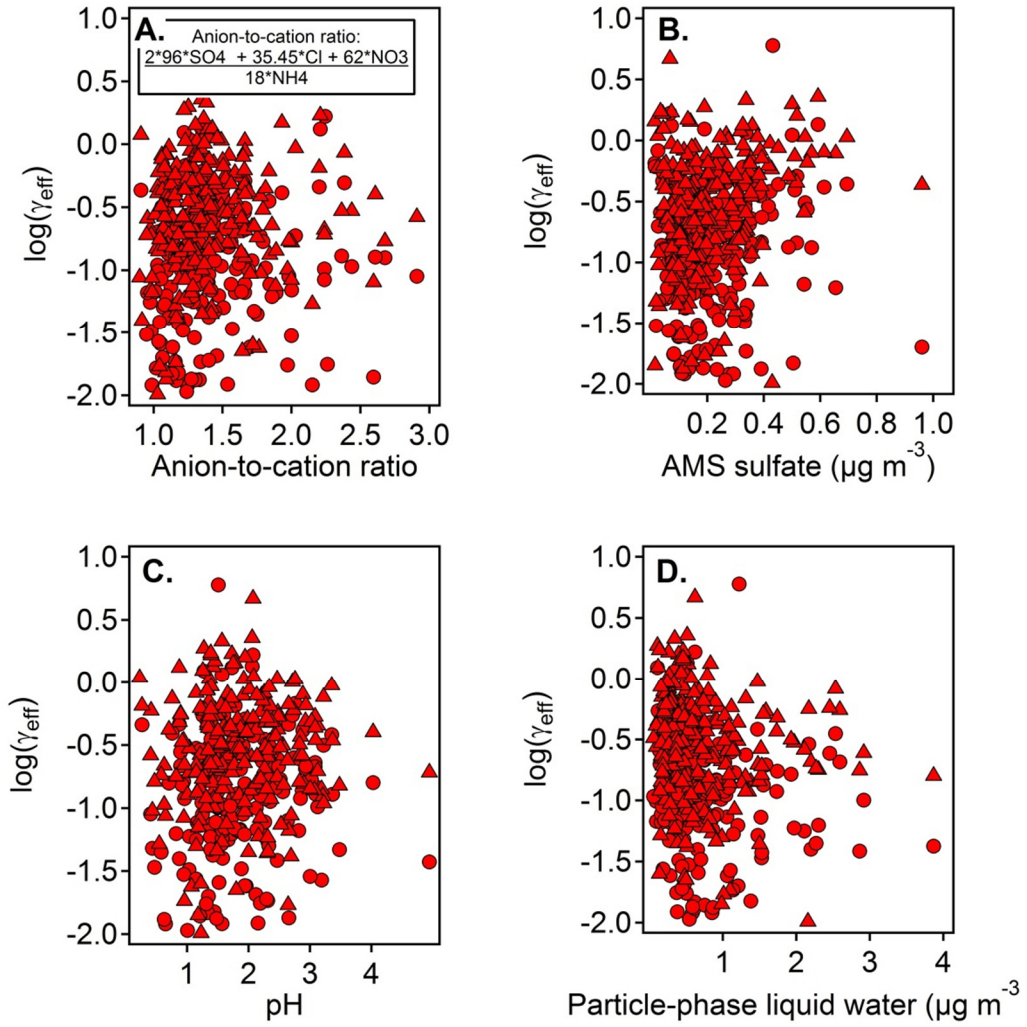

Figure E.1. Deviation of FP from predicted expressed as apparent activity coefficient, γ_{eff}, for 2-methylerythritol (red circles) and 2-methylthreitol (red triangles) during GoAmazon. A lack of correlation is shown with (a) AMS anion-to-cation ratio, (b) AMS sulfate, (c) E-AIM modeled pH, and (d) E-AIM modeled particle-phase liquid water.

E.2. Vapor pressure calculation from retention time of derivatized compounds

Previous work by this author (Chapter 2) and others (Hinckley et al., 1990; Jensen and Schall, 1966) has demonstrated that vapor pressure can be calculated from chromatographic retention time for compounds with similar polarity or functionality. That work is extended here to include derivatized compounds. The vapor pressures of 68 known compounds were calculated and compared to the chromatographic retention times (as alkane-based retention index) of their derivatized product. This analysis was performed by injection of a multi-component standard mixture on the SV-TAG instrument. Compounds include oxygenates with varying numbers of derivatized groups from none (i.e. ketones and esters) to four (i.e. tetrols). These compounds span most atmospherically relevant functionalities, including branched hydrocarbons, acids, diacids, hydroxyl acids, sugars, esters, ketones, alcohols and polyols. A complete list of

compounds is found in Table E.1. Vapor pressure calculated from structure-activity relationships (SIMPOL: Pankow and Asher, 2008) are compared in Fig. E.2 to retention index of the derivatized compounds. Note a clear linear relationship that depends on number of derivatized groups. A linear fit of all compounds yields an average error in log(vapor pressure) of 0.92 atm, which can be reduced to 0.45 atm by including the number of derivatized groups (as number of silicon atoms) in a two-variable regression. Classifying compounds as highly derivatized (2 or Si atoms) or less derivatized (0 or 1 Si atoms) yields an intermediate error in log(vapor pressure) of ~0.60 atm. These relationships determined here for calculating vapor pressure, ν_P, at 25 °C from alkane-based retention indices, t_I, on a relatively non-polar column (Rxi-5Sil MS) are:

All compounds: $\log \nu_P = 0.20 - (0.00429 t_I)$ Eq. E.3

0 or 1 derivatized group: $\log \nu_P = 0.58 - (0.00423 t_I)$ Eq. E.4

More than one derivatized group: $\log \nu_P = -1.27 - (0.00437 t_I)$ Eq. E.5

The slope with respect to elution time is largely independent of the number of derivatized groups, but the vapor pressure decreases by 1 to 2 orders of magnitude with increasing derivatization.

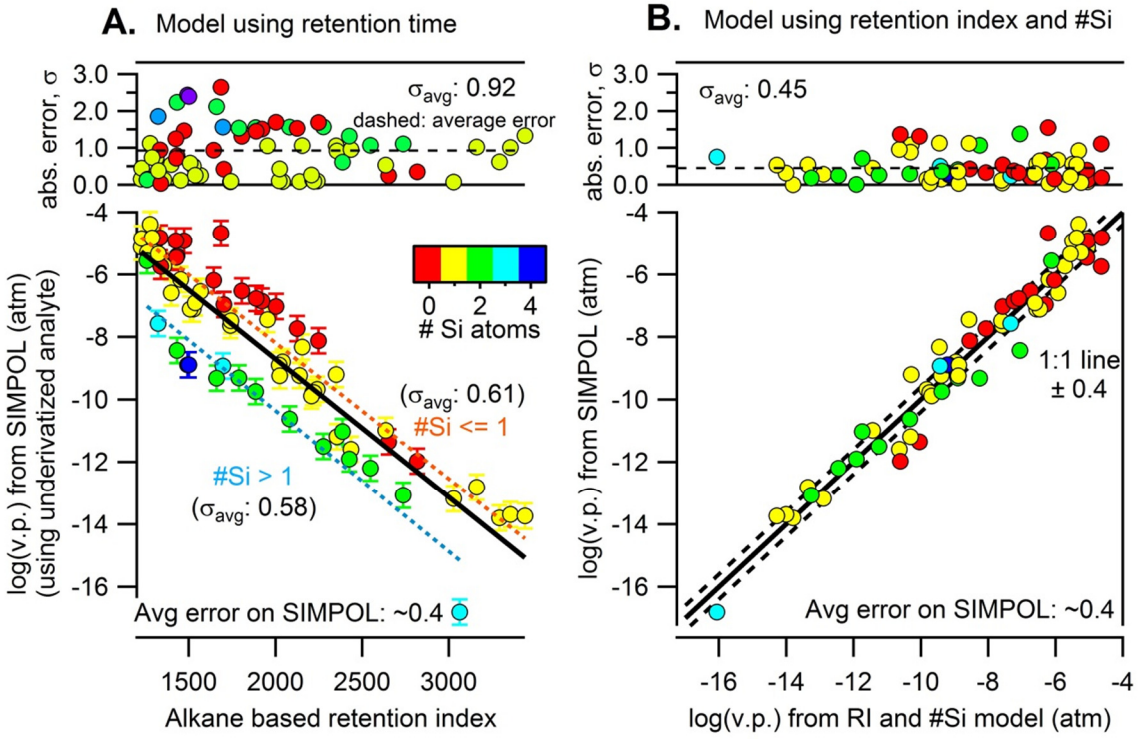

Figure E.2. (a) Vapor pressure calculated for the underivatized form of 68 oxygenated compounds as a function of GC alkane-based retention index, colored by the number of derivatized groups (1 Si atom = 1 derivatized group). Dash lines show the fit (and residual) for compounds containing 0 or 1 derivatized group (orange) or more than 1 (blue). (b) Vapor pressure calculated from SIMPOL compared to that modeled using a two-variable regression fit of retention index (t_I) and number. Top panel shows the absolute residual of the fit.

Table E.1. Compounds used in Fig. E.2 to calculate the relationship between calculation vapor pressure, alkane-based retention index, and, number of derivatized groups.

Compound Name	Retention Index (t_I)	log ν_P (atm)	#Si
2-methoxyphenol (Guaiacol)	1225	-4.93	1
Borneol	1228	-4.63	1
cis-3-methyltetrahydrofuran-3,4-diol	1259	-5.34	2
n-Octanoic acid	1262	-5.07	1
n-Nonadecanol	1276	-4.16	1
n-Decadecanol	1288	-4.59	1
Citronellol	1311	-4.70	1
2,3-Dihydroxypropanoic acid (Glyceric acid)	1324	-7.31	3
Terpineol	1325	-5.10	1
Cycloisolongifolene	1335	-4.62	0
Triacetin	1338	-5.53	0
n-Nonanoic acid	1357	-5.49	1
2,6-Dimethoxyphenol (Syringol)	1398	-6.36	1
Longifolene	1425	-4.70	0
Ionone	1429	-5.24	0
β-Caryophyllene	1432	-5.17	0
Dimethylglutaric Acid TMS	1433	-8.15	2
Decanoic acid	1453	-5.92	1
Alloaromadendrene	1473	-4.70	0
Threitol	1493	-8.59	4
Erythritol	1501	-8.59	4
Ketopinic acid	1507	-6.87	1
cis-Pinonic acid	1525	-6.87	1
3-Methoxy-4-hydroxybenzaldehyde (Vanillin)	1537	-6.67	1
2-Methoxy-4-propenylphenol (Isoeugenol)	1568	-6.31	1
Benzophenone	1643	-5.95	0
cis-Pinic acid	1661	-9.03	2
γ-Dodecalactone	1686	-4.46	0
Levoglucosan	1697	-8.63	3
2,6,10,14-tetramethylpentadecane	1703	-6.65	0
α-Bisabolol	1740	-7.33	1
n-Tridecanoic acid	1744	-7.19	1
1,9-Nonadioic acid	1789	-9.00	2
2,6,10,14-tetramethylhexadecane	1805	-6.22	0
1,10-Decadioic acid	1885	-9.43	2
Dodecyl benzene	1889	-6.47	0
Methyl palmitate	1923	-6.56	0
n-Hexadecanol	1955	-7.13	1
2-Octadecanone	2004	-6.74	0
cis-9-Hexadecenoic acid	2021	-8.57	1
Homosalate	2024	-8.94	1

n-Hexadecanoic acid	2041	-8.46	1
1,12-Dodecadioic acid	2082	-10.28	2
Methyl stearate	2126	-7.41	0
n-Heptanoic acid	2140	-8.89	1
n-Octadecanol	2154	-7.98	1
cis,cis-9,12-Octadecadienoic acid	2207	-9.53	1
cis-9-Octadecenoic acid	2214	-9.42	1
cis-11-Octadecenoic acid	2221	-9.42	1
n-Octadecanoic acid	2241	-9.31	1
Retene	2249	-7.80	0
1,14-Tetradecanoic acid	2277	-11.13	2
n-Eicosanol	2351	-8.83	1
Isopimaric acid	2355	-10.83	1
16-Hydroxyhexadecanoic acid	2387	-10.65	2
12-Hydroxyoctadecanoic acid	2426	-11.50	2
Abietic acid	2436	-11.22	1
Monopalmitin	2547	-11.77	2
n-Docosanoic acid	2636	-10.59	1
Squalane	2653	-10.90	0
Monostearin	2737	-12.62	2
Squalene	2819	-11.54	0
n-Hexacosanoic acid	3028	-12.71	1
Deoxycholic Acid	3062	-16.32	3
Cholesterol	3161	-12.39	1
β-Stigmasterol	3292	-13.35	1
β-Sitosterol	3356	-13.24	1
Lupeol	3439	-13.30	1

References

Adam, T. and Zimmermann, R.: Determination of single photon ionization cross sections for quantitative analysis of complex organic mixtures., Analytical and bioanalytical chemistry, 389(6), 1941-1951, doi:10.1007/s00216-007-1571-x, 2007.

Aiken, A. C., DeCarlo, P. F., Kroll, J. H., Worsnop, D. R., Huffman, J. A., Docherty, K. S., Ulbrich, I. M., Mohr, C., Kimmel, J. R., Sueper, D., Sun, Y., et al.: O/C and OM/OC Ratios of Primary, Secondary, and Ambient Organic Aerosols with High-Resolution Time-of-Flight Aerosol Mass Spectrometry, Environmental Science & Technology, 42(12), 4478-4485, 2008.

Allan, J. D., Delia, A. E., Coe, H., Bower, K. N., Alfarra, M. R., Jimenez, J.-L., Middlebrook, A. M., Drewnick, F., Onasch, T. B., Canagaratna, M. R., Jayne, J. T., et al.: A generalised method for the extraction of chemically resolved mass spectra from Aerodyne aerosol mass spectrometer data, Journal of Aerosol Science, 35(7), 909-922, doi:10.1016/j.jaerosci.2004.02.007, 2004.

Andreae, M. O.: Correlation between cloud condensation nuclei concentration and aerosol optical thickness in remote and polluted regions, Atmospheric Chemistry and Physics, 9, 543-556, 2009.

Angove, D. E., Fookes, C. J. R., Hynes, R. G., Walters, C. K. and Azzi, M.: The characterisation of secondary organic aerosol formed during the photodecomposition of 1,3-butadiene in air containing nitric oxide, Atmospheric Environment, 40(24), 4597-4607, doi:10.1016/j.atmosenv.2006.03.046 [online] Available from: http://linkinghub.elsevier.com/retrieve/pii/S1352231006003657 (Accessed 8 October 2014), 2006.

Arino, O., Ramos Perez, J. J., Kalogirou, V., Bontemps, S., Defourney, P. and Van Bogaert, E.: Global Land Cover Map for 2009 (GlobCover 2009), European Space Agency (ESA) & Université catholique de Louvain (UCL), doi:doi:10.1594/PANGAEA.787668, 2012.

Atkinson, R.: A Structure-Activity Relationship for the Estimation of Rate Constants for the Gas-Phase Reactions of OH Radicals with Organic Compounds, International Journal of Chemical Kinetics, 19, 799-828, 1987.

Atkinson, R.: Atmospheric Reactions of Alkoxy and B - Hydroxyalkoxy Radicals, International Journal of Chemical Kinetics, 29, 99-111, 1997.

Atkinson, R.: Kinetics of the gas-phase reactions of OH radicals with alkanes and cycloalkanes, Atmospheric Chemistry and Physics, 3(4), 4183-4358, doi:10.5194/acpd-3-4183-2003 [online] Available from: http://www.atmos-chem-phys-discuss.net/3/4183/2003/, 2003.

Atkinson, R. and Arey, J.: Atmospheric degradation of volatile organic compounds, Chemical Reviews, 103, 4605-4638, 2003.

Aumont, B., Szopa, S. and Madronich, S.: Modelling the evolution of organic carbon during its gas-phase tropospheric oxidation: development of an explicit model based on a self generating approach, Atmospheric Chemistry and Physics, 5, 2497-2517, doi:10.5194/acpd-5-703-2005, 2005.

Barsanti, K. C. and Pankow, J. F.: Thermodynamics of the formation of atmospheric organic particulate matter by accretion reactions - Part 1: aldehydes and ketones, Atmospheric Environment, 38(26), 4371-4382, doi:10.1016/j.atmosenv.2004.03.035, 2004.

Bench, G., Fallon, S., Schichtel, B., Malm, W. and McDade, C.: Relative contributions of fossil and contemporary carbon sources to PM 2.5 aerosols at nine Interagency Monitoring for Protection of Visual Environments (IMPROVE) network sites, Journal of Geophysical Research, 112(D10), 1-10, doi:10.1029/2006JD007708, 2007.

Bertram, A. K., Ivanov, A. V., Hunter, M., Molina, L. T. and Molina, M. J.: The Reaction Probability of OH on Organic Surfaces of Tropospheric Interest, Journal of Physical Chemistry A, 105, 9415-9421, 2001.

Blau, K. and Halket, J. M., Eds.: Handbook of Derivatives for Chromatography, 2nd Editio., John Wiley & Sons, England., 1993.

Blomquist, G. J. and Bagneres, A.-G., Eds.: Insect Hydrocarbons, Cambridge University Press, Cambridge, UK., 2010.

Bonn, B. and Moortgat, G. K.: New particle formation during α- and β-pinene oxidation by O3 , OH and NO 3 , and the influence of water vapour : particle size distribution studies, Atmospheric Chemistry and Physics, 2, 183-196, 2002.

Bonn, B. and Moortgat, G. K.: Sesquiterpene ozonolysis: Origin of atmospheric new particle formation from biogenic hydrocarbons, Geophysical Research Letters, 30(11), 1-4, doi:10.1029/2003GL017000, 2003.

Bonn, B., Schuster, G. and Moortgat, G. K.: Influence of Water Vapor on the Process of New Particle Formation during Monoterpene Ozonolysis, Journal of Physical Chemistry A, 106(12), 2869-2881, doi:10.1021/jp012713p, 2002.

Bouvier-Brown, N. C., Goldstein, A. H., Gilman, J. B., Kuster, W. C. and de Gouw, J. A.: In-situ ambient quantification of monoterpenes, sesquiterpenes, and related oxygenated compounds during BEARPEX 2007 – implications for gas- and particle-phase chemistry, Atmospheric Chemistry and Physics, 9(2), 5505-5518, doi:10.5194/acpd-9-10235-2009, 2009a.

Bouvier-Brown, N. C., Holzinger, R., Palitzsch, K. and Goldstein, A. H.: Large emissions of sesquiterpenes and methyl chavicol quantified from branch enclosure measurements, Atmospheric Environment, 43(2), 389-401, doi:10.1016/j.atmosenv.2008.08.039, 2009b.

Brock, C. A., Trainer, M., Ryerson, T. B., Neuman, J. A., Parrish, D. D., Holloway, J. S., Nicks Jr., D. K., Frost, G. J., Hubler, G., Fehsenfeld, F. C., Wilson, J. C., et al.: Particle growth in urban and industrial plumes in Texas, Journal of Geophysical Research, 108(D3), 1-12, doi:10.1029/2002JD002746, 2003.

Budisulistiorini, S. H., Canagaratna, M. R., Croteau, P. L., Marth, W. J., Baumann, K., Edgerton, E. S., Shaw, S. L., Knipping, E. M., Worsnop, D. R., Jayne, J. T., Gold, A., et al.: Real-Time Continuous Characterization of Secondary Organic Aerosol Derived from Isoprene Epoxydiols in Downtown Atlanta , Georgia , Using the Aerodyne Aerosol Chemical Speciation Monitor, Environmental Science & Technology, 2013.

Carlton, A. G., Pinder, R. W., Bhave, P. V. and Pouliot, G. A.: To What Extent Can Biogenic SOA be Controlled ?, Environmental Science & Technology, 44(9), 3376-3380, 2010.

Carlton, A. G., Turpin, B. I., Altieri, K. E., Seitzinger, S. P., Mathur, R., Roselle, S. J. and Weber, R. J.: CMAQ model performance enhanced when in-cloud secondary organic aerosol is included: comparisons of organic carbon predictions with measurements., Environmental science & technology, 42(23), 8798-802 [online] Available from: http://www.ncbi.nlm.nih.gov/pubmed/19192800, 2008.

Carlton, A. G. and Turpin, B. J.: Particle partitioning potential of organic compounds is highest in the Eastern US and driven by anthropogenic water, Atmospheric Chemistry and Physics Discussions, 13(5), 12743-12770, doi:10.5194/acpd-13-12743-2013 [online] Available from: http://www.atmos-chem-phys-discuss.net/13/12743/2013/ (Accessed 21 January 2014), 2013.

Carlton, A. G., Wiedinmyer, C. and Kroll, J. H.: A review of Secondary Organic Aerosol (SOA) formation from isoprene, Atmospheric Chemistry and Physics Discussions, 9(2), 8261-8305, doi:10.5194/acpd-9-8261-2009 [online] Available from: http://www.atmos-chem-phys-discuss.net/9/8261/2009/, 2009.

Cass, G. R.: Organic molecular tracers for particulate air pollution sources, Trends in Analytical Chemistry, 17(6), 356-366, doi:10.1016/S0165-9936(98)00040-5, 1998.

Chan, A. W. H., Isaacman, G., Wilson, K. R., Worton, D. R., Ruehl, C. R., Nah, T., Gentner, D. R., Dallmann, T. R., Kirchstetter, T. W., Harley, R. a., Gilman, J. B., et al.: Detailed Chemical Characterization of Unresolved Complex Mixtures in Atmospheric Organics: Insights into Emission Sources, Atmospheric Processing and Secondary Organic Aerosol Formation, Journal of Geophysical Research: Atmospheres, 118, 6783-6796, doi:10.1002/jgrd.50533 [online] Available from: http://doi.wiley.com/10.1002/jgrd.50533 (Accessed 6 June 2013), 2013.

Chan, M. N., Surratt, J. D., Claeys, M., Edgerton, E. S., Tanner, R. L., Shaw, S. L., Zheng, M., Knipping, E. M., Eddingsaas, N. C., Wennberg, P. O. and Seinfeld, J. H.: Characterization and quantification of isoprene-derived epoxydiols in ambient aerosol in the southeastern United States, Environmental science & technology, 44(12), 4590-6, doi:10.1021/es100596b [online] Available from: http://www.ncbi.nlm.nih.gov/pubmed/20476767, 2010.

Che, D. L., Smith, J. D., Leone, S. R., Ahmed, M. and Wilson, K. R.: Quantifying the reactive uptake of OH by organic aerosols in a continuous flow stirred tank reactor, Physical Chemistry Chemical Physics, 11(36), 7885-7895, doi:10.1039/b916865f, 2009.

Chen, Q., Farmer, D. K., Schneider, J., Zorn, S. R., Heald, C. L., Karl, T. G., Guenther, A., Allan, J. D., Robinson, N., Coe, H., Kimmel, J. R., et al.: Mass spectral characterization of submicron biogenic organic particles in the Amazon Basin, Geophysical Research letters, 36(L20806), 1-5, doi:10.1029/2009GL039880, 2009.

Chuong, B., Zhang, J. and Donahue, N. M.: Cycloalkene ozonolysis: collisionally mediated mechanistic branching., Journal of the American Chemical Society, 126(39), 12363-12373, doi:10.1021/ja0485412, 2004.

Claeys, M., Iinuma, Y., Szmigielski, R., Surratt, J. D., Blockhuys, F., van Alsenoy, C., Boge, O., Sierau, B., Gomez-Gonzalez, Y., Vermeylen, R., van Der Veken, P., et al.: Terpenylic Acid and Related Compounds from the Oxidation of a-Pinene: Implications for New Particle Formation and Growth above Forests, Environmental Science & Technology, 43(18), 6976-6982, 2009.

Claeys, M., Szmigielski, R., Kourtchev, I., van der Veken, P., Vermeylen, R., Maenhaut, W., Jaoui, M., Kleindienst, T. E., Lewandowski, M., Offenberg, J. H. and Edney, E. O.: Hydroxydicarboxylic acids: markers for secondary organic aerosol from the photooxidation of alpha-pinene., Environmental science & technology, 41(5), 1628-34 [online] Available from: http://www.ncbi.nlm.nih.gov/pubmed/17396652, 2007.

Claeys, M., Wang, W., Ion, A. C., Kourtchev, I., Gelencsér, A. and Maenhaut, W.: Formation of secondary organic aerosols from isoprene and its gas-phase oxidation products through reaction with hydrogen peroxide, Atmospheric Environment, 38(25), 4093-4098, doi:10.1016/j.atmosenv.2004.06.001 [online] Available from: http://linkinghub.elsevier.com/retrieve/pii/S1352231004004996 (Accessed 19 July 2012), 2004.

Clegg, S. L., Brimblecombe, P. and Wexler, A. S.: Thermodynamic Model of the System H+-NH4+-SO42--NO3--H2O at Tropospheric Temperatures, Journal of Physical Chemistry A, 102, 2137-2154, 1998.

Compernolle, S., Ceulemans, K. and Müller, J.-F.: EVAPORATION: a new vapour pressure estimation methodfor organic molecules including non-additivity and intramolecular interactions, Atmospheric Chemistry and Physics, 11(18), 9431-9450, doi:10.5194/acp-11-9431-2011 [online] Available from: http://www.atmos-chem-phys.net/11/9431/2011/ (Accessed 21 January 2014), 2011.

DeCarlo, P. F., Kimmel, J. R., Trimborn, A., Northway, M. J., Jayne, J. T., Aiken, A. C., Gonin, M., Fuhrer, K., Horvath, T., Docherty, K. S., Worsnop, D. R., et al.: Field-Deployable, High-Resolution, Time-of-Flight Aerosol Mass Spectrometer, Analytical Chemistry, 78(24), 8281-8289, doi:8410.1029/2001JD001213.Analytical, 2006.

Docherty, K. S. and Ziemann, P. J.: On-line, inlet-based trimethylsilyl derivatization for gas chromatography of mono- and dicarboxylic acids, Journal Of Chromatography A, 921, 265-275, 2001.

Donahue, N. M., Epstein, S. A., Pandis, S. N. and Robinson, A. L.: A two-dimensional volatility basis set: 1. organic-aerosol mixing thermodynamics, Atmospheric Chemistry and Physics Discussions, 10(10), 24091-24133, doi:10.5194/acpd-10-24091-2010, 2010.

Donahue, N. M., Huff Hartz, K. E., Chuong, B., Presto, A. A., Stanier, C. O., Rosenhørn, T., Robinson, A. L. and Pandis, S. N.: Critical factors determining the variation in SOA yields from terpene ozonolysis: A combined experimental and computational study, Faraday Discussions, 130, 295-309, doi:10.1039/b417369d, 2005a.

Donahue, N. M., Robinson, A. L., Huff Hartz, K. E., Sage, A. M. and Weitkamp, E. A.: Competitive oxidation in atmospheric aerosols: The case for relative kinetics, Geophysical Research Letters, 32(16), 1-5, doi:10.1029/2005GL022893, 2005b.

Donahue, N. M., Robinson, A. L., Stanier, C. O. and Pandis, S. N.: Coupled partitioning, dilution, and chemical aging of semivolatile organics., Environmental Science & Technology, 40(8), 2635-2643, 2006.

Donahue, N. M., Tischuk, J. E., Marquis, B. J. and Huff Hartz, K. E.: Secondary organic aerosol from limona ketone: insights into terpene ozonolysis via synthesis of key intermediates., Physical chemistry chemical physics, 9(23), 2991-2998, doi:10.1039/b701333g, 2007.

Edney, E. O., Kleindienst, T. E., Conver, T. ., McIver, C. ., Corse, E. . and Weathers, W. .: Polar organic oxygenates in PM2.5 at a southeastern site in the United States, Atmospheric Environment, 37(28), 3947-3965, doi:10.1016/S1352-2310(03)00461-8 [online] Available from: http://linkinghub.elsevier.com/retrieve/pii/S1352231003004618 (Accessed 15 July 2012), 2003.

Ehn, M., Thornton, J. a, Kleist, E., Sipilä, M., Junninen, H., Pullinen, I., Springer, M., Rubach, F., Tillmann, R., Lee, B., Lopez-Hilfiker, F., et al.: A large source of low-volatility secondary organic aerosol, Nature, 506(7489), 476-479, doi:10.1038/nature13032 [online] Available from: http://www.nature.com/doifinder/10.1038/nature13032 (Accessed 26 February 2014), 2014.

Ervens, B., Carlton, A. G., Turpin, B. J., Altieri, K. E., Kreidenweis, S. M. and Feingold, G.: Secondary organic aerosol yields from cloud-processing of isoprene oxidation products, Geophysical Research Letters, 35(2), L02816, doi:10.1029/2007GL031828 [online] Available from: http://doi.wiley.com/10.1029/2007GL031828 (Accessed 2 October 2014), 2008.

Ervens, B., Sorooshian, A., Lim, Y. B. and Turpin, B. J.: Key parameters controlling OH-initiated formation of secondary organic aerosol in the aqueous phase (aqSOA), Journal of Geophysical Research: Atmospheres, 119, 3997-4016, doi:10.1002/2013JD021021.Received, 2014.

Eschner, M. S., Welthagen, W., Gröger, T. M., Gonin, M., Fuhrer, K. and Zimmermann, R.: Comprehensive multidimensional separation methods by hyphenation of single-photon ionization time-of-flight mass spectrometry (SPI-TOF-MS) with GC and GCxGC., Analytical and bioanalytical chemistry, 398(3), 1435-1445, doi:10.1007/s00216-010-4021-0, 2010.

Fluka Chemie AG: Silylating Agents, Buchs, Switzerland., 1995.

Fraser, M. P., Cass, G. R. and Simoneit, B. R. T.: Gas-Phase and Particle-Phase Organic Compounds Emitted from Motor Vehicle Traffic in a Los Angeles Roadway Tunnel, Environmental Science & Technology, 32(14), 2051-2060, 1998.

Fraser, M. P., Cass, G. R. and Simoneit, B. R. T.: Particulate organic compounds emitted from motor vehicle exhaust and in the urban atmosphere, Atmospheric Environment, 33(17), 2715-2724, doi:10.1016/S1352-2310(98)00311-2, 1999.

Fraser, M. P. and Lakshmanan, K.: Using Levoglucosan as a Molecular Marker for the Long-Range Transport of Biomass Combustion Aerosols, Environmental Science & Technology, 34(21), 4560-4564, doi:10.1021/es991229l, 2000.

Gao, S., Keywood, M. D., Ng, N. L., Surratt, J. D., Varutbangkul, V., Bahreini, R., Flagan, R. C. and Seinfeld, J. H.: Low-Molecular-Weight and Oligomeric Components in Secondary Organic Aerosol from the Ozonolysis of Cycloalkenes and α-Pinene, Journal of Physical Chemistry A, 108(46), 10147-10164, doi:10.1021/jp047466e, 2004a.

Gao, S., Ng, N. L., Keywood, M. D., Varutbangkul, V., Bahreini, R., Nenes, A., He, J., Yoo, K. Y., Beauchamp, J. L., Hodyss, R. P., Flagan, R. C., et al.: Particle phase acidity and oligomer formation in secondary organic aerosol., Environmental science & technology, 38(24), 6582-6589, 2004b.

Gao, S., Surratt, J. D., Knipping, E. M., Edgerton, E. S., Shahgholi, M. and Seinfeld, J. H.: Characterization of polar organic components in fine aerosols in the southeastern United States: Identity, origin, and evolution, Journal of Geophysical Research, 111(D14314), 1-27, doi:10.1029/2005JD006601, 2006.

Geissler, R., Saraji-bozorgzad, M. R., Gro, T., Fendt, A., Streibel, T., Sklorz, M., Krooss, B. M., Fuhrer, K., Gonin, M., Kaisersberger, E., Denner, T., et al.: Single Photon Ionization Orthogonal Acceleration Time-of-Flight Mass Spectrometry and Resonance Enhanced Multiphoton Ionization Time-of-Flight Mass Spectrometry for Evolved Gas Analysis in Thermogravimetry : Comparative Analysis of Crude Oils, Analytical Chemistry, 81(15), 6038-6048, 2009.

Gentner, D. R., Isaacman, G., Worton, D. R., Chan, A. W. H., Dallmann, T. R., Davis, L., Liu, S., Day, D. A., Russell, L. M., Wilson, K. R., Weber, R. J., et al.: Elucidating secondary organic aerosol from diesel and gasoline vehicles through detailed characterization of organic carbon emissions., Proceedings of the National Academy of Sciences of the United States of America, 1-6, doi:10.1073/pnas.1212272109 [online] Available from: http://www.ncbi.nlm.nih.gov/pubmed/23091031 (Accessed 25 October 2012), 2012.

George, I. J., Vlasenko, A., Slowik, J. G., Broekhuizen, K. and Abbatt, J. P. D.: Heterogeneous oxidation of saturated organic aerosols by hydroxyl radicals: uptake kinetics, condensed-phase products, and particle size change, Atmospheric Chemistry and Physics, 7(16), 4187-4201, doi:10.5194/acp-7-4187-2007, 2007.

Geron, C. D., Arnts, R. R. and Pine, V.: Seasonal monoterpene and sesquiterpene emissions from Pinus taeda and Pinus virginiana, Atmospheric Environment, 44(34), 4240-4251, doi:10.1016/j.atmosenv.2010.06.054 [online] Available from: http://dx.doi.org/10.1016/j.atmosenv.2010.06.054, 2010.

Geron, C., Rasmussen, R., Arnts, R. R. and Guenther, A.: A review and synthesis of monoterpene speciation from forests in the United States, Atmospheric Environment, 34, 1761-1781, 2000.

Gloaguen, E., Mysak, E., Leone, S., Ahmed, M. and Wilson, K. R.: Investigating the chemical composition of mixed organic–inorganic particles by "soft" vacuum ultraviolet photoionization: The reaction of ozone with anthracene on sodium chloride particles, International Journal of Mass Spectrometry, 258(1-3), 74-85, doi:10.1016/j.ijms.2006.07.019, 2006.

Goldstein, A. H. and Galbally, I.: Known and unexplored organic constituents in the earth's atmosphere, Environmental Science & Technology, 41, 1514-1521, 2007.

Goldstein, A. H., Koven, C. D., Heald, C. L. and Fung, I. Y.: Biogenic carbon and anthropogenic pollutants combine to form a cooling haze over the southeastern United States, Proceedings of the National Academy of Sciences of the United States of America, 106(22), 8835-8840, 2009.

Goldstein, A. H., Worton, D. R., Williams, B. J., Hering, S. V., Kreisberg, N. M., Panić, O. and Górecki, T.: Thermal desorption aerosol comprehensive two-dimensional gas chromatographic resolution for in-situ measurements of organic aerosols, Journal of Chromatography A, 1186, 340-347, 2008.

de Gouw, J. A., Middlebrook, A. M., Warneke, C., Goldan, P. D., Kuster, W. C., Roberts, J. M., Fehsenfeld, F. C., Worsnop, D. R., Canagaratna, M. R., Pszenny, A. A. P., Keene, W. C., et al.: Budget of organic carbon in a polluted atmosphere: Results from the New England Air Quality Study in 2002, Journal of Geophysical Research, 110(D16), 1-22, doi:10.1029/2004JD005623, 2005.

Guenther, A., Hewitt, C. N., Erickson, D., Fall, R., Geron, C., Graedel, T., Harley, P., Klinger, L., Lerdau, M., Mckay, W. A., Pierce, T., et al.: A global model of natural volatile organic compound emissions, Journal of Geophysical Research, 100(94), 8873-8892, 1995.

Hallquist, M., Wenger, J. C., Baltensperger, U., Rudich, Y., Simpson, D., Claeys, M., Dommen, J., Donahue, N. M., George, C., Goldstein, A. H., Hamilton, J. F., et al.: The formation, properties and impact of secondary organic aerosol: current and emerging issues, Atmospheric Chemistry and Physics, 9, 5155-5236, 2009.

Hamilton, J. F.: Using comprehensive two-dimensional gas chromatography to study the atmosphere., Journal of Chromatographic Science, 48(4), 274-282, 2010.

Hanley, L. and Zimmermann, R.: Light and Molecular Ions : The Emergence of Vacuum UV Single-Photon Ionization in MS, Analytical Chemistry, (Ci), 4174-4182, 2009.

Hatch, L. E., Creamean, J. M., Ault, A. P., Surratt, J. D., Chan, M. N., Seinfeld, J. H., Edgerton, E. S., Su, Y. and Prather, K. A.: Measurements of Isoprene-Derived Organosulfates in Ambient Aerosols by Aerosol Time-of-Flight Mass Spectrometry-Part 2: Temporal Variability and Formation Mechanisms., Environmental science & technology, 45(20), 8648-55, doi:10.1021/es2011836, 2011.

Hayes, P. L., Ortega, a. M., Cubison, M. J., Froyd, K. D., Zhao, Y., Cliff, S. S., Hu, W. W., Toohey, D. W., Flynn, J. H., Lefer, B. L., Grossberg, N., et al.: Organic aerosol composition and sources in Pasadena, California, during the 2010 CalNex campaign, Journal of Geophysical Research: Atmospheres, 118(16), 9233-9257, doi:10.1002/jgrd.50530 [online] Available from: http://doi.wiley.com/10.1002/jgrd.50530 (Accessed 16 October 2014), 2013.

He, C., Liu, J., Carlton, A. G., Fan, S., Horowitz, L. W., Levy II, H. and Tao, S.: Evaluation of factors controlling global secondary organic aerosol production from cloud processes, Atmospheric Chemistry and Physics, 13(4), 1913-1926, doi:10.5194/acp-13-1913-2013 [online] Available from: http://www.atmos-chem-phys.net/13/1913/2013/ (Accessed 21 January 2014), 2013.

Hearn, J. D. and Smith, G. D.: A mixed-phase relative rates technique for measuring aerosol reaction kinetics, Geophysical Research Letters, 33(17), 1-5, doi:10.1029/2006GL026963, 2006.

Heimann, P. A., Koike, M., Hsu, C. W., Blank, D., Yang, X. M., Suits, A. G., Lee, Y. T., Evans, M., Ng, C. Y., Flaim, C. and Padmore, H. A.: Performance of the vacuum ultraviolet high-resolution and high-flux beamline for chemical dynamics studies at the Advanced Light Source, Review of Scientific Instruments, 68(5), 1945-1951, doi:10.1063/1.1148082, 1997.

Hildemann, L. M., Mazurek, M. A., Cass, G. R. and Simoneit, B. R. T.: Quantitative Characterization of Urban Sources of Organic Aerosol by High-Resolution Gas Chromatography, Environmental science & technology, 25(7), 1311-1325, 1991.

Hinckley, D. a., Bidleman, T. F., Foreman, W. T. and Tuschall, J. R.: Determination of vapor pressures for nonpolar and semipolar organic compounds from gas chromatograhic retention data, Journal of Chemical & Engineering Data, 35(3), 232-237, doi:10.1021/je00061a003, 1990.

Hodzic, A., Aumont, B., Knote, C., Madronich, S. and Tyndall, G.: Volatility dependence of Henry's law constants of condensable organics: Application to estimate depositional loss of secondary organic aerosols, Geophysical Research Letters, 41, 4795-4804, doi:10.1002/2014GL060649.Received, 2014.

Hodzic, A., Jimenez, J.-L., Prévôt, A. S. H., Szidat, S., Fast, J. D. and Madronich, S.: Can 3-D models explain the observed fractions of fossil and non-fossil carbon in and near Mexico City?, Atmospheric Chemistry and Physics, 10(22), 10997-11016, doi:10.5194/acp-10-10997-2010, 2010.

Holzinger, R., Lee, A., Mckay, M. and Goldstein, A. H.: Seasonal variability of monoterpene emission factors for a Ponderosa pine plantation in California, Atmospheric Chemistry and Physics, 6, 1267-1274, 2006.

Huff Hartz, K. E., Weitkamp, E. A., Sage, A. M., Donahue, N. M. and Robinson, A. L.: Laboratory measurements of the oxidation kinetics of organic aerosol mixtures using a relative rate constants approach, Journal of Geophysical Research, 112(D4), 1-13, doi:10.1029/2006JD007526, 2007.

Intergovernmental Panel On Climate Change: A report of Working Group I of the Intergovernmental Panel on Climate Change, 2007.

Isaacman, G., Chan, A. W. H., Nah, T., Worton, D. R., Ruehl, C. R., Wilson, K. R., and Goldstein, A. H.. Heterogeneous OH oxidation of motor oil particles causes selective depletion of branched and less cyclic hydrocarbons, Environmental Science & Technology, 46 (19), 10632-10640. 2012.

Isaacman, G., Kreisberg, N. M, Yee, L. D., Worton, D. R., Chan, A. W.H., Moss, J. A., Hering, S. V., and Goldstein, A. H.: On-line derivatization for hourly measurements of gas- and particle-phase Semi-Volatile oxygenated organic compounds by Thermal desorption Aerosol Gas chromatography (SV-TAG), Atmospheric Measurement Techniques, in press, 2014.

Isaacman, G., Kreisberg, N. M., Worton, D. R., Hering, S. V., and Goldstein, A. H.: A versatile and reproducible automatic injection system for liquid standard introduction: application to in-situ calibration. Atmospheric Measurement Techniques, 4, 1937-1942. 2011.

Isaacman, G. and Sueper, D.: TERN: TAG ExploreR and iNtegration, [online] Available from: https://sites.google.com/site/terninigor/, 2014.

Isaacman, G., Wilson, K. R., Chan, A. W. H., Worton, D. R., Kimmel, J. R., Nah, T., Hohaus, T., Gonin, M., Kroll, J. H., Worsnop, D. R. and Goldstein, A. H.: Improved resolution of hydrocarbon structures and constitutional isomers in complex mixtures using gas chromatography-vacuum ultraviolet-mass spectrometry, Analytical Chemistry, 84(5), 2335-2342, doi:10.1021/ac2030464, 2012.

Isaacman, G., Worton, D. R., Kreisberg, N. M., Hennigan, C. J., Teng, a. P., Hering, S. V., Robinson, A. L., Donahue, N. M. and Goldstein, A. H.: Understanding evolution of product composition and volatility distribution through in-situ GC × GC analysis: a case study of longifolene ozonolysis, Atmospheric Chemistry and Physics, 11(11), 5335-5346, doi:10.5194/acp-11-5335-2011, 2011.

Jaoui, M., Edney, E. O., Kleindienst, T. E., Lewandowski, M., Offenberg, J. H., Surratt, J. D. and Seinfeld, J. H.: Formation of secondary organic aerosol from irradiated a-pinene/toluene/NOx mixtures and the effect of isoprene and sulfur dioxide, Journal of Geophysical Research, 113(D09303), 1-12, doi:10.1029/2007JD009426, 2008.

Jaoui, M., Kleindienst, T. E., Lewandowski, M., Offenberg, J. H. and Edney, E. O.: Identification and quantification of aerosol polar oxygenated compounds bearing carboxylic or hydroxyl groups. 2. Organic tracer compounds from monoterpenes., Environmental science & technology, 39(15), 5661-73 [online] Available from: http://www.ncbi.nlm.nih.gov/pubmed/16124301, 2005.

Jaoui, M., Lewandowski, M., Kleindienst, T. E., Offenberg, J. H. and Edney, E. O.: β -caryophyllinic acid: An atmospheric tracer for β -caryophyllene secondary organic aerosol, Geophysical Research Letters, 34(5), 1-4, doi:10.1029/2006GL028827 [online] Available from: http://www.agu.org/pubs/crossref/2007/2006GL028827.shtml (Accessed 24 July 2012), 2007.

Jardine, K., Henderson, W. M., Huxman, T. E. and Abrell, L.: Dynamic Solution Injection: a new method for preparing pptv–ppbv standard atmospheres of volatile organic compounds, Atmospheric Measurement Techniques, 3(6), 1569-1576, doi:10.5194/amt-3-1569-2010, 2010.

Jardine, K., Yañez Serrano, A., Arneth, A., Abrell, L., Jardine, A., van Haren, J., Artaxo, P., Rizzo, L. V., Ishida, F. Y., Karl, T., Kesselmeier, J., et al.: Within-canopy sesquiterpene ozonolysis in Amazonia, Journal of Geophysical Research, 116(D19), D19301, doi:10.1029/2011JD016243 [online] Available from: http://doi.wiley.com/10.1029/2011JD016243 (Accessed 18 June 2014), 2011.

Jensen, D. J. and Schall, E. D.: Determination of Vapor Pressures of Some Phenoxyacetic Herbicides by Gas-Liquid Chromatography, Journal of Agricultural Food and Chemistry, 14(2), 123-126, 1966.

Jimenez, J.-L., Canagaratna, M. R., Donahue, N. M., Prevot, A. S. H., Zhang, Q., Kroll, J. H., DeCarlo, P. F., Allan, J. D., Coe, H., Ng, N. L., Aiken, A. C., et al.: Evolution of Organic Aerosols in the Atmosphere, Science, 326, 1525-1529, doi:10.1126/science.1180353, 2009.

Kalberer, M., Paulsen, D., Sax, M., Steinbacher, M., Dommen, J., Prevot, A. S. H., Fisseha, R., Weingartner, E., Frankevich, V., Zenobi, R. and Baltensperger, U.: Identification of polymers as major components of atmospheric organic aerosols., Science, 303(5664), 1659-62, doi:10.1126/science.1092185, 2004.

Kamens, R. M. and Coe, D. L.: Research Communications A Large Gas-Phase Stripping Device to Investigate Rates of PAH Evaporation from Airborne Diesel Soot Particles, Envi, 31(6), 1830-1833, 1997.

Karl, T., Harley, P., Emmons, L., Thornton, B., Guenther, A., Basu, C., Turnipseed, A. and Jardine, K.: Efficient atmospheric cleansing of oxidized organic trace gases by vegetation., Science, 330(6005), 816-9, doi:10.1126/science.1192534, 2010.

Karl, T., Potosnak, M., Guenther, A., Walker, J., Herrick, J. D. and Geron, C.: Exchange processes of volatile organic compounds above a tropical rain forest : Implications for modeling tropospheric chemistry above dense vegetation, Journal of Geophysical Research, 109(D18306), doi:10.1029/2004JD004738, 2004.

Kessler, S. H., Smith, J. D., Che, D. L., Worsnop, D. R., Wilson, K. R. and Kroll, J. H.: Chemical sinks of organic aerosol: kinetics and products of the heterogeneous oxidation of erythritol and levoglucosan., Environmental science & technology, 44(18), 7005-7010, doi:10.1021/es101465m, 2010.

Kleindienst, T. E., Jaoui, M., Lewandowski, M., Offenberg, J. H., Lewis, C. W., Bhave, P. V. and Edney, E. O.: Estimates of the contributions of biogenic and anthropogenic hydrocarbons to secondary organic aerosol at a southeastern US location, Atmospheric Environment, 41(37), 8288-8300, doi:10.1016/j.atmosenv.2007.06.045 [online] Available from: http://linkinghub.elsevier.com/retrieve/pii/S135223100700581X (Accessed 23 July 2012), 2007.

Kleindienst, T. E., Lee, S., Wang, Y., Russell, A. G., Doraiswamy, P., Hogrefe, C., Hao, W., Civerolo, K., Ku, J.-Y., Sistla, G., Fu, F., et al.: Contribution of Primary and Secondary Sources to Organic Aerosol and PM2.5 at SEARCH Network Sites, Journal of the Air & Waste Management, 60(11), 1388-1399, doi:10.3155/1047-3289.60.11.1388, 2010.

Kleindienst, T. E., Lewandowski, M., Offenberg, J. H., Jaoui, M. and Edney, E. O.: The formation of secondary organic aerosol from the isoprene + OH reaction in the absence of NOx, Atmospheric Chemistry and Physics, 9(2), 10015-10054, doi:10.5194/acp-9-6541-2009 [online] Available from: http://www.atmos-chem-phys-discuss.net/9/10015/2009/, 2009.

Kourtchev, I., Ruuskanen, T., Maenhaut, W., Kulmala, M. and Claeys, M.: Observation of 2-methyltetrols and related photo-oxidation products of isoprene in boreal forest aerosols from Hyytiälä, Finland, Atmospheric Chemistry and Physics, 5(3), 2947-2971, doi:10.5194/acp-5-2761-2005 [online] Available from: http://www.atmos-chem-phys-discuss.net/5/2947/2005/, 2005.

Kourtchev, I., Warnke, J., Maenhaut, W., Hoffmann, T. and Claeys, M.: Polar organic marker compounds in PM2.5 aerosol from a mixed forest site in western Germany., Chemosphere, 73(8), 1308-14, doi:10.1016/j.chemosphere.2008.07.011 [online] Available from: http://www.ncbi.nlm.nih.gov/pubmed/18710779 (Accessed 21 January 2014), 2008.

Kovats, E.: Gas-chromatographische Charakterisierung organischer Verbindungen. Teil 1: Retentionsindices aliphatischer Halogenide, Alkohole, Aldehyde und Ketone, Helvetica Chimica Acta, 41(7), 1915-1932, doi:10.1002/hlca.19580410703, 1958.

Kreisberg, N. M., Hering, S. V., Williams, B. J., Worton, D. R. and Goldstein, A. H.: Quantification of Hourly Speciated Organic Compounds in Atmospheric Aerosols, Measured by an In-Situ Thermal Desorption Aerosol Gas Chromatograph (TAG), Aerosol Science and Technology, 43(1), 38-52, doi:10.1080/02786820802459583, 2009.

Kroll, J. H. and Seinfeld, J. H.: Chemistry of secondary organic aerosol: Formation and evolution of low-volatility organics in the atmosphere, Atmospheric Environment, 42(16), 3593-3624, doi:10.1016/j.atmosenv.2008.01.003, 2008a.

Kroll, J. H. and Seinfeld, J. H.: Chemistry of secondary organic aerosol: Formation and evolution of low-volatility organics in the atmosphere, Atmospheric Environment, 42, 3593-3624, 2008b.

Kroll, J. H., Smith, J. D., Che, D. L., Kessler, S. H., Worsnop, D. R. and Wilson, K. R.: Measurement of fragmentation and functionalization pathways in the heterogeneous oxidation of oxidized organic aerosol, Physical Chemistry Chemical Physics, 11, 8005-8014, doi:10.1039/b916865f, 2009.

Kroll, J. H., Smith, J. D., Worsnop, D. R. and Wilson, K. R.: Characterisation of lightly oxidised organic aerosol formed from the photochemical aging of diesel exhaust particles, Environmental Chemistry, 9, 211-220, 2012.

Kubátová, A., Vermeylen, R. and Claeys, M.: Organic compounds in urban aerosols from Gent, Belgium: Characterization, sources, and seasonal differences, Journal of Geophysical Research, 107(D21), doi:10.1029/2001JD000556 [online] Available from: http://www.agu.org/pubs/crossref/2002/2001JD000556.shtml (Accessed 2 November 2012), 2002.

Kuhn, U., Andreae, M. O., Ammann, C., Araujo, A. C., Brancaleoni, E., Ciccioli, P., Dindorf, T. and Frattoni, M.: Isoprene and monoterpene fluxes from Central Amazonian rainforest inferred from tower-based and airborne measurements , and implications on the atmospheric chemistry and the local carbon budget, Atmospheric Chemistry and Physics, 7, 2855-2879, 2007.

Kuhn, U., Ganzeveld, L., Thielmann, A., Dindorf, T., Schebeske, G., Welling, M., Sciare, J. and Planck, M.: Impact of Manaus City on the Amazon Green Ocean atmosphere: ozone production, precursor sensitivity and aerosol load, Atmospheric Chemistry and Physics, 10, 9251-9282, doi:10.5194/acp-10-9251-2010, 2010.

Kwok, E. S. C. and Atkinson, R.: Estimation of hydroxyl radical reaction rate constants for gas-phase organic compounds using a structure-reactivity relationship: an update, Atmospheric Environment, 29(14), 1685-1695, 1995.

Lambe, A. T., Chacon-Madrid, H. J., Nguyen, N. T., Weitkamp, E. A., Kreisberg, N. M., Hering, S. V., Goldstein, A. H., Donahue, N. M. and Robinson, A. L.: Organic Aerosol Speciation: Intercomparison of Thermal Desorption Aerosol GC/MS (TAG) and Filter-Based Techniques, Aerosol Science and Technology, 44(2), 141-151, doi:10.1080/02786820903447206, 2010.

Lambe, A. T., Miracolo, M. A., Hennigan, C. J., Robinson, A. L. and Donahue, N. M.: Effective Rate Constants and Uptake Organic Molecular Markers in Motor Oil and Diesel Primary Radicals, Environmental Science & technology, 43(23), 8794-8800, 2009.

Lambe, A. T., Onasch, T. B., Croasdale, D. R., Wright, J. P., Martin, A. T., Franklin, J. P., Massoli, P., Kroll, J. H., Canagaratna, M. R., Brune, W. H., Worsnop, D. R., et al.: Transitions from Functionalization to Fragmentation Reactions of Laboratory Secondary Organic Aerosol (SOA) Generated from the OH Oxidation of Alkane Precursors., Environmental science & technology, 46(10), 5430-5437, doi:10.1021/es300274t, 2012.

Langenheim, J. H.: Higher plant terpenoids: a phytocentric overview of their ecological roles, Journal of Chemical Ecology, 20(6), 1994.

Lee, A., Goldstein, A. H., Keywood, M. D., Gao, S., Varutbangkul, V., Bahreini, R., Ng, N. L., Flagan, R. C. and Seinfeld, J. H.: Gas-Phase Products and Secondary Aerosol Yields from the Ozonolysis of Ten Different Terpenes, Journal of Geophysical Research, 111(D07302), doi:10.1029/2005JD006437, 2006a.

Lee, A., Goldstein, A. H., Kroll, J. H., Ng, N. L., Varutbangkul, V., Flagan, R. C. and Seinfeld, J. H.: Gas-Phase Products and Secondary Aerosol Yields from the Photooxidation of 16 Different Terpenes, Journal of Geophysical Research, 111(D17305), 2006b.

Lewandowski, M., Jaoui, M., Kleindienst, T. E., Offenberg, J. H. and Edney, E. O.: Composition of PM2.5 during the summer of 2003 in Research Triangle Park, North Carolina, Atmospheric Environment, 41(19), 4073-4083, doi:10.1016/j.atmosenv.2007.01.012 [online] Available from: http://linkinghub.elsevier.com/retrieve/pii/S1352231007000805 (Accessed 15 July 2012), 2007.

Lim, Y. B. and Ziemann, P. J.: Effects of molecular structure on aerosol yields from OH radical-initiated reactions of linear, branched, and cyclic alkanes in the presence of NOx., Environmental science & technology, 43(7), 2328-34, 2009.

Lin, Y.-H., Zhang, H., Pye, H. O. T., Zhang, Z., Marth, W. J., Park, S., Arashiro, M., Cui, T., Budisulistiorini, S. H., Sexton, K. G., Vizuete, W., et al.: Epoxide as a precursor to secondary organic aerosol formation from isoprene photooxidation in the presence of nitrogen oxides., Proceedings of the National Academy of Sciences of the United States of America, 110(17), 6718-23, doi:10.1073/pnas.1221150110 [online] Available from: http://www.pubmedcentral.nih.gov/articlerender.fcgi?artid=3637755&tool=pmcentrez&rendertype=abstract (Accessed 28 May 2013), 2013.

Lin, Y.-hsuan, Zhang, Z., Docherty, K. S., Zhang, H., Budisulistiorini, S. H., Rubitschun, C. L., Shaw, S. L., Knipping, E. M., Edgerton, E. S., Kleindienst, T. E., Gold, A., et al.: Isoprene Epoxydiols as Precursors to Secondary Organic Aerosol Formation : Acid-Catalyzed Reactive Uptake Studies with Authentic Compounds, Environmental Science & Technology, 46, 250-258, 2012.

Lindinger, W., Hansel, A. and Jordan, A.: On-line monitoring of volatile organic compounds at pptv levels by means of Proton-Transfer-Reaction Mass Spectrometry (PTR-MS) Medical applications , food control and environmental research, Internation Journal of Mass Spectrometry and Ion Processes, 173, 191-241, 1998.

Liu, P. S. K., Deng, R., Smith, K. a., Williams, L. R., Jayne, J. T., Canagaratna, M. R., Moore, K., Onasch, T. B., Worsnop, D. R. and Deshler, T.: Transmission Efficiency of an Aerodynamic Focusing Lens System: Comparison of Model Calculations and Laboratory Measurements for the Aerodyne Aerosol Mass Spectrometer, Aerosol Science and Technology, 41(8), 721-733, doi:10.1080/02786820701422278 [online] Available from: http://www.tandfonline.com/doi/abs/10.1080/02786820701422278 (Accessed 13 October 2014), 2007.

Liu, S., Ahlm, L., Day, D. a., Russell, L. M., Zhao, Y., Gentner, D. R., Weber, R. J., Goldstein, A. H., Jaoui, M., Offenberg, J. H., Kleindienst, T. E., et al.: Secondary organic aerosol formation from fossil fuel sources contribute majority of summertime organic mass at Bakersfield, Journal of Geophysical Research: Atmospheres, 117(D24), n/a-n/a, doi:10.1029/2012JD018170 [online] Available from: http://doi.wiley.com/10.1029/2012JD018170 (Accessed 16 October 2014), 2012.

Lough, G., Schauer, J. J. and Lawson, D.: Day-of-week trends in carbonaceous aerosol composition in the urban atmosphere, Atmospheric Environment, 40(22), 4137-4149, doi:10.1016/j.atmosenv.2006.03.009, 2006.

Lyman, W. J.: Environmental Exposure From Chemicals. Volume 1., edited by W. B. Neely and G. E. Blau, CRC Press, Inc., Boca Raton, FL., 1985.

Maksymiuk, C. S., Gayahtri, C., Gil, R. R. and Donahue, N. M.: Secondary organic aerosol formation from multiphase oxidation of limonene by ozone: mechanistic constraints via two-dimensional heteronuclear NMR spectroscopy, Physical chemistry chemical physics, 11(36), 7810-7818, doi:10.1039/b916865f, 2009.

Mao, D., Weghe, H. V. D., Lookman, R., Vanermen, G., Brucker, N. D. and Diels, L.: Resolving the unresolved complex mixture in motor oils using high-performance liquid chromatography followed by comprehensive two-dimensional gas chromatography, Fuel, 88(2), 312-318, doi:10.1016/j.fuel.2008.08.021, 2009.

Martin, S. J., Helanterä, H. and Drijfhout, F. P.: Is parasite pressure a driver of chemical cue diversity in ants?, Proceedings of the The Royal Society B: Biological sciences, 278(1705), 496-503, doi:10.1098/rspb.2010.1047, 2011.

Martin, S. T., Andreae, M. O., Artaxo, P., Baumgardner, D., Chen, Q., Goldstein, A. H., Guenther, A., Heald, C. L., Bracero, O. L. M., Mcmurry, P. H., Pauliquevis, T., et al.: Sources and Properties of Amazonian Aerosol Particles, Review of Geophysics, doi:10.1029/2008RG000280, 2010.

Mazurek, M. A.: Molecular Identification of Organic Compounds in Atmospheric Complex Mixtures and Relationship to Atmospheric Chemistry and Sources, Environmental Health Perspectives, 110, 995-1003, 2002.

Mazurek, M. A., Cass, G. R. and Simoneit, B. R. T.: Interpretation of High-Resolution Gas Chromatography and High-Resolution Gas Chromatography / Mass Spectrometry Data Acquired from Atmospheric Organic Aerosol Samples, Aerosol Science and Technology, 10(2), 408-420, doi:10.1080/02786828908959280, 1989.

McNeill, V. F., Yatavelli, R. L. N., Thornton, J. a, Stipe, C. B. and Landgrebe, O.: Heterogeneous OH oxidation of palmitic acid in single component and internally mixed aerosol particles : vaporization and the role of particle phase, Atmospheric Chemistry and Physics, 8(17), 5465-5476, 2008.

Mcmurry, P. H.: A review of atmospheric aerosol measurements, Atmospheric Environment, 34, 1959-1999, 2000.

Megharaj, M., Ramakrishnan, B., Venkateswarlu, K., Sethunathan, N. and Naidu, R.: Bioremediation approaches for organic pollutants: A critical perspective., Environment International, 37(8), 1362-1375, doi:10.1016/j.envint.2011.06.003, 2011.

van Midwoud, P. M., Janssen, J., Merema, M. T., de Graaf, I. A. M., Groothuis, G. M. M. and Verpoorte, E.: On-line HPLC Analysis System for Metabolism and Inhibition Studies in Precision-Cut Liver Slices, Analytical Chemistry, 83(1), 84-91, doi:10.1155/2009/953952., 2011.

Miracolo, M. A., Presto, A. A., Lambe, A. T., Hennigan, C. J., Donahue, N. M., Kroll, J. H., Worsnop, D. R. and Robinson, A. L.: Photo-oxidation of low-volatility organics found in motor vehicle emissions: production and chemical evolution of organic aerosol mass., Environmental science & technology, 44(5), 1638-1643, doi:10.1021/es902635c, 2010.

Mitschke, S., Welthagen, W. and Zimmermann, R.: Chromatography-Time-of-Flight Mass Spectrometry Using Soft and Selective Photoionization Techniques, Analytical Chemistry, 78(18), 6364-6375, 2006.

Mysak, E. R., Wilson, K. R., Jimenez-Cruz, M., Ahmed, M. and Baer, T.: Synchrotron Radiation Based Aerosol Time-of-Flight Mass Spectrometry for Organic Constituents spectrometer using tunable vacuum-ultraviolet (VUV), Analytical Chemistry, 77(18), 5953-5960, 2005.

NIST Mass Spec Data Center S.E. Stein director: Mass Spectra, in NIST Chemistry WebBook, NIST Standard Reference Database Number 69, edited by P. J. Linstrom and W. G. Mallard, National Institute of Standards and Technology, Gaithersburg, MD, 20899. [online] Available from: http://webbook.nist.gov, 2012.

NIST/SEMATECH: Section 2.3.6.7. Uncertainties of calibrated values, in e-Handbook of Statistical Methods. [online] Available from: http://www.itl.nist.gov/div898/handbook/, 2012.

Nah, T., Kessler, S. H., Daumit, K. E., Kroll, J. H., Leone, S. R. and Wilson, K. R.: Influence of molecular structure and chemical functionality on the heterogeneous OH-initiated oxidation of unsaturated organic particles., The journal of physical chemistry. A, 118(23), 4106-19,

doi:10.1021/jp502666g [online] Available from: http://www.ncbi.nlm.nih.gov/pubmed/24840787, 2014.

Ng, N. L., Chhabra, P. S., Chan, A. W. H., Surratt, J. D., Kroll, J. H., Kwan, A. J., McCabe, D. C., Wennberg, P. O., Sorooshian, A., Murphy, S. M., Dalleska, N. F., et al.: Effect of NOx level on secondary organic aerosol (SOA) formation from the photooxidation of terpenes, Atmospheric Chemistry and Physics, 7(4), 5159-5174, doi:10.5194/acpd-7-10131-2007, 2007.

Nguyen, T. B., Coggon, M. M., Bates, K. H., Zhang, X., Schwantes, R. H., Schilling, K. a., Loza, C. L., Flagan, R. C., Wennberg, P. O. and Seinfeld, J. H.: Organic aerosol formation from the reactive uptake of isoprene epoxydiols (IEPOX) onto non-acidified inorganic seeds, Atmospheric Chemistry and Physics, 14(7), 3497-3510, doi:10.5194/acp-14-3497-2014 [online] Available from: http://www.atmos-chem-phys.net/14/3497/2014/ (Accessed 5 August 2014a), 2014.

Nguyen, T. K. V., Petters, M. D., Suda, S. R. and Carlton, A. G.: Trends in particle phase liquid water during the Southern Oxidant and Aerosol Study, Atmospheric Chemistry and Physics Discussions, 14(6), 7469-7516, doi:10.5194/acpd-14-7469-2014 [online] Available from: http://www.atmos-chem-phys-discuss.net/14/7469/2014/ (Accessed 5 October 2014b), 2014.

Nguyen, T. L., Peeters, J. and Vereecken, L.: Theoretical study of the gas-phase ozonolysis of β-pinene (C10H16), Physical Chemistry Chemical Physics, 11(27), 5643-5656, doi:10.1039/b822984h, 2009.

Odum, J. R., Hoffmann, T., Bowman, F., Collins, D. R., Flagan, R. C. and Seinfeld, J. H.: Gas/particle partitioning and secondary organic aerosol yields, Environmental Science & Technology, 30, 2580-2585, 1996.

Offenberg, J. H., Lewandowski, M., Jaoui, M. and Kleindienst, T. E.: Contributions of Biogenic and Anthropogenic Hydrocarbons to Secondary Organic Aerosol during 2006 in Research Triangle Park, NC, Aerosol and Air Quality Research, 11, 99-108, doi:10.4209/aaqr.2010.11.0102, 2011.

Orasche, J., Schnelle-Kreis, J., Abbaszade, G. and Zimmermann, R.: Technical Note: In-situ derivatization thermal desorption GC-TOFMS for direct analysis of particle-bound non-polar and polar organic species, Atmospheric Chemistry and Physics, 11(17), 8977-8993, doi:10.5194/acp-11-8977-2011, 2011.

Ormeño, E., Gentner, D. R., Fares, S., Karlik, J., Park, J. H. and Goldstein, A. H.: Sesquiterpenoid emissions from agricultural crops: correlations to monoterpenoid emissions and leaf terpene content., Environmental science & technology, 44(10), 3758-64, doi:10.1021/es903674m, 2010.

Oss, M., Kruve, A., Herodes, K. and Leito, I.: Electrospray Ionization Efficiency Scale of Organic Compounds, Analytical Chemistry, 82(7), 2865-2872, 2010.

Ozel, M., Ward, M., Hamilton, J. F., Lewis, A., Raventos-Duran, T. and Harrison, R.: Analysis of Organic Nitrogen Compounds in Urban Aerosol Samples Using GCxGC-TOF/MS, Aerosol Science and Technology, 44(2), 109-116, doi:10.1080/02786820903410105, 2010.

Paatero, P. and Tappert, U.: Positive matrix factorization: a non-negative factor model with optimal utilization of error estimates of data values, Environmetrics, 5(April 1993), 111-126, 1994.

Pankow, J. F.: An absorption model of gas/particle partitioning of organic compounds in the atmosphere, Atmospheric Environment, 28(2), 185-188, doi:10.1016/1352-2310(94)90093-0, 1994.

Pankow, J. F. and Asher, W. E.: SIMPOL.1: a simple group contribution method for predicting vapor pressures and enthalpies of vaporization of multifunctional organic compounds, Atmospheric Chemistry and Physics, 8, 2773-2796, 2008.

Pankow, J. F. and Barsanti, K. C.: The carbon number-polarity grid: A means to manage the complexity of the mix of organic compounds when modeling atmospheric organic particulate matter, Atmospheric Environment, 43(17), 2829-2835, doi:10.1016/j.atmosenv.2008.12.050, 2009.

Park, J.-H., Fares, S., Weber, R. and Goldstein, A. H.: Biogenic volatile organic compound emissions during BEARPEX 2009 measured by eddy covariance and flux–gradient similarity methods, Atmospheric Chemistry and Physics, 14(1), 231-244, doi:10.5194/acp-14-231-2014 [online] Available from: http://www.atmos-chem-phys.net/14/231/2014/ (Accessed 19 August 2014), 2014.

Pathak, R. K., Stanier, C. O., Donahue, N. M. and Pandis, S. N.: Ozonolysis of a-pinene at atmospherically relevant concentrations: Temperature dependence of aerosol mass fractions (yields), Journal of Geophysical Research, 112, 1-8, doi:10.1029/2006JD007436, 2007.

Paulot, F., Crounse, J. D., Kjaergaard, H. G., Kürten, A., St Clair, J. M., Seinfeld, J. H. and Wennberg, P. O.: Unexpected epoxide formation in the gas-phase photooxidation of isoprene., Science, 325(5941), 730-733, doi:10.1126/science.1172910 [online] Available from: http://www.ncbi.nlm.nih.gov/pubmed/19661425 (Accessed 21 January 2014), 2009.

Perring, A. E., Bertram, T. H., Farmer, D. K., Wooldridge, P. J., Dibb, J., Blake, N. J., Blake, D. R., Singh, H. B., Fuelberg, H., Diskin, G. S., Sachse, G., et al.: The production and persistence of ΣRONO2 in the Mexico City plume, Atmospheric Chemistry and Physics, 10(15), 7215-7229, doi:10.5194/acp-10-7215-2010, 2010.

Pierce, J. R., Engelhart, G. J., Hildebrandt, L., Weitkamp, E. A., Pathak, R. K., Donahue, N. M., Robinson, A. L., Adams, P. J. and Pandis, S. N.: Constraining Particle Evolution from Wall Losses, Coagulation, and Condensation-Evaporation in Smog-Chamber Experiments: Optimal Estimation Based on Size Distribution Measurements, Aerosol Science and Technology, 42(12), 1001-1015, doi:10.1080/02786820802389251, 2008.

Pope, C. A. and Dockery, D. W.: Health effects of fine particulate air pollution: Lines that connect, Journal of Air and Waste Management, 56(6), 709-742, 2006.

Ramdahl, T.: Retene - a molecular marker of wood combustion in ambient air, Nature, 306, 580-582, 1983.

Renbaum, L. H. and Smith, G. D.: Artifacts in measuring aerosol uptake kinetics: the roles of time, concentration and adsorption, Atmospheric Chemistry and Physics, 11(14), 6881-6893, doi:10.5194/acp-11-6881-2011 [online] Available from: http://www.atmos-chem-phys.net/11/6881/2011/ (Accessed 16 August 2012), 2011.

Rinne, H. J. I., Guenther, A. B., Greenberg, J. P. and Harley, P. C.: Isoprene and monoterpene fluxes measured above Amazonian rainforest and their dependence on light and temperature, Atmospheric Environment, 36, 2421-2426, 2002.

Robinson, N. H., Hamilton, J. F., Allan, J. D., Langford, B., Oram, D. E., Chen, Q., Docherty, K., Farmer, D. K., Jimenez, J. L., Ward, M. W., Hewitt, C. N., et al.: Evidence for a significant proportion of Secondary Organic Aerosol from isoprene above a maritime tropical forest, Atmospheric Chemistry and Physics, 11(3), 1039-1050, doi:10.5194/acp-11-1039-2011 [online] Available from: http://www.atmos-chem-phys.net/11/1039/2011/ (Accessed 12 September 2014), 2011.

Rogge, W. F.: Molecular Tracers for Sources of Atmospheric Carbon Particles: Measurements and Model Predictions, California Institute of Technology., 1993.

Rogge, W. F., Mazurek, M. A., Hildemann, L. M., Cass, G. R. and Simoneit, B. R. T.: Quantification of urban organic aerosols at a molecular level: identification, abundance and seasonal variation, Atmospheric Environment, 27(8), 1309-1330, 1993.

Roldin, P., Eriksson, a. C., Nordin, E. Z., Hermansson, E., Mogensen, D., Rusanen, a., Boy, M., Swietlicki, E., Svenningsson, B., Zelenyuk, a. and Pagels, J.: Modelling non-equilibrium secondary organic aerosol formation and evaporation with the aerosol dynamics, gas- and particle-phase chemistry kinetic multilayer model ADCHAM, Atmospheric Chemistry and Physics, 14(15), 7953-7993, doi:10.5194/acp-14-7953-2014 [online] Available from: http://www.atmos-chem-phys.net/14/7953/2014/ (Accessed 12 August 2014), 2014.

Ruehl, C. R., Nah, T., Isaacman, G., Worton, D. R., Chan, A. W. H., Kolesar, K. R., Cappa, C. D., Goldstein, A. H. and Wilson, K. R.: The Influence of Molecular Structure and Aerosol Phase on the Heterogeneous Oxidation of Normal and Branched Alkanes by OH, Journal of Physical Chemistry A, 117, 3990-4000, 2013.

Ruehl, C. R. and Wilson, K. R.: Surface organic monolayers control the hygroscopic growth of submicrometer particles at high relative humidity., The journal of physical chemistry. A, 118(22), 3952-66, doi:10.1021/jp502844g [online] Available from: http://www.ncbi.nlm.nih.gov/pubmed/24866291, 2014.

Schauer, J. J., Kleeman, M. J., Cass, G. R. and Simoneit, B. R. T.: Measurement of Emissions from Air Pollution Sources. 1. C 1 through C 29 Organic Compounds from Meat Charbroiling, Environmental Science & Technology, 33(10), 1566-1577, doi:10.1021/es980076j, 1999a.

Schauer, J. J., Kleeman, M. J., Cass, G. R. and Simoneit, B. R. T.: Measurement of Emissions from Air Pollution Sources. 2. C 1 through C 30 Organic Compounds from Medium Duty Diesel Trucks, Environmental Science & Technology, 33(10), 1578-1587, doi:10.1021/es980081n, 1999b.

Schauer, J. J., Kleeman, M. J., Cass, G. R. and Simoneit, B. R. T.: Measurement of Emissions from Air Organic Compounds from Gasoline-Powered Motor Vehicles, Environmental Science & Technology, 36, 1169-1180, 2002.

Schauer, J. J., Rogge, W. F., Hildemann, L. M., Mazurek, M. A. and Cass, G. R.: Source apportionment of airborne particulate matter using organic compounds as tracers, Atmospheric Environment, 30(22), 3837-3855, 1996.

Schnelle-Kreis, J., Welthagen, W., Sklorz, M. and Zimmermann, R.: Application of direct thermal desorption gas chromatography and comprehensive two-dimensional gas chromatography coupled to time of flight mass spectrometry for analysis of organic compounds in ambient aerosol particles, Journal of Separation Science, 28(14), 1648-1657, doi:10.1002/jssc.200500120, 2005.

Sheesley, R. J., Deminter, J. T., Meiritz, M., Snyder, D. C. and Schauer, J. J.: Temporal trends in motor vehicle and secondary organic tracers using in situ methylation thermal desorption GCMS., Environmental science & technology, 44(24), 9398-9404, doi:10.1021/es102301t, 2010.

Shiraiwa, M., Zuend, A., Bertram, A. K. and Seinfeld, J. H.: Gas-particle partitioning of atmospheric aerosols: interplay of physical state, non-ideal mixing and morphology., Physical chemistry chemical physics : PCCP, 15(27), 11441-53, doi:10.1039/c3cp51595h [online] Available from: http://www.ncbi.nlm.nih.gov/pubmed/23748935 (Accessed 1 October 2014), 2013.

Shu, Y. and Atkinson, R.: Rate constants for the gas-phase reactions of O3 with a series of Terpenes and OH radical formation from the O3 reactions with Sesquiterpenes at 296 +/- 2 K, International Journal of Chemical Kinetics, 26(12), 1193-1205, doi:10.1002/kin.550261207, 1994.

Sieck, L. W.: Determination of Molecular Weight Distribution of Aromatic Components in Petroleum Products by Chemical Ionization Mass Spectrometry with Chlorobenzene as Reagent Gas, Analytical Chemistry, 55, 38-41, 1983.

Simoneit, B. R. T.: A review of current applications of mass spectrometry for biomarker/molecular tracer elucidation., Mass spectrometry reviews, 24(5), 719-65, doi:10.1002/mas.20036, 2005.

Smith, J. D., Kroll, J. H., Cappa, C. D., Che, D. L., Liu, C. L., Ahmed, M., Leone, S. R., Worsnop, D. R. and Wilson, K. R.: The heterogeneous reaction of hydroxyl radicals with sub-micron squalane particles: a model system for understanding the oxidative aging of ambient aerosols, Atmospheric Chemistry and Physics, 9, 3209-3222, 2009.

Speer, R. E., Edney, E. O. and Kleindienst, T. E.: Impact of organic compounds on the concentrations of liquid water in ambient PM2.5, Journal of Aerosol Science, 34, 63-77, 2003.

Spracklen, D. V., Jimenez, J.-L., Carslaw, K. S., Worsnop, D. R., Evans, M. J., Mann, G. W., Zhang, Q., Canagaratna, M. R., Allan, J., Coe, H., McFiggans, G., et al.: Aerosol mass spectrometer constraint on the global secondary organic aerosol budget, Atmospheric Chemistry and Physics, 11(23), 12109-12136, doi:10.5194/acp-11-12109-2011 [online] Available from: http://www.atmos-chem-phys.net/11/12109/2011/ (Accessed 20 February 2013), 2011.

Stockli, R., Vermote, E., Saleous, N., Simmon, R. and Herring, D.: The Blue Marble Next Generation - A true color earth dataset including seasonal dynamics from MODIS., NASA Earth Observatory, 2005.

Storey, J. M. E., Luo, W., Isabelle, L. M. and Pankow, J. F.: Gas/Solid Partitioning of Semivolatile Organic Compounds to Model Atmospheric Solid Surfaces as a Function of Relative Humidity. 1. Clean Quartz, Environmental science & technology, 29(9), 2420-2428, 1995.

Sueper, D.: ToF-AMS Analysis Software, [online] Available from: http://cires.colorado.edu/jimenez-group/wiki/index.php/ToF-AMS_Analysis_Software, 2012.

Surratt, J. D., Chan, A. W. H., Eddingsaas, N. C., Chan, M. N., Loza, C. L., Kwan, A. J., Hersey, S. P., Flagan, R. C., Wennberg, P. O. and Seinfeld, J. H.: Reactive intermediates revealed in secondary organic aerosol formation from isoprene., Proceedings of the National Academy of Sciences of the United States of America, 107(15), 6640-5, doi:10.1073/pnas.0911114107, 2010.

Surratt, J. D., Go, Y., Chan, A. W. H., Vermeylen, R., Shahgholi, M., Kleindienst, T. E., Edney, E. O., Offenberg, J. H., Lewandowski, M., Jaoui, M., Maenhaut, W., et al.: Organosulfate Formation in Biogenic Secondary Organic Aerosol, Journal of Physical Chemistry A, 112, 8345-8378, 2008.

Surratt, J. D., Murphy, S. M., Kroll, J. H., Ng, N. L., Hildebrandt, L., Sorooshian, A., Szmigielski, R., Vermeylen, R., Maenhaut, W., Claeys, M., Flagan, R. C., et al.: Chemical composition of secondary organic aerosol formed from the photooxidation of isoprene., Journal of Physical Chemistry A, 110(31), 9665-90, doi:10.1021/jp061734m [online] Available from: http://www.ncbi.nlm.nih.gov/pubmed/20108685, 2006.

Szmigielski, R., Surratt, J. D., Gómez-González, Y., Van der Veken, P., Kourtchev, I., Vermeylen, R., Blockhuys, F., Jaoui, M., Kleindienst, T. E., Lewandowski, M., Offenberg, J. H., et al.: 3-methyl-1,2,3-butanetricarboxylic acid: An atmospheric tracer for terpene secondary organic aerosol, Geophysical Research Letters, 34(24), L24811, doi:10.1029/2007GL031338

[online] Available from: http://doi.wiley.com/10.1029/2007GL031338 (Accessed 21 January 2014a), 2007.

Szmigielski, R., Surratt, J. D., Vermeylen, R., Szmigielska, K., Kroll, J. H., Ng, N. L., Murphy, S. M., Sorooshian, A., Seinfeld, J. H. and Claeys, M.: Characterization of 2-methylglyceric acid oligomers in secondary organic aerosol formed from the photooxidation of isoprene using trimethylsilylation and gas chromatography / ion trap mass spectrometry, Journal of Mass Spectrometry, 42(1), 101-116, doi:10.1002/jms, 2007b.

Tervahattu, H., Hartonen, K., Kerminen, V.-matti, Kupiainen, K., Koskentalo, T., Tuck, A. F. and Vaida, V.: New evidence of an organic layer on marine aerosols, Journal of Geo, 107(D7), doi:10.1029/2000JD000282, 2002.

Trebs, I., Mayol-bracero, O. L., Pauliquevis, T., Kuhn, U., Sander, R., Ganzeveld, L., Meixner, F. X., Kesselmeier, J., Artaxo, P. and Andreae, M. O.: Impact of the Manaus urban plume on trace gas mixing ratios near the surface in the Amazon Basin : Implications for the NO-NO 2 -O 3 photostationary state and peroxy radical levels, Journal of Geophysical Research, 117(2), 1-16, doi:10.1029/2011JD016386, 2012.

Turpin, B. J., Saxena, P. and Andrews, E.: Measuring and simulating particulate organics in the atmosphere : problems and prospects, Atmospheric Environment, 34, 2983-3013, 2000.

US EPA: Estimation Program Interface (EPI) Suite,, 2008.

Ulbrich, I. M., Canagaratna, M. R., Zhang, Q., Worsnop, D. R. and Jimenez, J.-L.: Interpretation of organic components from Positive Matrix Factorization of aerosol mass spectrometric data, Atmospheric Chemistry and Physics, 9, 2891-2918, 2009.

Vardag, T., Karger, N. and Ludemann, H.-D.: Temperature and Pressure Dependence of Self Diffusion in Long Liquid n-Alkanes, Berichte der Bunsengesellschaft für physikalische Chemie, 95(8), 859-865, 1991.

Wang, W., Kourtchev, I., Graham, B., Cafmeyer, J., Maenhaut, W. and Claeys, M.: Characterization of oxygenated derivatives of isoprene related to 2-methyltetrols in Amazonian aerosols using trimethylsilylation and gas chromatography/ion trap mass spectrometry., Rapid communications in mass spectrometry : RCM, 19(10), 1343-51, doi:10.1002/rcm.1940 [online] Available from: http://www.ncbi.nlm.nih.gov/pubmed/15856536 (Accessed 5 October 2014), 2005.

Weber, R. J., Sullivan, A. P., Peltier, R. E., Russell, A. G., Yan, B., Zheng, M., de Gouw, J. A., Warneke, C., Brock, C. A., Holloway, J. S., Atlas, E. L., et al.: A study of secondary organic aerosol formation in the anthropogenic-influenced southeastern United States, Journal of Geophysical Research, 112(D13302), 2007.

Weitkamp, E. A., Lambe, A. T., Donahue, N. M. and Robinson, A. L.: Laboratory Measurements of the Heterogeneous Oxidation of Condensed-Phase Organic Molecular Makers for Motor

Vehicle Exhaust, Environmental Science & Technology, 42(21), 7950-7956, doi:10.1021/es800745x, 2008.

Wexler, A. S. and Clegg, S. L.: Atmospheric aerosol models for systems including the ions H+, NH4+, NA+, SO42-, NO3-, Cl-, Br- and H2O, Journal of Geophysical Research, 107(D14), doi:10.1029/2001JD000451, 2002.

van Wilgenburg, E., Sulc, R., Shea, K. J. and Tsutsui, N. D.: Deciphering the chemical basis of nestmate recognition., Journal of chemical ecology, 36(7), 751-8, doi:10.1007/s10886-010-9812-4, 2010.

Williams, B. J., Goldstein, A. H., Kreisberg, N. M. and Hering, S. V.: An In-Situ Instrument for Speciated Organic Composition of Atmospheric Aerosols: Thermal Desorption Aerosol GC/MS-FID (TAG), Aerosol Science and Technology, 40, 627-638, doi:10.1080/02786820600754631, 2006.

Williams, B. J., Goldstein, A. H., Kreisberg, N. M. and Hering, S. V.: In situ measurements of gas/particle-phase transitions for atmospheric semivolatile organic compounds., Proceedings of the National Academy of Sciences of the United States of America, 107(15), 6676-81, doi:10.1073/pnas.0911858107, 2010a.

Williams, B. J., Goldstein, A. H., Kreisberg, N. M., Hering, S. V., Worsnop, D. R., Ulbrich, I. M., Docherty, K. S. and Jimenez, J.-L.: Major components of atmospheric organic aerosol in southern California as determined by hourly measurements of source marker compounds, Atmospheric Chemistry and Physics, 10(23), 11577-11603, doi:10.5194/acp-10-11577-2010, 2010b.

Williams, B. J., Goldstein, A. H., Millet, D. B., Holzinger, R., Kreisberg, N. M., Hering, S. V., White, A. B., Worsnop, D. R., Allan, J. D. and Jimenez, J.-L.: Chemical speciation of organic aerosol during the International Consortium for Atmospheric Research on Transport and Transformation 2004: Results from in situ measurements, Journal of Geophysical Research, 112(D10), 1-14, doi:10.1029/2006JD007601, 2007.

Winterhalter, R., Herrmann, F., Kanawati, B., Nguyen, T. L., Peeters, J., Vereecken, L. and Moortgat, G. K.: The gas-phase ozonolysis of beta-caryophyllene (C(15)H(24)). Part I: an experimental study, Physical Chemistry Chemical Physics, 11(21), 4152-72, doi:10.1039/b817824k, 2009.

Winterhalter, R., Neeb, P., Grossmann, D., Kolloff, A., Horie, O. and Moortgat, G. K.: Products and Mechanism of the Gas Phase Reaction of Ozone with β-Pinene, Journal of Atmospheric Chemistry, 35, 165-197, 2000.

Worton, D. R., Goldstein, A. H., Farmer, D. K., Docherty, K. S., Jimenez, J.-L., Gilman, J. B., Kuster, W. C., de Gouw, J. A., Williams, B. J., Kreisberg, N. M., Hering, S. V., et al.: Origins and composition of fine atmospheric carbonaceous aerosol in the Sierra Nevada Mountains,

California, Atmospheric Chemistry and Physics, 11(19), 10219-10241, doi:10.5194/acp-11-10219-2011, 2011.

Worton, D. R., Isaacman, G., Gentner, D. R., Dallmann, T. R., Chan, A. W. H., Ruehl, C., Kirchstetter, T. W., Wilson, K. R., Harley, R. A. and Goldstein, A. H.: Lubricating Oil Dominates Primary Organic Aerosol Emissions from Motor Vehicles, Environmental Science & Technology, 2014.

Worton, D. R., Kreisberg, N. M., Isaacman, G., Teng, A. P., McNeish, C., Górecki, T., Hering, S. V. and Goldstein, A. H.: Thermal Desorption Comprehensive Two-Dimensional Gas Chromatography: An Improved Instrument for In-Situ Speciated Measurements of Organic Aerosols, Aerosol Science and Technology, 46(4), 380-393, doi:10.1080/02786826.2011.634452, 2012.

Worton, D. R., Surratt, J. D., Lafranchi, B. W., Chan, A. W. H., Zhao, Y., Weber, R. J., Park, J.-H., Gilman, J. B., de Gouw, J. A., Park, C., Schade, G., et al.: Observational insights into aerosol formation from isoprene., Environmental science & technology, 47(20), 11403-13, doi:10.1021/es4011064 [online] Available from: http://www.ncbi.nlm.nih.gov/pubmed/24004194, 2013.

Xu, L., Guo, H., Boyd, C. M., Klein, M., Bougiatioti, A., Cerully, K. M., Hite, J. R., Isaacman-VanWertz, G., Kreisberg, N. M., Knote, C., Olsen, K., et al.: Effects of Anthropogenic Emissions on Aerosol Formation from Isoprene and Monoterpenes in the Southeastern United States, Proceedings of the National Academy of Sciences of the United States of America, 2014.

Youngsteadt, E., Guerra Bustios, P. and Schal, C.: Divergent chemical cues elicit seed collecting by ants in an obligate multi-species mutualism in lowland Amazonia., PloS one, 5(12), e15822, doi:10.1371/journal.pone.0015822, 2010.

Zhang, H., Ruehl, C. R., Chan, A. W. H., Nah, T., Worton, D. R., Isaacman, G., Goldstein, A. H. and Wilson, K. R.: OH-initiated heterogeneous oxidation of cholestane: a model system for understanding the photochemical aging of cyclic alkane aerosols., Journal of Physical Chemistry A, 117(47), 12449-12458, doi:10.1021/jp407994m [online] Available from: http://www.ncbi.nlm.nih.gov/pubmed/24152093, 2013.

Zhang, J., Huff Hartz, K. E., Pandis, S. N. and Donahue, N. M.: Secondary organic aerosol formation from limonene ozonolysis: homogeneous and heterogeneous influences as a function of NO(x)., Journal of Physical Chemistry A, 110(38), 11053-63, doi:10.1021/jp062836f, 2006.

Zhang, Q., Jimenez, J.-L., Canagaratna, M. R., Allan, J. D., Coe, H., Ulbrich, I. M., Alfarra, M. R., Takami, A., Middlebrook, A. M., Sun, Y. L., Dzepina, K., et al.: Ubiquity and dominance of oxygenated species in organic aerosols in anthropogenically-influenced Northern Hemisphere midlatitudes, Geophysical Research Letters, 34(L13801), 1-6, doi:10.1029/2007GL029979, 2007.

Zhang, Y., Sheesley, R. J., Schauer, J. J., Lewandowski, M., Jaoui, M., Offenberg, J. H., Kleindienst, T. E. and Edney, E. O.: Source apportionment of primary and secondary organic aerosols using positive matrix factorization (PMF) of molecular markers, Atmospheric Environment, 43(34), 5567-5574, doi:10.1016/j.atmosenv.2009.02.047, 2009.

Zhao, Y., Kreisberg, N. M., Worton, D. R., Isaacman, G., Gentner, D. R., Chan, A. W. H., Weber, R. J., Liu, S., Day, D. a., Russell, L. M., Hering, S. V., et al.: Sources of organic aerosol investigated using organic compounds as tracers measured during CalNex in Bakersfield, Journal of Geophysical Research: Atmospheres, 118(19), 11,388-11,398, doi:10.1002/jgrd.50825 [online] Available from: http://doi.wiley.com/10.1002/jgrd.50825 (Accessed 14 October 2014a), 2013.

Zhao, Y., Kreisberg, N. M., Worton, D. R., Isaacman, G., Weber, R. J., Liu, S., Day, D. A., Russell, L. M., Markovic, M. Z., Vandenboer, T. C., Murphy, J. G., et al.: Insights into secondary organic aerosol formation mechanisms from measured gas/particle partitioning of specific organic tracer compounds., Environmental science & technology, 47(8), 3781-3787, doi:10.1021/es304587x [online] Available from: http://www.ncbi.nlm.nih.gov/pubmed/23448102, 2013b.

Zhao, Y., Kreisberg, N. M., Worton, D. R., Teng, A. P., Hering, S. V. and Goldstein, A. H.: Development of an In Situ Thermal Desorption Gas Chromatography Instrument for Quantifying Atmospheric Semi-Volatile Organic Compounds, Aerosol Science and Technology, 47(3), 258-266, doi:10.1080/02786826.2012.747673 [online] Available from: http://www.tandfonline.com/doi/abs/10.1080/02786826.2012.747673 (Accessed 25 March 2013c), 2013.

Zhou, S., Shiraiwa, M., McWhinney, R. D., Pöschl, U. and Abbatt, J. P. D.: Kinetic limitations in gas-particle reactions arising from slow diffusion in secondary organic aerosol, Faraday Discussions, 165, 391, doi:10.1039/c3fd00030c [online] Available from: http://xlink.rsc.org/?DOI=c3fd00030c (Accessed 1 October 2014), 2013.

Zimmermann, R., Mühlberger, F., Fuhrer, K., Gonin, M. and Welthagen, W.: An ultracompact photo-ionization time-of-flight mass spectrometer with a novel vacuum ultraviolet light source for on-line detection of organic trace compounds and as a detector for gas chromatography, Journal of Material Cycles and Waste Management, 10(1), 24-31, doi:10.1007/s10163-007-0194-9, 2008.